SYNTHETIC SENSORS FOR SACCHARIDES AND GLYCOPROTEINS

Alexander J. Stephenson-Brown

A thesis submitted to The University of Birmingham
for the Degree of DOCTOR OF PHILOSOPHY

School of Chemical Engineering
College of Physical Sciences and Engineering
The University of Birmingham

ABSTRACT

The sensing of biological compounds is of vital importance to the screening and diagnosis of disease. The importance of such assays is due to the correlation observed between the observed levels of biological compounds and diseases such as cancer and diabetes mellitus. Compounds such as sugars and proteins are included in this useful class of molecules which can be used to detect pathology. Currently the detection of these compounds is achieved through the use of other biologically derived molecules- typically antibodies and enzymes. However, sensors based on these compounds can be limited in terms of their stability and suitability. Therefore there is a constant drive for novel detection methods for such molecules.

In this context, the aims of the work described herein, are to produce synthetic sensing systems for the selective detection of saccharides and glycoproteins. This work will use principles of nanotechnology and self-assembly to produce surface sensors which exploit the revisable interactions of boronic acids to bind compounds of interest, and which employ surface plasmon resonance spectroscopy to enable the label free reporting of these binding events.

Chapter 1 - This chapter aims to provide the reader with a prospective and an understanding about the current state of the art in the field of nanotechnology, self-assembly and sugar/glycoprotein sensing. Over the course of the subsequent pages a number of broad and varied topics will be introduced in order to allow the reader to appreciate the intricacies and applications of techniques discussed in subsequent chapters of this thesis.

Chapter 2 - In this chapter the various techniques and methods used to characterise materials and surfaces will be reviewed. The aim of this chapter is to provide a brief

explanation of the techniques which will be discussed in later chapters of this thesis. Particular attention will be paid to techniques suited to the investigation of modified surfaces.

Chapter 3 – This chapter will describe the fabrication of a glucose selective surface sensor. This sensor employs self-assembled monolayers on gold generated from a *bis*-boronic acid bearing a thioctic acid moiety, whose intramolecular distance between the boronic acid moieties is well defined. Using surface plasmon resonance, we are able to reveal this surface demonstrates a higher affinity towards glucose than other saccharides

Chapter 4 - In this chapter the design, synthesis and characterisation of components of a novel system for the production molecularly imprinted modified surface for the selective detection of glycoproteins will be described, along with subsequent surface reactions.

Chapter 5 - Following the design, synthesis and characterisation of each element of the proposed molecularly imprinted surface sensors, this chapter will detail their application. This chapter will describe the development of molecularly imprinted surface sensors to target compounds RNAse B and PSA. The ability of the produced sensors to bind these proteins along will be assessed and compared with other non-target proteins in order to demonstrate their affinity and selectivity.

Chapter 6 - Conclusions and future work

Chapter 7 – Methods

Chapter 8 – References

Acknowledgements

Firstly I would like to take the opportunity to thank my academic supervisors, Paula, John and Jon. Without their support, advice and patience, the completion of this thesis would have been impossible.

Next, there is a long list of support staff and fellow students who have been incredibly kind and helpful over the course of my PhD. I'll mention a few by name, this list is not exhaustive and if I miss anyone I only hope they will forgive me! From the support staff I'd like to thank Neil and Chi for keeping the analytical labs up and running, along with James Bowen for the help with equipment in Science City labs. Thanks also to the administrative staff in the School of Chemical Engineering, with special mention to Chris, Liz and Lynn.

There is a long list of current and former students/post-docs who made my time at Birmingham all the more memorable. From the Mendes group I'd like to thank Frankie, Cait, Olly, Paul, Alice, Elly, Aaron, Monika, Minhaj and Zarrar. From the School of Chemistry I'd like to thank Mark, Rama, Dan, Mariwan, Wenlei, Will, Sabrina and Antonio.

Finally, I must thank those friends and members of my family who have all helped get me here. Again I can't mention everyone, but special mentions must be given to my partner and teammate Natasha, my Mum, Dad and Denise, Grandma and Grandad, and siblings Ryan, Ellie, Charlotte and Lucy.

"An expert is a person who has made all the mistakes that can be made in a very narrow field."

— Niels Bohr

ABBREVIATIONS USED

AABA	(Acrylamido)phenylboronic acid
Az-OEG	O-(2-Azidoethyl)heptaethylene glycol
BA	Boronic acid
bis-BA	*Bis*-boronic acid
BE	*Binding energy*
BOC	*Tert*-Butyloxycarbonyl
BSA	Bovine serum albumin
CCD	Charged coupled device
CV	Cyclic voltametry
DCC	N,N'-Dicyclohexylcarbodiimide
DFC	Difunctional cysteine
DHU	Dicyclohexylurea
HRP	Horseradish peroxidase
IR	Infrared spectroscopy
MI	Molecular imprint
MS	Mass spectrometry
NHS	*N*-Hydroxysuccinimide
NMR	Nuclear magnetic resonance
NPA	n-phenylacramide
NSB	non-specific binding
OEG	of oligo(ethylene glycol)
PSA	Prostate Specific Antigen
RNAse	Ribonuclease
SPR	Surface Plasmon Resonance
TEGT	tri(ethylene glycol)-terminated thiol
TEMED	Tetramethylethylenediamine
TM	Transverse Magnetic
UHP	Ultra High Pure
XPS	X-Ray Photoelectron Spectroscopy

CHAPTER 1: INTRODUCTION

This thesis will describe the production of sensors for biologically relevant compounds. Molecular sensing relies on the success of two distinct processes: the selective binding of the target compound and the transduction of this interaction into a signal which can be measured, which is ideally proportionate to the concentration of the target compound present. This chapter aims to provide the reader with a prospective and an understanding about the current state of the art. Over the course of the subsequent pages a number of broad and varied topics will be introduced in order to allow the reader to appreciate the intricacies and applications of techniques discussed in subsequent chapters of this thesis.

1.1 Chapter Outline

This chapter aims to introduce a number of broad and varied topics in order to allow the reader to appreciate the intricacies and applications of techniques discussed in subsequent chapters of this thesis. It will begin by introducing simple carbohydrates- outlining their structures and the roles which they play in biological systems. This will then lead onto a brief overview of methods of sensing these compounds, with emphasis being placed on the detection of monosaccharides.

The next section then discusses how more complex carbohydrate groups are used to modulate the function of proteins in a process known as glycosylation. Here the roles of these structures in health and disease are discussed, with particular attention to how such structures could be exploited to improve the detection of malignancies such as prostate cancer. Next follows an account of the molecular tools commonly employed to bind carbohydrates, which will pay particular attention to boronic acids, and their application to sugar sensing including their use in nanoscale systems.

Next, a more detailed overview of nanotechnology will be discussed, which specifically focus on self-assembled systems, notably self-assembled monolayers and their application to sensor fabrication. In the final section, the concept of molecular imprinting will be introduced. Here its applications and limitations will be discussed to provide the reader with an overview of the current state of the art in this field of binding site fabrication.

1.2 Introduction to sugars

Saccharides represent a uniquely versatile class of molecule utilised by many physiological systems. They may be found in mechanical-structural compounds, energy sources and structures involved in cell communication and recognition. [3] In addition carbohydrate groups may be added to protein molecules as post-translational modifications that allows the modulation of protein function or half-life.[4] Their role in many biological systems drives the demand for methods of detection and measurement in a range of sample types. Current methods typically involve the use of saccharide specific enzymes, however such methodologies are limited as they consume the analytes of interest during the assay, require mediators and their sensitivity can be hindered by limited mass transport of target analytes. [5] These limitations have fuelled the development of new systems that are able to use alternative and novel methods of detection and quantification.

1.2.1 Carbohydrates

Monosaccharides are the simplest carbohydrates and can be defined as aldehydes or ketones which have two or more hydroxyl groups. The empirical formula for many monosaccharides is $(C\text{-}H_2O)_n$, where *n* is between three and seven. The structure of monosaccharide's is innately complex and heterogeneous, owing to the chain of chiral carbons which make up the backbone of their structure.[6]

There are a number of different methods to represent carbohydrates, which represent various aspects of their structures. Fischer projections are commonly used to show the overall structure of the open chain form of monosaccharides as they provide clear and simple views of the stereochemistry at each carbon centre (figure 1a). Haworth projections are commonly used to depict the cyclic structures of monosaccharides (figure 1b). [7]

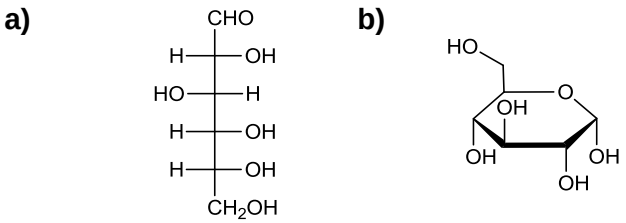

Figure 1: Diagram demonstrating a) Fischer projection and b) Haworth projection of α-D-glucose

Monosaccharide species are defined by the number of carbon atoms and configuration of hydroxyl groups around each chiral carbon- with the exception of the carbon furthest from the aldehyde or ketone group configuration of which is used to designate the 'L' or 'D' forms of each species, as shown in figure 2.[6]

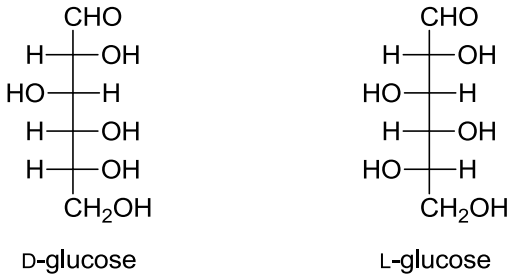

Figure 2: Chemical structures of D-glucose and L-glucose

The structures of some common ('D') monosaccharides are shown in figure 3. Examination of the species shown demonstrates that an increase in the length of the carbon chain is accompanied by an increase in structural diversity. For example the linear form of D-glucose contains four stereocentres, and consideration of the aldohexoses alone presents us with 16 stereoisomers, which translates to 8 monosachhrides species, each of which has a 'L' and 'D' isoform (figure 3).[8]

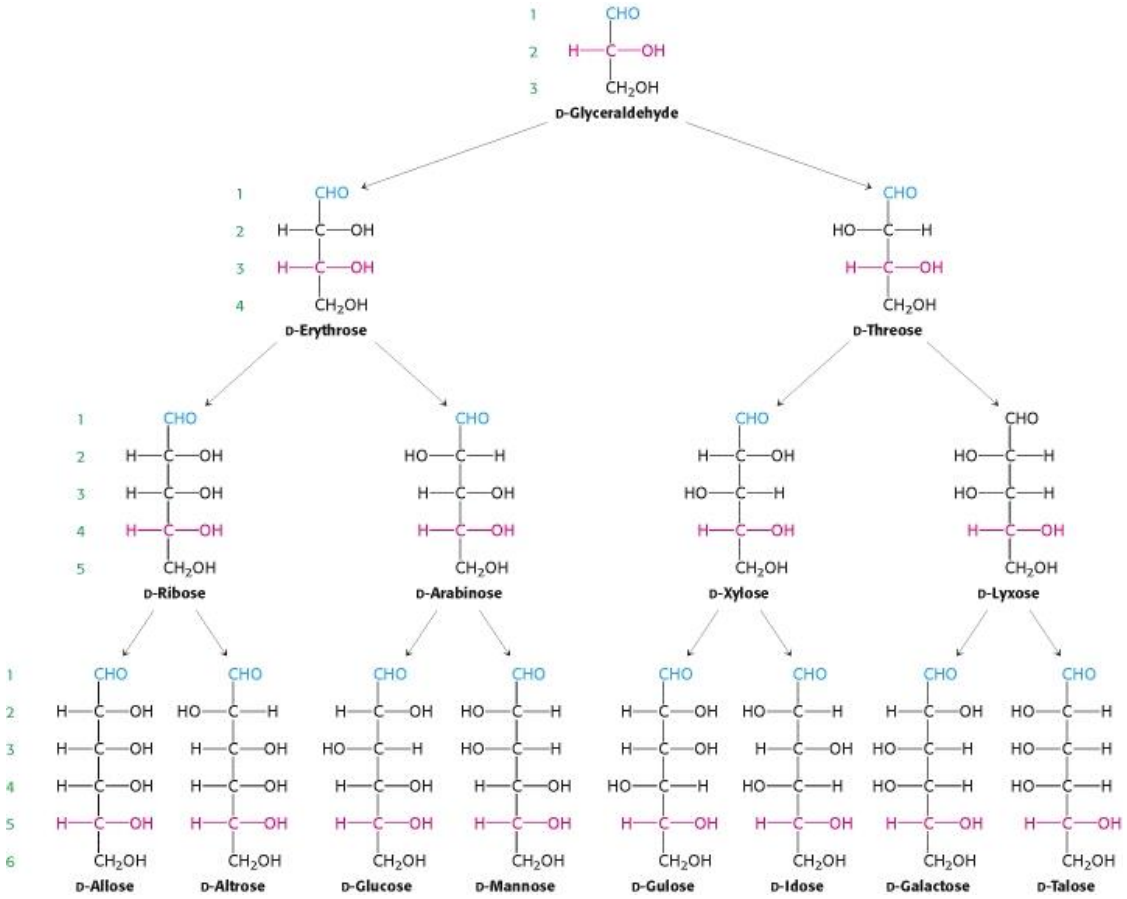

Figure 3: Chemical structures of some common monosaccharides.[6]

The structural properties of pentose and hexose monosaccharides is further complicated by the ability of these molecules, when placed in aqueous solution, to form ring structures. This occurs through the formation of an intramolecular hemiacetal or hemiketal, via reaction of the carbonyl group with the alcohol groups, often those of the most distal chiral carbon. Monosaccharides are able to from one of four ring structures, α-pyranose, β-pyranose, α-furanose, and β-furanose, as shown in figure 4. [5]

These ring structures are, for most species of monosaccharides, more energetically stable and predominate over the open chain form of the monosaccharide in solution.[9, 10] Ring formation results in the creation of a further asymmetric centre at the carbonyl carbon atom. This results in two possible isoforms of the ring structure, designated α- or

β- if the hydroxyl group occurs on the opposite or same side to the terminal carbon atom, respectively [6].

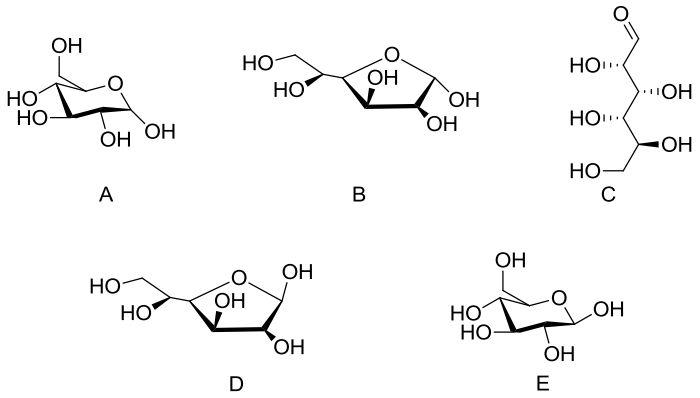

Figure 4: The various configurations adopted by glucose (A) α-pyransose, (B) α-furanose, (C) acyclic form, (D) β- furanose and (E) β- pyransose [9, 11]

The distribution of these structural forms in solution is in dynamic equilibrium: cleavage of the hemiacetal ring allows interconversion between the pyranose and furanose ring forms via an acyclic intermediate, with inversion of configuration at the anomeric centre equilibrating the α- and β- enantiomers, as shown for a glucose molecules in figure 5. [9] This process, termed mutarotation, can occur on a time scale of minutes and leads to a mixture of five forms. The distribution frequency is typical of each monosaccharaide species, for example the distributions of glucose and fructose, are shown in Table 1. [5] It should be considered that there is evidence that the solvent conditions have been reported to affect the rate of this exchange. For example, dimethyl sulfoxide is known to reduce the rate of mutarotation significantly, and can affect the distributions of molecular forms of some sugars including arabinose, ribose, and galactose, as evidenced by early NMR studies.[12-14]

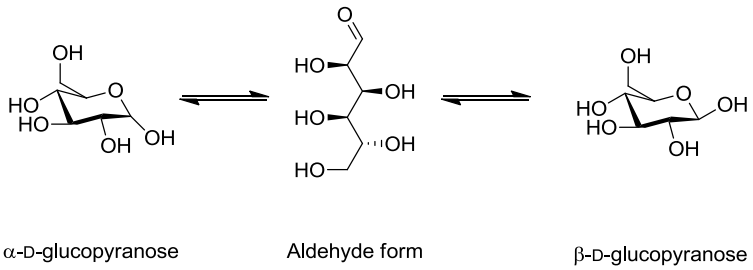

Figure 5: The process of maturation from the pyranose form to the furanose form via a cyclic intermediate , as shown for a glucose molecule.

Individual saccharide molecules are able to conjugate through the formation of glycosidic linkages. Chemically this bond is formed by a nucleophilic displacement of a leaving group, for example water.[15] In this way complex polysaccharide molecules can be produced, such as those seen in biological systems. *In vivo* this process is catalysed by two large group of enzymes glycosyltransferases, and glycosidases which are able to transfer saccharide groups from monosaccharide, oligosaccharide or activated glycosides onto the growing saccharide polymer.[16]

Table 1 The relative distributions of forms for the monosaccharides glucose and fructose in water, 293 K.

Sugar	**Form distribution (%)**			
	α-pyranose	*β-pyranose*	*α-furanose*	*β-furanose*
Fructose	39.4	60.2	0.2	0.21
Glucose	2.0	68	6.0	23.0

1.3 Sugar Sensors

1.2.1 Monosaccharide systems

In recent years a number of systems have been produced for the detection of monosaccharide species. The potential clinical application of glucose assays has led to these systems coming to the fore of current research. This interest is well deserved as such assays have potential uses in diagnosis and monitoring of diabetes mellitus, a chronic condition which current reports claim that worldwide up to 2.8% of all people may be affected, with this expected to rise to 4.4% by 2030. [17]

Some of the earliest methods of glucose quantification were based on chromogenic reduction of a copper solution by glucose. [18] Unfortunately, these methods were poorly selective and would be superseded by enzymatic assay. However, despite the inherent problems with specificity, non-enzymatic methods of glucose assay have continued to be developed through the 20th century to this day. [19] The detection element of non-enzymatic systems is commonly electrochemical or colorimetric and modern detection systems now use a variety of supports, including nanoparticles and carbon nanotubes to optimise the performance of such assays. [20, 21]

1.4 Introduction to glycosylation

Interest in the study of the molecular interactions of carbohydrates has grown significantly in recent years (Figure 6). This interest has been fuelled by an increased understanding of the role played by biologically active sugars in cellular recognition, signalling, protein function and how aberrations in these control and signalling systems can lead to pathologies- the most notable of which is cancer.[22-24] We now know that functions of proteins can be tuned by cells, through the addition non-peptide groups following their production, a process known as post-translational modification (Figure 7).[25] While the twentieth century saw dramatic advances in our understanding of the function of proteins and the process by which these molecules are encoded by cells, it is only now that we are beginning to understand the mechanisms used by cells to control the function of the proteins they produce.[26]

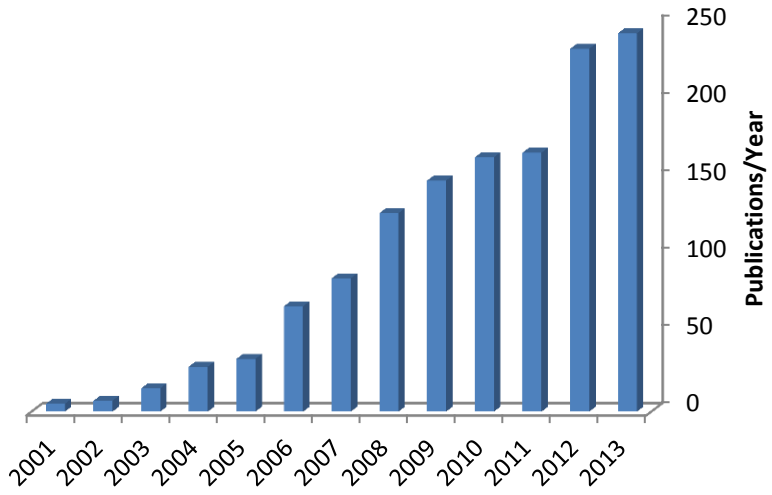

Figure 6: The number of publications by year on the subject of 'glycomics', taken from PubMed database (December 2013)

This lack of understanding, of what is acknowledged as fundamental processes in cellular biology, can be explained by the difficulty posed by the challenge of analysing

glycosylation structures. Their highly conserved structures make sugar species inherently difficult to discriminate and, furthermore, as they are assembled together in the large branched networks (commonly seen in protein glycans) this problem becomes ever more complex. [27, 28] Fortunately, as biotechnology and material science advances, methods of detecting and understanding the biological signals encoded by these glycosylations are becoming more wide spread. We are currently in an exciting phase of discovery whereby the advances in our understanding and technical ability serve to inform each other in a self-accelerating cycle.

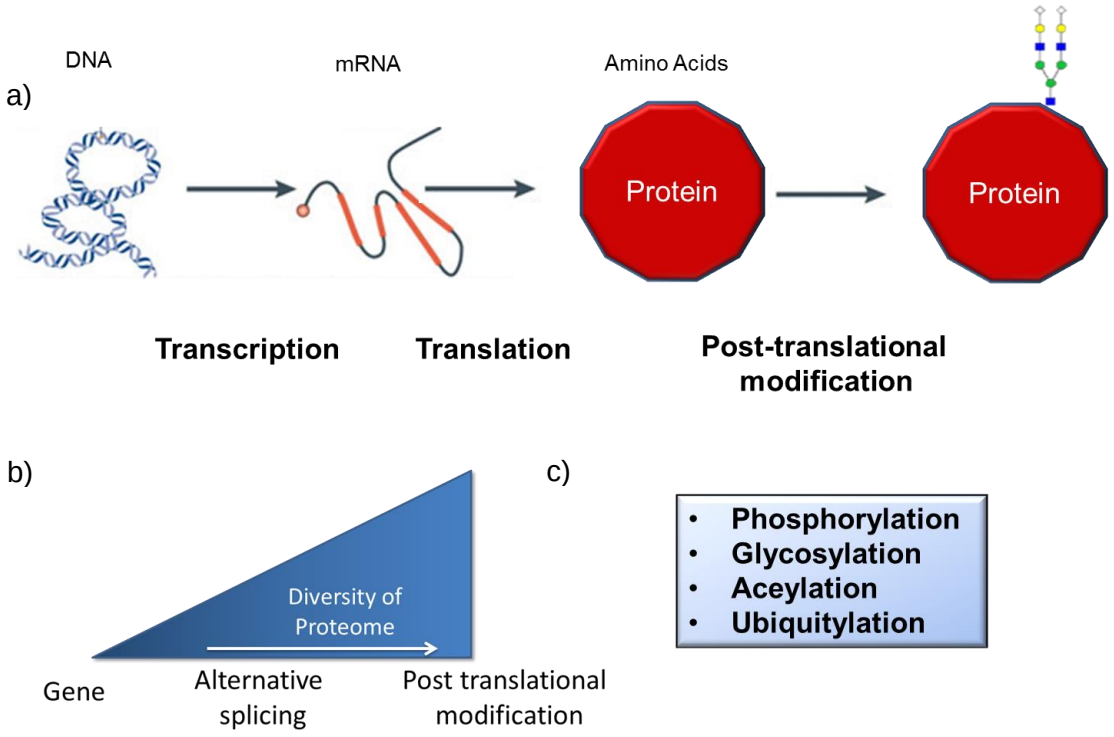

Figure 7: Outline of a) how post-translational modifications are added to proteins b) how such additions are able to increase the diversity of the proteome c) examples of post-translational modifications.

1.5 Roles of glycosylation in health and pathology

The post-translational modification of proteins is known to increase the size of the proteome (the spectrum of proteins produced by a cell) and acts to add diversity to protein function (Figure 7b).[25] In humans, more than 50% of the proteome is known to be glycosylated.[29] Glycosylation may occur in several different ways; N-linked glycosylation occurs through the linkage of glycans to proteins via aspargine residues; O-linked glycosylation is now known to be linked via serine and threonine, most commonly, but also in a smaller number of cases, by tyrosine and hydroylysine.[30]

Glycosylation is one of the most common co- or post-translational modifications made to proteins.[31] Inside cells, complex glycosylation pathways assemble these oligosaccharides and attach them to proteins and lipids as they travel to the cell surface.[32] Owing to their location, typically on the surface structures of cells, oligosaccharide epitopes on proteins or lipids exert key functions which are shown to be important in intercellular communication processes such as fertilization, immune response, cell adhesion, pathogen anchoring, healing and metastasis.[32-41]

Functional glycomics aims to define the paradigms by which protein-carbohydrate interactions mediate biological function.[42] Although the field is somewhat in its infancy, there are some known functional interactions which have already been well-characterised, notably those which are able to control the differentiation and phenotypic properties of cells. Specific types of glycosyl residues modulate particular signalling pathways and can regulate cell phenotypes.[43] Many glycan structures have been implicated in the modulation of cellular behaviour.[44] There have been suggestions that the over expression of some glycoslyations is able to subvert the immune system, resulting in suppression of immune cell function, including T-cell dysfunction and death.[45, 46] Thus glycans can play potentially vital roles in the transformation of cells into neoplasms and the establishment of such cells in cancer genesis.

1.5.1 Prostate cancer

Prostate cancer is the most common male malignancy in the western world.[47, 48] The two principle methods of prostate cancer detection are digital rectal examination of the prostate and through the measurement of serum levels of prostate specific antigen (PSA).[48] Unfortunately, increased PSA levels are poorly correlated with prostate cancer. Prostate disease, both malignant and benign, produces disruption to the structure of the prostate resulting in the escape of PSA into the blood stream.[48] As a result, such assays are associated with considerable problems with sensitivity and specificity, complicating the distinction of the various forms of prostate disease by such assays. The majority of patients (65–75%) who undergo a prostate biopsy due to a moderate PSA elevation have no evidence of cancer and a quarter of the prostate cancer patients are known to present with PSA levels within the normal range. [49]

Therefore one of the most urgent requirements in prostate cancer diagnosis is the development of a minimally-invasive test which is able to distinguish prostate cancer from the non-pathological condition of benign prostate hyperplasia.[50] Assessment of PSA glycosylation could be used to address this challenge. For example, it has been shown that a reduced level of glycosylation is associated with highly infiltrative histological patterns and behaviours of prostate carcinoma cells.[51] Indeed, abnormalities in protein glycosylation patterns have been observed in a majority of cancers, thus making this a vital area of research for the improvement of cancer detection and treatment. [52]

1.6 Boronic Acids and Lectins

1.6.1 Lectin History

Lectins are proteins which are able to bind carbohydrate groups, somewhat akin to antibodies and their ability to bind peptide antigens.[53] It is this property which has led to the interest in their use in glycomics applications. Many lectins are in fact plant proteins, for example Concanavalin A (ConA) was originally extracted from *Canavalia ensiformis* (commonly known as the Jack Bean) while *Sambucus nigra* agglutinin is extracted from the Common elder.[54] While there is some controversy, it is generally presumed that the biological role for these plant compounds is to act as a form of plant defence and immunity. Such molecules are able to protect the organism from invasive pathogens, such as bacteria, by recognition and agglutination and also can infer protection from predation due to the innate toxicity of some lectins.[55, 56]

1.6.2 Boronic acids

Boronic acids represent a potentially useful molecular species which can act as artificial lectin by forming intermolecular esters with glycols (Scheme 1).[57] The reversible interaction of boronic acids and polyols in water was first examined in detail in the ground-breaking study conducted by Lorand and Edwards.[58] Using the pH depression technique, they were able to demonstrate that the formation of ester complexes between phenylboronic acid and saccharides is more favourable at increased pH. This reaction is now known to proceed via the formation of reversible cyclic boronate esters between 1,2- and 1,3-diol found on glycan structures and the boronic acid centre.[59-64]

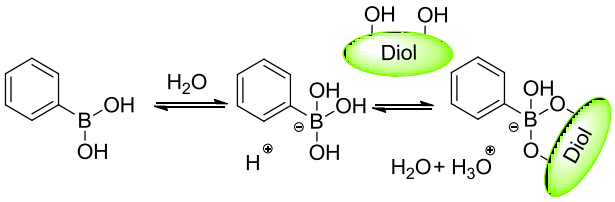

Scheme 1: Schematic of how boronic acids are able to form reversible esters with compounds containing diols

Boronic acids behave as Lewis acids, accepting electrons from bases, and in the process releasing protons. Although the molecular boronic acid is triganol planar in arrangement, when complexed with a diol the most favourable structure is found to be a tetrahedral complex. This is due to the hybridization of boron from sp^2 to sp^3 formation, the net result of this is a release of angle strain of the subsequent complex.[8] As this reaction occurs, an electron pair is accepted from hydroxide ions, which results in the generation of one proton and one water molecule.[65] However, as phenyl boronic acids are typically weakly acidic under neutral conditions (with a pKa of 8.8) the interaction between the boronic acid and diols is not favourable.[66] Therefore, many of the early attempts to use boronic acids as saccharide sensors required an elevated pH, dependent upon the pKa of both the boronic acid and the target species. Typically the pH required is above the pKa in order to favour the ionisation of the acid and subsequently its bond with the target diols.[66]

1.6.3 Boronic acids as sensor binding sites

Given that most biologically relevant species are found in media at mild physiological pH, it can be desirable for the interaction between boronic acids and diols to proceed well under such conditions. Several groups have investigated supramolecular strategies to enable this interaction to proceed efficiently at neutral pH. Examples include the use of electron withdrawing groups on the phenyl ring, such as carbonyl, nitro and sulphonyl groups, to promote the ionisation of the boronic acid, as demonstrated in the series of compounds in Figure 8.[2]

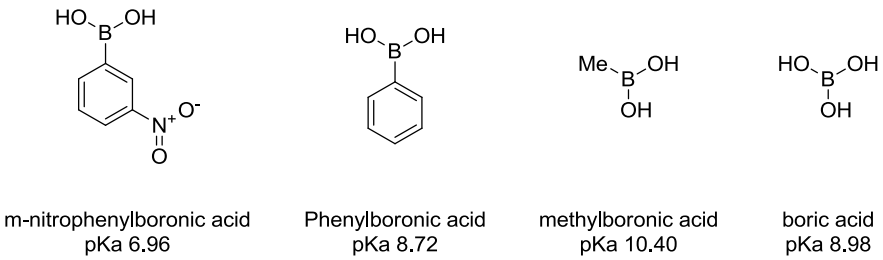

Figure 8: Examples of boronic acid species with their pKa values. The change in adjacent functional groups can be seen of affect the pKa and thus the properties of the bonric acid group [2].

A second method, pioneered by Wulff, uses intermolecular amines adjacent to the boronic acids to form co-ordinate complexes with the boronic acids, thus promoting their ionisation at lower pH due the amine stabilising the ionised form.[67, 68] The most common substituent used for this purpose is an adjacent secondary or tertiary amine. The nature of the nitrogen-boron (N-B) interaction may be considered to be comparable to a hydrogen bond.[69] However, in protic solvents, solvent insertion can occur to generate a zwitterionic species (Figure 9). The energy of nitrogen – boron interaction has been calculated to be between 15 and 25 kJ mol^{-1}, as demonstrated by potentiometric titration.[70]

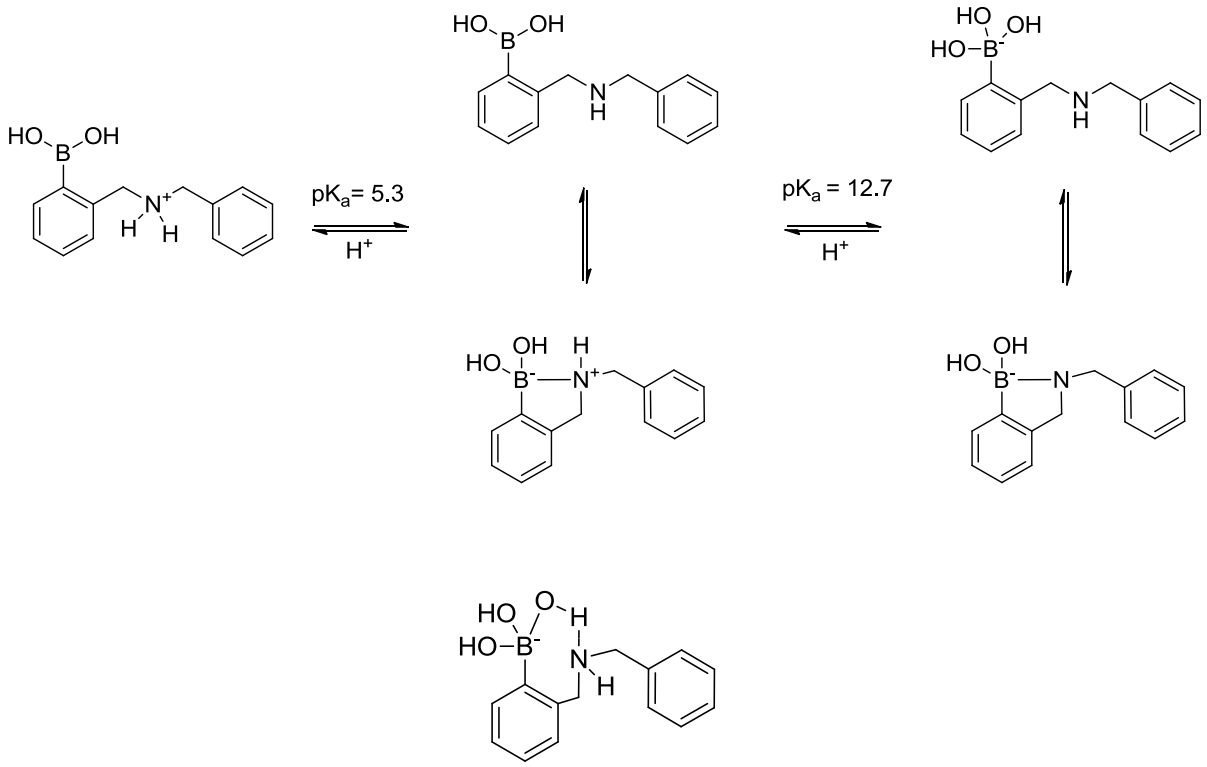

Figure 9: The mechanistic basis for the ability of adjacent nitrogen groups to allow the ionisation of boronic acids at lower pHs. [2]

More recently, the stabilising effect of N-B interactions have been shown to work intermolecularly, and have been demonstrated to stabilise the binding of boronic acids to nitrogen containing sialic acids at neutral pH with a much higher affinity than other glycols, particularly at lower pHs.[71] This effect has been exploited by Kataoka and co-workers to selectively target high sialic acid containing tumour cells with boronic acid functionalised micelles.[72] These structures were demonstrated to induce sialic acid selectivity in the polymers at both pH 7.4 and 6.5, when compared to other monosaccharides including glucose, mannose and galactose.

1.6.4 Monosaccharide selectivity

Boronic acids have been used extensively in recent years for the solution-phase detection of monosaccharides, many using elegant fluorescent reporting systems.[8, 73, 74] Despite the highly conserved nature of monosaccharide structures, boronic acids are able

to display different binding profiles to each monosaccharaide species. In their native form, phenyl boronic acids display a higher affinity to fructose than to other common saccharides. This is due to the geometric configuration of the fructose molecules in solution. [75] However, the clinical utility of fructose sensors is quite limited. In contrast, glucose selectively has been a topic of focus, given the huge health care burden posed by the increasingly common disease type 2 diabetes mellitus, which is typified by an increased concentration of glucose in the blood due to the collapse of physiological regulatory systems.[76]

The first glucose selective *bis*-boronic acid based sensor was pioneered by James and Shinkai (Figure 10).[77] The basic principle of the sensor is that two intramolecular boronic acid units are able to bind a single glucose molecule. In this compound the anthracene unit acts as both the core and the fluorophore. This acts to produce a much more stable bi-dentate type complex, and as a result the affinity of the interaction is increased significantly.[77]

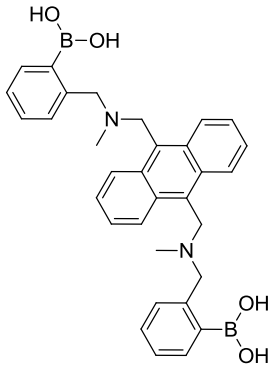

Figure 10: The first example of a *bis*-boronic acid compound, developed by James et al for the selective binding of glucose.[78]

Further works have since demonstrated that the selectivity of such sensors may be modulated by changing the spacing between the two boronic acid groups. In order to

facilitate this, modular series of boronic acids were synthesised and based upon the same core molecular design (Figure 11). By varying the length of the linker element, the spacing of the boronic acids was controlled, to produce a series of related compounds which contain boronic acids spaced by different number of carbons, and thus spaced by different distances.

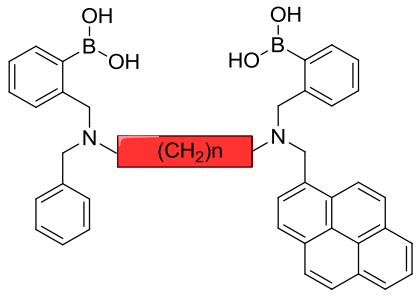

Figure 11: The structure of a modular *bis*-boronic acid species which was developed to investigate the effect of spatial separation on monosaccharide selectivity. Note; 'n' refers the number of carbons in the spacer unit between the boronic acids. The structures of the monosaccharides are included for reference.

Over the series it was observed that the glucose selectivity was favoured with links of between 4 and 6 carbons with the optimal affinity to glucose being recorded at 6 carbons. However any further extension to the linker group results in the loss of glucose selectivity, with galactose selectivity being observed (Figure 12a). Examination of the structures of glucose and galactose (Figure 12b) can help explain this observation; the 1, 2- and 4, 6-diols of D-glucose point in the same direction (down), but in D-galactose the 1,2-diol is down and the 4,6-diol is up. Thus the inter-diol distances of D-glucose are shorter than those of D-galactose.[79]

a)

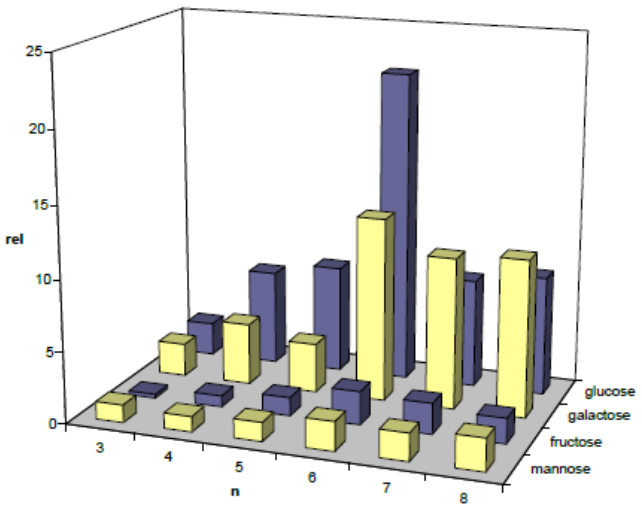

b)

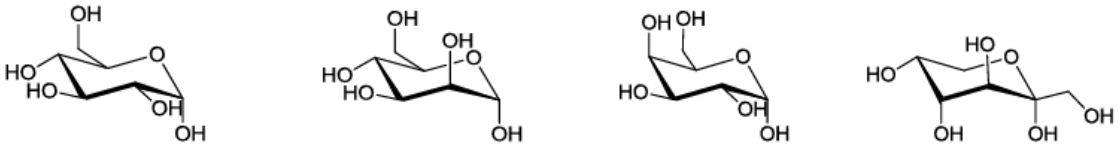

Figure 12: a) The observed relative stabilities of each member of the series of *bis*-boronic acid sensors with the monosaccharides glucose, mannose, galactose and fructose. 'n' refers the number of carbons in the spacer unit between the boronic acids. b) The structures of the monosaccharides are included for reference. [79]

1.6.5 Nanomaterials and Boronic acids

Compared with biological lectins, boronic acids have a number of advantages, which has made them popular targets for sensor fabrication research. Their popularity can be attributed to their diversity of application: they can be incorporated with relatively ease into a wide range of chemical synthesises, facilitating the fabrication of synthetic saccharide and glycoprotein binding systems. As compared to biological lectins, which contain a mixture of chemical groups homogenously dispersed among their structure, boronic acids afford molecular engineers a more defined and predictable chemical group to use in the synthesis of sensor platforms. In addition the physical size of the boronic acid groups are

considerably smaller than peptide lectins, which combined with their more defined chemical structure, allows for them to be incorporated with much greater ease into nanoscale detection systems. To this end, boronic acids have been engineered into nanostructures such as carbon nanotubes and nanoparticles to produce sensors with much larger surface areas to offer increasingly amplified binding signals.[80-87] These methods should help to produce increasingly sensitive systems which can then be used to detect quantities of analyte down to even the picomolar range.[88, 89] Boronic acid modified nanostructures have also been employed to facilitate the enrichment of glycoproteins from protein mixtures, including magnetic nanoparticles, which have been demonstrated to selectively enrich the glycoproteins from peptide mixtures.[80, 90, 91]

1.7 Nanotechnology

1.7.1 Self-assembly

The process of self-assembly is commonly found in nature; many cellular components, machinery and processes are reliant upon the principles of energetically favourable self-assembly.[92] However, the term self-assembly is now widely used in broadly related fields.

Self-assembly can be observed in many different systems, and a precise definition is often difficult. However, a number of general rules may be formulated which must be met in order for a process to be considered as self-assembly. In general the process must be exothermic (or at least energetically favourable) and able to produce a stable final state built from individual molecules.[92] In addition, it is often considered that the steps by which the final state is produced should not result in restricted intermediates; rather the intermediates must able to adjust or un-form to allow order to be introduced into the system. Without this ability, the system is likely to suffer from defects due to the inappropriate incorporation of monomer into the final macro-structure.[93]

Nature produces organisms which can be considered to be islands of order in a chaotic universe.[94, 95] To reinforce this proposition a great number of living processes are driven by self-assembly. The interactions of monomers and polymers of the three primary biological compounds, carbohydrates lipids and proteins, are all governed by such processes.[96] Take for example proteins; they are in basic terms, produced by cells as linear biological polymers which typically consist of heterogeneous amino acid subunits covalently joined. However at a higher level of structure, such peptide chains can coalesce via self-assembled mechanisms, governed by intermolecular forces, to produce globular protein subunits which themselves interact non-covalently to form dynamic functional structures.[97]

Examples of such structures are diverse and include structural components of cells including elements of the cytoskeleton, microtubules, actin filaments, and viral capsids[98]. Because most interactions are non-covalent, both assembly and disassembly are reversible reactions that can be readily controlled and adapted and although unwanted interactions are able to occur, as they are less stable, there is a constant force promoting desirable interactions and structures. [99]

1.7.2 Self-assembled monolayers

Self-assembled monolayers (SAMs) form spontaneously through the adsorption of an active surfactant, from liquid or vapour phase, on to a solid support. This process is mediated by the same intermolecular forces discussed above and the interactions between the chemical groups and properties inherent within the molecular units of the SAM play a critical role in the formation of its final structure. Thus, the physical properties of the SAM can be easily manipulated by control of the structures of the molecules.[100] Properties which can be controlled by the inclusion of specific chemical groups in the surfactant building blocks include: thickness; stability and surface energy. SAMs of thiols on gold and triethoxy silanes on silicon dioxide are two widely used examples of SAMs employed to modify the surface properties of metallic and inorganic substrates, respectively.[101]

The typical molecule used for the formation of SAMs has a structure which can be divided into three functionally distinct parts: the head group, backbone and terminal group (Figure 13). The head group guides the physical or chemical adsorption of the SAM molecules to the surface. Intermolecular interactions between the backbones are able to mediate the efficient packing of surfactant molecules into a monolayer structure, producing a densely packed monolayer.[102]

The terminal group provides the desired physiochemical properties of the SAM. It can be passive, affecting only the physical properties of the interface (such as the wettability) or it

may be chemically active, to provide an anchor point for additional modification of the monolayer (for example via the attachment of biomolecules and the formation of nanostructures).[103-105] The terminal group confers specific properties to the surface (hydrophilic, hydrophobic), and can also be used to anchor different molecules, biomolecules, or nanostructures by weak interactions or covalent bonds.[100]

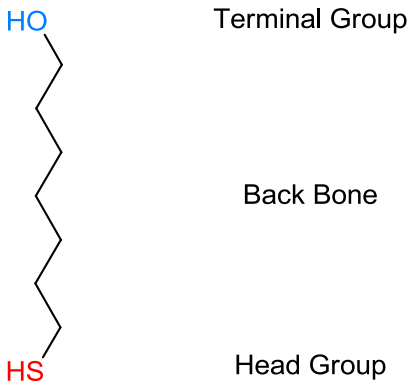

Figure 13: The general structure of a SAM molecule. The head group allows attachment of the compound to a surface, while the head group controls the physical and chemical properties of the monolayer formed.

SAMs can be characterised using a number of surface analytical techniques, including X-ray photoelectron spectroscopy (XPS), ellipsometry and contact angle goniometry. A detailed explanation and discussion of these techniques will be included in chapter 2 of this thesis.

1.7.3 Thiols on Gold

Beyond the examples observed from the natural world, in the more sterile laboratory environment, one of the best understood examples of self-assembly is the system of self-assembled monolayers, such as those formed from thiols on gold.[100] Such systems have been studied extensively and are relatively stable under ambient conditions and

versatile in their application. They can be easily modified with a wide range of functional groups and thus can display a range of physical properties.[100]This fact has since been exploited to investigate not only the effect of changing chemical properties on the self-assembly of the SAM, but also to probe the effect that modification of surface properties can have on other processes such as crystal formation on the SAM surface. [92] Beyond such fundamental research, SAMs have also been employed in the fabrication of modified surfaces for application in fields such as bio-recognition and sensor design, microfluidics and self-healing surfaces.[106]

SAMs of octadecanethiol on clean Au(111) surfaces are, perhaps, the archetype system of thiol based systems. Through the studies of such systems the fundamental physical processes which underpin the formation of these structures has been investigated. It is now known that the formation of SAMs from dilute solutions of thiols occurs in two main distinct phases.[101] Kinetics studies of SAM formation indicate that the first step is a fast process which occurs within minutes cleaned gold surfaces being immersed into thiol solution.[107] Here, the relatively rapid adsorption of the SAM molecules is able to occur through physisorption of molecules to the surface (figure 14b). During this phase the physical characteristics of the SAM begin to become apparent, with thickness and contact angles moving towards 80-90% of their final values.[107] The second step is generally considered to be much slower, occurring over several hours, although the time taken for this phase can be dependent on a number of factors including SAM molecular structure and solvent conditions.[108] During this phase the molecules adsorbed onto the surface begin to form covalent bonds with the gold substrate (figure 14c). Finally, through a process of desorption and reabsorption, the order of surface components increases (Figure 14d). This process can be considered similar to the formation of a two-dimensional crystal.[101]

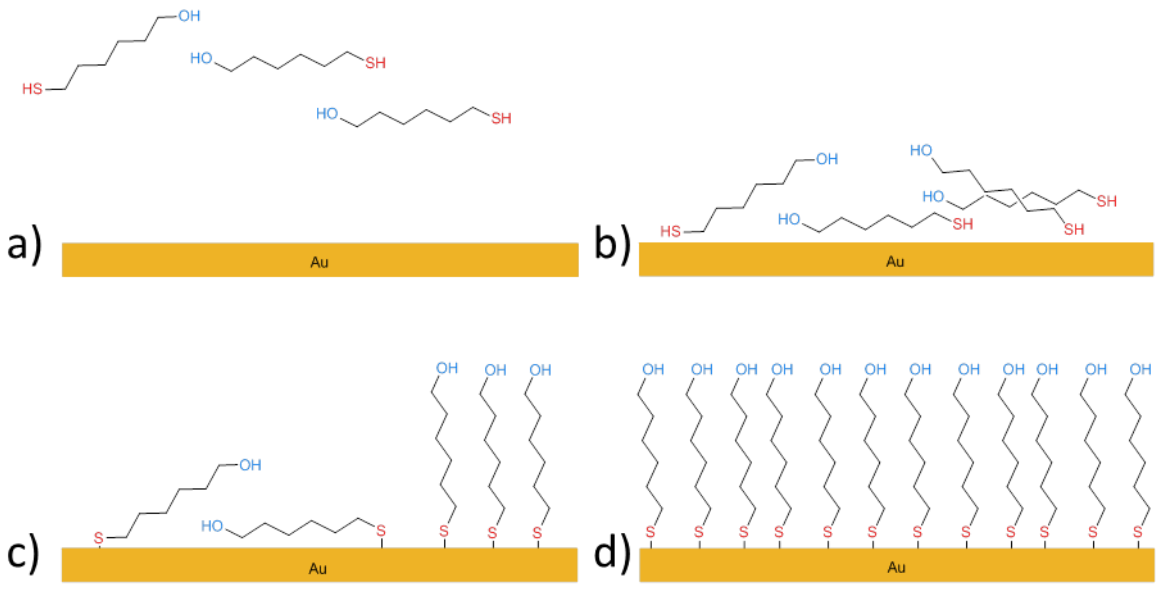

Figure 14: Schematic of process of SAM formation. As the SAM molecules reach the gold surface (a), they becoming physisorbed (b). this step occurs almost instantly. The next, slower, step occurs as chemical bonds are formed between the sulphur head groups of the SAM molecules and the gold surface (c). Finally as more SAM molecules become chemisorbed, the order of the film increases forming a complete SAM (d).

The head group guides the self-assembly process on each type of substrate, acting to link the molecule to the metal surface through a strong bond with a specific surface site. In the case of thiol gold SAMs this is via the formation a gold-sulphur covalent bond. The formation of this bond is an energetically favourable and exothermic process, and the resultant bond is relatively strong, with an enthalpy change of around 210 kJ mol^{-1}.[109] The interactions among backbone hydrocarbon chains (involving van der Waals and hydrophobic forces) ensure an efficient packing of the monolayer and contribute to stabilize the structures with increasing chain length. Such interactions also play a role in the formation of SAMs, as the intermolecular interactions between chains act to promote the organisation of adsorbed surfactants into islands structures of higher order.[110] Over time, as additional adsorption of surfactant takes place, these island structures coalesce, leading to the final structures of complete SAMs.[100]

The two phases of this process can be written as the following reactions, in this case a generic alkanethiol (RSH), where R is a alkyl carbon chain, is chosen to represent the surfactant:

$$RSH + Au \rightarrow RSH_{phys}Au \quad (1)$$

$$RSH_{phys}Au \rightarrow RS\text{-}Au + 1/2H_2 \quad (2)$$

Reaction (1) corresponds to the physical adsorption of the surfactant onto a gold surface, while reaction (2) illustrates the overall chemisorption process. However, while the overall reaction is known, there is currently no single consensus on the exact mechanism followed by this process. It has been assumed that the reaction proceeds via oxidative adsorption of the thiol RS-H bond to the gold surface, however it is not known whether this involves an ion, radical or other species. This lack of understanding is rooted in the fact the kinetics of SAM formation have been shown to be affected by a number of factors, including surface coverage, the surfactant species and the cleanliness of the gold substrate. [108]

The adsorption process is believed to be similar for other sulphur containing species, such as disulphides, which are also known to form bonds with gold. Disulphides are an interesting species for the investigation of such phenomena, due to the steric constrains imposed upon them; in order for disulphides to adsorb they require two adjacent and available gold absorption sites, as suggested by reaction three.[102]

$$RS\text{-}SR + 2Au \rightarrow 2\ RS\text{-}Au \quad (3)$$

This overall reaction has been confirmed with data from experiments comparing SAMs formed from both disulphides and thiols showing that, following SAM formation, the resultant sulphur species are indistinguishable by detailed examination by XPS, therefore indicating that both sulphurs are involved with bonding to the gold. [111] However, investigations have suggested that the adsorption of thiols and disulphides may occur at a

different rate, with thiols adsorbing more readily, assuming that chemical structures of the molecules are otherwise comparable.[112]

Together such observations lead to the conclusion that, in the case of disulphides, as there are only a finite number of binding sites on the gold surfaces, sulphur groups already bound to the surface must be able to rapidly diffuse and migrate across the surface to provide space for the adsorption of further disulphides. Further evidence for this hypothesis can be observed in experiments which demonstrate the ability of adsorbed surfactant molecules to exchange with those in solution.[113]

The ability of disulphides to form SAMs has been increasingly exploited in recent years, as they can offer several advantages when compared to thiol systems. Principally, they are easy to store and resistant to oxidation[114]. This chemical stability can also simplify synthetic procedures, as they generally do not require the addition of protecting groups during synthetic steps sometimes required for thiols. There is also evidence that disulphides are more resistant to surfactant exchange reactions than thiols.[115]

Finally, there are several organically derived compounds which contain both disulphides and other functional groups which facilitate the facile synthesis of SAMs with a wide range of functionalities using only simple and well established chemical methods and reactions. Taken together this makes them desirable for incorporation in the design and fabrication of biosensors.[116] Two examples of such compounds commonly found in literature are cystine and thioctic acid (Figure 15).[117-119]

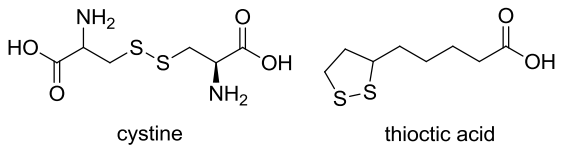

Figure 15: The structures of cystine and thioctic acid, two compound which can be easily modified to produce molecules suitable for formation of SAMs.

Surface orientation of SAM Molecules

The final structure of thiol and disulphide SAMs on gold has been shown to be dependent upon a number of factors, including the structures of the surfactant molecules themselves, the condition of the gold substrate and the solvent conditions. It is no coincidence that the factors which affect the kinetics of SAM formation are also at play in governing the final configuration adopted by such structures, as the two are intimately linked.[102]

Packing and structural modes of thiol and disulphide SAM systems on Au are mainly determined by the Au-S interaction, inter-chain van der Waals interactions, and interchain functional group interactions.[120] Studies of SAMs formed from alkyl chains which contain 12 or more methyl units form well-ordered, dense monolayers on Au (111) surfaces, with the majour intra molecular force driving their formation being the van der Waals interactions between adjacent chains. Thiols are believed to attach to the three fold hollow sites of the gold surface, which are arranged in a hexagonal geometry, an arrangement known as the $(3\sqrt{} \times 3\sqrt{})R30°$ over layer structure.[101] When considering Au (111), the distance between each adsorption sites is 0.497 nm, which results in each adsorbed molecule being placed in an area of 0.214 nm^2 since the van der Waals diameter of an alkanethiol is too small to completely occupy this area, is it energetically favourable to the chains to adopt a tilted formation, with an angle of approximately 30-35° relative the surface normal.[100]

In addition to the effect of interactions between the alkane chains, the final macro-structure and stability of SAMs can also be affected by the other groups present in the surfactant molecules. Typically, these are the chemical species contained in the terminal group of the molecule.[101, 121, 122] However, evidence also suggest that interactions such as hydrogen bonding between groups ‘buried’ within the SAM can also influence the final structure and stability of the monolayer.[123]

The interplay between these factors can vary with the functional groups and chain lengths present within the SAM molecules; investigations show that as the length of the SAM chain is reduced, the greater the relative effect of functional groups on SAM formation and structure.[124] For example, the adsorption of L-cysteine molecules on Au (111) has been reported to yield an ordered monolayer with a (4√ x 7√) R19° structure, due to the hydrogen bonding between the carboxylic acid groups (Figure 16).[117] However, there remains some controversy regarding this conclusion as other structures of cysteine SAMs have been reported.[120, 125, 126] Furthermore, it has been demonstrated that change in the pH of the SAM formation solution can also produce differently structured SAMs, notably for amino terminated surfactants a raised pH can produce alternative binding mechanisms such as nitrogen mediated adsorption. [118, 127]

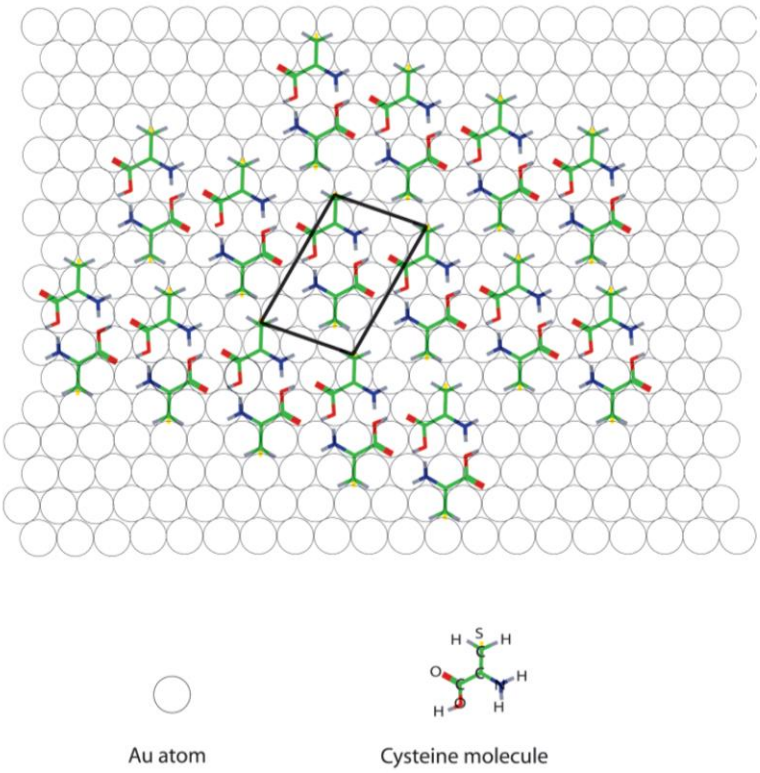

Figure 16: The proposed organisation adopted by cysteine molecules on gold, with a (4 x √7) R19 [117]

1.7.4 SAM defects

In many publications which one may find in literature, SAMs are presented as perfect monolayers, free from defects with all molecule, well packed arrangement. However, in reality there are a number of defect types known to exist in SAMs that the reader should be made aware of. The most common defect types are pin hole defects, disorder defects and domain defects. Pin hole defects (Figure 17a) are characterised by small areas of the surface where there can be a small number of missing molecules. In domain defects (Figure 17b), the imperfection occurs at sections of the SAM where frontiers of the crystalline lattice meet. This can occur at the boundary between regions of the same lattice structure which contain molecules in a mismatching orientation and also between areas where two lattice types meet. [102, 113] Disorder defects (Figure 17c) refer to regions of the monolayer where the hydrocarbon chains of the surfactants are not fully extended, and instead adopt a gauche configuration which is defined as an area of disorder in the SAM, caused by the interruption of a sequence of ordered SAM components. Typically this is caused by an approximately 120° rotation about the backbone bond. [128]

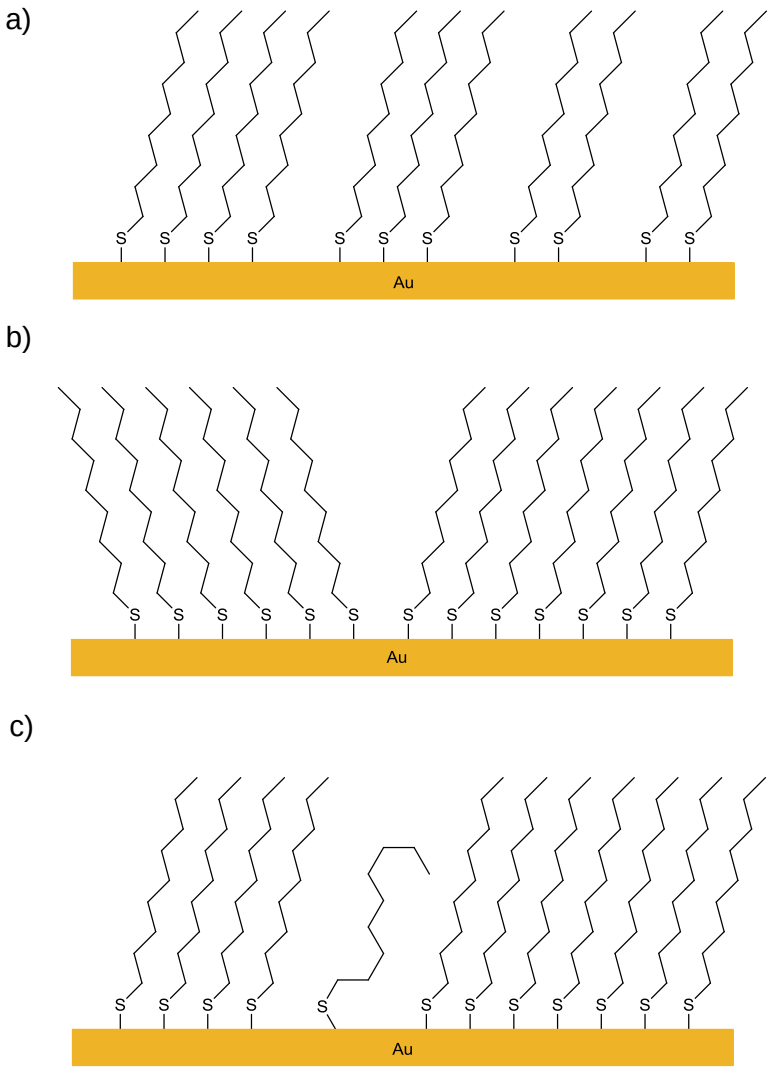

Figure 17: Examples of SAM defects which can affect the formation of complete monolayers. a) Pin hole defects are caused by missing SAM molecules leading to small 'hole' defect in the surface. b) Domain defects are found where two (incompatible) super structures of SAMs meet. c) Disordering of the chains of the SAM molecules leads to poor packing in areas of the SAM.

1.7.5 Mixed SAMs

While the discussion to this point has focused on SAMs comprised of single componets, it is important to stress that mixed solutions of thiolated compounds have been observed to form mixed monolayers. The results of producing mixed monolayers can be varied and may have mutiple benefits as the use of different surfactants can produce surfaces which have hybrid properties when compared pure SAMs of each surfactant type.[129] This technique of producing SAMs from multiple components has been used increasingly for the fabrication of engineered surfaces, such as those seen in the field of biosensors. An

example of this can be seen in the formation of mixed oligoethylene glycol thiol (OEGT) and biotinylated peptides to produce surfaces able to resist the non-specific adoption of ‘unwanted’ proteins yet simultaneously take part in the selective binding of neutravidin.[130] A second common application of mixed SAMs is to reduce the steric hindrances which may occur between adjacent molecules in the monolayer. A mixture of SAM components can be used to effectively space out ‘active’ (i.e. binding site containing) molecules with ‘passive’ surfactant molecules.[131] The aim of such a strategy is to reduce the risk of steric hindrances for binding complex formation between the surface bound anchor sites and their respective ligands (Figure 18), which is of great importance in biosensor fabrication. This principle can also be found in published works which investigate the fabrication of switchable surfaces. Here, mixed SAMs are required for effective switching to take place; without them there is not the ‘space’ for the movement of switching components on the surface.[130-132]

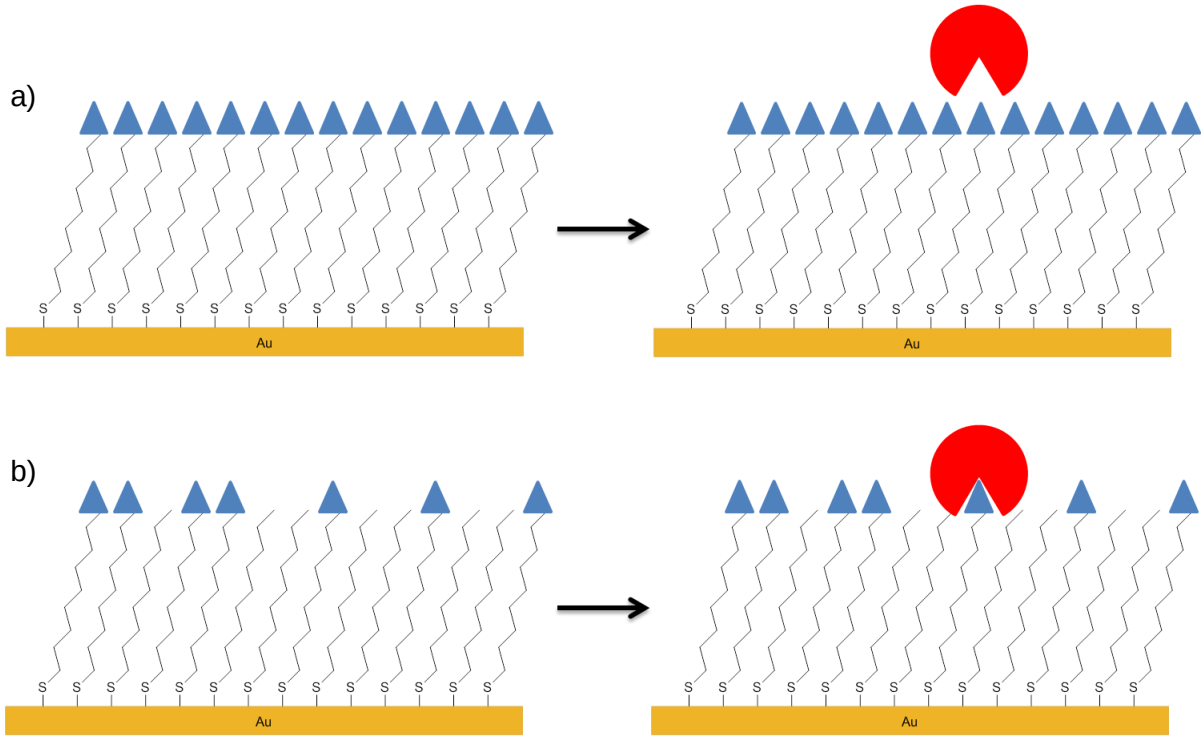

Figure 18: Examples of how steric hindrance can affect functionalities of monolayers (a) by blocking the interactions of immobilised ligands with their solution analytes, and how these problems can be overcome using mixed monolayers to reduce the crowding of functional groups via the addition of spacer molecules (b).

Depending upon the desired structure and subsequent function of a mixed SAM, the ratios of components can be important. However, although it is easy to calculate the ratios of these components in solution, it is seldom the case that the ratio of components adsorbed to the surface follows solution concentration, due to the preferential adsorption of one of the components.[130] This finding highlights the importance of surface characterisation techniques to accurately determine the exact surface composition of mixed SAMs.[130, 133] Such methods will be discussed in detail later chapters of this thesis.

1.8 Applications of SAMs

SAMs have found applications in a number of fields of research including biosensing, catalysis, and generation of biocompatible and protein resistant surfaces.[100, 134] Among these, the generation of biocompatible and protein resistant surfaces used in biosensor fabrication will now be discussed in detail.

1.8.1 Generation of Biocompatible and Protein Resistant Surfaces

The ability of protein to adhere to surfaces can be considered to be a natural phenomenon; in living creatures the ability of specific proteins to bind with self and non-self, and subsequently elicit activation of biological pathways is vital for many immune and homeostatic processes.[135] The importance of such events can be highlighted by the fact that in multicellular organisms cell growth is regulated by attachment of cells to basement membranes and support tissues.[136] In bacterial cells adhesion to surface can bring about changes in cellular phenotype and or behaviour.[137] However, while vital to cellular functions, these phenomena can be undesirable in industrial and some medical contexts.

In industrial, processing and marine applications, the build-up of organic matter is problematic due to its ability to reduce the efficiency of industrial machinery and processes.[138] In fields of healthcare and medicine, challenges are found due interactions between proteins and materials found in prostheses, catheters and implants, as these unwanted interaction can impact on the function of such devices.[139] This can be particularly problematic with devices which are implanted into individuals - contact of such devices with blood and tissue fluid can give rise to the adhesion and activation of platelets, leading to thrombus generation, and recruitment and activation of immune cells which act to reduce the functionality of the devices.[140] All such processes are commonly initiated by non-specific interaction between protein and surfaces. Typically this interaction is undesirable, and represents one of the first steps in bio-fouling which can

ultimately result in loss of function in materials such as nanofabricated surfaces and can lead to limitations the useful life span of such technologies.[141] Therefore, the generation of biocompatible surfaces is vital for a number of biological and medical applications. Proteins are the most common and functionally diverse group of biological macromolecules and surfaces are the points at which biological and synthetic systems meet. Thus, the ability to tailor and control the ways in which proteins and surface interact is vital to the design and production of functional materials.[142]

One common strategy employed to render interfaces resistant to protein adsorption is to modify surfaces with chemical groups. Ethylene glycol derivatives, such as poly(ethylene glycol) (PEG) and oligo(ethylene glycol) (OEG), have become popular compounds for this application.[143] Their success in this application has been attributed to the high surface water retaining capacity, charge neutrality, as well as steric repulsion and surface exclusion effects. [144] However, the exact mechanism of how ethylene glycol derivatives are able to facilitate a resistance to protein adhesion remains open to debate, as different model system may operate via different mechanisms.[145] The picture of the interactions that occur between glycols and proteins is complex; despite the well documented ability of PEG to resist protein adsorption, there have been studies which demonstrate that in free solution, PEG is able to interact with proteins.[146] This finding combined with investigations into the of the effect of PEG graft density on surfaces ability to resist protein suggests that the protein resistance observed is a property of the bulk PEG on a surface rather than an intrinsic property of the molecule itself.[140, 147-151] A general explaination for these observations is that if the surface contains large amounts water in a similar state to the surrounding bulk water, then no free energy can be gained via adsorption of protiens to the surface.[152]

Many works have described how surfaces which are unable to resist the adsorption of proteins can be chemically modified to reduce protein adsorption. For example, works by

Wu et al have demonstrated that protein resistance can be introduced to surfaces which are non-resistant to adsorption by the introduction of PEG chains.[153] These surfaces were also able to selectively bind plasminogen (via lysine residues incorporated into the surface) which was able to retain functionality, forming plasmin and degrading clotting proteins compared with non-plasminogen modified surfaces. PEG dendrimers have also been conjugated to thioctic acids molecules to produce SAMs able to resist nonspecific adsorption of proteins.[154]

Although there is not a set of surface properties which provide protein resistance that can be easily defined, there appears to be some common properties found between different protein resistant surfaces. The most commonly shared properties are that the surfaces are hydrophilic and non-charged. Proteins are known to adhere more easily to hydrophobic surfaces, though if such surfaces are modified to become more hydrophilic protein adsorption may be suppressed.[155] However, it would appear that charged groups should be avoided despite hydrophilic groups being required for the proteins resistance- there is considerable evidence that charged groups can promote the adhesion of proteins and also cells at interfaces.[132] Despite this observation, some degree of charge can be used in protein resistant surfaces if the net charge of the surface is neutral such as those described in reports which have demonstrated that the use of zwitterionic surfaces can produce protein resistance.[156]

Literature on protein adsorption to hydrophobic surfaces, in general, reports that ,when exposed to proteins, hydrophobic surfaces will quickly become fouled. This observation is believed to be caused by hydrophobic residues in the proteins interacting with the hydrophobic groups on the surface to exclude water and thus providing an entropic driving force for adsorption.[157] Typically, this event leads to the denaturation of the protein, a process which is allows the exposure of further hydrophobic residues which would normally be ‘buried’ in the core of the protein to become exposed to the

surface.[158] This effect is well known for many hydrophobic polymers and the effect of the adherence of like-hydrophobic groups can result in the denaturation of the adsorbed proteins.[139, 159]

1.8.2 Biosensor Fabrication

SAMs have found popularity in the field of sensor fabrication. They provide a foundation from which sensors can be built, using an array of biologically and synthetically derived components. Perhaps the most common sensor type which utilises SAMs is the biosensor. Here, the SAM is used to immobilise biological molecules which are able to bind or interact with the analyte of interest. The most common biomolecules employed in such sensors are antibodies and enzymes, which offer a high affinity binding site for the target molecules.[160] More recently nucleic acids have also been employed as recognition units, in the form of aptamers.[161] When combined with an appropriate reporting strategy, binding events occurring at these recognition sites can be monitored. In the case of enzymes, this strategy is often based upon the consumption or generation of electrochemically detectable species, which is monitored via voltammetry or other similar methods, to produce a signal with magnitude proportional to analyte concentration (Figure 19).[162] However, while enzymes generally offer a high affinity binding site and convenient reporter method, they are not ideal, they commonly rely on co-factors for effective function, result in the breakdown of the analyte of interest and can suffer from poor stability, limiting their use and shelf-life.[79]

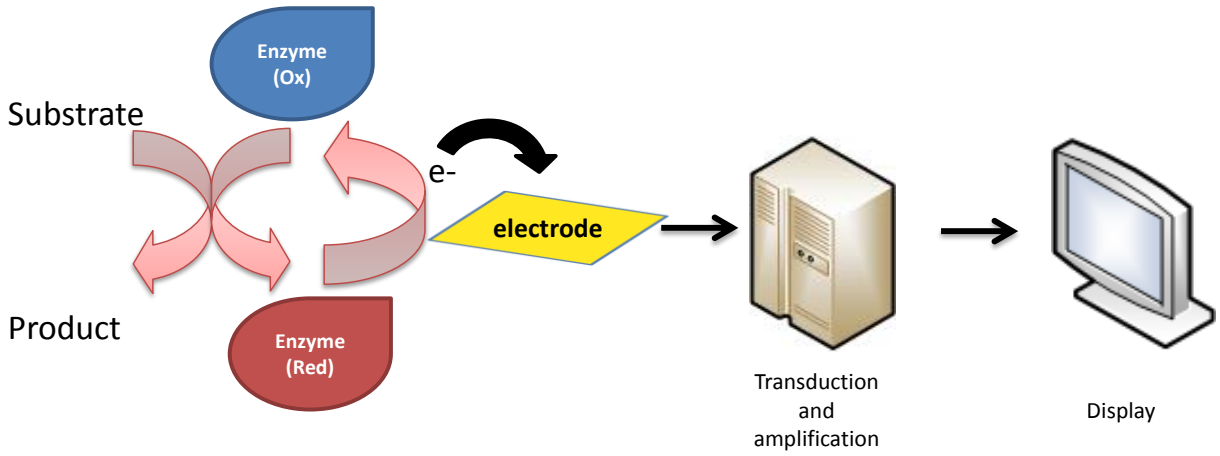

Figure 19: Schematic of an enzymatic biosensor. The reduction of the active enzyme or co-factors can be used to generate a electrochemical signal upon encountering an analyte. [163]

Antibodies and aptamers offer less destructive alternative binding elements to enzymes. In antibody based sensors, the reporting method used is commonly different to that used in enzymatic sensors. For example, additional binding interactions may be required to fluorescently or enzymatically label and detect the bound analyte.[164] Such arrangements can be used to probe the analyte content in a range of sample types. If the fabrication of the sensor is appropriate, then detection can be achieved even in complex matrices.[165] If such materials are combined with techniques such as Surface plasmon Resonance (SPR) , then the binding kinetics of analytes with their binding sites on the sensor may be monitored in real time.[166] This is a powerful method of investigating biological interactions and will be discussed further in chapter 2. However, both protein and nucleic acid based sensors can face problems in the due to their potential instability. Aptamers can be limited due to their sensitivity to nucleases, while protein based recognition units are susceptible to thermal damage and break down by proteases, resulting a limited shelf-life.[161] Typically the effective number of active molecules will reduce over time due to the degradation of the biological elements of the sensor and in addition there is often a requirement of cold storage of these proteinaceous elements of the sensor, which is a limit to their commercial application.[167]

1.9 Molecular Imprinting

Molecular imprinting is a technique which allows production of materials possessing specific cavities designed to provide complementary binding sites for target molecules.[168] It offers the possibility of producing molecular structures which can act as synthetic binding sites and has the potential to offer alternatives to the antibody-based binding sites commonly seen in many sensors.[169] In addition, as the structures are synthetic, there is a much greater scope for the rational design of binding site components which can improve their efficacy.[170]

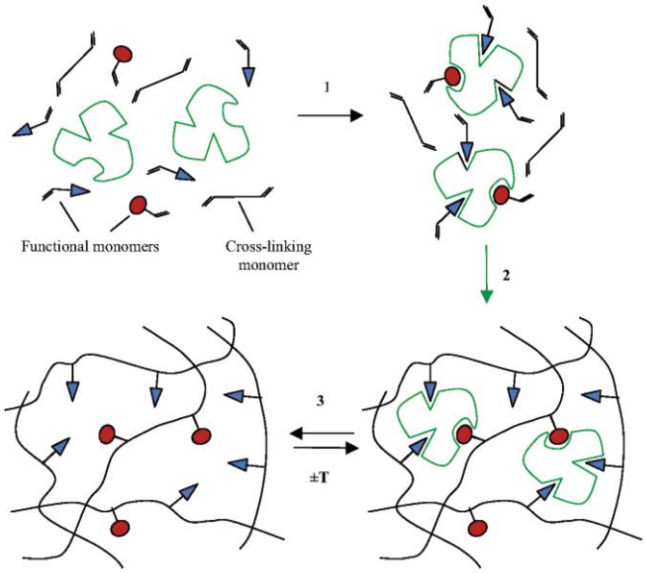

Figure 20: Diagram illustrating the general principle used in a) 'traditional' polymer monolith molecular imprinting. Here the target compound is mixed with functional monomers and crosslinking monomers (1) allowing the functional monomers to interact with complementary sites on the target. (2) The polymerisation of this monomer-target complex in the presence of the crosslinking monomer acts to 'fix' the functional monomers in position producing an imprint of the target. (3) The target is then removed, leaving behind the empty imprint of the target. This process occurs in three dimensions, producing a monolith imprinted structure.[171]

Molecularly imprinted binding sites are produced by using target molecules as templates around which molecular structures are produced.[169] A typical strategy is to use a mixture of functional and crosslinking monomers and the target molecule in a suitable

solvent. The functional monomers initially form a complex with the target molecule which then is co-polymerised with the crosslinking groups to form a three-dimensional and rigid polymer network around the target molecule.[172] Subsequent removal of the imprint molecule leaves cavities with a size, shape and chemical functionality complementary to those of the template (Figure 20). In this way, a 'molecular memory' is introduced into the polymer, which is capable of selectively binding the target with affinities comparable to those of immunosorbents.[168]

The choice of the compounds used to interact with the target molecules is of vital importance in order to produce a selective imprint system.[173] A wide range of monomers containing differing functional groups have been used to in attempts to exploit a number of interactions types including non-covalent interactions, reversible covalent interactions, or metal ion mediated interactions. [174] For molecules of low molecular weight such as organic compounds, antibiotics and herbicides large numbers of differing molecular imprinting methodologies have been reported.[171, 175] Of these approaches, methods which utilise a strategy based around non-covalent interactions appear to be the most common.[176]

Small organic compounds have, in general, well defined structures and are soluble in organic solvents. This is convenient for the design and production of molecular imprints of such compounds as it allows for the selection of monomers with ideal properties to produce effective binding sites. For example, imprints have been produced for drug molecules such as diazepam and theophylline which utilise methacrylic acid as a functional monomer in order that the carboxylic acid groups present in the imprint structures are able to form ionic and hydrogen bonds with the amine and polar groups present in the target compounds respectively (Figure 21).[177] However, techniques for bio-macromolecular targets such as proteins are not so widely reported.[178]

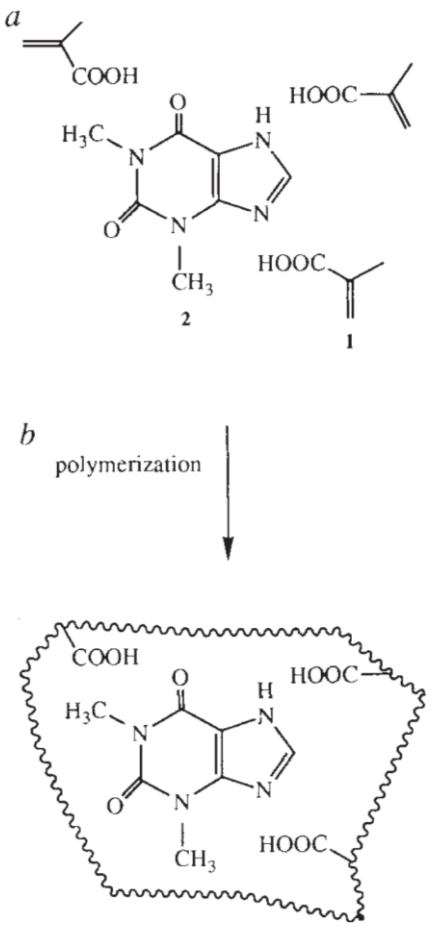

Figure 21: An example of a molecular imprint formed by the exploitation of carboxylic acid groups present in the imprint structures to form ionic and hydrogen bonds with amine and polar groups present in the target compounds.[177]

Although in many examples of molecular imprint formation a single type of interaction is used to mediate the imprint formation, there are also examples of molecular imprinting methods which utilise both covalent and non-covalent interactions to produce the final imprint. For example, previous publications have described using a covalent interaction to attach the target compound to imprint monomers prior to their polymerisation. Following polymerisation, this strategy then allowed the covalent bond to be broken and the target to be released, while maintaining the rest of the imprinted binding site. In addition the method used to degrade the covalent bond also generated a potential biding site via the formation of a hydroxyl group which is then able to participate in hydrogen bonding with

the target compound (cholesterol) (Figure 22). It was found that these methods were able to distinguish cholesterol from is structural isomers, which suggests that this method of controlling orientation can be very effective for producing successful molecular imprints.[179]

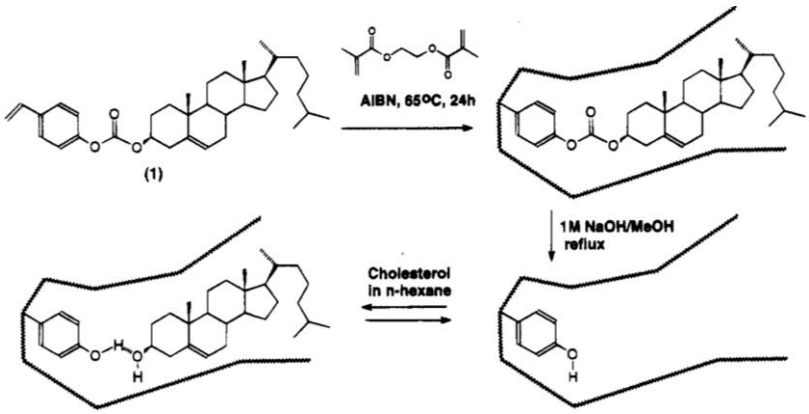

Figure 22: An illustrated example of a molecular imprint prepared by covalent immobilisation of the target compound prior to polymerisation. Following production of the molecular imprint, the covalent interaction between the target and the imprint is degraded to allow release of the target and facilitate subsequent rebinding. [179]

1.9.1 Molecularly imprinting proteins

One of the challenges to the production of molecularly imprinted sensors specific for bio-macromolecules such as proteins is the potential fragility of these targets.[180] Unlike small molecules such as drugs, herbicides and antibiotics (all of which have successfully being used in molecular imprints), proteins and other biological molecules are vulnerable to changes in temperature, UV exposure and organic solvent conditions.[171] This acts to severely limit the options for template formation, as all reactions are limited to aqueous media and mild conditions of temperature and pH, limiting the chemical strategies available for use.[181]

Molecular size, complexity, conformational flexibility and solubility can also be problematic—traditional polymer-based molecularly imprinted monoliths tend to be

relatively dense, leading to difficulty in a macromolecular template reaching (or leaving) any formed binding site. Such poor mass transport and permanent entrapment results in inadequate recognition properties.[182] This also limits the choice of monomers available for selection as many monomers commonly used in molecular imprints of small molecules are insoluble or partially soluble in water. This makes imprinting in aqueous solutions necessary to produce systems with optimal selectivity, as specific imprints of proteins should be tailored to the native structure to be of any use in an assay or sensor system.[180] The influence of water competing for binding sites is an important factor that has to be considered, but it has been shown that this effect is more pronounced with small molecule binding, and thus using a macromolecular template with increased surface interactions can lower or remove this effect.[171]

Due to their complex nature, bio-macromolecules contain many sites that could potentially serve as molecular recognition sites, such as charged amino acids and regions of differing hydration. The result is that the variation of the molecular imprints produced to target these compounds can be high.[176] This heterogeneity produces a greater potential for non-specific binding to occur in molecularly imprinted systems based on such target compounds.[183] As a consequence, appropriate selection of imprint components is vital to produce a functional and selective system. In addition, there is a requirement that the methods used to produce protein imprints must be suitable for use in aqueous conditions, in order to avoid damage and changes to the conformation of the protein.[170] This requirement is evidenced by the effect of ‘solvent memory’- where molecular imprints produced in organic solvents perform poorly when used in aqueous conditions.[176] Akin to the common methods used in examples of molecular imprints produced for small molecules, protein targets have been successfully imprinted using non-covalent type systems. In such systems, a number of relatively weak interactions are able to come together to produce the final imprint. Typically, these methods use only one simple type of interaction to produce the sensor. One such example uses polymerised sugar groups as

hydrogen bonding sites to produce imprints to proteins. Here, the hydroxyl groups are able to form hydrogen bond interactions with the amino acid side groups present in the proteins (Figure 23). Using such a system, the authors were able to produce imprints selective for several proteins. However, the assay relied on labelling based detection method which limits is potential application.[184]

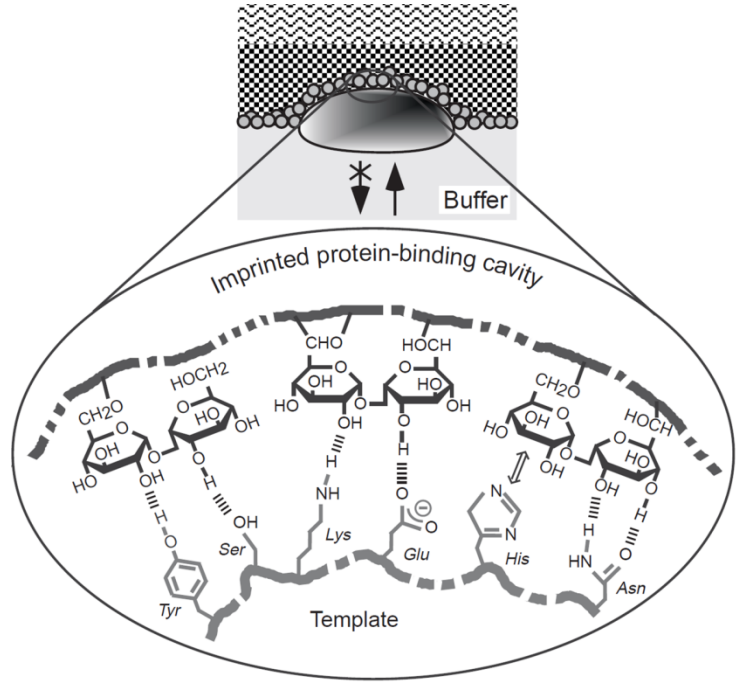

Figure 23: Illustration of the non-covalent interactions between the hydroxyl groups present on surfaces and the amino acid side chains present on proteins.[184]

More recent publications have begun to focus on the development of increasingly selective and more sensitive methods for monitoring binding events on a time scale more suitable for use in high throughput clinical settings. Recently, a method was described employing the use of polyphenol to produce binding sites as part of nanofabricated surface sensors for detection of the proteins human ferritin and calmodulin. In this example, imprinted polymers were formed on the top of nanotubes which were embedded in a second supporting polymer (Figure 24). Here, the affinity of the surface to the proteins was mediated by the non-covalent interaction between the protein and the

polymer. The non-conducting properties of the polyphenol are then used to allow detection of protein binding by electrical impedance spectroscopy, as the binding of proteins to their binding sites produced an increase in the resistance of the system. While this system is effective at detection down to very low levels, the system still suffers with protein entrapment in the imprint sites, which could inhibit the performance of the sensor.[169]

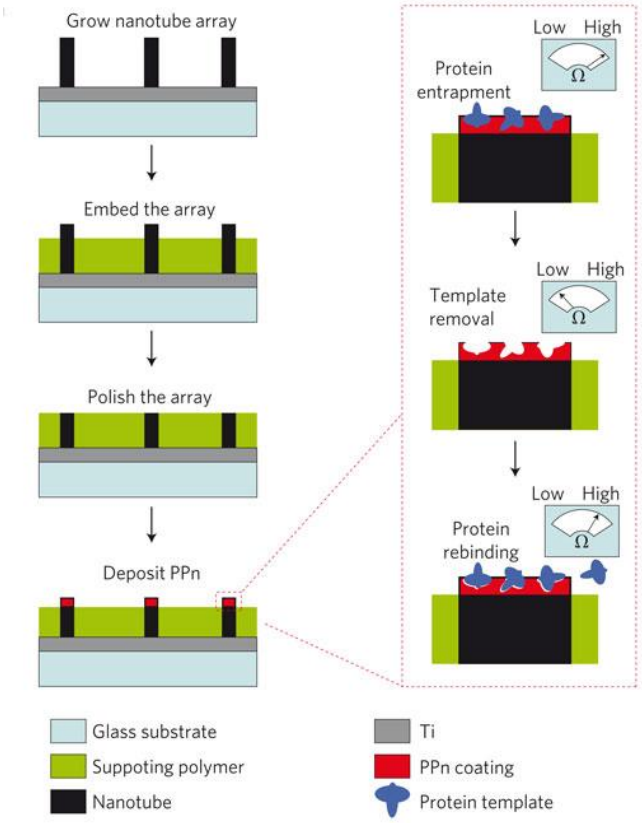

Figure 24: a) Illustration of a molecularly imprinted sensor formed on the tips of a nanotube array, and b) detection of protein re-binding to the sensor by electrical impedance spectroscopy [169]

Boronic acids have also been investigated for use in molecular imprints, and have been found to offer some useful characteristics, such as the ability to form covalent interaction which can be controlled by pH to allow the binding and release of target compounds, particularly target molecules which contain diols.[175] However, to date, the full potential of boronic acids in molecular imprints remains to be realised. The potential of boronic

acids and their derivatives can be attributed to their physical and chemical properties. In addition to their well-documented ability to form reversible covalent interactions with diols, they are also able to act as hydrogen bonding groups, and can offer the possibility of ionic and electrostatic interactions. Together these possibilities make boronic acids extremely interesting compounds from which to produce molecular imprinted sensors for proteins and glycoproteins.

1.9.2 Surface imprints

Recently, there have been published examples of a new class of molecular imprinted sensors which move away from the production of large polymer networks. Instead, imprints are produced in thin films or fixed to a supporting surface.[171] By producing molecular imprints in such a manner, limitations of bulk polymer imprints can be avoided, producing systems with high mass transfer, easy integration with sensor platforms, and increased robustness.[185] A recent example of a surface imprinted system has demonstrated that imprinting is possible using a relatively simple SAM-based method. Here, 11-mercapto-1-undecanol was used to form SAMs in the presence of the target molecules (Figure 25), such as proteins and virus structures and shown to be effective at producing imprints, although the selectivity/promiscuity of the protein imprints was not investigated. However, the virus template SAMs were shown to be able to discriminate between two species of virus based on their molecular size- imprints Poliovirus (27 nm) and adeno virus (70-100 nm).[186, 187] Although this technique was demonstrated to work with the targets investigated, its application to a wider range of targets is limited due to the presence of cysteine groups in proteins which would act to bond the protein to the gold surface which may also act to cleave sulphur bridges present in many proteins. Additionally, it is known that proteins can irreversibly attach and subsequently change conformation or denature when exposed to a bare gold surface.[188-190]

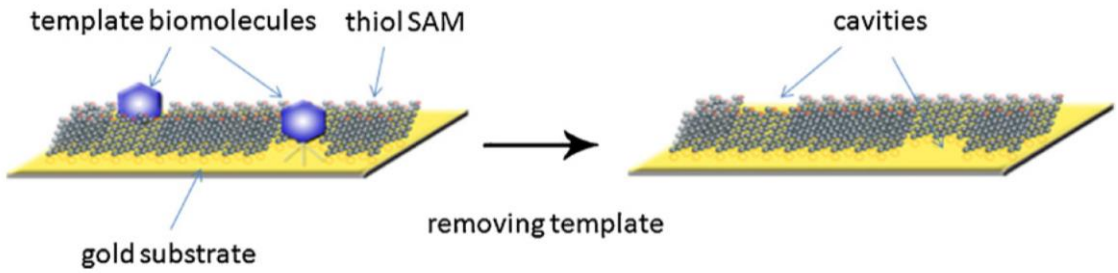

Figure 25: Illustration of a method of producing molecular imprints using SAM based system, employing 11-mercapto-1-undecanol as the SAM molecule. [191]

Surface imprints are, however, not without limitations. A commonly cited problem is that the surface methodology can produce unwanted interaction due increased levels of heterogeneity in the binding sites produced (Figure 26). This can be compared to the differences in selectivity and cross reactivity observed with monoclonal and polyclonal antibodies- here monoclonal species have little or no variation in their structure while polyclonal antibodies have a wide variation, resulting in comparably lower levels of cross reactivity in monoclonal antibodies.[192] Thus, there remains a great potential for the improvement of molecular imprinted sensors through the development of new methods and technologies for their production, in order to improve both the selectivity and sensitivity of molecular imprinted binding sites to proteins.

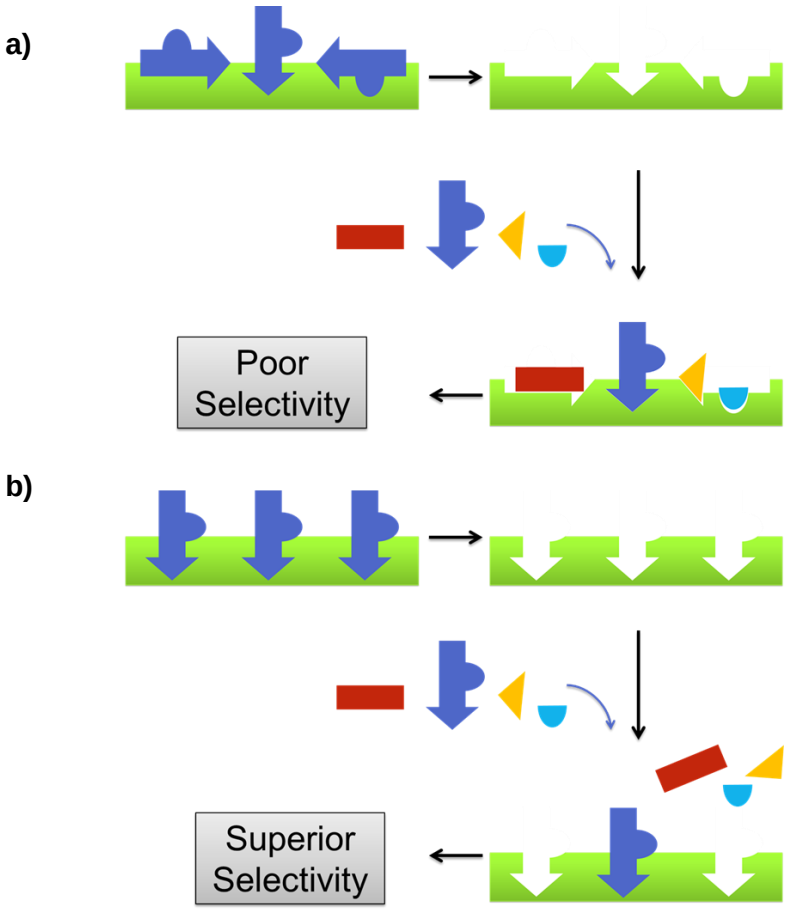

Figure 26: Illustration of how molecular imprints homogeneity affects selectivity. In a) a low degree of homogeneity produces binding sites with an increased variation, producing more sites for the potential cross reactivity of other compounds. In b) an imprint is formed with high homogeneity and subsequently the potential for cross reactivity with unwanted compounds is reduced.

1.10 Concluding remarks

As understanding of the roles played by post-translational modifications, such as glycosylation, grows so does the need and desire to produce technology able to detect such changes. Currently the 'gold standard' methods of detection and profiling of glycosylation, that is to say HPLC and mass spectrometry, are used for preliminary research work, but they are poorly suited to the needs of more large scale investigations. This is due to the fact that such technologies rely on extensive samples preparations and instruments which have high setup and running costs. Therefore, novel methods for the

easy detection of glycoproteins are becoming increasingly sought after for applications in biology, healthcare and medicine. In particular, those methods which offer a cost effective and high throughput potential would be highly valued, as they would facilitate the large scale investigation of links between glycosylation changes and diseases, such as cancer. Furthermore, these qualities would also be desirable in order for such technologies to be employed as clinical screening tools.

In this chapter, we have discussed a number of topics which, in the subsequent chapters, will be brought together to produce sensing systems which aim to meet the needs just described. Thus, the remained of this thesis will describe the fabrication of a sensor system which is able to detect saccharides and glycoproteins which are associated with human pathology. In addition, these systems act as proof of principles of the production of synthetic sensors able to distinguish different glycoforms of the same protein. This aim can be divided into the following two goals:

- Production of a *bis*-boronic acid surface sensor for the selective detection of the monosaccharide species glucose.
- The design, synthesis and characterisation of a molecular imprinted surface sensor which is able to detect glycoproteins.

Both of these systems will be based around self-assembled monolayer systems and contain boronic acids which act as binding units. As these systems are fabricated on a nanoscale, specialist methods of characterising the structures are needed. Discussion and explanation of the techniques will now follow in chapter two.

CHAPTER 2: SURFACE CHARACTERISATION TECHNIQUES

In this chapter the various techniques and methods used to characterise materials and surfaces will be reviewed. The aim of this chapter is to provide a brief explanation of the techniques which will be discussed in later chapters of this thesis. Particular attention will be paid to techniques suited to the investigation of modified surfaces. Techniques such as ellipsometry (for surface thickness), X-ray photoelectron spectroscopy (XPS) (for surface elemental analysis), contact angle (wettability and surface composition) and cyclic voltammetry (CV) (for surface chemistry and stability) are employed to characterise prepared surfaces. Other techniques such as Surface Plasmon Resonance (SPR) are discussed, as they provide a convenient means to study the interactions between solutions based species and surfaces.

2.1 Introduction

One of the challenges of nanoscale science is the confirmation that structures and modifications on this scale have been effective. Fortunately, there exists a number of characterisation techniques which can be used to overcome these problems. The methods used in the following chapters of this thesis will be concerned with investigating the properties of modified surfaces. Such techniques provide information about the composition and structures of modified surfaces, including the elemental composition, the thickness and physical and chemical properties of surfaces. A summary of the methods available is shown in Figure 27. In the rest of this chapter the methods will each be discussed in turn.

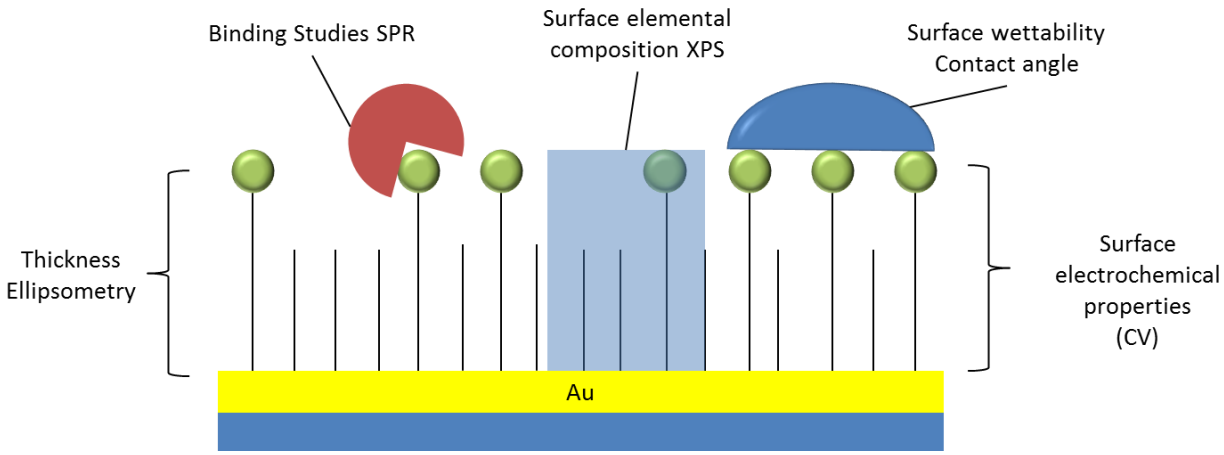

Figure 27: Illustration of some of the various surface characterisation techniques involved in this thesis.

2.2 Ellipsometry

Ellipsometry, is a non−destructive optical technique which can be used to calculate, *in−situ,* changes in polarisation of light upon reflection from a surface, in order to probe the dielectric properties of a sample. As changes in the polarization are measured, rather than the absolute intensity of light, ellipsometry sensitive to changes in surface properties, such as those induced by thin films such as self-assembled monolayers (SAM). The

origins of the technique can be traced to the late 19th century, when P. Drude (1863-1906) was the first to build an instrument to investigate the effect of surface adsorbed compounds on the optical constants of metals.[193] The equipment built by Drude is surprisingly very similar to many types of ellipsometry instruments in use today. However, the technique received little attention until the 1970's and 1980's, when ellipsometry became widely utilized.[194]

Ellipsometry uses elliptically polarized monochromatic light to determine the thickness of a SAM surface.[195] Before discussing this further a definition of the components of light is included for completeness:

An electromagnetic wave, such as light, consists of an electric field E and a magnetic field B. The field vectors are mutually perpendicular and also perpendicular to the propagation direction as given by the wave vector *k*. All states of polarization for such waves are classified according to the electrical field vector during one period. The electric field vector can be described by the sum of two components, defined 's' and 'p' which are perpendicular to each other and the direction of the waves travel.[196] To produce linearly polarised light, the electric field vector, E, must oscillate within a plane, and in order for this to happen the 's' and 'p' components of E must be in phase (figure 28a). If the components are out of phase, then the result is that the E vector of light rotates as the wave propagates (Figure 28b). If the amplitude of 's' and 'p' components are equal then the wave will rotate in a circular motion, however, if the amplitudes of these components are different, then the wave will trace the shape of an ellipse as it propagates. [194]

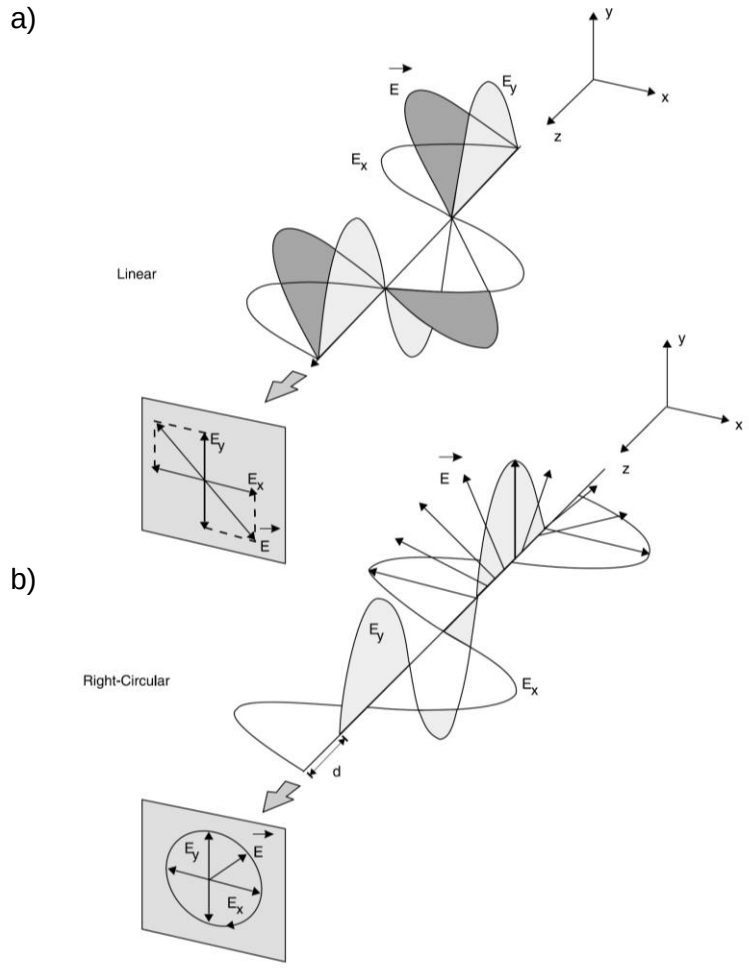

Figure 28: Diagram illustrating the ‘s’ and ‘p’ components of a) linearly polarised light and b) circularly polarised light [194]

When linearly polarized light interacts with the SAM surface at an angle, it resolves into its ‘s’ and ‘p’ component due to the refraction of light by surface appended molecules, producing changes in the phase and amplitude of the components of the light. When the reflected ‘s’ and ‘p’ polarized components are combined, the result is the elliptically polarized light (Figure 29).[194]

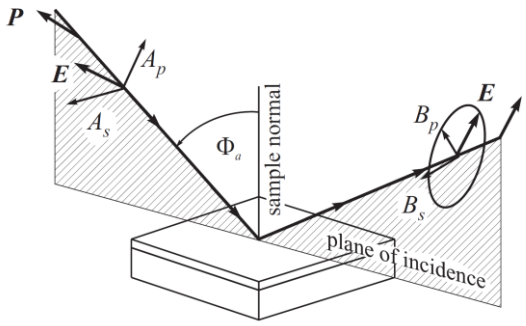

Figure 29: Digram demonstrating how the polarisation of light is changed from linear to elliptical following interaction with a surface [197]

A typical ellipsometry experimental set up is depicted in Figure 30. Light with a well-defined state of polarization is shone on a sample and differences in its state of polarization and are measured and quantified in an ellipsometry experiment. An ellipsometric measurement allows one to quantify the phase change between ‘s’ and ‘p’ and the change in the ratio of their amplitudes. This polarisation change allows the calculation of the reflection coefficient, ρ, which is equal to the ratio between the reflection coefficients of the ‘p’ and ‘s’ polarised light and can also be expressed in terms of the amplitude ratio, Ψ, and the phase difference, Δ, as depicted in Equation 1.[194]

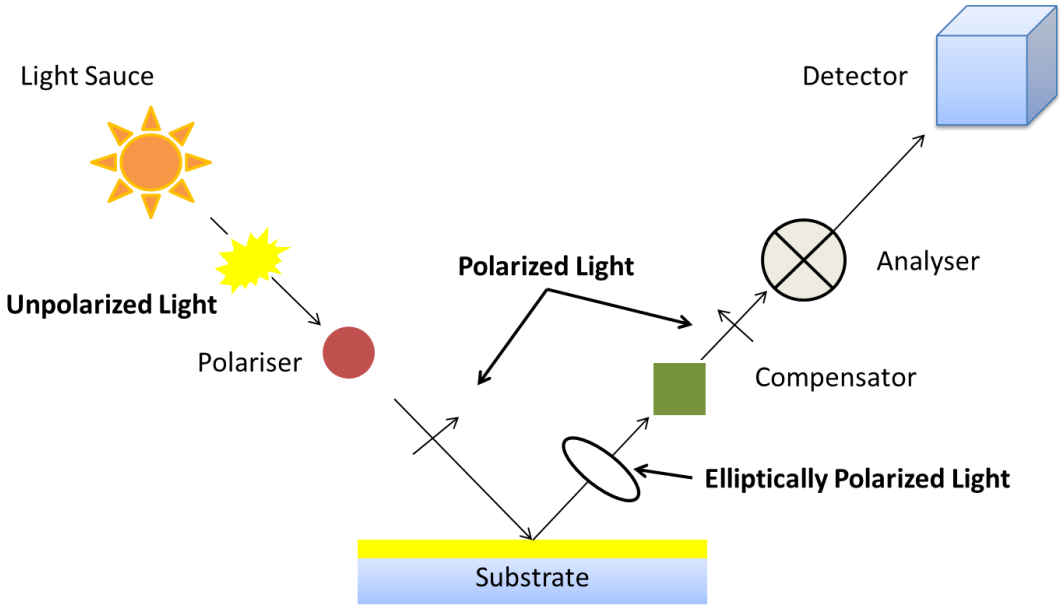

Figure 30: Illustrated representation of the experimental set up used in ellipsometry measurements

Eq. 1 $$\rho = \frac{r_p}{r_s} = \tan(\Psi)e^{i\Delta}$$

As ellipsometry is an indirect method, the measured parameter such as Ψ and Δ cannot be converted directly into a thickness measurement for the sample. Therefore, a model is required which is able to take into account the refractive index and thickness parameters of all layers forming the sample. By using the model and by applying an iterative procedure (least−squares minimisation) the unknown optical constants and/or thickness parameters are varied, and Ψ and Δ values are calculated using the Fresnel equations. The calculated Ψ and Δ values which best match the experimental data are used to provide the optical constants and thickness parameters of the sample. The self-assembled monolayers (SAMs) thickness value is based on the model of Air/SAM/Solid in which SAMs are assume to be defect free (homogenous) and with a refractive index of 1.51. This model is based on the Cauchy equation, which considers the SAMs as a transparent layer.[198]

2.3 Contact angle goniometry

A contact angle goniometer measures the static and dynamic contact angle of a drop of solvent on a surface. Contact angle is defined as the angle formed at the intersection between the boundaries of the solid liquid interface and the liquid vapour interface (Figure 31). The technique can be traced back to the to the early 17th century, however the origin of the technique in its modern form can be pinned down a publication by Thomas Young in 1805, where he correctly identified the forces acting on a sessile liquid drop on a solid surface.[199]

Contact angle measurement, although simple to conduct, can be useful to probe the properties of surfaces and modified surfaces, such as SAMs.[200] Furthermore, the assessment of the contact angles can be used to infer other, more difficult to measure, surface properties.[201]

The general set up of a contact angle goniometer consists of a syringe filled with a solvent (e.g. water), a fibre optic capable for illuminating the surface and a charge-coupled device (CCD) camera connected to a computer for analysis. The solvent is added as a droplet onto the surface for contact angle measurements.[202]

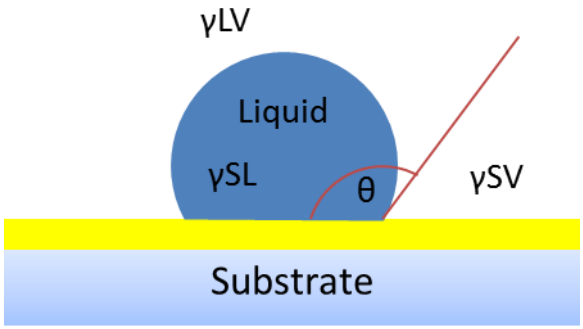

Figure 31: A liquid drop on a solid surface forming a contact angle.

The contact angle (θ) is formed at a point of contact between the solid, liquid and vapour phases. The angle is the tangent measured at the three phase contact point, as shown in

figure 31. The contact angle is governed by Young's Equation (Equation 2) where γSL is the free energy of solid surface in contact with liquid, γLV is the free energy of the liquid-vapour interface and γSV is the free energy between the solid and the vapour. [200, 201]

Eq. 2 $$\gamma SL + \gamma LV\cos\theta = \gamma SV$$

When a water droplet is in contact with a hydrophilic surface, the water spreads onto the surface to minimise free surface energy, which produces a low contact andgle (<30 °). In contrast, hydrophobic surfaces tend to have lower free surface energy and the water droplet does not spread onto the surface, therefore, producing a high contact angle (>100 °) as shown in Figure 32.

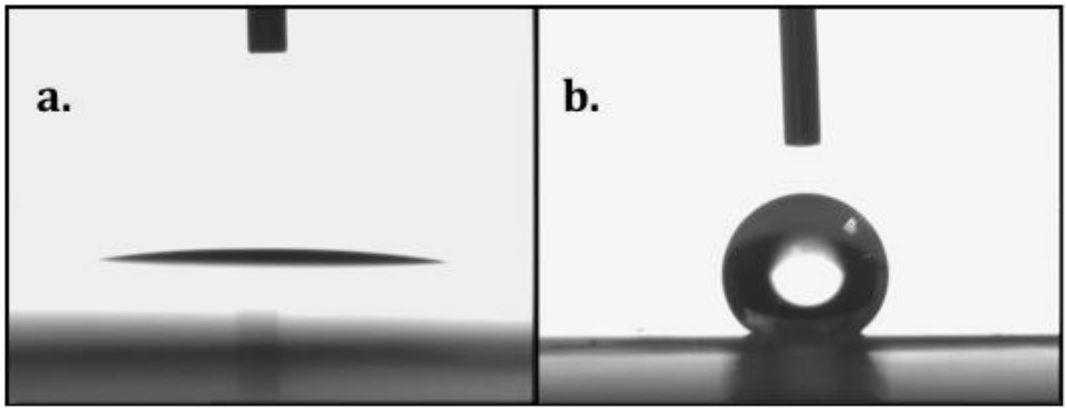

Figure 32: A liquid drop on a solid surface forming a contact angle on a) a hydrophilic surface and b) a hydrophobic surface.

The contact angle is measured by a free standing drop of a liquid on the surface, known as static contact angle (no syringe) or measured by a captive drop of liquid known as dynamic contact angle (with syringe) (Figure 33). All contact angles discussed in this thesis were measured using the captive drop technique. The dynamic contact angle is measured by adding and withdrawing water through the needle, where the addition of water produces the advancing contact angle (θa) and the withdrawal of water produces the receding contact angle (θr).

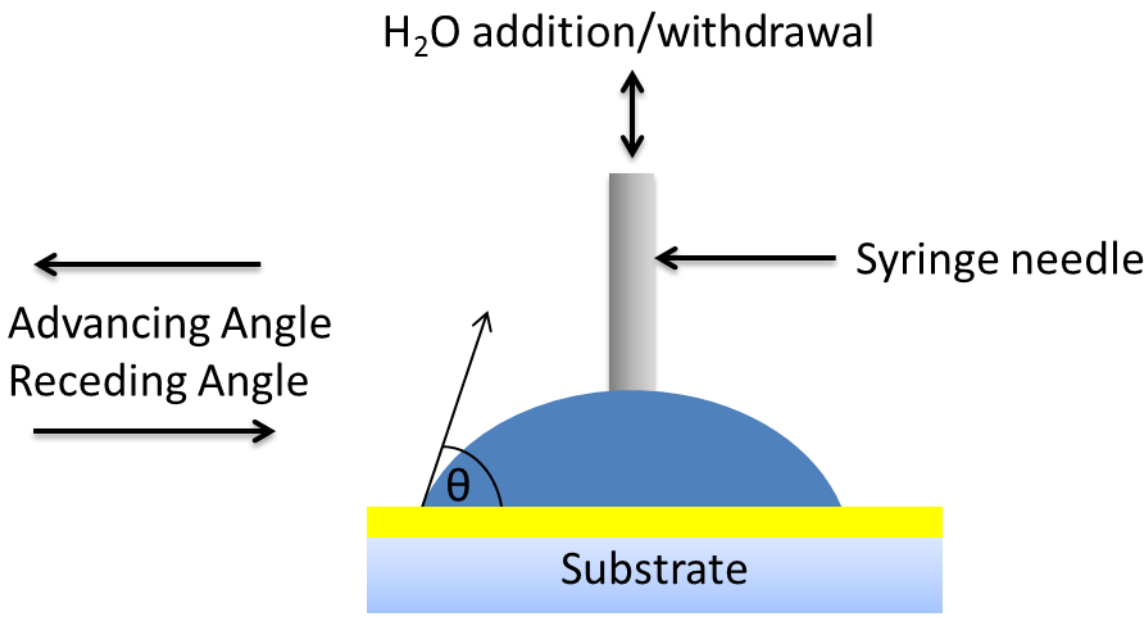

Figure 33: An illustrated representation of advancing and receding contact angles when water is added to or withdrawal from the surface.

The difference between the advancing and receding contact angles is known as the contact angle hysteresis ($\Delta\theta = \theta a - \theta r$). A small hysteresis (greater than ~ 5 °-10 °) indicates a homogenous, well ordered and crystalline SAM, whereas a large hysteresis suggests the surface is contaminated, non-homogenous and/or relatively rough.[201]

2.4 X-Ray Photoelectron Spectroscopy

X-Ray photo electron spectroscopy (XPS) is a technique which is able to provide both qualitative and quantitative information about the compounds present within a sample.[203] It a based upon the photoelectric effect; an x-ray photon is used to induce the ejection of an electron from either a tightly bound core level orbital or from more weakly bound valence and molecular orbitals from atoms within the sample, and the energy of the emitted photoelectrons is analysed by the spectrometer to produce a graph of intensity vs electron energy.[204] A schematic of the experimental set up is shown in Figure 34.

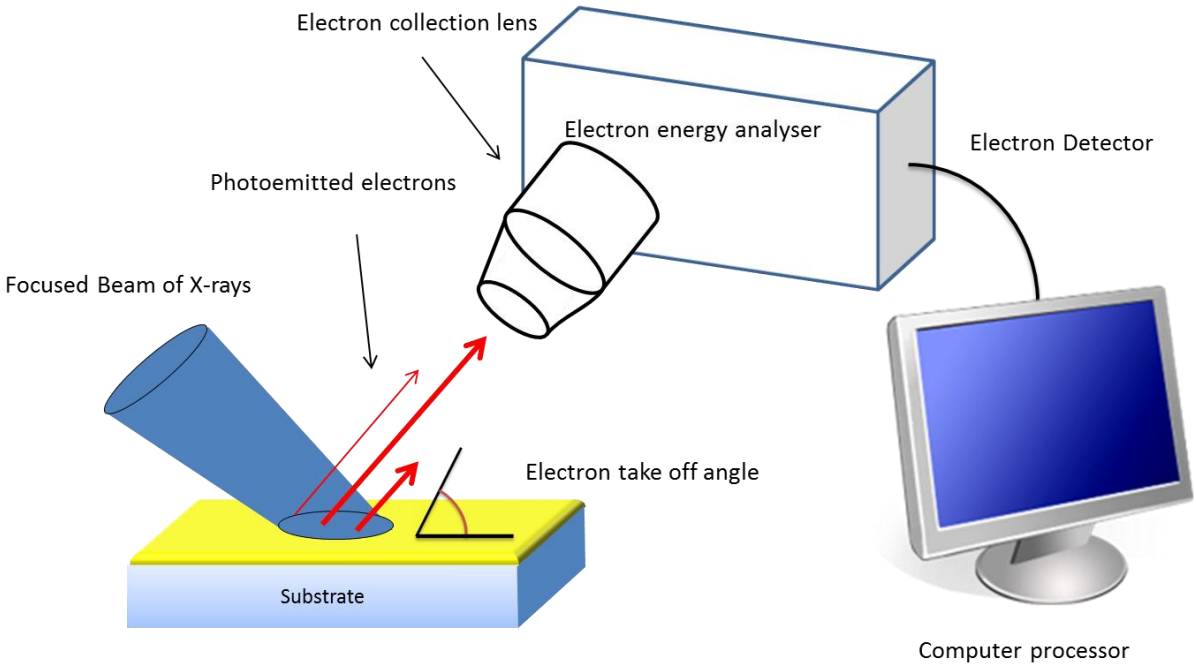

Figure 34: A schematic of the experimental setup used for XPS analysis

The raw data from the experiment is measured in units of electron kinetic energy. This value, however, is not absolute; it is dependent on the photon energy of the x-rays used. Therefore it is common place for the kinetic energy values to be converted into a value known as binding energy (BE), which is given by the following equation;

Eq. 3 $$E_B = hv - E_K - W$$

Where *hv* is the photon energy, E_K is the kinetic energy of the electron, and *W* is the spectrometer work function. As all the values are known or measureable, it is simple matter to calculate the binding energy of the electron.[205]

The spectra produced by XPS analysis can be thought of as a reproduction of the electronic configuration of the element being analysed, with the electronic radius extending out with the growing kinetic energy, or conversely with decreasing binding energy. The well-defined peaks observed are caused by electrons which are able to escape the pull of the atomic nuclei without loss of energy, while ejected electrons which are inhibited in their escape by inelastic scattering produce the broad and decaying signal

observed between the sharp peaks due to the loss of energy caused by such interactions.[206]

By its nature XPS, is best suited to the analysis of surfaces and surface structures such as SAMs and thin films.[203] This effect is due to two factors; firstly the energy of photons generated by typical x-ray sources are able to penetrate only a short distance into the bulk of the sample in the order of 1 μm, therefore most generated photoelectrons will originate near or at the surface of the sample. Secondly, generated photoelectrons at or close to the surface have a much greater probability of leaving the solid without energy loss than photoelectrons generated from within the bulk of the sample.[207] Taken together, such factors result in XPS being useful for characterisation of materials within 10 nm of the sample surface.[206]

Due to the ease at which low energy electrons can be scattered by other particles such as gasses, there is a requirement for XPS systems to be operated under ultra-high vacuum (UHV) conditions, where pressures of 10^{-8} to 10^{-10} mbar. Loss of vacuum will result in a decrease in the total intensity of the spectra will decrease while the noise spectra will increase. An important consideration for experimental design is the samples ability to conduct; if the sample is insulating there is the requirement for methods of charge compensation.[208] Due to the ejection of electrons, if the sample is insulating, there will be a build-up of positive charge on the sample surface. This issue is most severe in the case of highly focused monochromic X-ray sources, which can produce localised regions of highly differential charge, which in turn can broaden and distort specta. [206] To avoid this problem the sample can be earthed with a conducting material or the positive charge can be mitigated by the use of a ‘flood-gun’ which provides a source of low energy electrons to neutralise any differential in surface charge.[205]

Using most common x-ray sources, XPS spectra containing signals from at least one core level for each element may be observed, with the exception of Hydrogen and Helium.

Furthermore, the binding energies of the signal peaks on the are generally distinct enough to permit the identification of the signal, although for a small number of elements there can be overlap between signal peak which can prove problematic. This is especially the case for first row elements, as these compounds contain only the 1s level. For compounds with more complex electronic configurations, overlapping signals can be more easily resolved by considering the peaks for other orbitals.[206]

Elemental analysis of a sample can therefore be achieved using a wide 'survey' scan, assuming appropriate resolution and signal: noise ratio. Furthermore, as the intensity of a peak is directly proportional to the density of atoms from which it is produced, XPS is inherently quantitative. Therefore, in a homogenous sample the relative atomic concentration of any chosen element, A, can be obtained from the following equation:

Eq. 4 $$C_A = \frac{\frac{I_A}{S_A}}{\sum_n \left(\frac{I_n}{S_n}\right)}$$

Where C_A is commonly expressed as the atomic % of all elements determined, excluding hydrogen, and S_n is the relevant sensitivity factor for each element.[209]

In addition to elemental composition, XPS data can reveal information about the chemical environment inhabited by atoms. Such insight can be provided as although the core-level binding energy of elements are unique enough to allow elemental identification, they are not fixed values; the same atom in different chemical can give rise to distinct core level signal components. Such relative shifts in the BE, known as chemical shifts, are, in molecular solids, influenced primarily by the electronegativity of surrounding atoms.[207] Although a rather simplified view, in general atoms adjacent to strongly electronegative atoms will exhibit an increase in signal BE. However, the magnitude of chemical shifts for any element is actually quite small, typically less than 10 eV.[206] Since peak widths are in the order of 1 eV, discrete signals due to chemical shifts are not always observed. This can lead to the need to engage in curve fitting to de-convolute the contributions made by

over lapping chemical shift signals. An example of such fitting can be seen, along with assignments for each signal, in figure 35.

An additional effect which should also be recognised when interpreting chemical shifts is the appearance of additional peaks due to the reorganisation of the electronic configuration caused by the ejection of core level electrons. To the valence electrons, such photo emissions are equivalent to an increase in nuclear charge. This results in the major reorganisation of valence electrons, and can lead to a final state in which a valence electron is promoted to a higher unfilled level. However, as the energy required for this transition is not available to the primary photoelectron, this is a two electron process, producing a discrete structures at the higher BE side of the primary peak.[206]

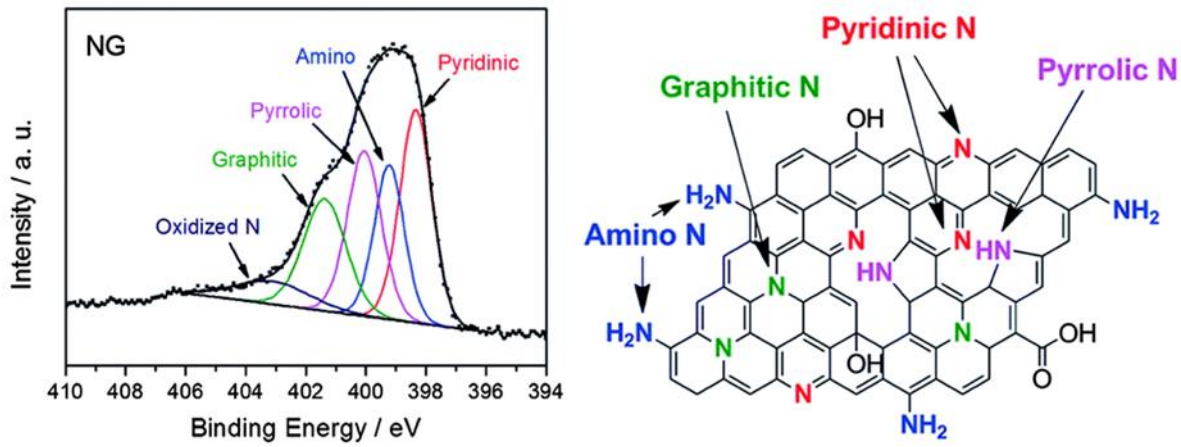

Figure 35: Examples of a high resolution spectra of the nitrogen region for the nitrogen doped graphene. As indicated on the spectra, nitrogen atoms in different chemical environments produce distinct signals in the spectra which are proportional to their relative abundance. [210]

2.5 Surface Plasmon Resonance

The phenomenon of surface plasmon resonance was first observed by Woods in 1902, when during experiments with metal-backed diffraction gratings, Transverse Magnetic (TM) polarised light was shone through such a grating, he noted the appearance of unusual dark bands in the reflected light (Figure 36). Interestingly this effect only

appeared with TM polarised light, and only if the light's electric vector was at right angles to the grating ruling. [211-213]

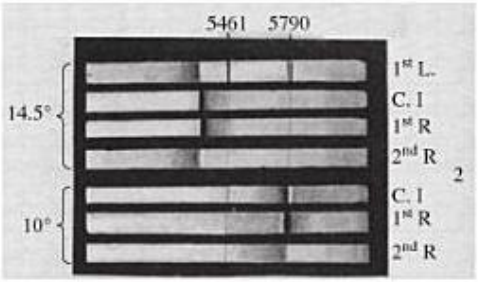

Figure 36: An example of the Wood's anomalies observed in the reflection spectra of diffraction gratings.[214]

Wood's observations of these bands, now referred to as Wood's anomalies, were examined by several of his contemporaries, including Lord Rayleigh, one of the early pioneers of the theory of diffraction gratings.[213] However, despite the efforts of several scholars, a satisfactory explanation for these anomalies was not reached until 1941 when Fano correctly identified their source as the resonant excitation of surface electro-magnetic waves, and it was not until 1968 that the experimental excitation of surface plasmons was demonstrated by Otto, Kretschemann and Raether. Due to its versatility, the experimental setup used by latter is still is use to this day in commercially available SPR instruments. [213, 214]

Surface plasmon resonance is a charge-density oscillation that may exist at the interface of two media with dielectric constants of opposite signs, for example, a metal and a dielectric. The charge density wave is associated with an electromagnetic wave, the field vectors of which reach their maxima at the interface and decay into both media.[211] There are several approaches that all result in the dispersion relation for a surface plasmon, that is, a relationship between the angular frequency, ω, and the wave vector, k. For any interface between two media, the complex reflection coefficient, r_p , for p-polarized incident light electric field is described by Fresnel's equations, where E_i and E_r

are the incident and reflected electric fields, respectively, and the angles α and β are defined as the angle of incidence and refraction, respectively, as shown in Equation 5.[213]

Eq. 5 $$r_{\mathrm{p}} = \frac{E_{\mathrm{i}}}{E_{\mathrm{r}}} = \left|\frac{\tan(\alpha-\beta)}{\tan(\alpha+\beta}\right| e^{i\varphi}$$

The angles α and β are related by Snell's law and in addition, a phase change *j* of the reflected field relative to the incident field occurs, depending on the refractive indices of the materials involved. For the reflectance, R_p, defined as the ratio of the reflected intensities, the following relationship holds, as shown in Equation 6.

Eq. 6 $$R_{\mathrm{p}} = \left|r_{\mathrm{p}}\right|^2$$

These relationships lead to two circumstances where interesting phenomena become apparent: if α+β= π/2, then the denominator of Equation 5 becomes very large and as a result reflectance becomes zero. This situation describes the Brewster angle, where there is no reflection for p-polarized light. The other special case occurs when α-β= π/2- here reflectance becomes infinite as there is a large E_r for a very small E_i. This circumstance corresponds to resonance, and is the effect that is exploited to produce SPR sensor systems. However, this effect cannot be immediately utilised as the wave vector and angular frequency cannot be matched appropriately with 'normal' light to cause resonance of surface plasmons.[213]

Fortunately, optical excitation of the surface plasmon can be achieved in the so-called Kretschmann configuration, where p-polarised, light beam undergoes total internal reflection through a prism, at a glass/thin-metal-film/dielectric interface, as depicted in figure 37d) . Here, the two interfaces require two dispersion equations- one for each interface. It can be observed that the line representing the dispersion relation for 'normal' light in medium 1 (line b) intersects the SP dispersion line for the metal/medium 3

interface. This indicates that light incident from medium 1 can achieve the required wave vector to produce resonance with the surface plasmons. Therefore by proper adjustment of the incoming angle α (Figure 37d), we can tune the incoming wave vector to match the wave vector necessary for SP excitation. In this way, any wave vector between the two lines in figure X a and b in Figure 37, can be set. As an example, one such line, labelled c, is indicated.[213]

The angle at which the resonance occurs is extremely sensitive to any change in the refractive index of the medium adjacent to the metal surface, which in the case of biosensors is typically the buffer system. Such changes can be monitored by recording intensity of reflected light when the system goes out of resonance, for example when addition molecules are adsorbed onto the environment next to the surface.[212]

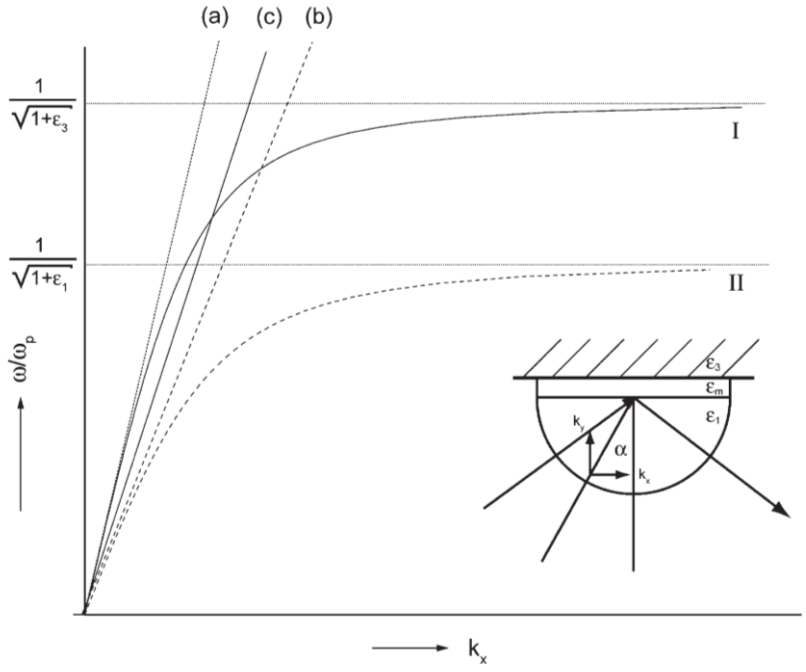

Figure 37 Dispersion relation for surface plasmons. Curves I and II represent the surface plasmon dispersion for the interfaces $\varepsilon_3/\varepsilon_m$ and $\varepsilon_1/\varepsilon_m$, respectively. The lines a and b are the dispersion relations for 'normal' light in medium ε_1 and ε_3, respectively, which are dependent on the angle of incidence a in the experimental setup as indicated in the inset. By varying a, any line c between the lines a and b can be realized. [213]

In order to demonstrate how these effects produce an effective sensor for molecular interactions, a situation can be imagined where molecules, such as proteins, are allowed to adsorb to the water/metal interface. This process can be imagined as an event where water molecules in the environment close to the metal suface are replaced by protein molecules. Because, generally, the refractive indices (and consequentially the dielectric constants) for the protein will be different to the water, the average dielectric constant close to the interface will change, which produces a change of the wavevector k_x required to achieve resonance which can be monitored by the SPR instrument. In addition, as the surface plasmon field is evanescent in the direction perpendicular to the interface, a change of the dielectric constant e_2 is only detectable in surface plasmon characteristics if this change occurs within the penetration depth of the field. Consequently, an SPR sensor will only be sensitive to adsorption events which occur at a distance to the metal surface that is roughly half the wavelength of the used light.[215]

We now understand that an essential requirement for the production of an SPR signal is the presence of free electrons at the interface between two materials. In practice this essentially means that one of the materials must be a metal, where free conduction electrons are abundant. However, in the case of SPR spectrometry, the second material must be a dielectric, such as aqueous buffer.[211] In this case, due to the properties of the metal (its large plasma frequency) the wave vector of the light required will be beyond the properties of visible light radiation, leading to an inability for such radiation to induce resonant excitement of the surface plasmons in the sample. One method (commonly known as the Kretschmann configuration or attenuated total reflection) to produce larger wave vectors using visible light is to launch a wave inside a second dielectric medium with an incidence angle greater than the critical angle. This third medium is often a glass prism, as shown in Figure 38.[215] The wave is totally internally reflected and has a wave vector property which is high enough to couple with surface plasmons, which allows the generation of an evanescent wave on the other side of the interface, in the metal layer

and out into the sample. An additional advantage of this arrangement is that the total internal reflection of the light can be used to detect the angle at which the resonance occurs and monitor change in this angle bought about by changes in the resonant properties of the surface plasmons.[216]

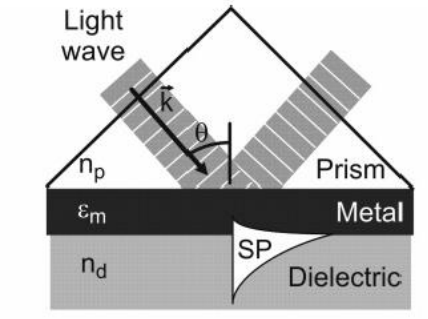

Figure 38: Schematic of the Kretschmann configuration commonly used in SPR biosensors. [215]

Prism couplers represent the most frequently used method for optical excitation of surface plasmons. In the Kretschmann configuration of the attenuated total reflection method, a light wave passes through a high refractive index prism and is totally reflected at the base of the prism, generating an evanescent wave penetrating a thin metal film. The evanescent wave propagates along the interface with the propagation constant, which can be adjusted to match that of the surface plasmon by controlling the angle of incidence. Thus, the matching condition can be fulfilled, allowing the evanescent wave to be coupled to the surface plasmon.

2.6 SPR Biosensors

SPR spectroscopy has become a commonly used system for the development of label free sensor systems. In general, and in the case of SPR spectroscopy, the second material will be a dielectric, i.e. the sample (e.g. a self-assembled monolayer) and surrounding buffer. Typically for biosensor applications, the materials will be gold and an aqueous buffer, and with a light source of wave length 700 nm, this will produce a wave

which is able to penetrate each gold and water/buffer to depths of 26 nm and 238 nm respectively.[213] Therefore changes in the refractive indices of the materials within the scope of the evanescent wave will have an effect on the resonance property of the Plasmon wave. In the case of a sensor, if the content of the buffer close to the surface is altered, such as by the adsorption of a protein molecule, the refractive index of the material proximal to the surface will change. As a result the properties of the light, the angle required to produce the resonance will also change. It is this phenomenon which is monitored by SPR spectrometers.[217] Thus, a surface immersed in a solution into which a surface active molecule can be injected can be monitored by SPR to reveal the characteristics of adsorption events.

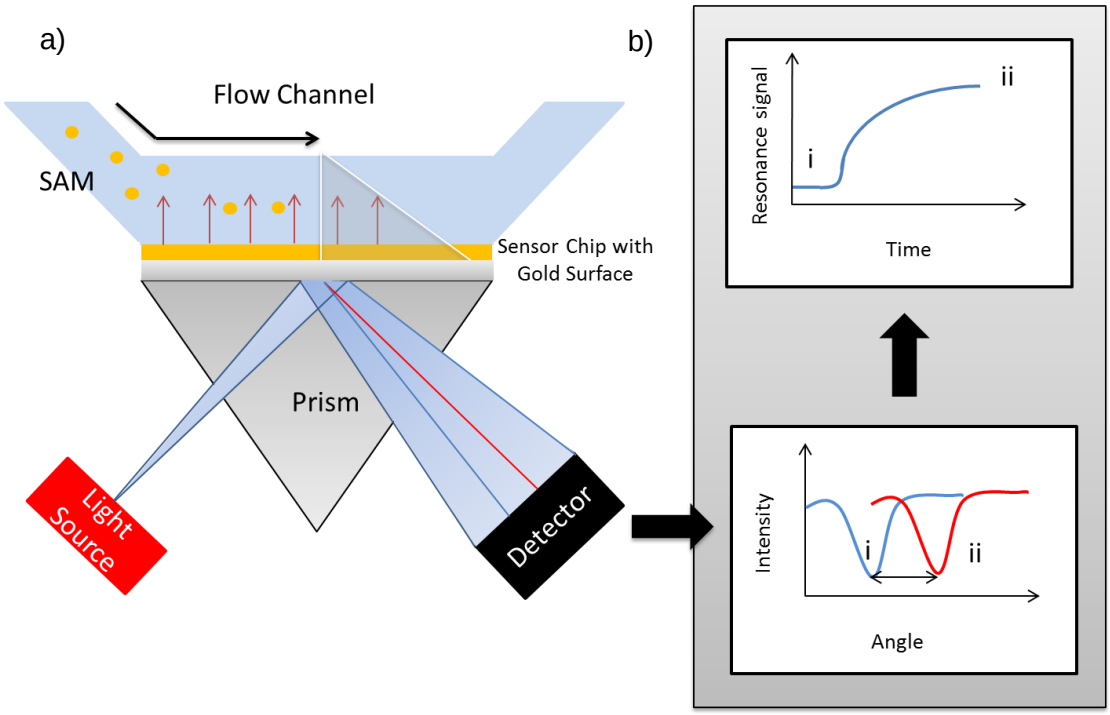

Figure 39: a) Illustration of the the experimental set up for an SPR instrument. b) representation of how changes in the resonances frequency of the reflected light is tracked to produce the SPR plot.

SPR systems can be further divided into three sub-groups, depending on the methods used to monitor change in the refractive index of the surface: fan-shaped beam, fixed angle and angle scanning instruments. Results described in this thesis are obtained using

the fan-shaped beam system, and a general schematic of the instrumental setup is shown in Figure 39a. Therefore, this system is described in greater detail.

In a fan-shaped beam instrument, a converging or diverging beam of p-polarised light is coupled to the higher refractive index medium (sensor chip) using a cylindrical or triangular prism. In a converging beam fan-shaped instrument, the beam focuses on a very narrow line on the sensor chip, whereas the diverging fan-shaped beam focuses on a large area on the sensor chip. A photodiode array detector is used to detect the reflected diverging beam with the SPR dip as shown in Figure 39b.[213]

Commonly the change in the resonance angle is plotted against time to produce a sensorgram, such as the one shown in Figure 40. The typical SPR experiment is performed as a cycle. The first part of this cycle is the setting of a stable baseline by flowing buffer over the surface. This is then followed by an injection of the analyte (in the same buffer) over the surface. As this injection proceeds, binding events are monitored by the change in SPR response. Once the injection is complete, buffer is once again passed over the surface, and a dissociation phase is produced as bound analyte is removed from the surface. The surface is then re-conditioned using a regeneration solution to remove any analyte which remain on the surface following the dissociation phase. The regeneration returns the SPR response to its original value and experiment can be repeated. The complete sequence is shown in figure 41.

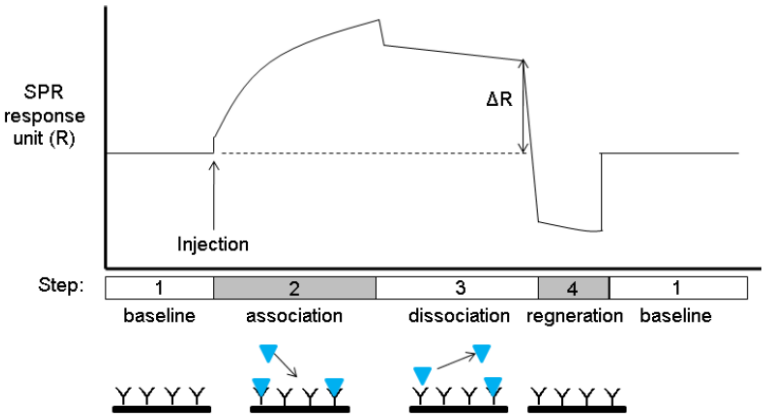

Figure 40: The steps commonly involved in an SPR experiment. Following the establishment of a baseline, injection of analyte produces the association phase. Once the injection is completed, buffer is once again flowed over the surface, leading to the dissociation of bound analyte. Finally the surface is regenerated before a baseline is re-established and the sequence may be repeated.

2.7 Cyclic Voltammetry

The earliest examples of cyclic voltammetry can be traced back to the 1980's, with examples of being published by Armstrong-James et al as early as 1981. Although the presentation of data is different when compared to contemporary methods, the essential details of the experiment are present.[218] Later this technique was used by Millar and co-workers to quantify biologically relevant compounds, primarily for neuroscience research applications.[219]

The typical cyclic voltammetry experiment involves applying a potential to a working electrode which changes over time. Over the course of the experiment the potential is swept reversibly between E1 and E2, resulting in a triangular potential cycle as shown in Figure 41.[220]

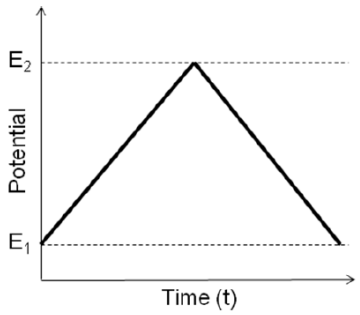

Figure 41: The wave form of the potential applied to the working electrode over the course of a cyclic voltammetry experiment.

Over the course of the experiment, a graph is produced demonstrating the current flowing through the working electrode as a function of potential. This plot is known as a 'voltammogram' and an example of such as plot, for a single electron process, is shown in figure 16. The cyclic voltammogram produced can be used to detail a wide range of information about the electrochemical behaviour of the surface.[221] The peaks observed are due the oxidation and reduction of compounds being examined, as shown in Equation 7.

Eq. 7 a) Oxidation $A^- \rightarrow A + e^-$

b) Reduction $A + e^- \rightarrow A^-$

As the potential is swept, either the oxidation or reduction reaction is driven, producing the currents observed in the voltammogram due to the acceptance or liberation of electrons to or from the working electrode. In this example, it is assumed that the solution contains only a single electrochemical reactant. In the voltammogram displayed in Figure 42, the potential applied (V_1) is initially positive to ensure that the species of interest are completely oxidised as the experiment commences (A). The potential, V_1, is then swept from the initial voltage to lower values, until the the lower limit of the potentials to be examined is reached. During this processes, as the reduction potential ($-V^{red}_p$) of A is approached, the current will increase until a maximum value ($-i^{red}_p$) is observed depicting

the reduction of A to A–. following this peak, the current will be observed to reduce as the concentration of A is depleted close to the electrode surface (V_2), thus reducing the rate of electron transfer.

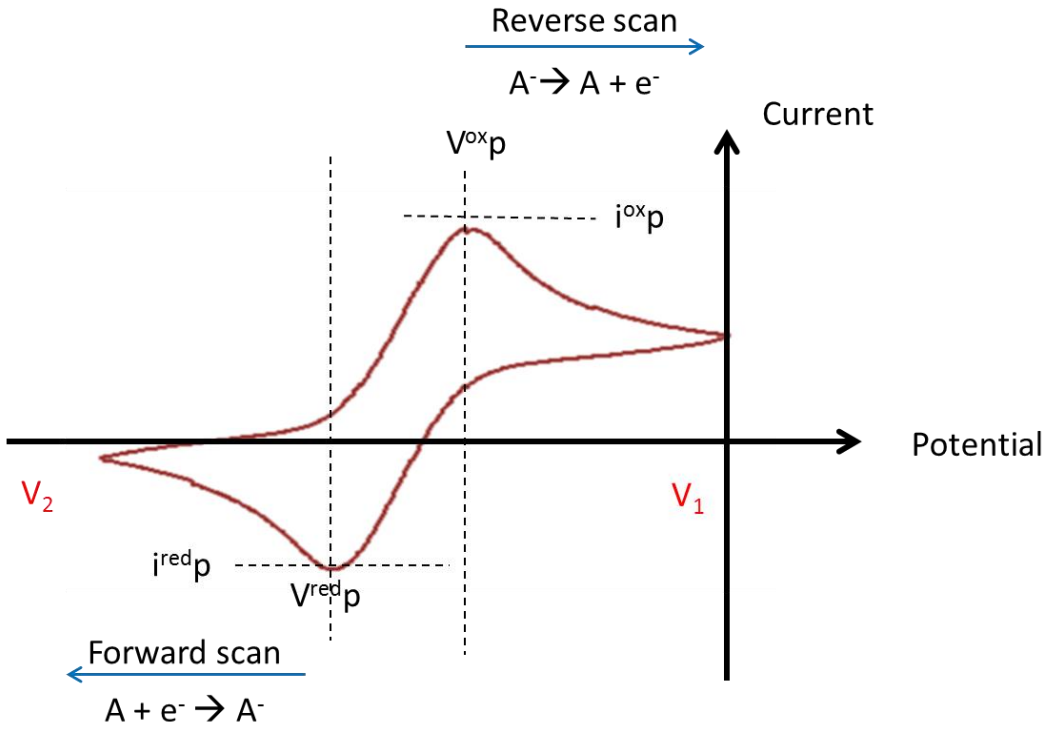

Figure 42: A typical voltammogram produced by cyclic voltammetry. See text for detailed discussion.

If the electrochemical process being investigated is chemically reversible, when the applied potential sweep is reversed, it will reach a potential (V^{ox}_p) that will re-oxidise A^- to A, producing a current of reverse polarity from the forward scan (i^{ox}_p) caused by the transfer of electrons back from the electroactive species to the working electrode. Typically, this oxidation peak will have a comparable shape to the reduction peak. As a result, information about the redox potential and electrochemical reaction rates of the compounds is obtained.[221]

CHAPTER 3: GLUCOSE SELECTIVE SPR-BASED *BIS*-BORONIC ACID SURFACE SENSOR

This chapter is based on the manuscript "Glucose selective Surface Plasmon Resonance-based *bis*-boronic acid sensor" Stephenson-Brown, A. Wang, H. C. Iqbal, P. Preece, J. A. Long, Y. Fossey, J. S. James, T. D. Mendes, P. M. *Analyst*, 2013, **138**, 7140-7145

Saccharides – a versatile class of biologically important molecules – are involved in a variety of physiological and pathological processes, but their detection and quantification is challenging. Herein, we describe the fabrication of a glucose selective surface sensor. This sensor employs self-assembled monolayers on gold generated from a *bis*-boronic acid bearing a thioctic acid moiety, whose intramolecular distance between the boronic acid moieties is well defined. Using surface plasmon resonance, we are able to reveal this surface demonstrates a higher affinity towards glucose than other saccharides probed, namely D-galactose, D-fructose and D-mannose.

3.1 Introduction

Carbohydrates play a vital role in a great number of varied and functionally diverse biological processes ranging from cellular recognition to respiratory metabolism (Figure 43). The monosaccharide glucose is a universal nutrient preferred by most organisms and serves fundamental roles in energy supply, carbon storage, biosynthesis and cell wall formation.[222-224] However, in humans, the aberrant control of glucose metabolism leads to the condition of diabetes mellitus, a chronic and potentially debilitating disease, which is estimated to affect 2.8% of the global population- a figure expected to rise to 4.4% by 2030.[17] Delayed detection and poor control of blood glucose in sufferers is correlated with poor clinical outcomes and increased risk of co-morbidities. Thus; to reduce complications, improve patient management and quality of life; the sensitive, timely and selective methods of glucose measurement are required to improve diagnosis and management of disease.

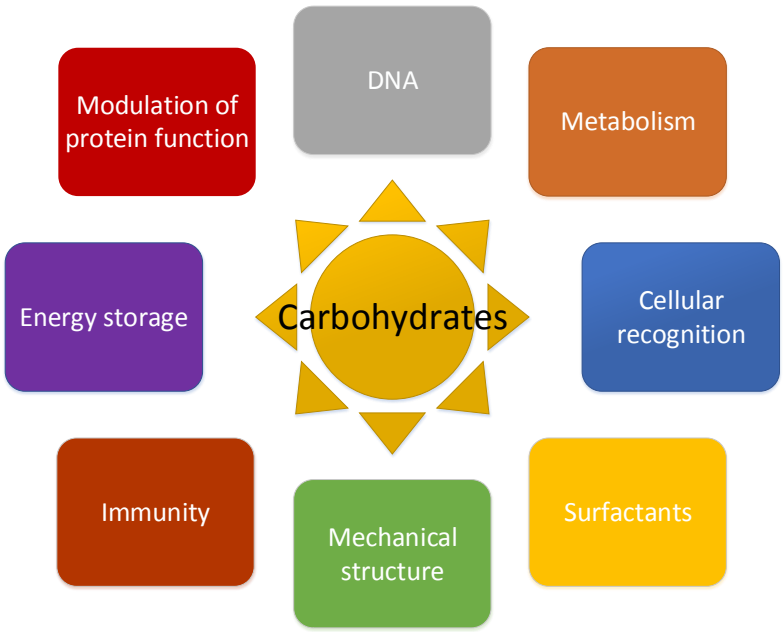

Figure 43: The varied and central role played by carbohydrates in living systems. Carbohydrates are involved in fundamental processes such as energy and information storage, recognition and immunity, and mechanical applications such as cell wall formation and maintenance of structural integrity in their roles as surfactants.

Despite quantitative analysis and detection of saccharides and saccharides-containing biomolecules being of paramount importance, reliable and accurate non-enzymatic sensors are not widely available.[225] The development of convenient, rapid and precise glucose monitoring systems has been studied extensively. The majority of clinically applicable glucose sensors used today are enzyme based and utilise glucose oxidase to catalyse the transformation of glucose to gluconolactone, producing H_2O_2 as a co-product.[226] This reaction has been exploited by several detection strategies, including electrochemical peroxide measurement where, at a constant voltage, the current generated across the electrochemical cell is proportional to the concentration of hydrogen peroxide, which is in turn proportional to the glucose.[11] Other methods used have included monitoring changes in mechanical and optical properties of polyelectrolyte gels induced by glucose oxidation, and subsequent changes produced in the gels ionic environment.[227, 228]

Despite their widespread use, enzyme-based sensor systems for glucose often suffer from a number of limitations. Notably, they result in the consumption of the analyte of interest from samples, can be dependent on local oxygen concentrations and, like all proteins, are poorly heat stable and prone to reduced activity over time owing to loss of functional enzyme due to denaturation.[229] Due to these limitations, there is a drive towards non-protein dependent systems, which harbour the potential for vast improvements to current glucose monitoring technologies.[230]

One group of compounds which is well suited to this challenge is boronic acids, which are able to readily and reversibly form cyclic boronate esters with diols in aqueous basic media (Scheme 2). [59-64] Since saccharides contain 1,2- and 1,3-diol units, they provide an ideal structural framework for binding to boronic acids.[231] It is this property which in recent years has led to a growing interest in the development of detection and sensor

systems that employ boronic acid groups as “synthetic lectins”.[60, 225, 232-236] The most favoured class of boronic acid-based sensors utilise an amine group proximal to a phenylboronic acid group, in which the Lewis acid–Lewis base interaction between the boronic acid and the tertiary amine enables the formation of boronate esters to proceed at neutral pH.[61, 62, 235] However, interactions between phenylboronic acids and saccharides are generally of limited selectivity and typically display a high affinity for fructose over other monosaccharides.[64, 237]

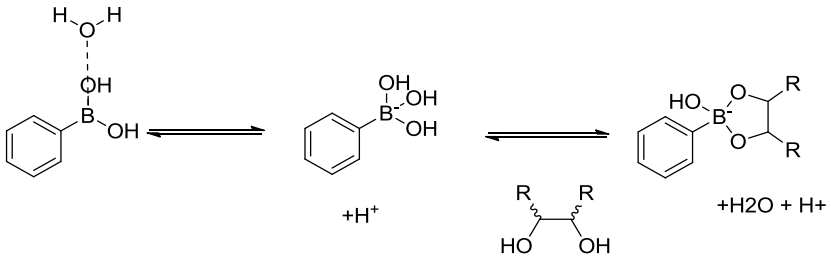

Scheme 2 The overall interaction between boronic acids and diols.

The difficulty posed by the selective identification of monosaccharides becomes more obvious when their structures are examined. The chemical structures of the monosaccharides fructose, glucose, mannose and galactose are shown in Figure 44. Inspection of these structures leads to the realisation that, in fact, all these compounds are simply isomers of each other; each molecule containing the same chemical functionalities; 6 carbons, 5 hydroxyl groups and 1 carboxyl group. Glucose, mannose and galactose all contain a terminal carboxyl group, leading to them being termed aldoses due to this aldehyde group. In contrast, fructose contains an internal carboxyl (ketone) group, and thus is known as a ketose. The structures of glucose, mannose and galactose differ only in the position of the hydroxyl groups in the molecules, thus these compounds are known as diastereoisomers.[6]

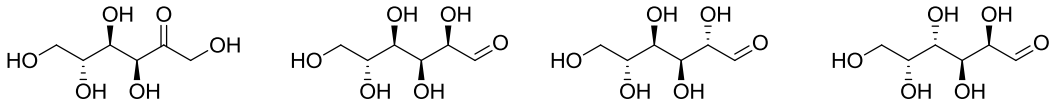

Figure 44: The chemical structures of the monosaccharides using in this investigation.

In addition to the open chain form, monosaccharides are able to form one of four ring structures,(α-pyranose, β-pyranose, α-furanose, and β-furanose). The distribution of these structural forms in solution is in dynamic equilibrium: Cleavage of the hemiacetal ring causes interconversion between the pyranose and furanose ring forms, via an acyclic intermediate. [11] This process, termed mutarotation, can occur over a time scale of minutes and leads to a mixture of five forms. The distribution frequency of each form is typical for each monosaccharaide species. This non-uniform distribution is thought to partially explain the differences observed in the affinities of boronic acids to different monosaccharide species, for example an increased affinity to monosaccharides which display a preference to the furanose forms, such as fructose (Table 2). [5]

Saccharide (Structure)	Relative percentage (%)	$K_{obs(}dm^3\ mol^{-1)}$
D-glucose (β-D- glucofuranose)	0.14	110
D-mannose (β-D- mannofuranose)	0.3	170
D-galactose (α-D- galactofuranose)	2.5	280
D-arabinose (β-D- arabinofuranose)	2	340
D-fructose (β-D- fructofuranose)	25	4400

Table 2 Relative abundances of the furanose form and stability constants observed with phenylboronic acid for a selection monosaccharides. One can observe that as the abundance of the furanose form increases, so does the stability of complexes formed between the monosaccharides and phenylboronic acid[11]

The large proportion of fructose in the furanose form goes some way in to explaining the high affinity for fructose displayed by boronic acids. However, despite this preference for fructose, it has been demonstrated that by employing two intramolecular phenylboronic acid receptor units, selectivity in favour of other monosaccharides may be achieved.[77]

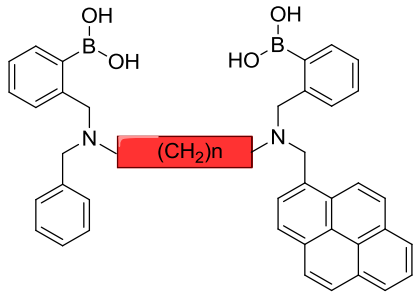

Figure 45: The structure of the modular *bis*-boronic acid sensor compound. The length of the carbon linker can easily be controlled.

By using a modular design (Figure 45), it is possible to control the length of the carbon chain used to link the two boronic acid units, making it possible to optimise the saccharide selectively. Using such techniques it has been demonstrated that glucose selectivity may be achieved using a six carbon linker unit (Figure 12).[79]

The mechanism of the selectivity towards glucose was therefore demonstrated to be due to the ability of the *bis*-boronic acid (*bis*-BA) binding motifs to form complexes using multiple sets of diols present on a single glucose molecule forming stable cyclic 1:1 complexes, such as those shown in Figure 46a. This mechanism of binding results in the glucose complex displaying a higher stability than other saccharides such as fructose, galactose and mannose.[61, 238] Additionally, there have been investigations, using a closely related sensor compound, which suggest that the exact mechanism of this interaction is further complicated by a transformation of the bound glucose to its furanose ring form resulting in binding occurring between all five glucose hydroxyl groups (Figure 46b). The speed of this effect is affected by solvent conditions, but is observed to occur almost instantly in the presence of water. [239]

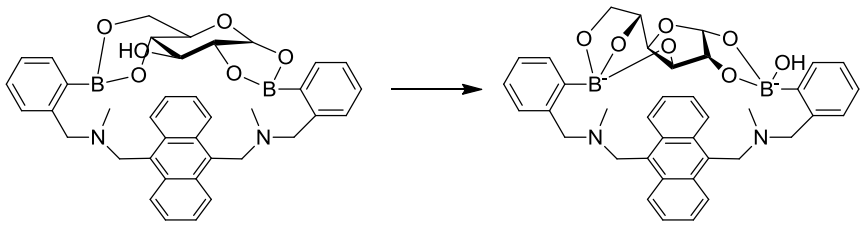

Figure 46: The proposed transformation of glucose from the pyranose form to the furanose form, upon binding to the *bis*-boronic acid compound shown. [239]

3.1.1 Our approach

While investigations such as those outlined in the previous section have been incredibly useful to provide insight into the mechanisms at work, such sensors have some limitations which hinder their application. One of the most problematic aspects of the molecular structures which make up these sensors is their solubility- The large aromatic structures present in such molecules, while elegant in their ability to provide fluorophores, mean that the sensors are poorly soluble in aqueous conditions. Furthermore, when in the solution phase, it is difficult to recover the sensor compound following analysis.

In order to facilitate the development of a surface sensor system, the modular *bis*-boronic acid (*bis*-BA) sensor was adapted to contain a disulphide group, to allow surface attachment (Figure 47). The design and synthesis of this compound was carried out by collaborators in the group of Prof. Tony James at the University of Bath. Details of the synthesis of this compound, including characterisation, can be found in a recent publication by Wang et al.[240]

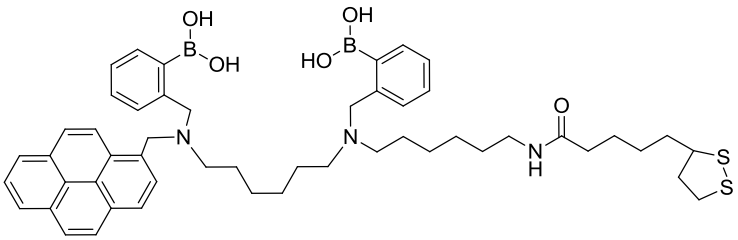

Figure 47: The *bis*-BA molecule. The two boronic acid groups are separated by a six carbon linker, which should favour glucose interactions. The molecule also contains a disulphide group to allow surface attachment.

This chapter will describe the design and fabrication of a glucose selective surface sensor, using the aforementioned *bis*-BA species as the glucose binding unit. The strategy employed takes advantage of the principle of self-assembly to form the sensor surface and can successfully monitor binding events with the need for labelled analytes by employing surface plasmon resonance (SPR) spectroscopy to detect and measure the relative binding of analyte to the surface.

3.1.1 Motivation for Label Free Detection

In order for a sensor system to be useful in 'real world' scenarios, it is desirable that it is able to function without the need for labelled targets to be produced. The modular *bis*-boronic acid was designed to function as a fluorescent sensor; binding of diols to the boronic acids groups results in increased fluorescence.[79] Unfortunately, such a strategy could not be used with surfaces such as gold due to its optical absorption of electromagnetic energy over the both the excitation and emission wavelengths of the fluorophore.[241] However, there are a number of technologies which are well suited to the production of surface sensors and able to monitor molecular interactions. One such technology is SPR spectroscopy.

3.2 Sensor Surface Design

Although in solution, previous works have demonstrated that the *bis*-boronic acid binding site is able to selectively bind glucose, surface attachment of the group can lead to undesirable effects such as steric hindrances.[242] Fortunately, by employing co-surfactants to act as spacers such problems can be minimised.[243] In addition, by careful choice of co-surfactant, it is possible to produce surfaces which have properties more suited for aqueous biological sample types, and should avoid the need for the use of other solvents such as methanol, as has been previously described for this type of sensor.[238] Therefore we chose to use a tri(ethylene glycol)-terminated thiol (TEGT) compound for use as a co-surfactant (Figure 48). TEGT has been previously demonstrated to be suitable to space out surface components to reduce steric hindrance and also inhibit the non-specific binding of proteins to modified surfaces.[130]

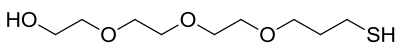

Figure 48: The structure of the TEGT molecule.

The functional sensing surface was fabricated by formation of a two-component, mixed SAM on a gold surface (Figure 49a). One of the components of the SAM is the previously described *bis*-BA derivative (separated by a six-carbon linker) which now bears a thioctic acid appended unit for binding to the gold surface.[231] A TEGT, described previously, was used as the second SAM component to ensure adequate separation between adjacent *bis*-BA on the surface, and eliminate the possibility of neighbouring boronic acid groups inhibiting saccharide binding or selectivity.[130] In addition a control surface was also produced in the same manner but with a non-active compound (diamine) in place of the *bis*-BA (Figure 49b). The control molecule was structurally similar to the *bis*-BA molecule except for the absence of the phenylboronic acid moieties.

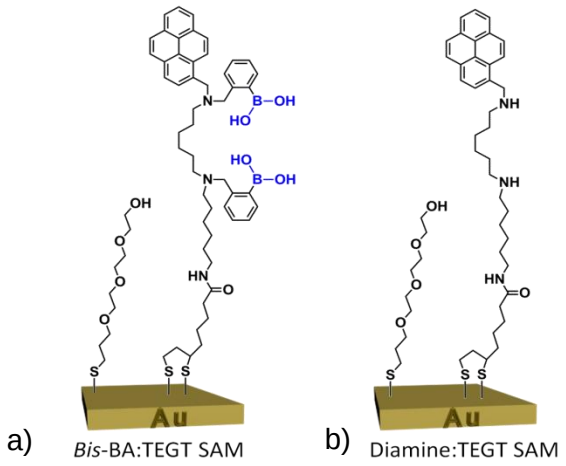

Figure 49: a) Two-component, mixed SAM formed from a *bis*-BA derivative and a TEGT-terminated thiol. b) A control surface produced from a two-component mixed SAM, of diamine and TEGT molecules. The diamine compound lacks the phenylboronic acid moieties but otherwise has the same structural back bone.

3.3 Results and discussion

3.3.1 Kinetics of SAM formation

3.3.1.1 Contact angle

In order to produce the desired surfaces, the first step was to investigate the kinetics of SAM formation using both the TEGT and the *bis*-BA surfactants individually. This was accomplished by conducting contact angle and ellipsometry at various time points over a 48 hour period. In order to form the SAMs at the indicated time intervals cleaned gold substrates were placed in methanolic solutions of each surfactant for the specified time. Gold chips were cleaned by immersion in piranha solution for 10 minutes, before being rinsed with liberal amounts of water for 1 minute, and then rinsed with HPLC grade methanol for a further minute. Following immersion in the SAM solution for the specified time, the chips were removed and rinsed with pure HPLC grade methanol, to 'quench' the SAM formation. Dried samples were then analysed by contact angle and ellipsometry. The results of these investigations are presented in Figure 50.

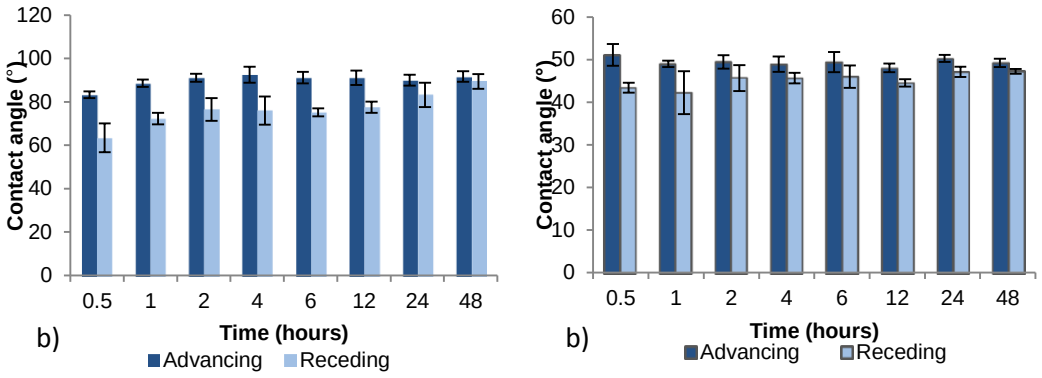

a) b)

Figure 50: Kinetics of SAM formation, investigated by water contact angle on a) *bis*-BA SAMs and b) TEGT SAMs. Formation kinetics were monitored over the following time points; 0.5, 1, 2, 4, 6, 12, 24 and 48 hours. Measurements were taken in triplicate, error bars indicate standard deviations from the mean.

The results obtained are consistent with a full monolayer being formed after around 24 hours of incubation for *bis*-BA (Figure 50a), and after 4 hours of incubation for TEGT monolayers (Figure 50b). The data suggests that SAM formation for the *bis*-BA molecule proceeds at a slower rate than for the TEGT.

Inspection of the advancing contact angle reveals that *bis*-BA SAM reaches a maximum contact relatively quickly indicating that adsorption of *bis*-BA surfactant occurs in a short time. The processes of SAM formation can be investigated further by examination of the hysteresis between the advancing and receding measurements- a large hysteresis is considered a sign of SAM disorder.[244] It can be seen that over a 24 hour period, the receding contact angle increase while the advancing contact angle remains relatively constant. The net result is a decrease in hysteresis, consistent with an increase in order of the SAM, which finally falls to around 5° after 24 hours. This distinct two- phase SAM formation is in agreement with literature on the mechanism of SAM formation. [100, 101]

A similar effect is observed for TEGT SAMs; the advancing contact angles quickly reach a static value, while receding angles take longer to become consistent. The pattern of

formation is similar, however, the time taken for this to happen is considerably shorter for the TEGT SAM. This observation is likely due to the more complex, bulkier structure of the *bis*-BA compound, which will act to increase steric hindrance on the surface resulting in a longer period of disorder before the SAM structure becomes stable. In contrast, the relatively simple structure of TEGT should lead to reduced hindrances and therefore an increased rate of adsorption and surface organisation.

3.3.1.2 Ellipsometry

Ellipsometry measurements appear to support the conclusions drawn from the contact angle investigations. For TEGT a steady film thickness is reached within 2 hours while the thickness of *bis*-BA monolayers remains unstable until 4 hours, when it begins to stabilise (Figure 51a and 51b). The larger error associated with these measurements may be due to a large degree of heterogeneity present on the surface. This hypothesis would appear to be in consensus with the observed contact angle data. The measurements also demonstrate that there is no formation of double layers which can be a potential pitfall for SAMs with hydrogen bonding groups.[245] The pattern of change in the measured thickness of each SAM can be attributed to the time-dependant changes in the organisation of the adsorbed molecules These observed changes are in good agreement with the result of our own contact investigations and there are reports of similar phenomena in the literature. [246]

The final measured thicknesses of the surfaces, along with calculated theoretical values for each SAM type are outlined in Table 1. It is notable that the measured values are lower than the calculated values. However this is not surprising given the tilt observed for thiol SAMs on gold and the fact that the molecules are unlikely to adopt a completely stretched out conformation on the surface (for example, TEGT is known to adopt a non-extended conformation). [247] In addition, a control surface was also produced using a ‘diamine’ compound which was the same as the sensor compound but without the two

boronic acid groups (Figure 50). For the diamine molecule, similar results to *bis*-BA surface were observed.

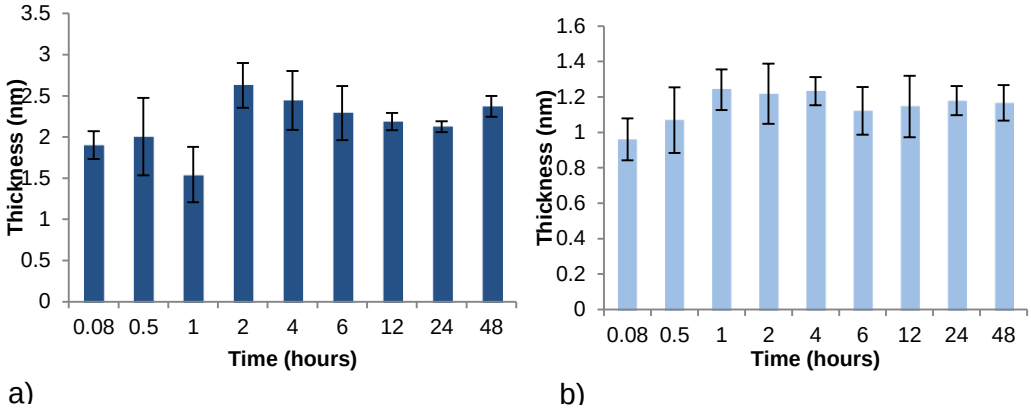

Figure 51: Kinetics of SAM formation ellipsometry data from a) *bis*-BA SAMs and b) TEGT SAMs . Formation kinetics were monitored over the following time points; 0.8, 0.5, 1, 2, 4, 6, 12, 24 and 48 hours. Measurements were taken in triplicate. , error bars indicate standard deviations from the mean.

3.3.2 Formation of Mixed SAMs

Following contact angle and ellipsometric characterisation of the pure SAMs, studies were conducted to optimise a *bis*-BA:TEGT SAM ratio of 1:1 on the gold surface. This optimum ratio should enable maximum sugar binding capacity while avoiding steric hindrance from neighbouring *bis*-BA molecules in the SAM.[130]

SAM	Contact Angle (°)		Thickness (nm)	
	Advancing	*Receding*	*Theoretical* [a]	*Experimental*
***Bis*-BA**	90.0 ± 2.5	83.3 ± 5.6	3.61	2.12 ± 0.12
Diamine	85.4 ± 2.1	79.1 ± 3.2	3.61	2.35 ± 0.23
TEGT	50.3 ± 1.8	47.1 ± 2.1	1.66	1.17 ± 0.11
1:1 *Bis*-BA:TEGT	77.8 ± 1.5	64.2 ± 3.9	-	2.17 ± 0.35
1:1 Diamine:TEGT	69.4 ± 0.7	60.4 ± 3.0	-	2.10 ± 0.34

[a] Theoretical thickness was determined using ChemBio 3D Ultra 11.0

Table 3 Advancing and receding water contact angles and ellipsometric thickness values for the different SAMs formed for 24 hours.

As reported in previous literature, when producing mixed SAMs, the ratio of two-components in solution are rarely identical to those observed in the SAM, due to the preferential adsorption of one of the components.[237, 248, 249] Thus, systematic studies were carried out in order to understand how the ratios of SAM components in solution diverge from the ratios in the formed SAM. A simple method of quantifying this was to use the relationship proposed by Cassie[250] which relates the contact angle of a surface of mixed composition to those of pure SAMs (Equation 8).

Eq. 8 $$\cos\theta_{Adv} = x\cos\theta_{Adv1} + y\cos\theta_{Adv2}$$

Where θ_{Adv} is the water advancing contact angle on the mixed SAM, θ_{Adv1} and θ_{Adv2} are the contact angles related to the pure SAMs formed from *bis*-BA and TEGT, respectively, and x and y are their corresponding surface molar ratios (x+y=1). Contact angles measured on mixed SAMs formed from different solution concentration ratios of *bis*-BA and TEGT (1:1, 1:5, 1:10 and 1:40) suggest that the *bis*-BA and TEGT components are adsorbed at different rates. An examination of the calculated ratios demonstrates that with an equimolar concentration in solutions SAMs are formed with an excess of the *bis*-BA component on the surface. This suggests that the *bis*-BA compound is adsorbed in preference the TEGTs compounds (Figure 52). Indeed, this trend is observed across all the ratios investigated.

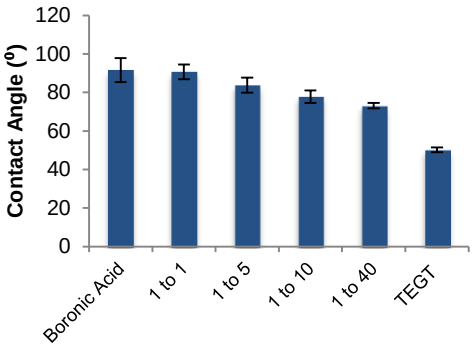

Figure 52 Water contact angles observed on mixed SAMs formed from various solution ratios. The contact angles suggest that the *bis*-boronic acid compound is adsorbed in preference the TEGTs compounds. , Error bars indicate standard deviations from the mean.

Using Equation 8, molar ratios (*bis*-BA:TEGT) in the SAMs of 3:1 3:2, 1:1 and 2:3 were obtained respectively and are presented in Table 3. These results indicated that in order to produce the desired 1:1 *bis*-BA:TEGT SAM a solution ratio of components in a 1:10 ratio (*bis*-BA:TEGT) is required.

In order to ensure that the control surfaces were formed via the same dynamics, analysis of contact angles from pure diamine SAMs were examined along with SAMs formed from solution ratios of 1:10 (control :TEGT). The resulting mixed monolayers of the diamine:TEGT SAMs were found to have a contact angle of 77.8°. Using this data, calculations of the surface composition were conducted using the Cassie equation. Surfaces formed from a 1:10 control:TEGT solution were found to have a 1:1 surface ratio, suggesting that the mechanism of SAM formation is the same for both molecules despite the absence of the phenyl boronic acid groups on the control compound.

Ratio of components in Solution (Boronic acid: TEGT)	Calculated Ratio of components on surface (Boronic acid: TEGT)
Pure Boronic Acid	1:0
1 to 1	3:1
1 to 5	3:2
1 to 10	1:1
1 to 40	1:2
Pure TEGT	0:1

Table 4 The calculated surface ratios of mixed SAMs formed from mixed solutions of *bis-boronic acid and TEGT of known component ratio.* The indicated surface ratios of SAM components were determined using the Cassie equation

As shown in Table 4, and consistent with a mixed monolayer, the 1:1 *bis*-BA:TEGT and 1:1 diamine:TEGT SAMs exhibited contact angle and thickness values between those of the pure monolayers. Furthermore, the heterogeneity of the surface due to the presence of both molecules, either *bis*-BA and TEGT or diamine and TEGT, has led to a greater contact angle hysteresis on the 1:1 mixed surfaces than on the pure monolayers.

3.3.3 X-ray Photoelectron Spectroscopy (XPS)

Following the characterisation of the surfaces using the ellipsometry and contact angle goniometry XPS was used to investigate the elemental composition of the surfaces. XPS confirmed the formation of pure and mixed SAMs, showing expected signals from C (1s), O (1s), B (1s) and S (2p). High resolutions scans of the boron and nitrogen regions for each surface are presented in Figure 53, while sulphur and carbon spectra are presented in Figure 54. High-resolution scans of the N (1s) and B (1s) regions (Figure 53) confirm the presence of nitrogen and boron on the pure *bis*-BA SAMs and *bis*-BA:TEGT mixed SAMs. As expected, no boron peaks were observed in the mixed diamine:TEGT SAMs. XPS also confirmed the absence of nitrogen and boron on the pure TEGT SAM.

For both a pure *bis*-BA SAM and *bis*-BA:TEGT mixed SAM, the B (1s) spectra display a peak at 192 eV, which is consistent with the values reported for other boronic acid derivatives.[251] The N (1s) spectra can be deconvoluted into two peaks, the first one,

centred at 400.2 eV, is characteristic of amide and amine moieties, while the second peak, centred at 402.0 eV, is attributed to protonated amino groups.[252, 253] This finding is not surprising given the structure of the *bis*-BA molecule. Previous studies have observed that the pyrene group is able to promote the protonation of the adjacent nitrogen groups.[254] In addition, the mildly acidic nature of the methanol used as a SAM solvent could facilitate the protonation of the *bis*-BA and diamine molecules observed.

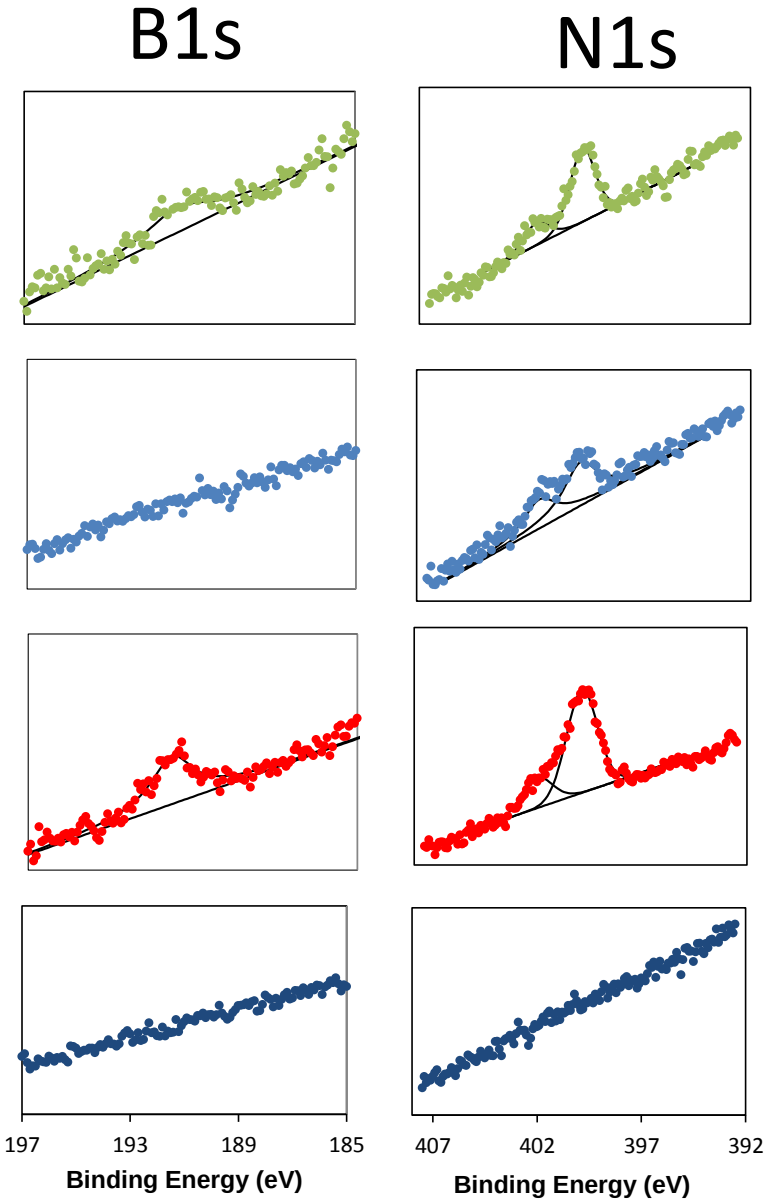

Figure 53 XPS Spectra of B (1s) and N (1s) from pure *bis*-BA: TEGT (green), diamine: TEGT (light blue), pure *bis*-BA (red), pure diamine (maroon) and pure TEGT SAMs (navy blue).

With the XPS analysis, the ratio of *bis*-BA:TEGT and diamine:TEGT on the mixed SAM can be further calculated. By integrating the area of the S (2p) and N (1s) peaks for the mixed monolayers, a S:N ratio of 1:1 was obtained. Since both, the *bis*-BA molecule and the diamine compound, consist of 3 N atoms and 2 S atoms and TEGT has no N and 1 S atom only, a S:N ratio of 1:1 corresponds to a ratio of 1:1 of *bis*-BA: TEGT and 1:1 of diamine:TEGT on the mixed SAM. Thus, the surface ratio determined by XPS is in close agreement to that determined using the Cassie equation.

Upon examination of the carbon spectra from the various surfaces it is also possible to observe differences between the different surfactants used. The TEGT SAM shows a major peak at 286.5 eV, with another considerably smaller peak at 284.6 eV. This pattern of splitting has been reported before with such compounds and can be explained due to the two carbon types in the TEGT molecules.[255] The carbons involved in ester bonds, C-O, are known to exhibit a higher binding energy and therefore can be assigned the peak at 246.5 eV, while the reaming peak at 264.6 eV can be assigned to the alkane, C-C, carbons.[256]

In contrast, the carbon spectra for the pure *bis*-BA SAM shows a major peak at 284.9eV. The major peak is the signal from carbon-carbon bonds, which is expected given the structure of the *bis*-BA molecule. This major peak can be fitted to contain two peaks centred at 285 eV and 284.7 eV which represent aromatic and aliphatic carbons, respectively. The ratio of these components was calculated to be 1.26 (aromatic: aliphatic) and found to be very close to the predicted ratio of 1.22. [257] In contrast the minor peak is due to the carbonyl, C=O, groups present in the molecule. [258]

The carbon spectra for the diamine SAM was found to be quite similar to the *bis*-BA SAM, however the results of fitting demonstrate that the ratios of the aromatic: aliphatic carbons are different. This is expected given the loss of the phenyl boronic acid groups. The ratio

of these carbon types was found to be 0.73 which is in close agreement to the predicted ratio of 0.76.

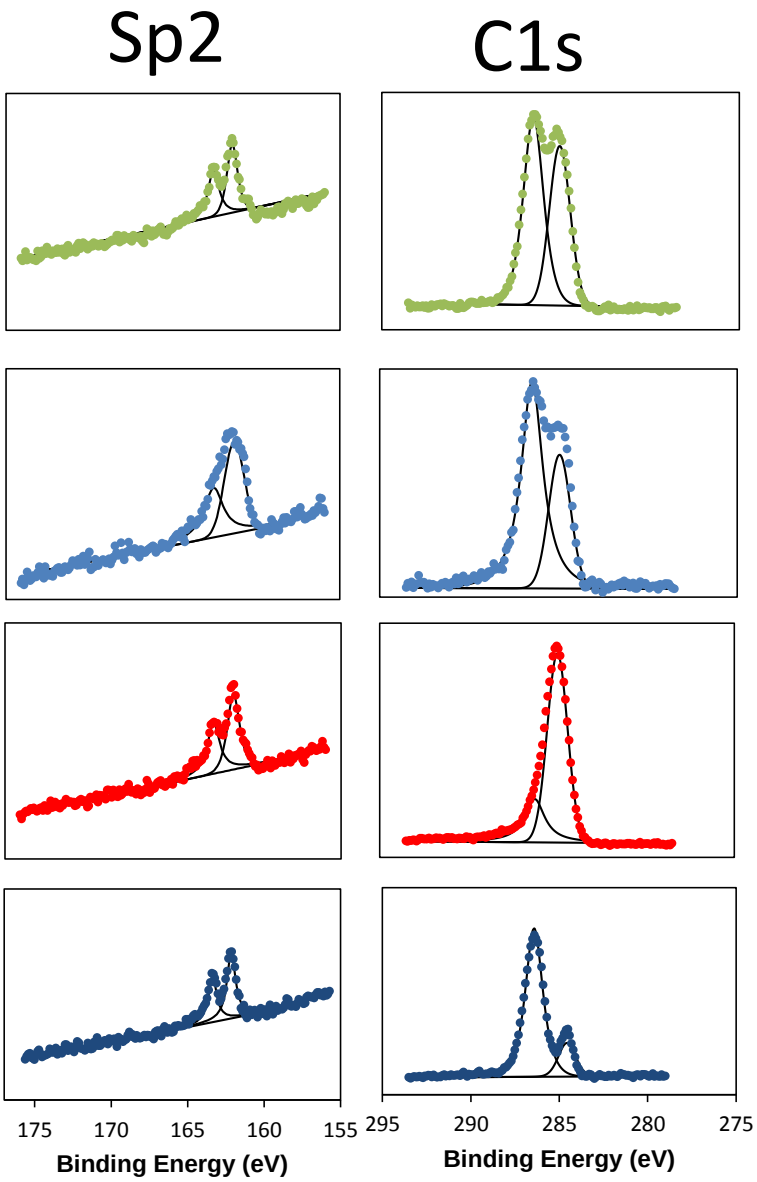

Figure 54 XPS Spectra of S (2p) and C (1s) from pure *bis*-BA: TEGT (green), diamine: TEGT (light blue), pure *bis*-BA (red), pure diamine (maroon) and pure TEGT SAMs (navy blue).

The different energies in the major carbon peaks observed for the TEGT and *bis*-BA surfaces is also useful for confirmation of the composition of the mixed SAMs, as the mixed SAM displays to large signals at 285eV and 286.5eV which correspond to the C-C and C-O chemical groups

respectively. The same is observed in mixed SAMs of diamine and TEGT, however here there is a relative drop in the signal from aromatic carbons which is consistent with the expected chemical composition of the surface.

3.4 Detection of Saccharide Binding *via* SPR

Following the characterisation of the modified-gold surfaces, attention was turned to the investigation of the saccharide binding ability of the 1:1 *bis*-BA:TEGT SAM surfaces. Measurements of the interaction between either glucose, galactose, fructose or mannose and 1:1 *bis*-BA:TEGT SAMs was performed by SPR. Different concentrations of saccharides (0.6 mM, 1.25 mM, 2.5 mM, 5 mM, 10 mM and 20 mM) in PBS solution were used. The concentration range of saccharides was chosen to reflect the range of blood glucose concentrations observed in healthy and diabetic patients. While the definition of a clear diagnostic cut off has proven to be divisive within the medical community, healthy adults would be expected to have a blood glucose level of around 4 mM, while diabetes is commonly diagnosed when blood glucose levels are raised above 7 mM.[259] Each saccharide solution was injected over a mixed *bis*-BA:TEGT surface for 5 min to reach equilibrium, followed by a dissociation phase with only PBS buffer flowing over the chip (Figure 55). It should be noted that for each saccharide all six curves presented in figure 13 were performed using the same SAM surface. After the dissociation phase the chip was regenerated for 2 min with an acidified (pH=5) 3:1 (v/v) ethanol:PBS solution to ensure that all bound saccharide was removed from the surface. Regeneration was verified by a return to the baseline established prior to each run.

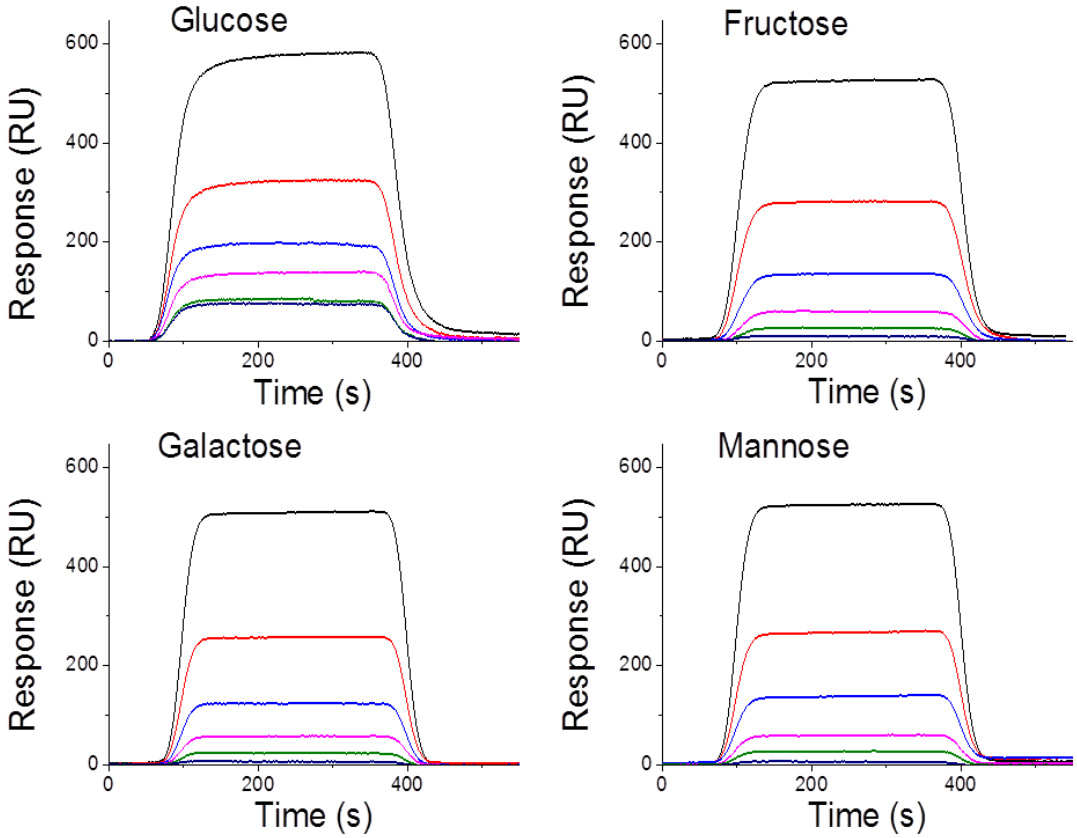

Figure 55. SPR kinetic measurements showing the binding of D-glucose, D-galactose, D-fructose and D-mannose to 1:1 *bis*-BA:TEGT SAMs using different saccharide concentrations (0.6 mM, 1.25 mM, 2.5 mM, 5 mM, 10 mM and 20 mM). Measurements taken at 297 K.

When considering the SPR data, all hexose sugars exhibited clear concentration dependent-responses, although the intensities differed among the individual sugars. Across all concentrations, glucose produced the largest change in SPR response. To derive affinity binding constants for the interaction between the immobilised boronic acid moieties and the different saccharides in solution, equilibrium analyses were utilised because they avoid problems resulting from mass transport limitations.[260] In order to correct for bulk refractive index contributions arising from the differing buffer composition and some possible nonspecific binding to the *bis*-BA:TEGT SAMs, SPR responses from the control mixed diamine:TEGT were subtracted from those obtained from the *bis*-BA:TEGT SAMs. The corrected SPR responses at equilibrium (R_{eq}) were plotted against

the concentration of injected saccharide (C_S) (Figure 56) and fitted to a 1:1 steady-state affinity model. The model utilises a nonlinear least-squares regression method to fit data to the Langmuir adsorption isotherm (Equation 9). K_D is the dissociation constant of the BA-sugar complex and R_{max} is the maximum response if all available BA binding sites are occupied. The calculated K_D were inversed, to give the association constant, K_A, to allow comparison with data obtained previously from solution. [231] These values are presented in Table 4.

Eq. 9 $$R_{eq} = \left(\frac{C_S}{C_S + K_D}\right) R_{max}$$

The K_A results illustrate that the surfaces exhibit a higher affinity for glucose, with a comparatively reduced affinity to other hexose sugar isomers, including over double the affinity for glucose compared to fructose (Table 5). These results are comparable with stability constants (K_{OBS}) previously observed in solution, producing the same orders of saccharide binding affinities as previously determined. While the absolute values differ this is likely to be caused by the different steric constraints imposed by the surface attachment.

Saccharide	Surface K_A (M^{-1})	Solution K_{OBS}/M^{-1} [231]
D-Glucose	203.25(6) [a]	962
D-Fructose	95.2(1)	784
D-Galactose	33.9 (4)	657
D-Mannose	22.9 (7)	74

[a] Values in parentheses are standard deviations (S.D.) on the last significant figure.

Table 5 Table showing calculated K_A values for each saccharide. Solution stability constants, K_{OBS} are included for reference.

The affinity to glucose of the surface is comparable to some biological glucose ligands which have been previously investigated; for example, bacterial binding proteins utilised in an SPR based sensor have been found to have similar affinities for glucose.[261]

Furthermore, the sensor produced here displays a sensitivity range which is useful to a clinical setting, unlike previously described sensors which have been only useful over much lower saccharide concentrations before the surface becomes saturated.

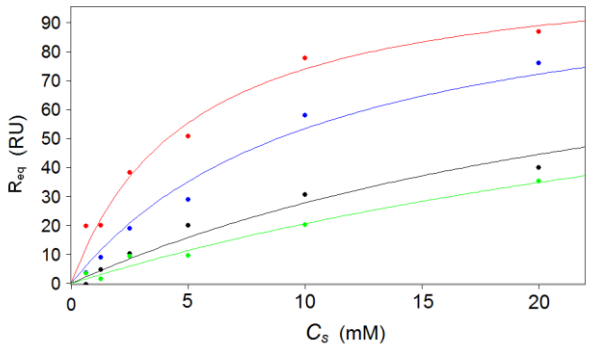

Figure 56 Calibration curve of control subtracted SPR response change for *bis-BA* sensor vs glucose (red), fructose (blue), galactose (black) and mannose (green) (0.6 mM, 1.25 mM, 2.5 mM, 5 mM, 10 mM 20 mM).

The results demonstrate that the surfaces are able to produce a dynamic detection range over the clinically relevant concentrations of saccharides analysed (Figure 56). Although a response from the other hexose isomers is observed, the impact on glucose measurements in clinical samples would be minimal as glucose is by far the most prevalent saccharide found in blood and other bodily fluids (typically found in concentrations orders of magnitude greater than other saccharides).[222]

3.5 Conclusions

In summary, we have demonstrated for the first time, through the marriage of supramolecular design and surface modification the fabrication of a glucose selective sensor surface is possible. Utilising an SPR detector system, the fabricated sensor is able to operate at clinically relevant saccharide concentrations. This offers a range of opportunities for the production of flow past sensors and also the utilisation in miniaturised systems.

This work also demonstrates the suitability of surfaces modified with synthetic receptors for biological molecules to function as sensor devices, when coupled to a suitable detection technique such as SPR. The surface attachment of the binding motifs is such as this *bis*-boronic acid is useful as such receptors have previously been effectively single use, due to the difficulty of separating sensor and analyte following detection. In addition, surface modification allowed for the use of co-surfactant to enhance the biological compatibility of the sensor compounds, which have previously been shown to be unsuitable for use in aqueous buffers, requiring high concentrations of co-solvents such as methanol which can affect the functions and structures of compounds such as proteins which would likely be present in biological samples.

It was observed that following the surface attachment of the compounds to the surface, there was an overall decrease in the affinity of the sensor to all saccharides compared to the previously reported solution based sensor compounds. This finding is likely due to the reduced degrees of freedom of the compounds following surface attachment, and the lower affinity likely to be caused by the steric hindrances induced by surface attachment. In addition, the change in buffer could have an impact on the rate of mutorotation of the sugars, which could also go some way to explaining the effect observed.[262] Despite this, the overall affinity behaviour of the compounds was found to be consistent with the solution based sensor.

In conclusion, the successful incorporation of *bis*-boronic acid receptor into a modified surface, and the demonstration of it selectivity towards the specific monosaccharide, glucose, provides evidence for the suitability of the use of boronic acids in surface sensors. In the following chapters, the use of boronic acids in the production of self-assembled synthetic sensors for the selective detection of glycoproteins will be discussed.

CHAPTER 4: SYNTHESIS AND CHARACTERISATION OF COMPONENTS FOR MOLECULAR IMPRINTED SURFACES

The post-translational modification of proteins is fast becoming recognised for the important role it plays in a great number of fundamental biological processes. In this process pre-synthesised proteins are augmented with additional groups such as sugars phosphates and lipids. However, at present, there are very few methods of detecting and quantifying post-translational modification of proteins in a fast, high throughput and cost effective manner. In this chapter the design, synthesis and characterisation of components of a novel system, along with subsequent surface reactions, for the production molecularly imprinted modified surface for the selective detection of glycoproteins will be described.

4.1 Introduction

Antibodies are currently widely used for the detection, quantification and purification of many proteins, toxins and small molecules.[263] They are employed as the site of molecular recognition in many commercially available assays, which commonly link binding events occurring at the antibody to a reporting mechanism such as fluorescent or enzymatic tags to facilitate the quantification of the analyte in question. The most common example of such technology is the now ubiquitous enzyme-linked immunosorbent assay or ELISA. However, the production of antibodies is an expensive and time consuming exercise and it is not without its limitations; the peculiarities of intracellular machinery, which is utilized in the commercial production of antibodies, is not ideally suited for the production of high affinity antibodies against carbohydrate based antigens.[264] In addition, as antibodies themselves are proteins, they are susceptible to degradation by conditions of high temperature, moderate change in pH and UV light.[265-268] For these reasons, a more robust synthetic alternative is highly sought after.

In this chapter, a novel method of molecular imprinting will be described. The method is based upon the design and fabrication of an imprinted surface which is able to distinguish between imprinted proteins and non-imprinted proteins to a high degree of selectivity. In addition, the surface also shows an ability to distinguish between glycosylated and non-glycosylated forms of proteins. The design of the sensor components allows for a high degree of flexibility in the chemical groups used to form the imprinted surface; using two surface cross-coupling groups affords the ability to separately control the introduction of functional groups within the surface, allowing the binding properties to be tuned to the target. In addition, as the imprint architecture is built on a monolayer system, common problems observed in larger molecularly imprinted surfaces and monoliths should be avoided.[171]

4.1.1 Chapter outline

This chapter will describe the production of a molecularly imprinted surface which is capable of selectively binding proteins. Furthermore, this surface is able to distinguish between glycosylated and non-glycosylated forms of the same protein.

The chapter will begin with an outline of the approach that will be implemented, outlining the strategy of how the molecularly imprinted surfaces will be created. Next, the design and synthesis of the novel compounds from which the molecularly imprinted surface are formed will be discussed. This will include an outline of the chemical techniques which can then be used to modify surfaces which are functionalised with our novel molecules.

In the next section, the ability of the novel compound to form self- assembled monolayers will be investigated. This will include analysis by a number of surface characterisation techniques, such as contact angle goniometry, ellipsometry and x-ray photoelectron spectroscopy. The following sections will the cover development of protocols for the modification of the surface via two distinct chemical groups. The success of these methods will then be assessed by surface characterisation techniques.

4.2 Our approach

A principle which underlies this work is that any methodology should be designed to be easily be tuned to the target compound, and that given the scale of most compounds, mechanisms of self-assembly should be utilised to build binding sites. SAMs on gold provide a well understood method of developing modified surfaces. Furthermore, a major advantage of preparing the recognition site on thiol-gold SAM surfaces is that the protein interactions with the recognition site may be monitored via optical, label free methods of detecting and quantifying binding, such as SPR.

Our approach to sensor generation is outlined in Figure 57. A ‘foundation’ self-assembled monolayer was prepared on gold surfaces, onto which the components of the molecular imprint structure can be grafted. The chemical groups within the SAM should allow the control of assembly of two distinct elements: boronic acids and oligo(ethylene glycol) chains, side by side. Boronic acids are able to form reversible interactions with the diol group, while the glycol groups provide both hydrogen bonds within the sensor cavity as well as an element of resistance to non-specific binding (NSB) of protein on non-imprinted areas of the surface. An advantage provided by the ‘foundation’ SAM approach is that it removes the risk of proteins interacting directly with the underlying gold substrate. This is potentially problematic as gold is known to catalyse the cleavage of disulphide groups with in proteins which leads to protein denaturation and can result in the covalent attachment of peptides to the gold surface via gold-sulphur bonds.[269, 270]

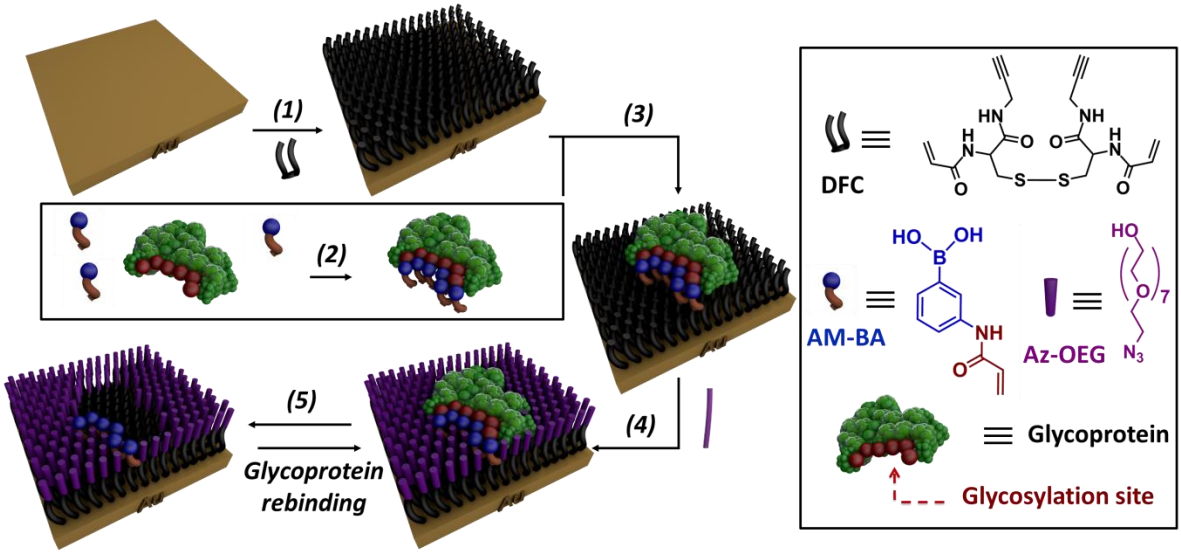

Figure 57: The overall approach can be divided into five distinct steps. 1) the formation of a foundation monolayer; 2) the interaction and formation of complexes between boronic acids and sugar groups of the target glycoprotein; 3) attachment of the target glycoprotein-boronic acid complex to the foundation monolayer; 4) attachment of glycol chains to the foundation monolayer around the target protein to produce a surface cavity; 5) removal of target protein to leave a vacant binding site.

4.3 SAM Molecule Design

In order to produce the desired imprinted surface, a suitable SAM molecule on to which the synthetic recognition platform could be built was required. In order for the method to be successful, the molecule would require three distinct functional groups; a group is needed to anchor the molecule to the surface and two more groups are required to build the imprint surface and also control the incorporation of other binding groups, such as boronic acids. In reality, as we wish to produce the synthetic recognition platform on a gold surface, we have to use a sulphur group for the anchor site. The choice of chemical groups for the functionalities, however, can be more flexible.

Given these requirements, we chose to use cystine as the starting point for the SAM molecule. Cystine is a natural amino acid, and therefore easily obtainable from commercial sauces at low cost. It also contains a sulphur group (Figure 58).

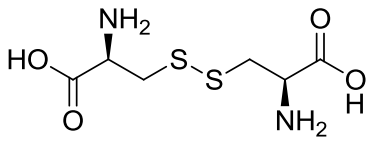

Cystine

Figure 58 The structure of cystine.

Cystine was chosen over cysteine as it is more resistant to oxidation than cysteine. Furthermore, it is known that the disulphide group is able to spontaneously break when exposed to gold, allowing the dimer to split in to two molecules which are each individually anchored to the gold substrate.[125]

The two remaining groups on the cystine offer the ability to chemically modify the cystine with relative ease using well established chemical synthetic techniques, such as those used in peptide synthesis. After reviewing the literature of possible chemical modification

strategies, it was decided that two suitable chemical groups would be an acrylic group and an alkyne group. These groups were chosen as they both can be selectively controlled to take part in aspects of the formation of the synthetic recognition platform, via acrylic cross coupling and click chemistry, respectively. The final SAM molecule design is outlined in Figure 59, and will be referred to as Di-Functional Cystine (DFC).

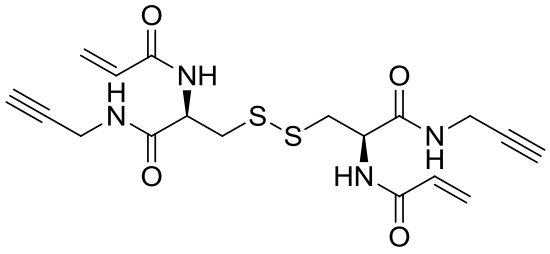

Figure 59: Structure of the DFC molecule, which is based upon a cystine skeleton. The compound contains three functionally distinct chemical groups; a disulphide, a terminal alkyne and an acrylic group.

The alkyne group was chosen as it is suited to use in the crosslinking reactions commonly referred to as click chemistry. The second functional group chosen for the SAM molecule was the acrylic group. Acrylic functional groups offer the possibility of incorporation of a relatively wide range of chemical groups through a common polymerisation strategy. Furthermore, the use of acrylic groups to produce molecularly imprinted polymers and thin films is well established.[271, 272]

4.3.1 Click Chemistry

The principles of ‘click’ chemistry were proposed by Sharpless and co-workers in 2001. This field of chemistry aims to produce modular, high yielding reactions which produce no offensive by-products and, where appropriate, be stereo specific.[273]

Currently, one of the more widely used click reactions is the Huisgen 1,3-dipolar cycloaddition, commonly known as a copper(I)-catalyzed azide-alkyne cycloaddition

(Cu-AAC) reaction (Scheme 3). In fact, this reaction has become so synonymous with click chemistry that it is often referred to as *the* click reaction.[274] It may be considered a pure fusion process as there are no side products produced directly from the reaction.

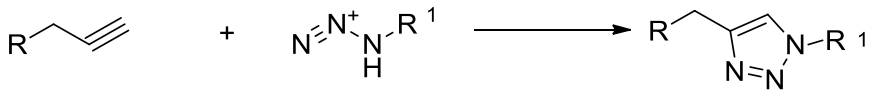

Scheme 3 The overall reaction between azides and terminal alkynes, commonly referred to as the click reaction.

This reaction has found application in a wide range of fields, owing to the fact that alkyne and azide components can be easily incorporated into a wide range of substituents. However, the first non-catalysed reaction was of limited scope due to the slow reaction rate, need for harsh conditions and poor product selectivity. Fortunately, these issues were overcome in 2002 when several groups independently reported the utility of copper (I) catalysts; its employment results not only in the increase in reaction rate, but also the exclusive formation of the 1,4-substituted 1,2,3-triazole.[275, 276]

The appeal of this reaction is multi-faceted. For the purposes of the imprinted surface design, click chemistry was attractive due to its ability to proceed well under aqueous conditions, which is vital for solvent compatibility with target proteins. In addition, the azide and alkyne groups are seldom found in biological systems, therefore there was little to no risk of cross reaction of the functional groups with protein based targets.[275, 277] Furthermore, it tolerates most organic functional groups, proceeds in a variety of solvents, tolerates a wide range of pH values, and performs well over a broad temperature range at high yield.[278]

4.3.2 Mechanism

The overall reaction of the Huisgen 1,3-dipolar cycloaddition is shown in Scheme 4. As the scheme depicts the usefulness of this reaction is that a crosslink between two

compounds can be easily formed. However, the underlying mechanism is believed to be somewhat more complex as shown by Scheme 4.

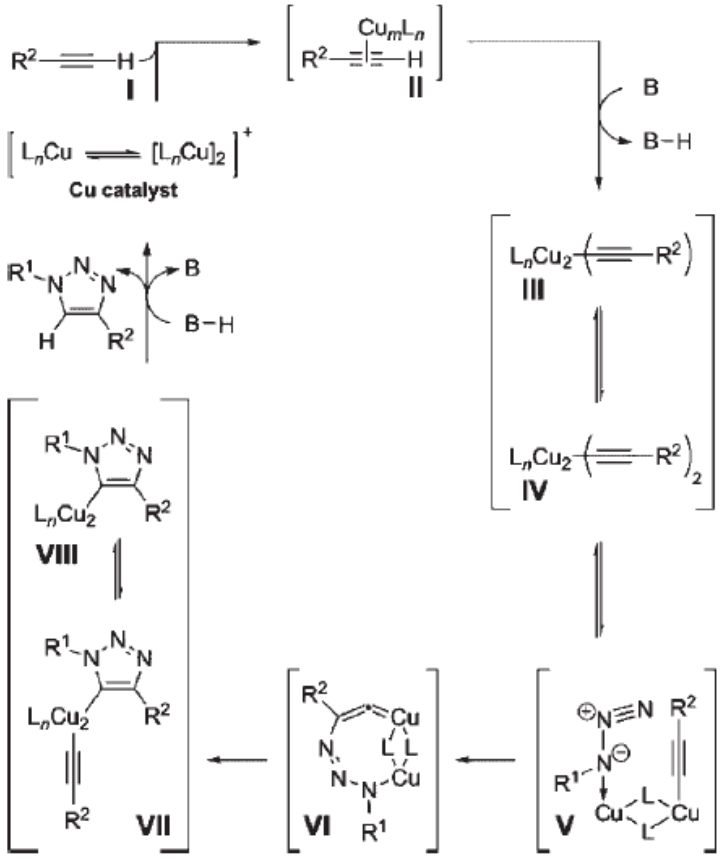

Scheme 4 The proposed mechanism of copper catalysed Huisgen 1,3-dipolar cycloaddition.[278]

It is proposed that the copper mediated catalytic cycle begins with Cu^{I} insertion into the terminal alkynes, forming a Cu^{I} acetylide species via a π complex **3** (Scheme 5). This step is believed to be exothermic in aqueous conditions, which is consistent with observations of increased reaction rate in water. Computational calculations also indicate that copper coordination lowers the pK_a of the alkyne C–H by up to 9.8 pH units, thus making deprotonating in aqueous systems possible without the addition of a base. [278, 279]

The exact nature of the next step is not fully resolved: Following the formation of the active copper acetylide species, azide displacement of one ligand generates a copper acetylide-azide complex, such as the dicopper species **IV** (Scheme 5). Complexation of

the azide activates it toward nucleophilic attack of acetylide carbon C(4) at N(3) of the azide (numbers based on traditional triazole nomenclature), generating metallocycle **VI**. Protonation of triazole-copper derivative **VII** followed by dissociation of the product ends the reaction and regenerates the catalyst (Scheme 4). Limited deuteration studies suggest that protonation occurs through interaction with a protonated external base or solvent molecule but further studies are needed to conclusively establish the proton source.[278, 280]

4.4 Synthetic strategy

In order to synthesise the final SAM molecule depicted in figure 5 a synthetic pathway was designed (Scheme 5) which takes advantage of the well-known and robust DCC coupling reactions.

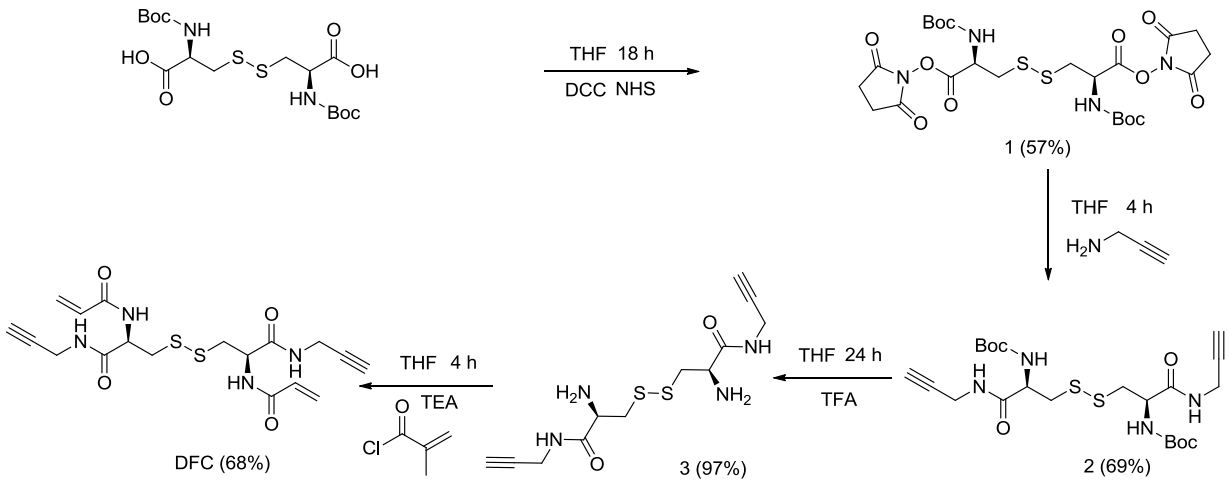

Scheme 5 The synthetic scheme designed to produce the desired DFC SAM molecule. Details of reaction conditions and purification methods can be found in the experimental section of this thesis.

The di-functional cystine (DFC) compound was synthesised through a multistep route as illustrated in Scheme 6. The carboxylic acid groups of the commercially available starting material Nα,Nα′-di-Boc-L-cystine were activated with dicyclohexylcarbodiimide (DCC) and coupled with *N*-hydroxysuccinimide (NHS) over 18 hours at room temperature, to produce

the NHS ester **1**. **1** was then reacted with propargylamine over 4 hours at room temperature to produce **2**. Deprotection of the boc protected amines in **2** was achieved using trifluoroacetic acid over 24 hours at room temperature to produce **3**. Acrylic groups were then coupled to the free amines of **3** via reaction with acryloyl chloride over 4 hours at room temperature to obtain DFC.

4.4.1 DCC/NHS coupling chemistry

The strategy of producing activated NHS esters from carboxylic acids for use in crosslinking reactions is now a common strategy for the production of modular systems due to the wide availably of the reagents and the wide range of application. An outline of the general overall reaction between carboxylic acid and NHS/DCC is shown in Scheme 7. DCC and carboxylic acid form an O−acylisourea intermediate. The reaction proceeds with the addition of the alcohol, in this case NHS, to the activated carboxylic acid to form the stable dicyclohexylurea (DHU) and the desired NHS ester.

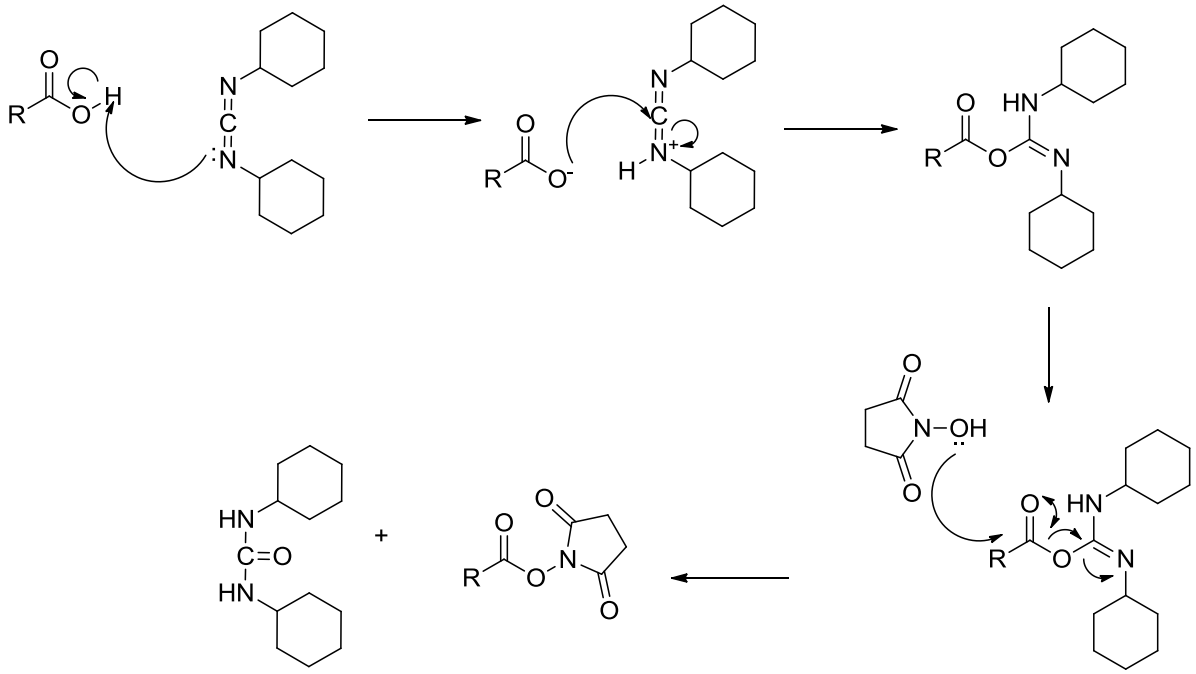

Scheme 6: The overall reaction which occurs between carboxylic acids, DCC and NHS to produce the activated NHS ester.

Once formed the NHS ester is relatively stable until it is exposed to a nucleophile. In our case, the nucleophile is an amine, propargylamine, which is then able to attack the NHS ester, liberating the NHS leaving group and cross linking the amine and carboxylic acid via an amine bond, as outlined in Scheme 8.

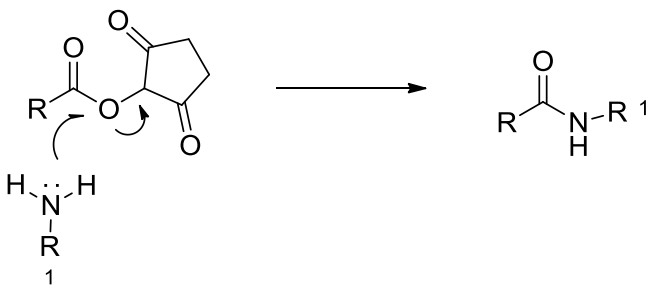

Scheme 7: Nucleophilic attack of an amine to produce the amide bond from an activated carboxylic acid- NHS ester.

The tert-butyloxycarbonyl (boc) group is a commonly used protecting group due its simple removal to regenerate the free amine. Here, we use the acid hydrolysis of this group to produce the free amine.[281, 282]

The final step of the reaction was the addition of the acrylic groups which were added via coupling to the free amine. This was possible using achronyl chloride, which is the acid chloride of N-methylacrylamide. This step can be potentially problematic due to the ability of the acid produced as a side product of this reaction to initiate the polymerization of the acrylic groups therefore this step was carried out in the presence of excess base to ensure that produce was not lost as polymer.

4.4.2 Characterisation

The ^{1}H NMR spectrum of the final product can be found in Figure 61, along with the proton assignment. Some of the coupling observed in the NMR spectra is quite interesting, and warrants discussion. Perhaps most notably the splitting observed in the

‘B’ protons is quite surprising; the protons appear to be split by the amine proton, I, and also by the alkyne proton, ‘A’. Although at first this seems a little unlikely, upon examination of the signal for protons ‘A’ it can be seen this is also split to a triplet, rather than the singlet which might be expected. Likewise the amide proton ‘I’ is also observed to be split into a broad triplet. Such splitting patterns may be explained by the ability of acetylic compounds to produce long range proton coupling. [283]

The protons of the second amide group, ‘H’ also display coupling, producing a doublet. Protons ‘D’ and ‘F’ occupy different spectral positions due to these protons being chemically inequivalent and both are coupled due to each other and also to ‘E’. This produces geminal coupling due the cys-trans positional differences in the portions resulting in the being non-equivalent. Protons J and G can be observed as two distinct doublet of doublets. This effect is due to their diastereotopic nature resulting in each proton being non-equivalent. Thus these protons couple to each other and also the proton ‘C’ producing a doublet of doublets for each proton. The roofing observed in the spectra of many of the protons is caused by the coupling that occurs between these protons being large relative to the differences in their chemical shifts. All coupling relationships were confirmed by COSY NMR experiments, as shown in Figure 61.

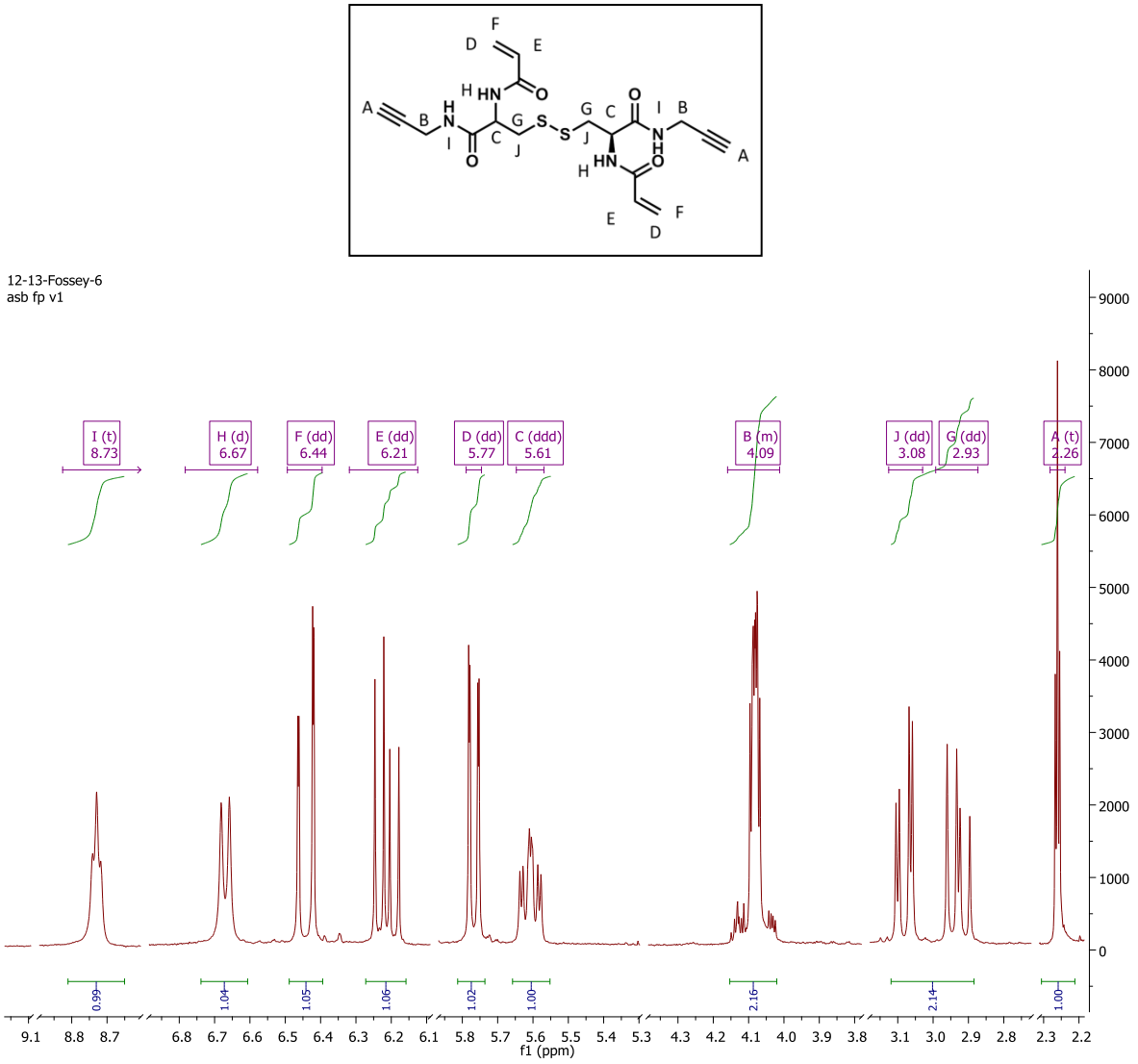

Figure 60: Proton NMR for DFC SAM molecule, with assignments. NMR taken in $CDCL_3$.

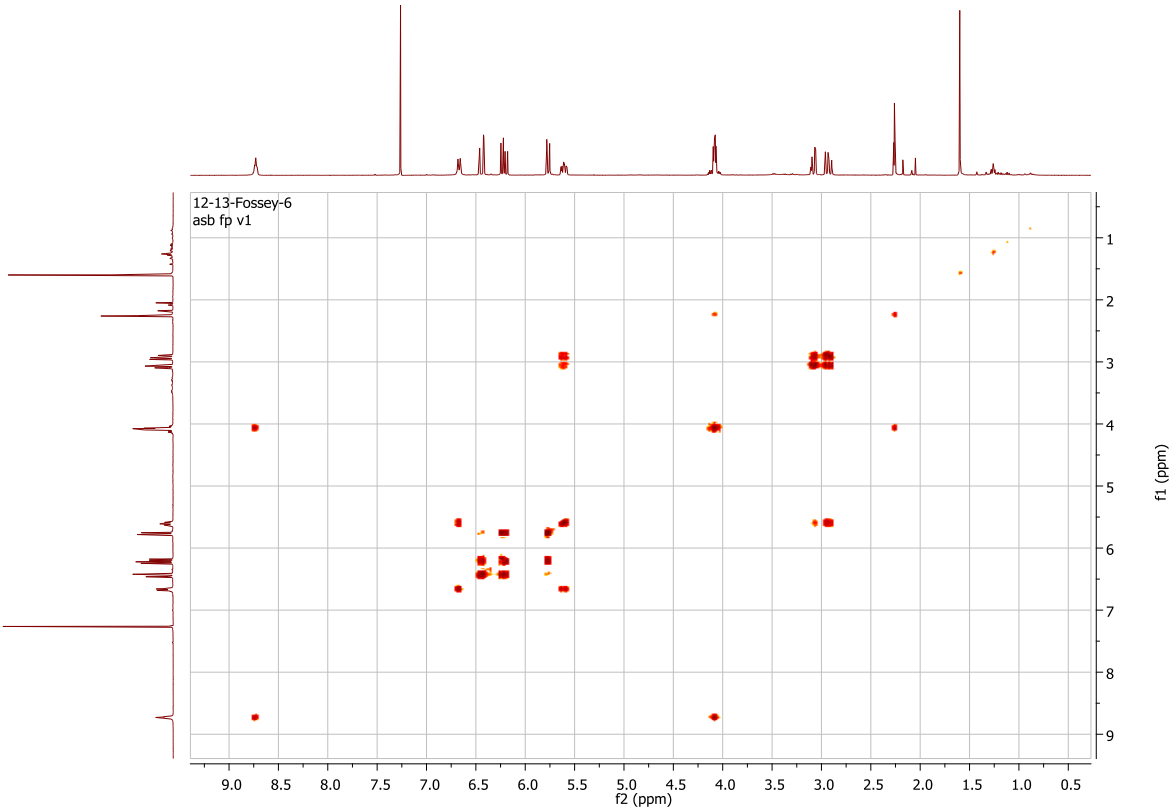

Figure 61: COSY NMR spectra of the DFC molecule.

The molecular weight of the compound was confirmed using electron spray mass spectrometry, in positive ion mode. The predicted mass of the DFC molecule was calculated to be 422.11. A peak was observed with a mass of 445.1 which can be assigned to a sodium adduct of the DFC compound ($[M+Na]^+$). This was confirmed with high resolution mass spectrometry, the calculated mass of the sodium adduct was 445.0980 and the observed mass was found to be 445.0967 [M+Na]. The samples were analysed by FTIR, with the major adsorptions observed at the following wavelengths which are consistent with the functional groups present in the molecule. IR (cm^{-1}) 3277; m, br; NH 1623; S; C=O amide 1647; S; C=O amide 1529; S; alkene.

4.5 Surface Preparation and Characterisation.

4.5.1 SAM formation

SAMs were formed on cleaned gold surfaces. Polycrystalline gold substrates were purchased from George Albert PVD., Germany and consisted of a 50 nm gold layer deposited onto a glass covered with a thin layer of chromium. In order to determine the time required for SAM formation studies of the kinetics of formation were undertaken. This was accomplished by conducting contact angle goniometry measurements at various time points over a 48 hour period. In order to form the SAMs at the indicated time intervals cleaned gold substrates were placed in methanolic solutions of DFC surfactant for the specified time. Gold chips were cleaned by immersion in piranha solution for 10 minutes, before being rinsed with liberal amounts of water for 1 minute, and then rinsed with HPLC grade methanol for a further minute, prior to being placed a 0.1 mM solution of DFC in methanol. Following immersion in the SAM solution for the specified time, the chips were removed and rinsed with pure HPLC grade methanol, to ‘quench’ the SAM formation, and dried with argon. Dried samples were then analysed immediately. The results of these investigations are presented in Figure 62.

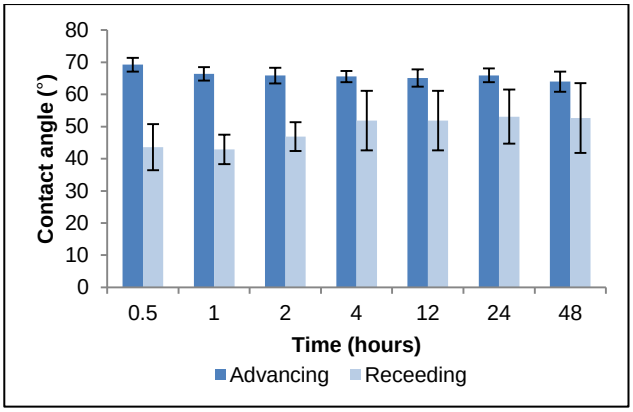

Figure 62: Kinetics of SAM formation, investigated by water contact angle on DFC SAMs. Formation kinetics were monitored over the following time points; 0.5, 1, 2, 4, 12, 24 and 48 hours. Error bars indicate standard deviation.

The results obtained are consistent with a full monolayer being formed after around 12 hours of incubation for DFC. Inspection of the advancing contact angle reveals that DFC reaches a consistent contact relatively quickly indicating that adsorption of DFC surfactant occurs rapidly, with values becoming constant after 2 hours. The processes of SAM formation can be investigated further by examination of the hysteresis between the advancing and receding measurements.[244] It can be seen that over the course of the investigation, the receding contact angle increase while the advancing contact angle remains relatively constant. The net result is a decrease in hysteresis, consistent with an increase in order of the SAM. Hysteresis reaches a minimum after 12 hours of incubation and remains constant thereafter. This distinct two- phase SAM formation is in agreement with literature on the mechanism of SAM formation. [100, 101]

The results observed with contact angle are somewhat lower than literature values observed for pure alkyne SAMs, which have previously been reported to be in the region of 75-85 degrees.[284-286] However, as there are two functionalities present in the DFC molecule it is expected that the contact angle of the surface should be influenced by both functionalities. Thus, the observed contact angle can be explained by the contribution of

the acrylic functional group, which are known have hydrophilic properties, with published contact angles being below 10 ° in some related surface initiated systems.[287]

Table 6 Results of contact angle and ellipsometry investigations conducted on DFC SAMs.

SAM	Contact Angle (°)		Thickness (nm)	
	Advancing	*Receding*	*Theoretical*	*Experimental*
DFC SAM	65.1 ±1.15	46.94±3.84	0.91	0.42 ±0.12

Ellipsometry was used to confirm that the DFC modified surfaces had formed monolayers, free from multi-layer formation which can occur in some SAM structures. The results of these investigations are presented in Table 6, and demonstrate that the thickness of the DFC SAMs is half of the calculated length of the DFC compound, which suggests that a monolayer has been formed successfully, and is an agreement with results observed for related compounds.[288] This disparity between calculated molecular lengths and monolayer thickness is expected due the conformations adopted by the molecules on surfaces.[120]

XPS- DFC SAM

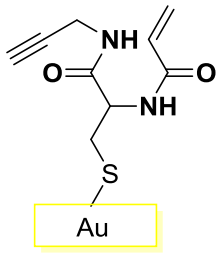

Figure 63 Expected structure for the DFC SAMs

XPS analysis confirmed the formation of DFC SAMs (Figure 63). XPS survey spectrum revealed the presence of the elemental species S, N, C, O and Au on the DFC SAM surface. High resolution spectra of S 2p, N 1s and C 2s were acquired in order to unambiguously demonstrate the presence of the DFC SAM on the gold surface. All

elements were observed in ratios close to those predicted by the molecular structure of the DFC molecule (Table 7), which is consistent with the successful formation of SAMs of the DFC compound.

Table 7 Expected and measured elemental ratios observed for the Az-OEG modified DFC surfaces, as determined by XPS.

Element	Expected Ratio	Measured Ratio
C/S	9	10.7
N/S	2	2.0

High resolution scans for the sulphur, nitrogen and carbon elements are shown in figure 67. The S 2p spectrum (Figure 64a) consists a doublet peak, at 162.1 eV (S $2p_{3/2}$) and 163.3 eV (S $2p_{1/2}$), indicating that the sulphur is chemisorbed on the gold surface.[289] The N 1s spectrum (Figure 64b) can be assigned to a single peak centred at 399.7 eV, which can be ascribed to the amide groups in the DFC molecule.

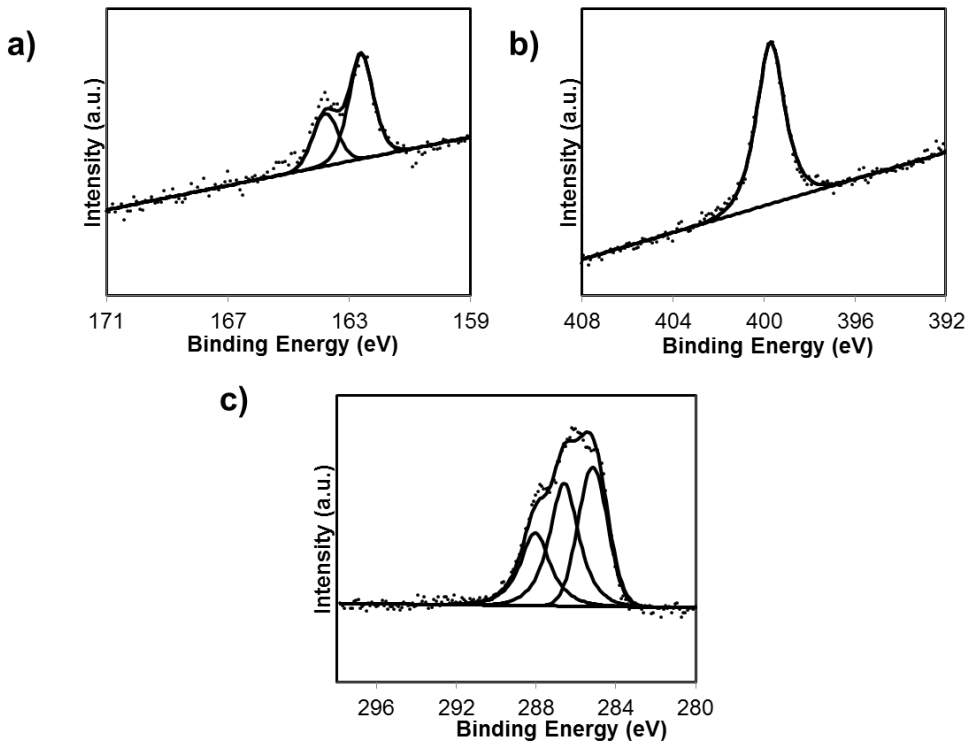

Figure 64: XPS spectra of the a) S 2p, b) N 1s, c) C 1s and peak regions of DFC SAMs.

The C 1s spectrum (Figure 64c) can be deconvoluted into three peaks, which is consistent with the structure of the DFC compound. The peaks can be assigned to the carbon species present in the compound; C-C which is centred around 285.2 eV; C=O centred around 288.0 eV and a third peak at 286.6 eV which can be attributed to the accumulation of different contributions of the remaining carbon species C-S and C-N.[290] The ratio of these carbon types are in good agreement with expected ratios (Table 8).

Table 8: Carbon species ratio for DFC surface

Peak BE	Ratios with respect to 288 eV		Species
	Expected	*Measured*	
288.0	1	1	C=O
286.6	1.5	1.6	C-S, C-N
285.2	2	1.8	C-C C=C

4.5.2 Acrylic Reactions

4.5.2.1 Models

There are many published strategies for the initiation of acrylic polymerisation. Therefore, in order to determine the most effective method to use in aqueous conditions investigation was required. In order to determine the most efficient conditions, a simple experiment was carried out to screen a number of possible conditions. The commercially available starting material, *N,N'*-methylenediacrylamide (*bis*-acrylamide) (Sigma Aldrich, UK), is soluble in aqueous conditions, but its polymer is not, therefore polymerisation could be monitored by the production of insoluble gel precipitate formation (figure 68).

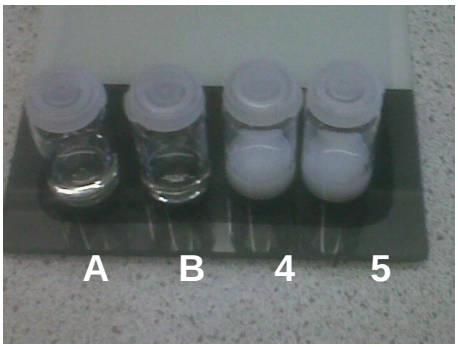

Figure 65: Photo demonstrating the results of the initiator investigations. The vials marked A and B show the acrylic solution before addition of initiator. Vials marked 4 and 5 show the solution following polymerisation under conditions 4 and 5 as described in Table 3.

The free radical polymerisation reaction requires an initial source of free radical to proceed. The two most common methods of generating free radicals can be devided into

two groups: chemical and photochemical. Ammonium persulphate (APS) is commonly used a chemical source of free radicals while riboflavin in combination with a light source can be act as a photochemical source of free radicals. *N,N,N′,N′*-Tetramethylethylenediamine (TEMED), a base, was also investigated as an additional catalyst. TEMED interacts with APS at neutral to basic pH to enhance the production of free radicals.[291] An additional advantage of the TEMED is that it has been shown to increase the yield of Cu-AAC reactions.[284] Riboflavin may also be used as source of free radicals, however it requires irradiation to generate them.[292] The conditions investigated all used a 1 M solution of *bis*-acrylamide and to this were added a number of different initiator types and/or conditions. The details of reaction conditions and observed results are shown in Table 9. The results indicate that the best conditions appear to be those detailed in entries 4 and 5 of Table 9. Given that the two results appear to be essentially the same, it was decided that the best conditions to move forward to surface reactions would be entry 4, as UV radiation maybe lead to degradation of the SAMs.

Table 9 Results and conditions investigated for initiation of acrylic polymerisation

Entry	Conditions (final vol = 3mL)	Result
1	1 mM Amonium Persulphate and 1 M *bis*-acrylamide	No change
2	0.1 mM Ammonium per sulphate, 1 M HLC, 1 M *bis*-acrylamide	No change
3	5% (vol:vol) 40mg/mL Ammonium persulphate, 30ul TEMED, 1 M Bis Acrylamide	While Gel formed
4	1 mM riboflavin, 1 mM ammonium persulphate, 1 M *bis*-acrylamide w/ UV exposure	White gel formed
5	As above but with 30 µl TEMED	White ppt formed
6	1 mM riboflavin, 15 ul TEMED, 1 M *bis*-acrylamide	Small amount of ppt formed.
7	1 M *bis*-acrylamide, 60°C 6 hours	No change

The conditions identified were then taken forward for use with SAMs. However, the concentration of the N,N'-methylenediacrylamide was reduced to 1 mM and 10 mM to avoid gel formation. The overall reaction is outlined in Scheme 8. The experiment was carried out as follows: SAMs of DFC were formed over 18 hours, as previously described. SAMs were then placed in a solution of the N,N'-methylenediacrylamide and the initiators were added. Reactions were allowed to continue for 4 hours. After this time the SAMs were removed for the solutions, and rinsed with large volumes of methanol, before being sonicated and rinsed with water. The physical properties of the SAMs were then investigated by contact angle and ellipsometry. In addition, samples were also probed electrochemically via cyclic voltammetry using a ferricyanide redox probe.

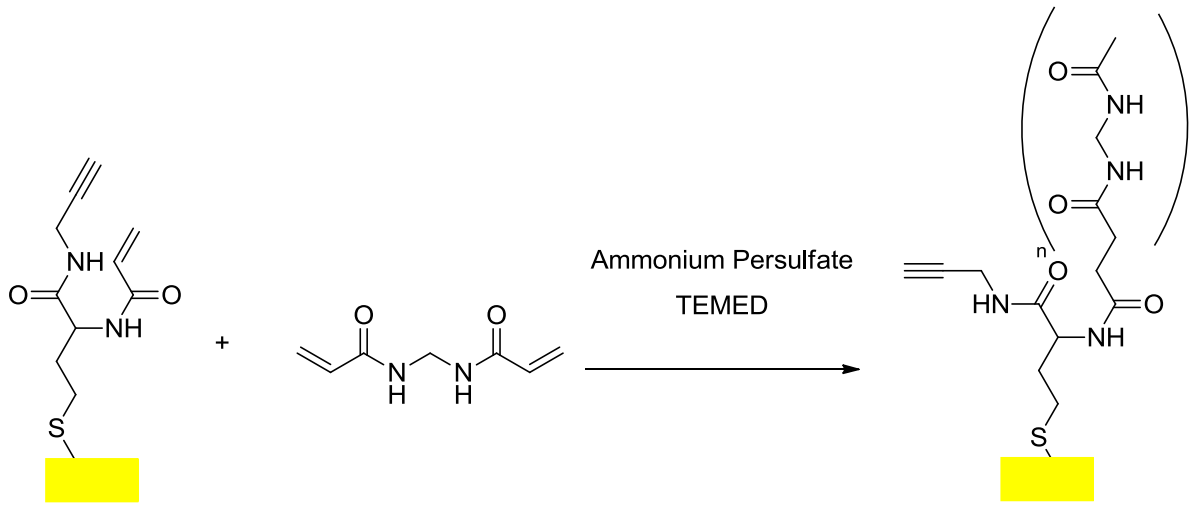

Scheme 8 Addition of acrylic polymer to preformed DFC SAMs.

The results demonstrate that the surfaces display a change in thickness and wettability following the modification with the acrylic compound (figure 69). Initially, the wettability contact angle of the surfaces of the DFC SAMs was found to be 65.1^{o}. However, following the modification with the 1mM *bis*acrylic solution with was observed to fall to 38.5^{o}, indicating the surface becoming more hydrophilic with the addition of the acrylic polymer which is in agreement with other literature on acrylic terminated surfaces

(Figure 66a).[293, 294] This effect becomes even more pronounced when the 10 mM solution is used, as the advancing contact angle falls to 13.6^{o}. This observation can be explained by the conformation of the surfaces as surface initiated polymerisation can produced hydrogel-type structures, which have been reported to have comparable contact angles.[295] In addition, other polymers with high bis acrylamide content have also shown low contact angles.[296]

Examination of the ellipsometry results for these surface also demonstrate that the thickness of the modified surfaces increase proportionally to the concentration of the N,N'-methylenediacrylamide. The unmodified DFC SAM is measured to have thickness of 0.46 nm, which is consistent with calculated molecular length, demonstrating the formation of a single monolayer (Figure 66b). When reacted with the 1 mM bis-acrylic solution, the surfaces were measured to increase in thickness of 1.73 nm. The surface reacted with the 10 mM solution was observed increase to a thickness of 12.0 nm. These results are consistent with the hypothesis that the change in the hydrophillicity of the surface is proportional to the content of poly-bisacrlyamide, as evidence with increases in thickness of the surfaces observed here and in agreement with other investigations into surfaces modified with bis-acrylamide.[287]

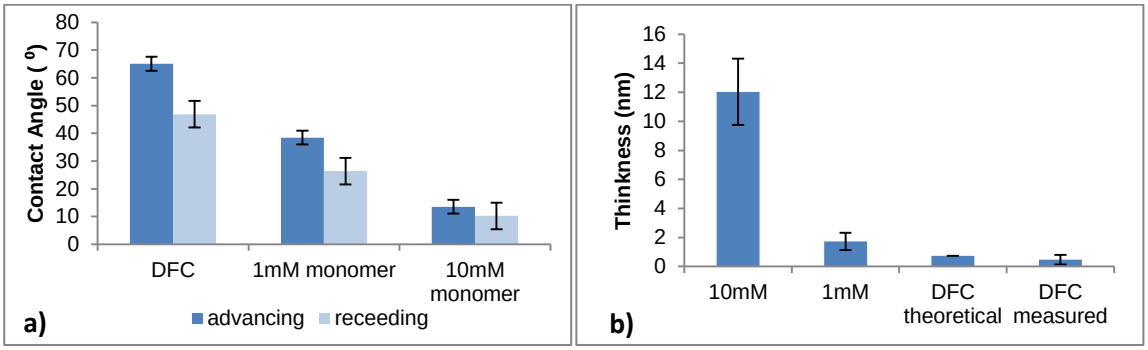

Figure 66 Results of a) ellipsometric and b) contact angle investigations of surface acrylic reactions. With higher concentrations of acrylic monomer a film of increased thickness is formed, as shown by the increased film thickness and decreasing contact angle. . Error bars indicate standard deviation.

4.5.2.3 Electrochemical analysis

The results of contact angle and ellipsometric investigations suggest that acrylic groups were able to covalently attach to the SAM surface. However, to add further certainty, electrochemical investigations were also carried out. This experiment is based around the oxidation/reduction cycles of an iron complex which is able to exist in both the 3+ and 4+ oxidation state.[297] This overall reaction is outlined in Equation 10:

Eq. 10 $$Fe(CN)_6^{3-} + e^- \rightleftharpoons Fe(CN)_6^{4-}$$

Cyclic voltammetry experiments consist of cycling the potential of an electrode, which is immersed in an unstirred solution, and measuring the resulting current. The experimental set up is detailed in Figure 67, where modified DFC surfaces were used as the working electrode.

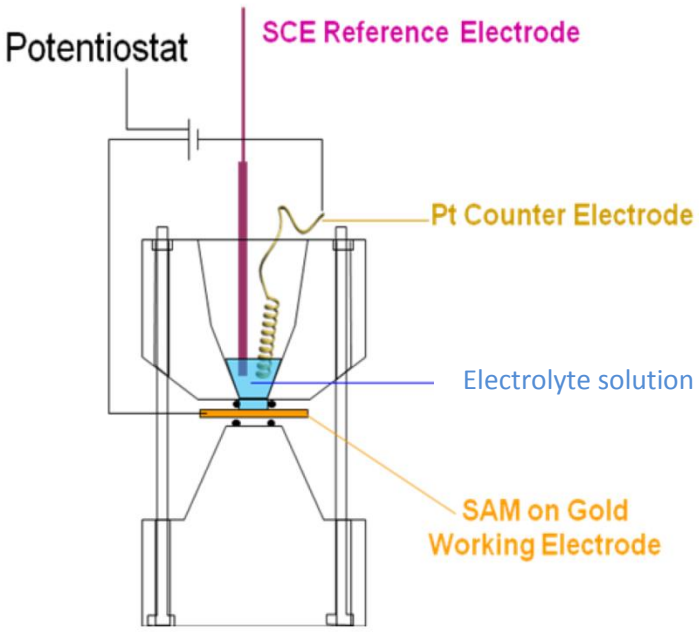

Figure 67: A schematic representation of the electochemical cell used to investigate the modifed surfaces.

CV experiments can be used to investigate a number of properties of solutions and electrode surfaces, and has been used in some cases as a reporting mechanism in

sensor systems, including molecularly imprinted surfaces.[298] In this case, the parameter being investigated is the physical structure of the electrode it's self- in this case the modified SAM surface. The basis of this investigation is that the electrochemical behaviour of the probe is influenced by the properties of the surface. The cyclic voltamagrams obtained on each of the surfaces is shown in Figure 68. It can be seen that with the unmodified DFC surfaces large oxidation and reduction peaks are observed. Furthermore, the separation of these peaks is small, which suggests that both the 3+ and 4+ species are able to rapidly exchange electrons with the surface.[297, 299]

In contrast, examination of the results obtained with the modified surfaces demonstrates that the behaviour of the electrode have changed - the peak currents of the oxidation and reduction reactions are reduced on both modified surfaces, with the peaks being reduced further on the 10 mM modified surface than the 1 mM surface. In addition, the separation between the oxidation and reduction peaks is also increased on both surfaces and again this effect is more pronounced with the 10 mM surface. The results demonstrate that as the acrylic layer increases in thickness the ability of the ferricyanide probe to take part in the redox cycle is inhibited, which is consistent with the acrylic groups inhibiting the ability of the probe to access the surface and take part in redox processes (figure 14).

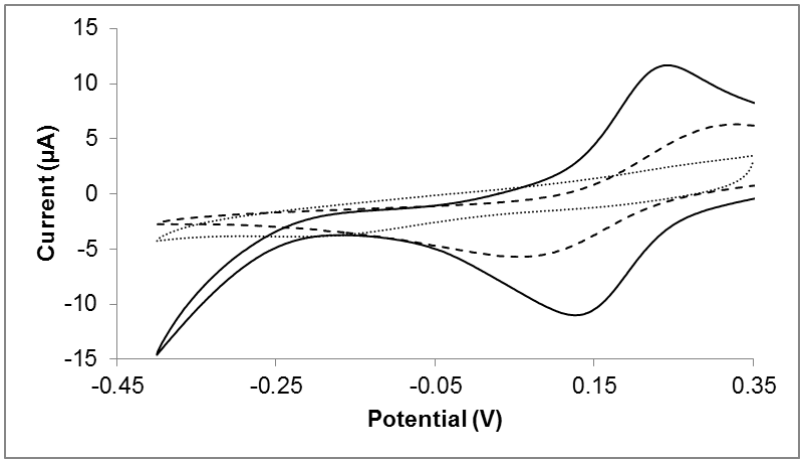

Figure 68 Results of cyclic voltammetry investigations of surface acrylic reactions. Solid line is DFC SAM, dashed line and dotted line are 1 mM and 10 mM acrylic modified SAMs, respectively. An

increase in the resistance of electron transfer can be observed with increased acrylic monomer concentration.

4.5.2.2 Incorporation of acrylic boronic acid

Following the establishment of the polymerisation initiation conditions using model acrylic groups, the same conditions were used with a commercially available acrylic boronic acid, 3-(Acrylamido)phenylboronic acid (AABA) (Sigma Aldrich, UK). In addition, a control surface was produced using a compound similar to AABA but without the boronic acid groups, N-phenylacrylamide (NPA). The molecular structure of the compounds is outlined in figure 15. Preformed DFC SAMs were reacted with 0.1 mM solutions (1mL) of the AABA and NPA monomers for 6 hours in the presence of initiators as described in entry 5, Table 9.

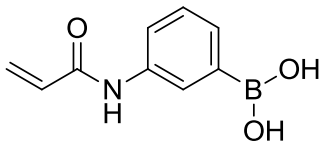

3-(Acrylamido)phenylboronic acid

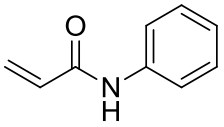

N-phenylacrylamide

Figure 69: The structures of the acrylic boronic acid and the control compound *N*-phenylacrylamide.

The attachment of the compounds to the surface was monitored by contact angle. Contact angle results demonstrate that following the reaction of the AABA with the surface, an increase in the surfaces hydrophobicity was observed, the results are presented in figure 73. The advancing contact angle was observed to change from 65.1 ° with the DFC surface to 44.5 °, following the reaction with the AABA. Comparison with published results from related surfaces, such as those outlined by Uvdal and co-workers of 31.5 ° reveal these values to be higher than might be expected for a pure boronic acid terminated surface. However, this result can be explained by the presence of the hydrophobic alkyne present on the surface.

Eq. 11 $$\cos\theta_{Adv} = x\cos\theta_{Adv1} + y\cos\theta_{Adv2}$$

Using the Cassie equation (Equation 11) allows this hypothesis to be checked by calculating the surface proportions of the alkyne and boronic acid components, using the literature values of 31.5 ° boronic acid and the measured value of 65.1 ° as a reference for the DFC. The results of this calculation suggest that the measure value of 44.4 ° is the result of a near perfect 1 to 1 (0.56 to 0.44) surface ratio of the boronic acid and alkyne components (Figure 70).

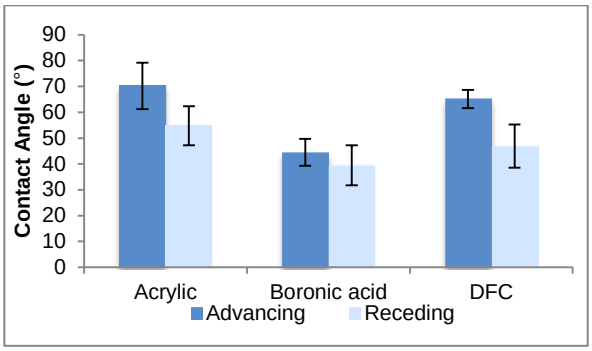

Figure 70: Observed advancing and receding contact angles for DFC SAMs modified with NPA and AABA. Unmodifed DFC contact angle included for reference. Error bars indicate standard deviation.

In contrast, the result obtained when the DFC surface were reacted with the control compound reveal an increase in the hydrophobicity of the surfaces, with contact angles increasing to 70.8 °. This result compares well to previously published values for aromatic-terminated SAMs, which have reported as 74.1 °. [300] The Cassie equation was again used to calculate the component ratios of the phenyl and alkyne groups in the surface. As with the AABA modified surface, surface component ratios were determined to be close to 1:1 (0.58 to 0.42.).

4.5.2.3 XPS – AABA modified DFC

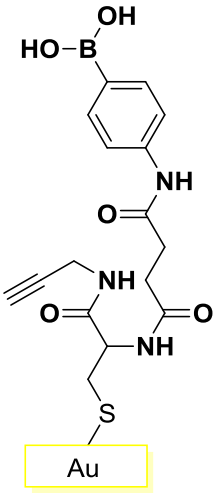

Figure 71: Expected structure for the DFC SAMs modified with Acrylamidophenylboronic acid.

XPS analysis confirmed the AABA modification of DFC surfaces. XPS survey spectrum revealed the presence of the elemental species S, N, C, O and Au on the DFC SAM surface. High resolution spectra of S 2p, N 1s, B1s and C 2s were acquired in order to unambiguously demonstrate the presence of the DFC SAM on the gold surface. The measured elemental ratios are compared to their expected ratios (for a 1:1 stoichiometric reaction, Figure 71) in Table 10. Examination of these results suggests that the acrylamide boronic acids are able to crosslink to the DFC surface in close to 1:1 stoichiometry.

Table 10 Expected and measured elemental ratios observed for the AM-BA modified DFC surfaces, as determined by XPS

Element	Expected Ratio	Measured Ratio
C/S	20	21.4
N/S	3	3.1
B/S	1	1.1

High resolution scans for the sulphur, nitrogen, carbon and boron elements are shown in Figure 72. The chemical state of the sulphur atom was probed using the XPS spectra of

the S 2p emission (binding energy range of 160 eV to 170 eV) (Figure 72a). The S 2p spectrum consists of a single doublet peaks 162.1 eV (S $2p_{3/2}$) and 163.3 eV (S $2p_{1/2}$), indicating that the sulphur is chemisorbed on the gold surface.[289] The N 1s spectrum (Figure 72b) contained a single peak centred at 400.4 eV is attributed to amide (C=O) moieties.[301] The C 1s spectrum (Figure 72c) can be deconvoluted into three peaks, which are attributed to five different binding environments. The peak at 285.1 eV is attributed to C-C bonds.[302] The observation of this peak is consistent with values previously reported for such similar surfaces.[284] The peak at 286.5 eV corresponds to C 1s of the three binding environments of C-S, C-N and C-B.[302] The third and smaller peak (288.4 eV) is assigned to the C 1s photoelectron of the carbonyl moiety, C=O.[302] The ratios of these peaks is in good agreement with the ratios predicted from the compounds structure (Table 11).

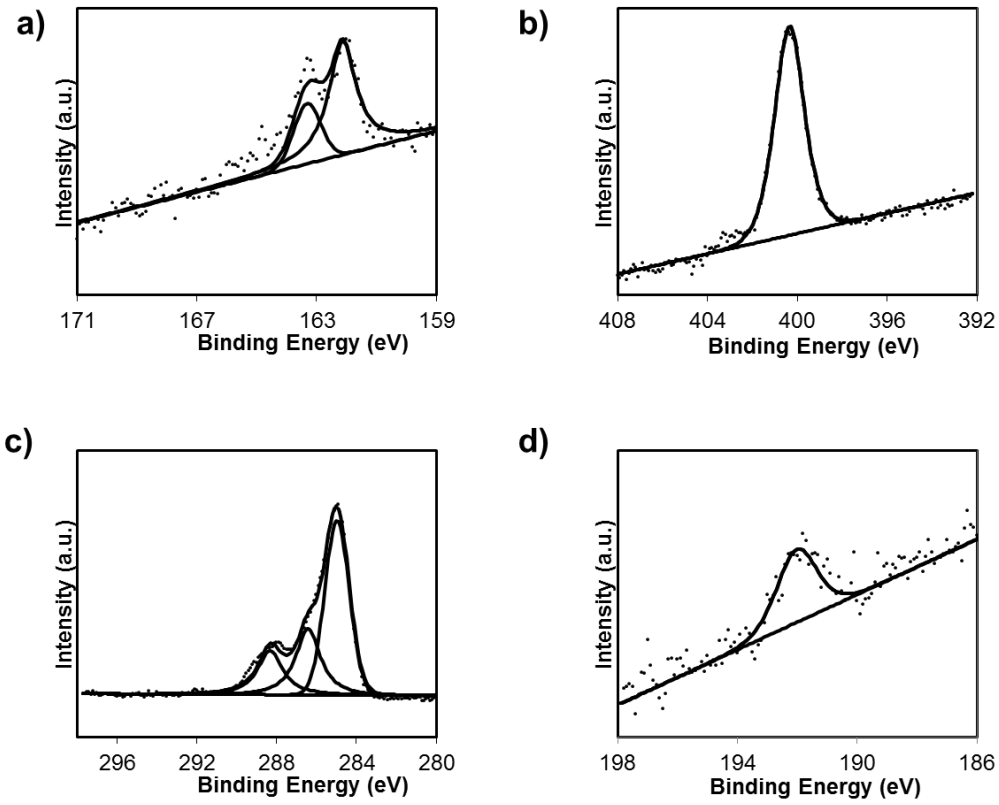

Figure 72 XPS spectra of the a) S 2p, b) N 1s, c) C 1s d) B 1s peak regions of DFC-BA SAMs.

The XPS spectrum of the boron region (Figure 72d) was observed to contain a single peak centred at 192.0 eV which can be attributed to the boronic acid group.[303]

Table 11 Carbon species ratios for the AMBA modified surface

Peak BE	**Ratios with respect to 288 eV**		**Species**
	Expected	*Measured*	
288.33	1	1	C=O
286.56	1.6	1.424168	C-S, C-N, C-B etc.
285	2.7	3.008036	C-C

In addition, using XPS we were able to monitor the kinetics of the reaction over time, by monitoring the nitrogen content of the samples after various reaction times. Briefly, preformed DFC SAM chips were placed in solution of the AABA and initiators added to being the surface modification reaction. At the indicated time periods, the chips were removed and rinsed with pure HPLC grade methanol, to 'quench' the SAM formation. XPS analysis was then used to calculate the nitrogen to sulphur ratios in each sample. This ratio was then used to infer the progression of the reaction, with a ratio of 1:2 (S:N) being taken as 0% complete and a ratio of 1:3 being taken to be 100% reaction. The reaction was observed to go to completion after two hours (Figure 73). This result is consistent with contact angle data, suggesting that the AABA monomer attaches to the surfaces in a 1:1 molar ratio.

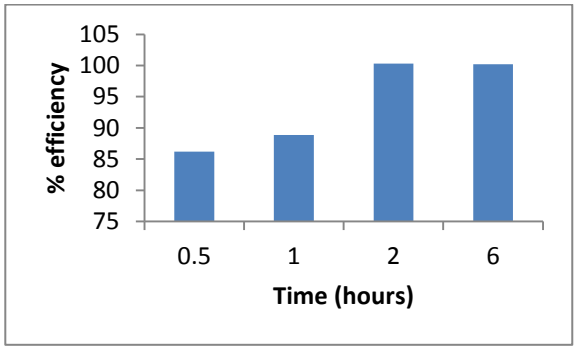

Figure 73 Kinetics of surface reactions of AABA and DFC surfaces, as determined by N/S ratios, via XPS.

4.5.3 Click reaction optimisation

4.5.3.1 Surface Click Reaction Optimisation

Surface click reactions were investigated using SAMs of DFC and Az-OEG. Cu-AAC reactions were conducted in aqueous conditions based on a literature procedure.[304] This method employed in situ generation of Cu^{I} from copper sulphate by reduction via sodium ascorbate. The success of the reaction was monitored via ellipsometry and contact angle, and the results of such investigations are outlined in Table 12.

Table 12 Results of contact angle and ellipsometry investigations into the properties of DFC and modified DFC SAMs

SAM	Contact Angle (°)		Thickness (nm)	
	Advancing	*Receding*	*Theoretical*	*Experimental*
DFC	65.1±0.6	46.9±3.84	0.9	0.4±0.2
Clicked Surface	39.9±3.5	31.3 ± 3.2	2.9	2.0±0.12
Glycol Reference [247, 305, 306]	30-50	-	-	-
Alkyne Reference[285, 307]	75-85	-	-	-

Following reaction with click reagents, the contact angles of the surface were observed to fall from 65.1 ° observed with the unmodified DCF SAMs to 39.9 °. This result illustrates that the modified surfaces have adopted a much more hydrophilic property, which is close to the literature values expected for OEG SAMs, suggesting that the click reaction has been successful. Ellipsometry results indicate an increase in thickness for the 'clicked' surfaces, which were found to be 1.95 nm in thickness as compared to the unmodified DFC SAM which was only 0.42 nm in thickness. Although the measured thickness is below the theoretical molecular length of the glycol, this result is not surprising as glycols are known to adopt a collapsed structural conformation when not hydrated.[247] Together with the contact angle data, this data provides strong evidence for the success of the surface click reactions.

4.5.3.2 Electrochemical analysis

CV experiments were also conducted to investigate the success of the Cu-AAC reaction. As with the acrylic modified surfaces, the basis of this investigation is that the electrochemical behaviour of the probe is influenced by the properties of the surface. The cyclic voltamagrams on DFC and DFC appended with Az-OEG via a Cu-AAC reaction are shown in Figure 74. It can be seen that with the unmodified DFC surfaces large oxidation and reduction peaks are observed. Furthermore, the separation of these peaks is small, which suggests that redox couple of both the 3+ and 4+ species are able to rapidly exchange electrons with the surface.[297, 299]

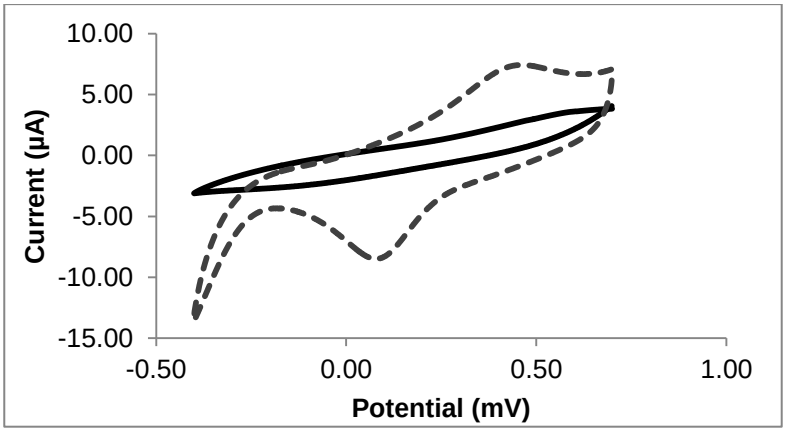

Figure 74: Results of cyclic voltammetry investigations of surface Cu-AAC reaction. Solid line is DFC SAM and the dashed line is the result for the Az-OEG appended SAMs. An increase in the resistance of electron transfer can be observed following the Cu-AAC reaction.

In contrast, examination of the results obtained with the Az-OEG-modified surface (6 hour reaction time) demonstrates that the behaviour of the electrode has changed - the peak currents of the oxidation and reduction reactions are reduced on the modified surface. In addition, the separation between the oxidation and reduction peaks is also increased on the Az-OEG-modified surface. The results demonstrate that the presence of the Az-OEG molecule on the surface inhibits the ability of the ferricyanide probe to take part in the redox cycle.

4.5.4 Click DFC XPS

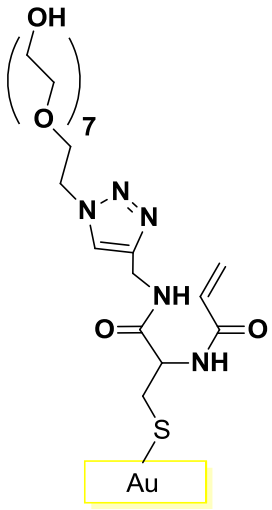

Figure 75 Expected structure for the DFC SAMs modified via copper catalysed azide alkyne cycloaddition reaction with Az-OEG

XPS analysis confirmed the success of the Cu-AAC surface reaction to produce Az-OEG modified DFC (Figure 75). XPS survey spectrum revealed the presence of the elemental species S, N, C, O and Au on the DFC SAM surface. High resolution spectra of S 2p, N 1s and C 2s were acquired in order to unambiguously demonstrate the presence of the Az-OEG modified DFC SAM on the gold surface. XPS analysis confirmed the success of surface modification via copper catalysed azide alkyne cycloaddition reaction. All elements were observed in the ratios expected (Table 13), and were consistent with a near quantitative yield for the surface Cu-AAC reaction.

Table 13: Expected and measured elemental ratios observed for the Az-OEG modified DFC surfaces, as determined by XPS

Element	Expected Ratio	Measured Ratio
N/S	5	4.8
C/S	25	24.9
O/S	10	10.8

High resolution scans for the sulphur, nitrogen and carbon elements are shown in Figure 76. The chemical state of the sulphur atom was probed using the XPS spectra of the S 2p emission (binding energy range of 160 eV to 170 eV). The S 2p spectrum (Figure 76a) consists of a single doublet peaks at 163.4 eV (S $2p_{1/2}$) and 162.3 eV (S $2p_{3/2}$), indicating that the sulphur is chemisorbed on the gold surface.[289] The N 1s spectrum (Figure 76b) can be deconvoluted into two peaks; the peak centred at 399.5 eV is attributed to the accumulation of both the N=N and amide nitrogen atoms, which are known to occupy the same spectral area. [308] The second peak centred at 400.6 eV is assigned to the N-C atom present in the triazole ring.[309] No peaks were observed at higher binding energies, such as those which may be produced by the electron deficient nitrogen present in the azide starting material.[310] The ratio of these peaks was found to be close to the expected ratio (Table 14).

Table 14 Nitrogen species ratio for the DFC Az-OEG surface

Peak BE	**Ratio with respect to 400 eV**		**Species**
	Expected	*Measured*	
399.5	4	3.9	NC=O, N=N
400.6	1	1	N-N

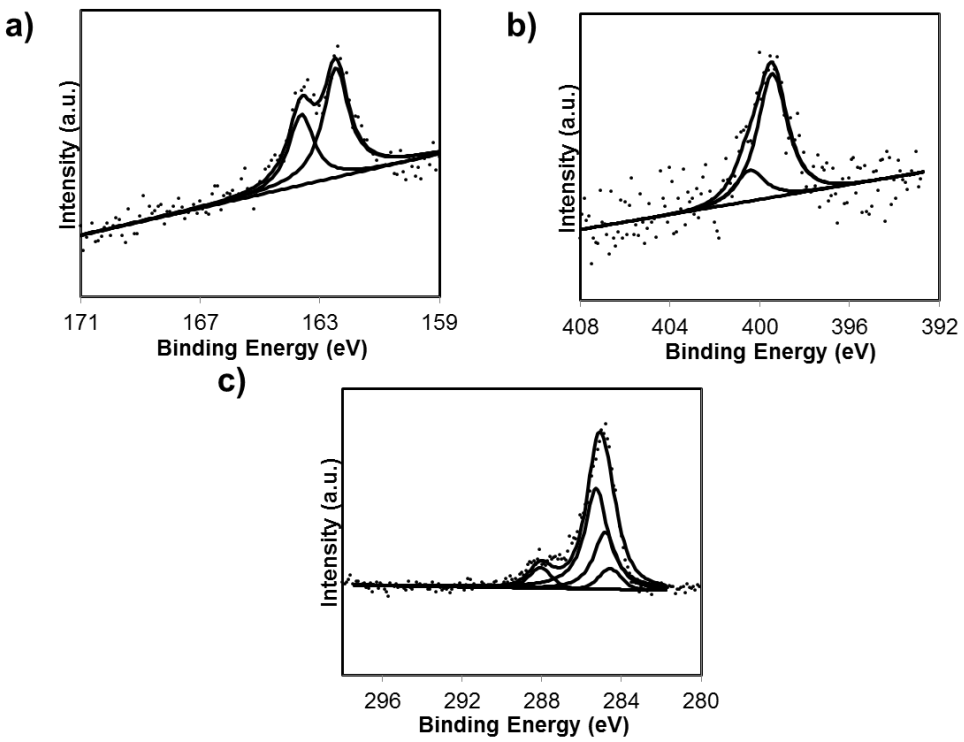

Figure 76: XPS spectra of the a) S 2p, b) N 1s and c) C 1s peak regions of DFC Az-OEG surface.

The C 1s spectrum (Figure 76c) can be deconvoluted into four peaks. The peak at 284.6 eV is attributed to C-C bonds,[302] while the peak at 284.8 eV corresponds to the superstition of the remaining C 1s of the three binding environments of C-S, C-N and C-OH.[302] The third peak centred around 285.3 eV is attributed to the C-O carbons of the OEG group. The fourth peak (288.1 eV) is assigned to the C 1s photoelectron of the carbonyl moiety, C=O.[302] The ratio of these peaks was found to be close to the expected ratio of the carbon environments (Table 15). Taken together with the spectra observed in the nitrogen regions this finding is consistent with a near quantitative reaction of the surface alkyne groups.

Table 15 Carbon species ratio for Cu-AAC modified surface

Peak BE (eV)	Ratio with respect to 288 eV		Species
	Expected	*Measured*	
284.6	2	1.9	C-C
284.8	7	6.8	C-N, C-S,
285.3	14	13.6	C-O
288.1	2	2.0	C=O

4.6 Conclusion

In this chapter the concept, design and synthesis of compounds to form the basis of a novel sensor platform have been outlined. The DFC was produced and demonstrated to form SAMs spontaneously when exposed to a clean gold surface. Following the formation of DFC SAMs the functional groups within the compound were demonstrated to successfully take part in the subsequent chemical reaction to produce modified DFC SAM surfaces. Following this promising start the compounds and reactions discussed here will be investigated further in subsequent chapter to engineer functional sensors.

CHAPTER 5: MOLECULAR IMPRINTED SURFACES: SELECTIVE DETECTION OF GLYCOPROTEINS

Following the design, synthesis and characterisation of each element of the proposed molecularly imprinted surface sensors, this chapter will detail their application. This chapter will describe the development of molecularly imprinted surface sensors to target compounds RNAse B and PSA. The ability of the produced sensors to bind these proteins along will be assessed and compared with other non-target proteins in order to assess their affinity and selectivity. The compatibility of these sensors with complex biological media will then be assessed.

5.1 Introduction

Following the optimisation of the surface modification strategies outlined in the previous chapter, attention will turn to using these strategies to fabricate the molecularly imprinted surface sensor. The chapter will begin be examining the effect of the various surface modification has on the surfaces ability to interact with proteins. This will be followed by investigation into the production of imprinted surface specific for target proteins, and in particular, investigations into imprinted surfaces to which are able to distinguish between glycosylated and non-glycosylated version of the same proteins.

Next, the suitability of the methods for production of a sensor selective for the biologically relevant glycoprotein, Prostate specific antigen (PSA), will be assessed. This will be followed by examining the suitability of the system to function with complex biological matrices.

5.2 Protein resistance of click surfaces

To ensure that the surface reactions were able to produce the desired physical properties on the surfaces, the ability of the surface to resist non-specific adsorption of proteins was investigated via SPR. SAMs of oligo(ethylene glycol) (OEG) thiol SAMs have been used as a 'gold standard' of protein resistance, as it is a well-known and well characterised surface method of reducing adhesion of proteins.[311] Therefore, an OEG SAM was prepared as per a published method using a hexaethylene glycol thiol to allow the investigation of an 'ideal' protein resistant surface.[312] Over this surface a series of BSA protein solutions were injected and binding monitored. The BSA solutions were prepared by serial 2 x dilutions to produce 7 protein solutions ranging from 1 mg/mL to 0.0156 mg/mL. Solutions were injected in order of ascending concentration. Each injection and wash phase lasted for 15 minutes, with a flow rate of 25 µL/min. As expected, OEG SAMs were able to resist the adsorption of protein up to concentrations of

up to 1 mg/mL (Figure 77). However, it can be seen that at the higher concentrations of protein some signal change is observed. This can be attributed to the 'bulk effect' of the high concentration of protein, which is able to produce a change in the refractive index of the bulk solution, which is picked up by the SPR, rather than a true interaction with the surface. [313]

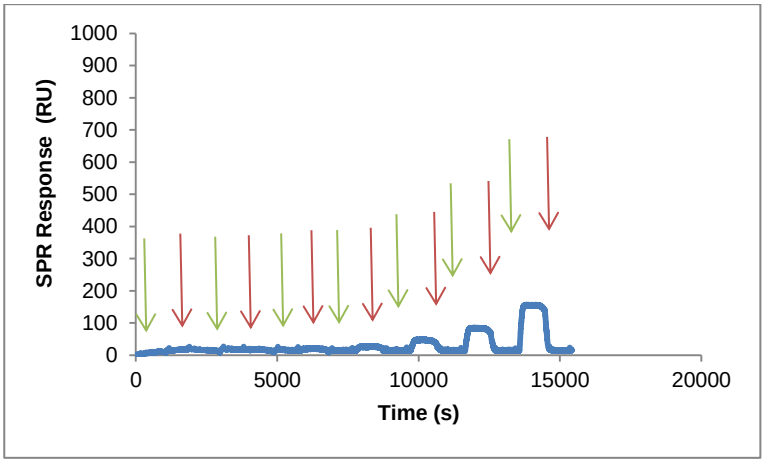

Figure 77: Representative SPR sensorgram demonstrating injections of BSA over a OEG SAM. Green arrows indicate the start of and injection and red arrows indicate the beginning of a wash. Protein concentrations were prepared by serial 2x dilutions ranging from 1 mg/mL (final injection) to 0.0156 mg/mL (first injection).

In contrast, the results of the observed interaction of SAMs of DFC (figure 66) with BSA demonstrate that SAMs of these molecules are unable to resist the non-specific binding (NSB) of protein. The similar experiment is conducted using an unmodified DFC surface. BSA solutions were prepared as before using a 2x serial dilution, however this time the highest concentration used was 0.25 mg/mL, as it was anticipated that surface would have become saturated with protein before the reaching higher concentrations. Thus, 5 solutions were produced ranging from 0.0156 mg/mL to 0.25 mg/mL. These solutions were then injected over the unmodified DFC surfaces. Results of these injections are shown by the blue line in Figure 78. It can be seen even the lowest concentration solutions of 0.0156 mg/mL BSA produce a large and mostly irreversible response. As the

injection continues, the relative increase in SPR signal beings to decrease, which is consistent with the surfaces becoming saturated with adsorbed proteins.[314] This behaviour is typical for surfaces which have not been optimised for the resistance of NSB of proteins.

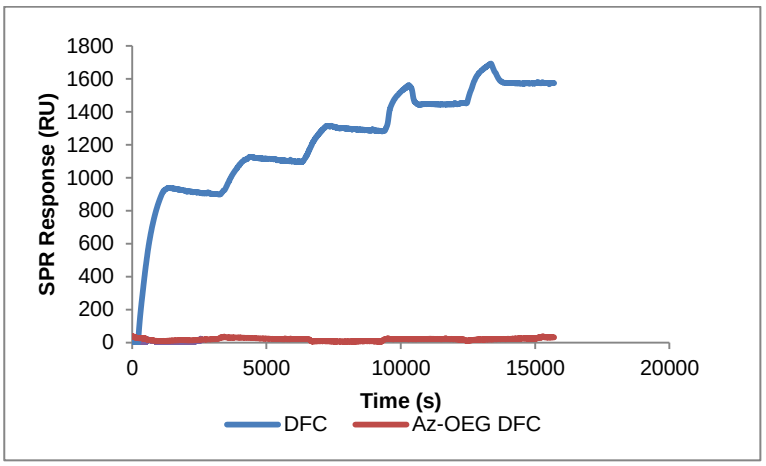

Figure 78: Representative SPR sensorgram demonstrating injections of BSA over an unmodified DFC SAM (blue line) and a Az-OEG DFC SAM (red line).

In order to assess the effectiveness of the click reactions to modify the surface properties, the same experiment was then conducted using DFC surfaces that were modified via click chemistry to be OEG-terminated. The same BSA protein solutions were then injected over these modified DFC surfaces. The results are shown by the red line in figure 81. It can be seen that there is a marked decrease in the protein interactions with the surface, with adsorption being reduced to a level which comparable with the OEG SAM investigated. Thus it can be concluded that the surface modification strategies are successfully able to modify the physical properties of the SAM surfaces, including the ability to resist the non-specific adsorption of protein (BSA), producing results comparable to an OEG surface.

5.3 Boronic acid surfaces ability to bind RNAse A and B

The cellular enzyme ribonuclease (RNAse) offers a well understood model for investigation of glycoproteins and is particularly useful as it has two isoforms, RNAse A, which is non-glycosylated isomer of the protein and RNAse B which has the same amino acid structure, but with the addition of a single glycosylation site. For this reason, we chose to use these proteins as models to build molecularly imprinted surfaces for glycoproteins, as we hypothesise that additional glycans present will result in enhanced affinity for RNAse B due to the formation of glycan-boronic acid complexes, as depicted in Figure 79.

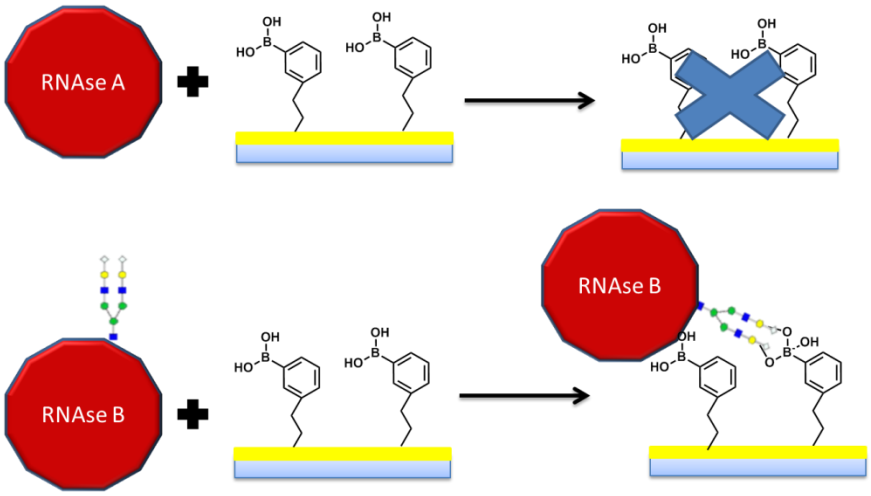

Figure 79: Schematic diagram of the interactions between boronic acid-terminated surface and RNAse A and RNAse B. RNAse A and B have the same peptide sequence, however RNAse B contains a glycosylation group, shown schematically in the diagram. This boronic acid group permits the formation of complexes between sugar diols and the boronic acids on the surface which not possible with RNAse A due to the lack of glycosylation.

The ability of boronic acids to interact with diols is a pH dependant process. This is due to the process being reversible (see Scheme 9), with each step in the process resulting in the liberation of protons.

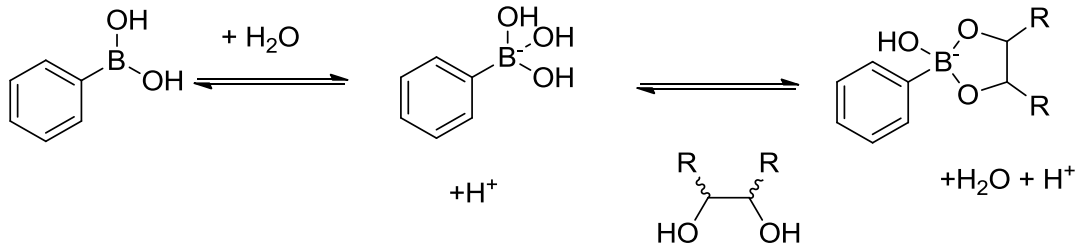

Scheme 9 The reversible interaction between boronic acids and diols.

Therefore, an increase in the pH acts to push this equilibrium across to the right, promoting the formation of boronic-diol complexes. To ensure that we conducted SPR experiments at the ideal pH, we looked at the ability of boronic acid SAM to bind simple sugars at various pHs. DFC SAMs modified with acrylic boronic acids were used as the sensor surface. The monosaccharide fructose was used as a ligand due the increased stability of complexes formed between it and boronic acids compared to other monosaccharides, thus producing the largest possible SPR response.[11] Solutions of fructose in the buffers adjusted to the relevant pH were injected over the surface for 10 minutes and equilibrium values were monitored. The equilibrium results can be seen in Figure 80. The results suggest that the optimum pH would be 8.5, which is in agreement with other published works.[315-317] In addition, we used boron NMR to ensure that the case was the same in bulk solution with boronic acid which was not surface bound.

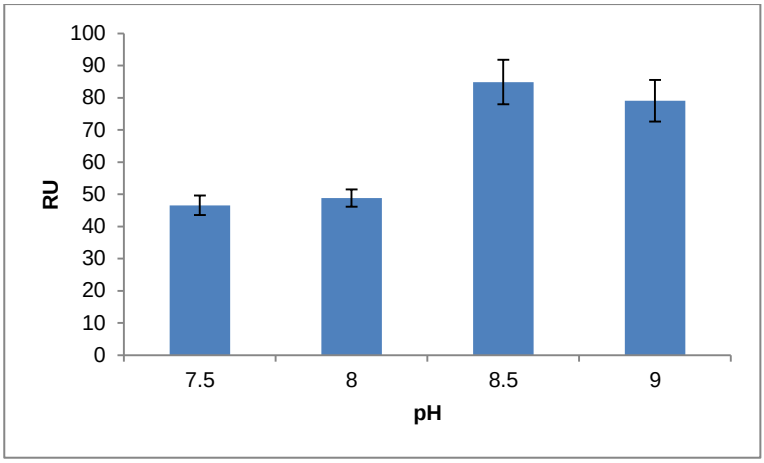

Figure 80 SPR responses of boronic acid modified DFC surfaces to fructose at differing pHs. Error bars indicate standard deviation.

Boron NMR can be used to determine the proportion of the boronic acid species that are complexed to diols. Adoption of the tetrahedral form of boronic acids causes a distinct chemical shift in the boron NMR spectra, producing a second peak at 10 ppm around 20 ppm lower than the trigonal form of boron, which is seen at around 30 ppm.[318] Solutions of aminophenylboronic acids and fructose were produced in a 1:1 mixture of duterated methanol acid and D_2O, which were pH adjusted to the indicated values using sodium hydroxide. The final concentration of boronic acid and fructose was 30 mM and 300 mM, respectively. The results shown in Figure 81 demonstrate that as the pH of the solutions was increased, the size of the second peak increases. This finding agrees well with the results of the SPR pH experiments, as both experiments indicate that a greater number of complexes are formed at higher pH. These results are also in agreement with published literature.[319]

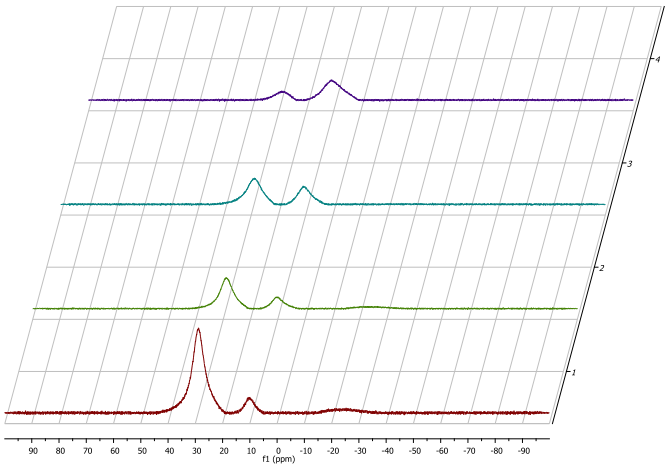

Figure 81: Boron NMR of mixtures of phenyl boronic acids and fructose in solutions at varying pHs; pH 7 red line, pH 7.5 green line, pH8 blue line, pH 8.5 purple line.

5.3.1 Ability to Bind RNAse B

To provide proof of principle that boronic acids can be used to differentiate between RNAse A and B, we fabricated a surface of DFC and then carried out the acrylic boronic acid reaction, to produce a pure boronic acid terminated surface. Over this surface, we then injected a solution of each protein, at a concentration of 100 µg/mL. The results demonstrate that these boronic acid surfaces have an inherently higher affinity to the glycosylated RNAse B, compared to RNAse A (Figure 82). This increased affinity is presumably due to the interactions of the boronic acid groups with diols present the sugar residues of the glycosylation group of the RNAse B molecule. Notably, however, there is a significant response from the non-glycosylated RNAse A protein.

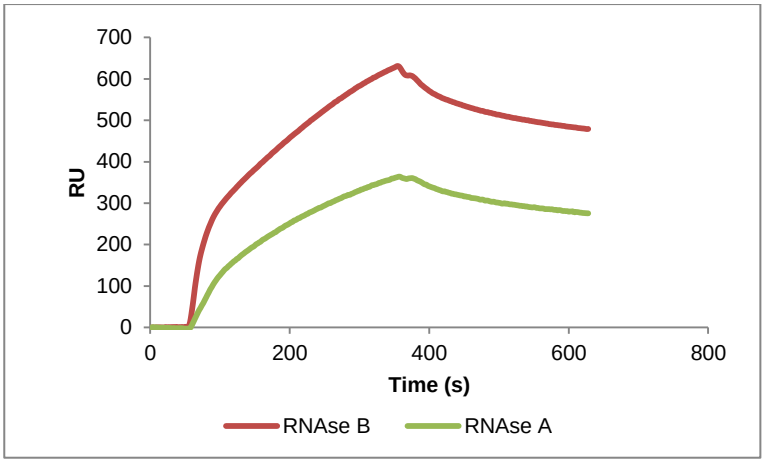

Figure 82: Representative SPR sensorgram demonstrating injections of RNAse A (green line) and RNAse B (red line) over a AABA modified DFC SAM

This suggests that the boronic acids are not only interacting directly with the diol moieties but could also be acting as hydrogen bonding sites for groups within the peptide backbone of the protein. Additionally, there is some evidence reported previously which suggests that boronic acids are also able to form the covalent interactions with the diol-like groups on multiple serine residues while the RNAse peptide is known to contain several points at which there is di-serines, which could explain the affinity for the non-glycosylated RNAse A.[73, 320]

While the results obtained with the AABA modified DFC, with a higher affinity displayed for the glycoprotein RNAse B, are promising, this surface does will likely not be selective for any particular protein. To test this hypothesis, a series of proteins, RNase B (glycosylated), Lysozyme (non-glycosylated) and α-1-Acid glycoprotein (glycosylated), at a number of concentrations were prepared and injected over the surfaces. The results of the equilibrium SPR response of each protein are shown in Figure 83. It can be see that although RNAse B produces the highest responses, there is also a significant response from the other proteins, even though they are non-glycosylated. This suggests that the boronic acid groups are able to interact not only with the glycol groups but also able to

interact with proteins through non-covalent interactions such as hydrogen bonding and ionic interactions.

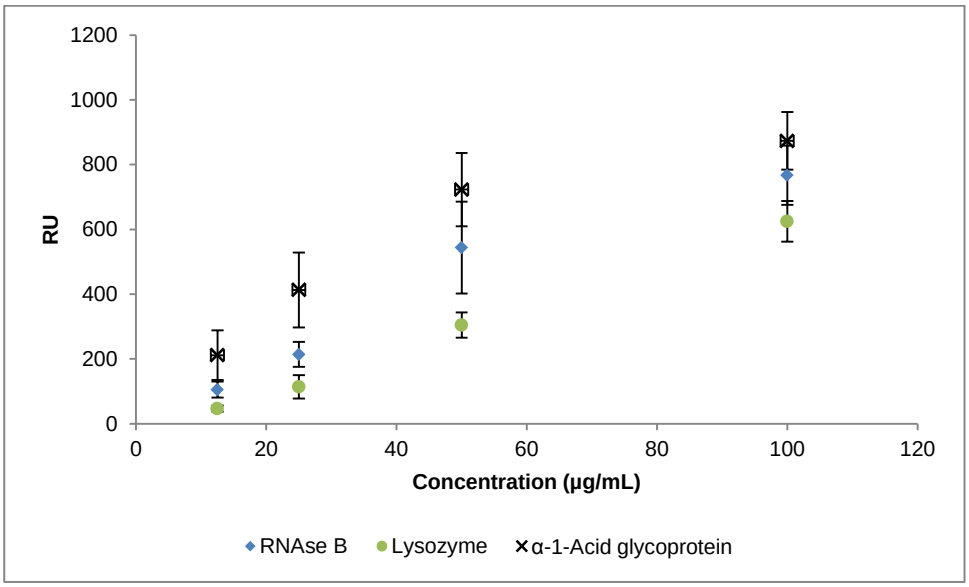

Figure 83: SPR equilibrium responses of boronic acid modified DFC surfaces to RNAse B, α-1-Acid glycoprotein and lysozyme. Measurements conducted at at 298 K.

5.3.2 Imprinted Surfaces

Following from establishing the suitability of boronic acids to interact with proteins, and interact more strongly with glycosylated proteins, attentions were turned to producing an imprint site, so that only desired interactions between target proteins with the surface were promoted. To enable this we used the sugar chains to be act as the molecular imprint, and produce binding sites on the surface as outlined in the schematic shown in Figure 84.

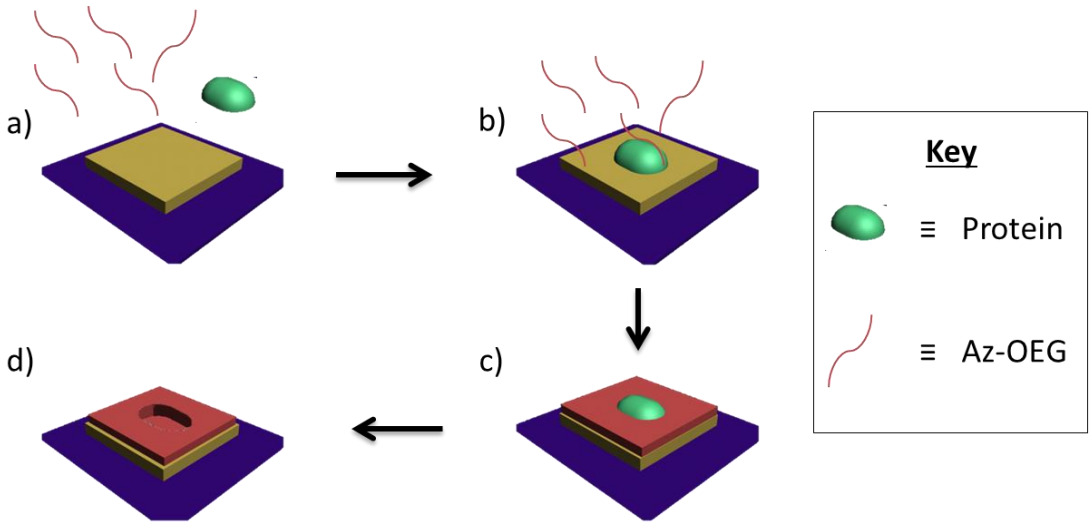

Figure 84: The outline of the scheme of molecular imprinting using sugar chains. a) A pre-prepared DFC surface is mixed with the target protein in the presence of Az-OEG b) the surface and Az-OEG allowed to interact with the proteins, c) using the Cu-AAC reaction the glycol chains are added around the protein d) the protein is removed leaving behind the imprint site

Briefly, preformed DFC SAM was placed in solutions containing both the target protein RNAse B and the azide glycol. To this solution, the click reaction initiators were added and the mixture allowed to react for 4 hours, after which the SPR chips were removed from the solution and washed with liberal amounts of water to remove template proteins. The ability of the surfaces to bind the target proteins was then assessed via SPR. When the sensor was then exposed to both RNAse A and B, a response was observed from both proteins, although it can be seen that RNAse A produced a larger response (Figure 85). It is also notable that both RNAse A and B produce a smaller response on this surface than on the pure boronic acid-modified surface, which suggests that the boronic acid is able to enhance the interactions of the protein, most significantly RNAse B, presumably due to interaction with diols present only in the glycoprotein.

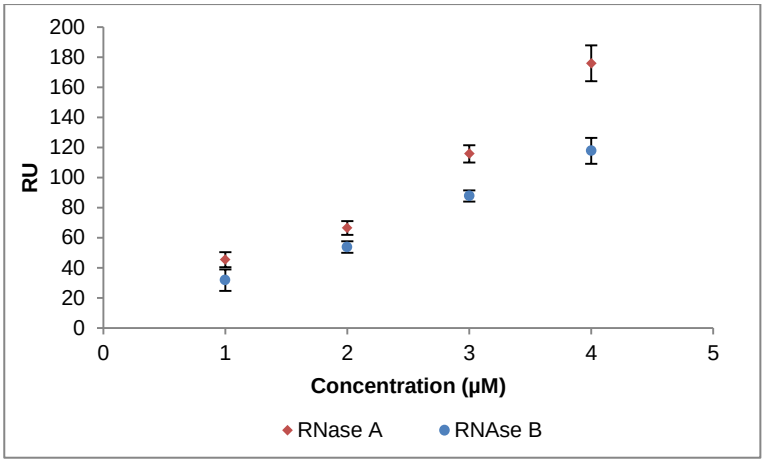

Figure 85: SPR responses of RNAse B molecularly imprinted surfaces prepared in the absence of boronic acid to RNAse A (red points) and RNAse B (blue points) Measurements conducted at at 298 K.

In addition, it suggests that a RNAse A has a higher affinity to the glycol scaffold. This effect was at first puzzling, as one may expect the two proteins to have the same affinity to the imprinted surfaces. However, after consulting the literature there is evidence to suggest that the increased affinity of the RNAse A may be increased due to interactions with the acrylic groups on the imprinted surface. [321, 322]

To ensure that this effect was due to the effective imprinting of the proteins, a non-imprinted surface was produced on preformed SAM of DFC, which was then modified with the glycol groups in the absence of target protein. This process would produce an essentially glycol-terminated SAM. The ability of these surfaces to interact with the RNAse A and B was then assessed via SPR (Figure 86). The results show that the pure glycol control SAM shows little binding for any of the proteins used in the study, and thus confirm that the enhanced response seen in figure 88 is due to the imprinting process.

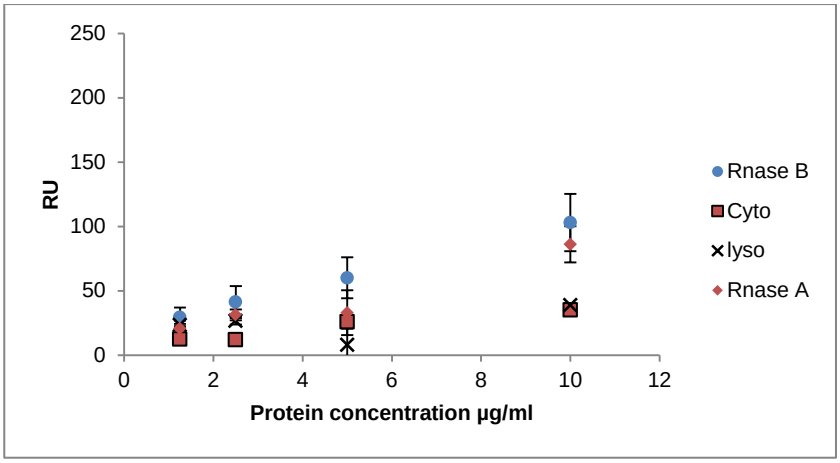

Figure 86 SPR responses of control (non-molecularly imprinted) Az-OEG DFC modified surfaces, prepared in the absence of template compound, to RNAse A, RNAse B, Lysozyme and BSA and other proteins. Measurements conducted at 298 K.

5.4 Molecular Imprints with AABA and Az-OEG

5.4.1 Optimum boronic acid ratio

Following the proof of principle that the OEG and boronic acid elements of the sensor design were suitable for the imprinting and glycoprotein selectivity, respectively, the two elements were brought together to produce functional sensors. Detailed methods of molecular imprint formation can be found in the methods chapter of this thesis. However, a brief outline of the procedure is as follows: Imprinted surfaces were formed on SPR chips which had been modified with a DFC monolayer. To form the imprinted surfaces these preformed DFC SAMs and the imprint components, AABA and Az-OEG, were incubated with samples of the template protein. The imprinted surface fabrication was then controlled by the addition of the initiators for each of the acrylic and Cu-AAC reactions. Acrylic reactions were initiated first by the addition of APS and TEMED and allowed to proceed for 30 min. After this, the click reactions were initiated via the addition of a copper sulphate and sodium ascorbate. The mixture was then allowed to react for a further 4 hours. Following formation, sample chips were removed for the formation mixture and rinsed for several minutes with large quantities of water to remove template molecules.

In order to determine the optimal amount of boronic acid required a series of molecular imprints, using RNAse B as a template, were made using differing molar equivalents of boronic acids. The ability of the resulting imprinted surfaces to bind RNAse A and B was investigated via SPR. The results of this investigation are presented in Figure 87. The results show that as the equivalent of boronic acids are increased, the overall ability to bind the two proteins increases, as demonstrated by the increase in the calculated affinity for the two proteins. However, the absolute affinity is not the only factor to consider; the selectivity of the imprints to the desired glycosylated RNAse B must also be considered. In order to do this, the calculated affinity for RNAse A was divided by the calculated

affinity for RNAse B to provide an indication of the selectivity demonstrated by each surface. The result of this calculation demonstrated that the optimum equivalent of boronic acid was ten times that of the protein template. Although high levels of boronic acid produce a higher absolute response to the template, RNAse B, then also produced a larger response the competing RNAse A, and ultimately reducing the selectivity of the surface.

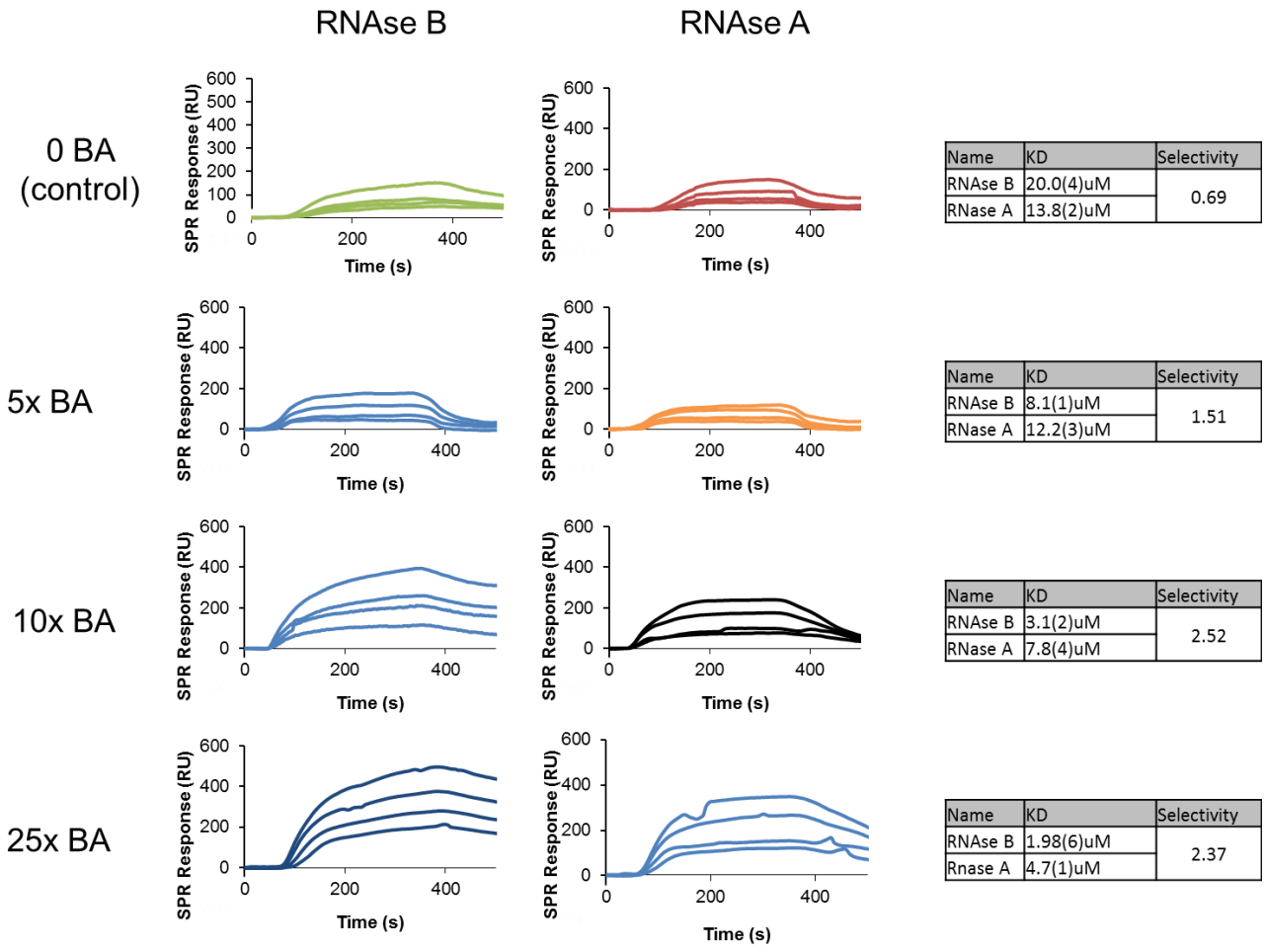

Figure 87: SPR investigation into the effects of boronic acid content on RNAse A and B selectivity in molecular imprinted surfaces. Measurements conducted at at 298 K.

5.5 RNAse B imprinted Sensor

5.5.1 Assessment of sensor affinity and selectivity

Following optimisation, the selectivity of the RNAse B imprinted sensors was investigated by assessing their ability to bind proteins, both template and competing, via SPR. The properties, such as size and isoelectric point, of all the proteins investigated are presented in Table 16.

Table 16 Properties of the proteins used in moleclar imprinting studies

Protein	RNAse B/A	Lysozyme	α-1-acid glycoprotein	BSA	PSA	HPA	α-1-antitrypsin
Molecular weight	14700/ 13700	14600	44000	66500	28400	44000	52000
Glycosylation (%)	9/ 0	0	45	0	8.30	21	5
Dimensions (nm)	3.8x2.8x2.2 [323]	2.8x3.2x3 [324]	5.9x4.2x3.9 [a]	14.x4.0x4.0 [26]	4.4x4.1x5.1[a]	4.0x6.7x11.7 [325]	7x3x3 [326]
Isoelectric point	9.2- 9.6 [327]	11.1[328]	2.8-3.8[329]	4.7[330]	6.2-7.5[49]	9 [331]	4.5-5.5[332]

[a] *calculated from crystallography data using ChemBioDraw 3D*

The result of SPR investigations in to the binding of each protein to the molecular imprinted surface is presented in Figure 88. We observed that the response to template proteins was significantly higher than that to non-imprinted proteins, which produced a response similar to that expected from non-imprinted surfaces. This demonstrates that the molecularly imprinted surfaces were able to distinguish between the target protein and non-target proteins with a high degree of selectivity.

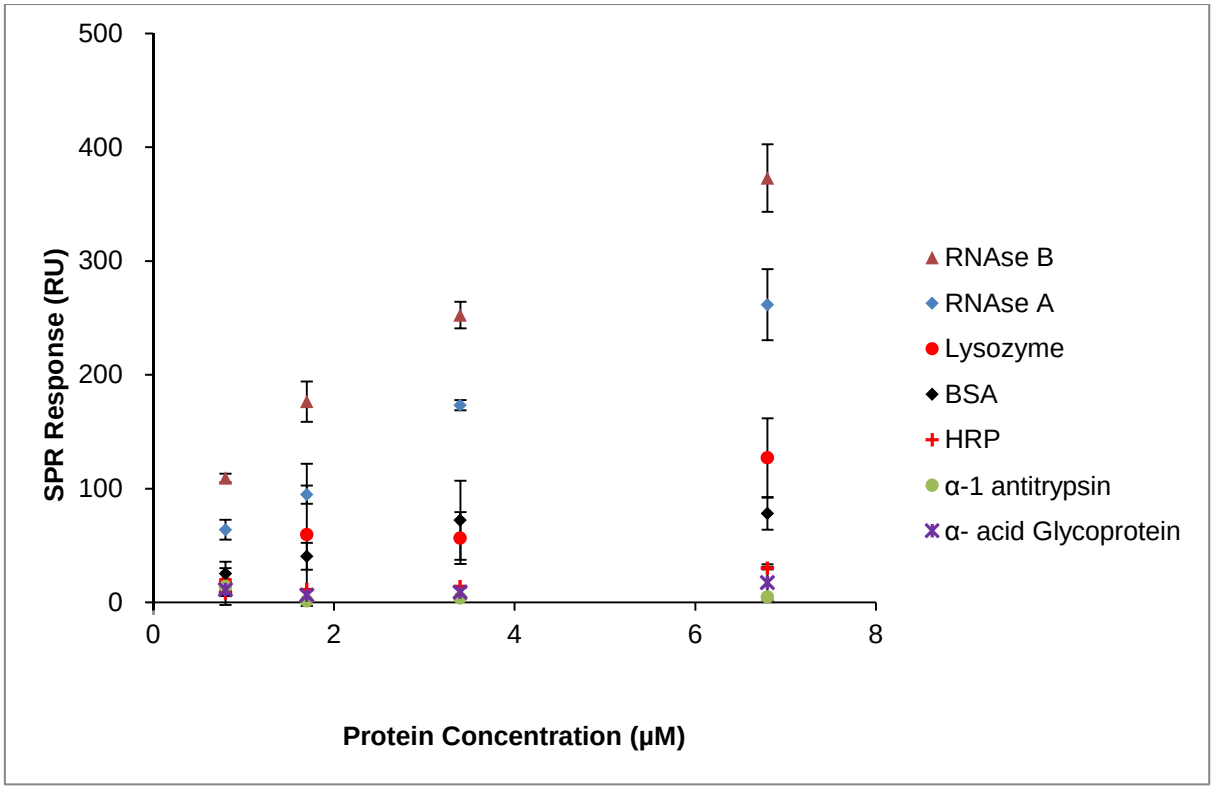

Figure 88: SPR responses of RNAse B specific molecularly imprinted DFC surfaces to RNAse B and other proteins. Measurements conducted at 298 K. Error bars indicate standard deviation.

5.5.2 Discussion of sensor affinities

For the surfaces which were engineered to be specific to RNAse B, we observe the affinities shown in Table 17. The highest affinity is observed with the target protein, RNAse B, thus suggesting that binding sites on the surface are complementary in size and arrangement to this molecule. RNAse A is the non-glycosylated isomer of RNAse B. Both compounds share the same protein structure, however, RNAse B contains an additional post-translational modification - a single glycosylated site. Therefore, the observation that RNAse A shows the closest affinity to RNAse B from all the proteins examined is expected.

Table 17 Calculated affinties between proteins and RNAse B molecularly imprinted sensor

Protein	K_D (μM)
RNAse B	3.89 ± 0.1
RNAse A	8.01 ± 0.1
Lysozyme	24.3 ± 1.0
BSA	33.8 ± 6.0
HRP	119 ± 2.0
α-1-acid glycoprotein	201 ± 7.0
α-1-antitrypsin	570 ± 50

We observe that the lysozyme is also able to interact with the surface, but to lesser degree than the target protein, with an affinity around 6 times lower. Although this compound is not glycosylated, it is similar in molecular weight and dimension to the template compound, (2.8 × 3.2 × 3.0 nm vs 3.8 x 2.8 x 2.2 nm).[333] Furthermore, is carries a net positive charge, which could facilitate the interaction with the negatively charged boronic acid groups on the surface. In addition, the peptide sequence of lysozyme is known to contain several serine residues which could also offer sites to which boronic acids could interact.[334]

The remaining proteins examined produced only negligible binding with the sensor surface, as shown by the calculated affinities, some of which are orders of magnitude less than the target protein. This finding was interesting given that the several of the proteins are glycosylated. We initially hypothesised that such compounds may display non-specific interactions with the surface, due to the sugar residues. However, examination of the properties of these proteins suggests that these proteins are too large to interact with the surface imprints - all the proteins have larger molecular dimensions than the target, RNAse B. In addition, these proteins are commonly negatively charged which may also inhibit their interaction with the surfaces due to the repulsion between the charges on the proteins and the negative charge on the boronic acids.

5.6 PSA Imprinted Sensor

Following the optimisation of an imprinted surface specific for RNAse B, we attempted to produce an imprinted surface which was able to selectively interact with the clinical marker PSA. Prostate cancer is the most common male malignancy in Europe and the United States, and the second leading cause of death from cancer.[335-337]

PSA is a glycoprotein, and increase in its levels, is correlated with an increased risk of developing prostate cancer. Furthermore, there is evidence to suggest that the glycolaslation seen on the proteins could correlate with the development of malignant prostate disease.[338] Therefore, this protein was chosen as a clinical marker for sensor development. The PSA imprinted surface was produced in the same manner as described previously, with the exception that PSA was used as a template molecule. Following the fabrication of the imprinted surfaces, solutions of target proteins and a number of competing proteins were each injected injected over the surfaces and interactions of each protein with the surface were monitored using SPR. The results of this investigation are presented in Figure 89.

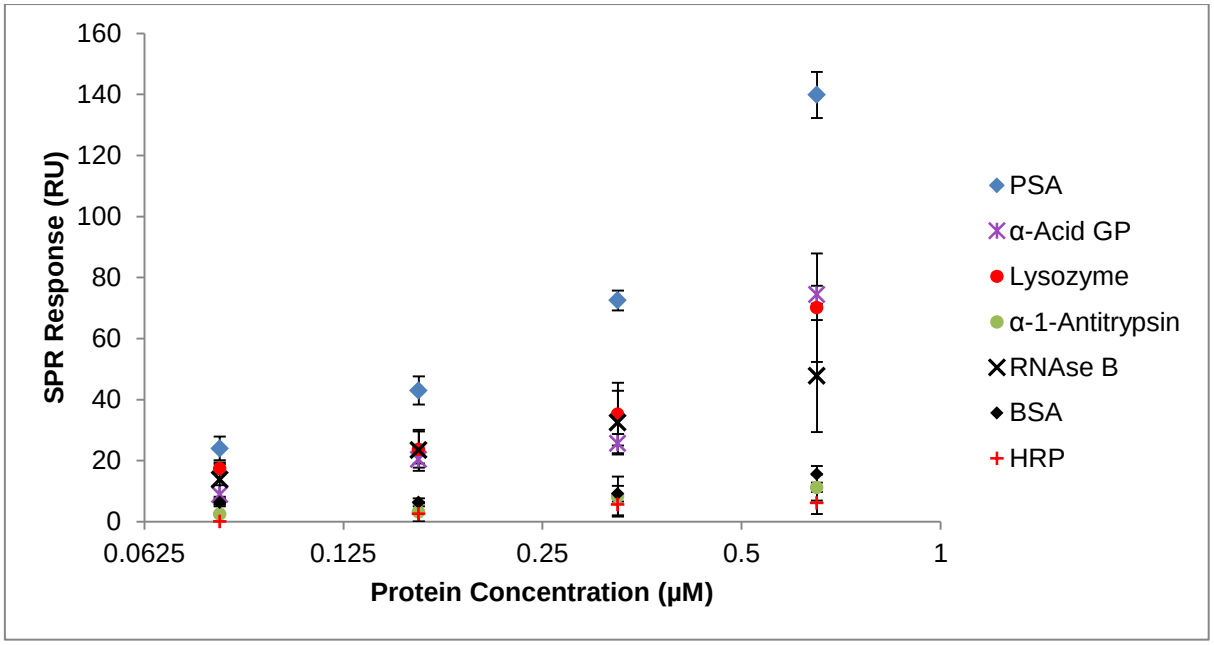

Figure 89: SPR responses of PSA specific molecularly imprinted DFC surfaces to PSA and other proteins. Measurements conducted at at 298 K. Error bars indicate standard deviation.

5.6.1 Assessment of affinity and selectivity of PSA Surface

Following examination of the interactions of surfaces imprinted with PSA with other proteins, we observe the affinities shown in Table 18. We observed that PSA produces the highest response and affinity, which is expected as it is the target protein. This high affinity is expected as the molecular imprints should be complementary to the PSA, and its glycosylation groups. As observed with RNAse B-imprinted surfaces, molecular size appears to be a factor affecting the binding of other competing proteins to the molecular imprints. The proteins RNAse B, Lysozyme and α1-acid glycoproteins are all similar or smaller in size to the target PSA and display binding affinities that are higher than that of the other lager proteins examined (see Table 16). We observe that the α-1 acid glycoprotein produces the second highest affinity to the surface, which we hypothesise that this is due to the protein having a similar molecular diameter to PSA and also due to the high levels of glycans present on this protein. This combination permits the protein to 'fit' into the imprint sites and facilitate the interactions between the boronic acid groups

and the glycans present on the protein, producing the observed affinities. Comparison with the response of the RNAse B MI surface and PSA MI surface to α1-acid glycoprotein shows that on the RNAse B surface the protein produced a very low affinity, while on the PSA surface the response is considerably higher. We hypothesise that this is due to the increased size the imprint sites due to the lager target compound, PSA, which allows the α1-acid glycoprotein to access the binding site, producing an enhanced affinity.

Table 18 Calculated affinties between proteins and PSA molecularly imprinted sensor

Protein	K_D (μM)
PSA	1.8 ± 0.07
Lysozyme	4.84 ± 0.1
α-1-Acid glycoprotein	5.3 ± 0.1
RNAse B	6.7 ± 0.5
BSA	21.6 ± 0.6
α-1-Antitrypsin	30.9 ± 0.9
HRP	52.5 ± 2.0

RNAse B shows some interactions with the surface. However, its affinity is approximately 4 times less than the affinity of PSA towards the surface. This is presumably due to the fact RNAse B has dimensions which should allow it to 'fit' into the molecular imprint sites, however, the binding site will not be complimentary to the structure of the protein-producing the reduced affinity observed.

Lysozyme, as with the RNAse B surface, is able to interact to some degree with the PSA MI surface. Presumably this is due to its small size, facilitating access to the MI binding sites. However, as the protein is not glycosylated we hypothesised that this interaction is mediated via electrostatic interactions between its net positive charge and the negative charge of the boronic acids in the binding sites. The remaining proteins BSA, HRP and α-1-antitrypsin display negligible interaction with the surface. These proteins are all larger in their molecular dimensions than the target PSA, and so are unable to access the binding sites in the surface, and so produce a very weak interaction with the surface.

The SPR data was also fitted using a kinetic modelling, which produced affinity values comparable to the equilibrium affinity data. The fitting is shown in Figure 90. Using this fitting method a K_D value of 1.92µM was determined.

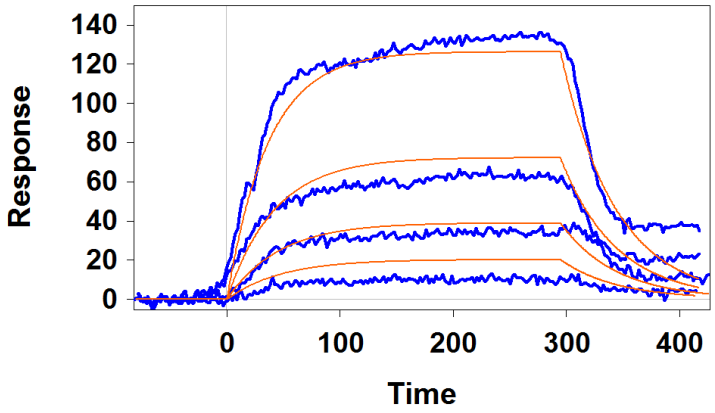

Figure 90: Kinetic model fitting of the PSA SPR sensor gram, for the PSA MI surface vs the PSA. Measurements conducted at at 298 K.

5.7 Sensor Reusability

In order to assess the surface sensors suitability to reuse, a cycle of sample binding and surface regeneration was used. An RNAse B solution (3.65 µM) was used to examine the cycles of binding and regeneration of the surface (Figure 91).

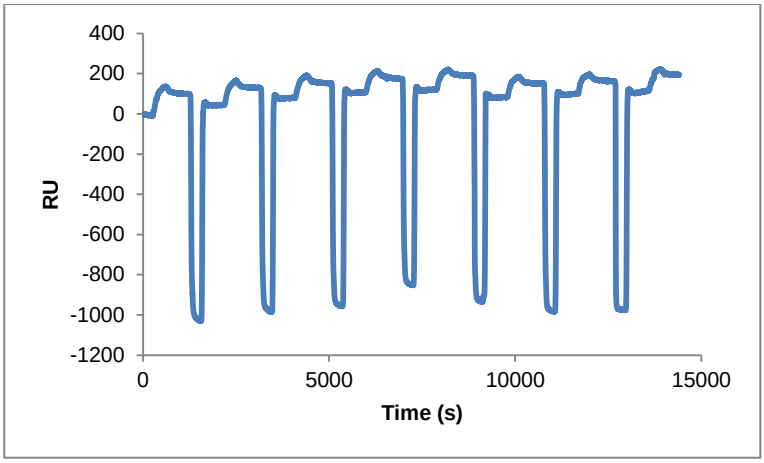

Figure 91: Representative SPR sensorgram demonstrating cycles of binding and regeneration of RNAse B to RNAse B molecularly imprinted surfaces. Injections of 3.65 µM samples were injected for 5 minutes followed by a 5 minute dissociation period. Following this a regeneration solution was then injected over the surfaces for 5 minutes.

This procedure was repeated 10 times and in triplicate, and the SPR response at equilibrium was monitored. The results (Figure 92) demonstrate that for the first 10 replicates the loss of sensor function is minimal, which is comparable if not better than the regeneration behaviours of antibody based sensors.[339, 340]

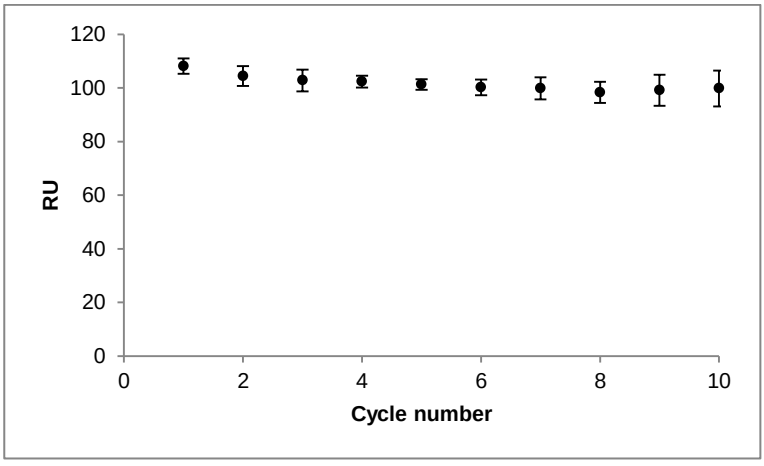

Figure 92: Plot of the equilibrium responses for a 3.65 µM RNAse B solution over RNAse B MI surface after various numbers of binding-regeneration cycles. Error bars indicate standard deviation.

5.8 Serum compatibility

In order for the surfaces to be useful in a clinical setting, there will be a requirement for the surfaces to be suitable to work in the presence of complex matrixes. This requirement stems for the fact that many clinically relevant glycoproteins which are potential biomarkers are likely to be found in sample types such as serum, urine and prostate secretions. All such sample types contains a large number of proteins, carbohydrates and lipids, which have the potential to cross react with the imprinted surface and affect performance. Fortunately, the OEG groups from which the imprinted surface is fabricated are known to offer effective resistance to the non-specific adsorption of proteins and other biological compounds. In order to be sure that the MI surface was able to resist the adsorption of unwanted compounds, while maintaining the ability to bind the desired targets, experiments were conducted using the complex media, serum. In these experiments 0.5% serum was added to the buffer used for all SPR experiments. RNAse B protein dilutions were prepared in this 0.5% serum buffer and then each concentration of the protein was injected over the sensor surface as normal. The results of these investigations demonstrate that the surface were able to perform adequately 0.5% serum, although the responses produced were diminished, presumably due loss of some binding sites due to the non-reversible adsorption of some serum components (Figure 93).

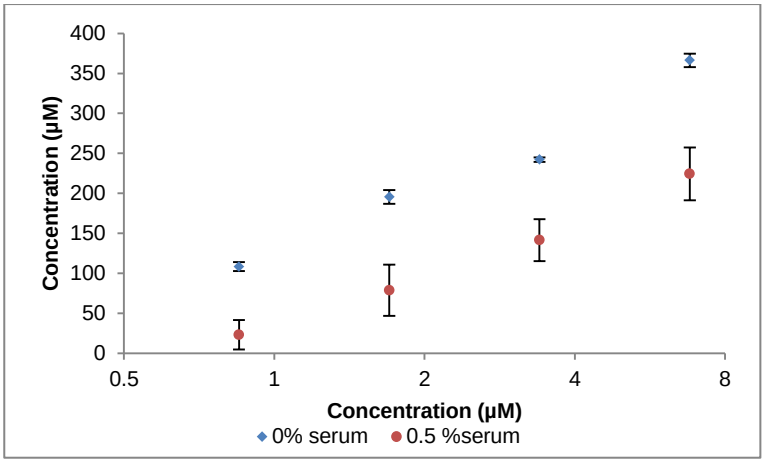

Figure 93: SPR responses of RNAse B specific molecularly imprinted DFC surfaces to RNAse B with 0.5% serum. Measurements conducted at at 298 K. Error bars indicate standard deviation.

5.9 Conclusion

In conclusion, the fabrication of a synthetic molecularly imprinted surface sensor system for the detection of glycoproteins has been described, based upon a novel di-functionalised SAM molecule. In addition, the system is able to selectively identify glycosylated forms of the target protein, in preference to non-glycosylated forms, via the incorporation of boronic acid units. The methodology has been demonstrated to be adaptable and able to be used to generate sensors of several proteins including the biologically relevant prostate specific antigen, which is a clinical marker for prostate cancer. The affinities of the resulting sensor surfaces were calculated and have shown to be in the range of some antibodies, however they were found to be lower than some high high-affinity monoclonal antibodies.[341] The sensor surfaces have been demonstrated to be suitable for use in complex matrixes, such as serum, with minimal loss of performance. It is hoped that further work with this system will allow the development of system which are capable of analysing clinical samples to take this technology forwards towards ‘real world’ applications.

CHAPTER 6: CONCLUSIONS AND FUTURE WORK

6.1 Conclusion

The work performed in this thesis has described the fabrication of surface sensors for the selective detection of glycoproteins and monosaccharides. This work has demonstrated that through the design of molecular components and binding sites, synthetic sensors can be fabricated. Furthermore, it has been illustrated that such systems offer the possibility to produce sensor systems with functionally comparable to that observed in biologically derived sensors, such as those which rely on antibodies and enzymes for molecular recognition.

These devises were produced using principles of self-assembly to modify surfaces and impart upon them the physical and chemical properties which are required to achieve the goal of molecular recognition. Key to this has been the employment of boronic acids groups which are able to offer a solution to sugar detection via the formation of reversible esters with the diol groups present on sugar compounds. We demonstrate that this interaction can be combined with supramolecular concepts to produce surface attachable compounds for the selective binding of a target monosaccharide, glucose, with higher affinity than other closely related monosaccharide compounds.

In the second section of this thesis we describe the concept, design and synthesis of compounds to use in a novel molecular imprinted surface sensor. The final target compound, DFC, contained three separate functional groups to allow the control of three aspects of sensor formation: attachment to the gold surface and the addition of two separate sensor components, boronic acid and glycol chains. The sensors which were created with using this system were shown to be able to selectively bind target proteins, including the biologically relevant protein PSA. Additionally we demonstrate that this system is able to distinguish between a glycosylated and non-glycosylated isoform of the same protein, RNAse. While this finding certainly represents progress towards synthetic sensors for detecting changes in glycosylations of proteins, further work would be helpful

to realise this lofty goal. Ideas for how this project could be further developed will now be discussed.

6.2 Future Work

The ultimate goal of this research is to produce systems which are able to differentiate between different glycoforms of specific target glycoproteins. Currently, the only methods by which this can be achieved are time consuming and costly techniques such as HPLC. We aim to produce a simple synthetic sensor system which is able to achieve this goal in a single step process, akin to ELISA. Whilst we have been able to produce a system which is able to differentiate between glycosylated and non-glycosylated proteins, the challenge of detecting and quantifying different glycoforms of the same glycosylated protein remains.

6.2.1 The Problem- Highlighted by Prostate Cancer

Prostate cancer is the most commonly diagnosed male malignancy in the western world.[47] Prostate disease, both malignant and benign, produces disruption to the structure of the prostate resulting in the escape of PSA into the blood stream.[48] Although PSA assays are widely used for detection of prostate cancer such assays are associated with poor sensitivity and specificity. Therefore one of the most urgent requirements in cancer diagnosis and treatment is the development of a minimally-invasive test which would be able to distinguish prostate cancer from the non-pathological condition of benign prostate hyperplasia.[50]

Glycosylation is one of the most common co- or post-translational modifications made to proteins. Critically, changes to patterns of glycosylation of proteins is known to change in cancerous disease, including prostate cancer, and so offers a promising target for new biochemical assays.[32] However, due to the inherent difficulties in the characterization of protein glycosylation structures by traditional methods, there is currently no single test

able to distinguish between prostate cancer and benign prostate disease. Our previous research has produced synthetic sensor surfaces which are able to selectively bind specific monosaccharides and glycoproteins, including PSA, using boronic acids and molecular imprinted surfaces.[305] The advantage of the systems produced is that they are well suited to the high throughput and simple sample preparation required by clinical practice. Thus, the goal of future research stemming from the work described in this thesis will be to develop a single sensor system which is able to selectively bind and distinguish PSA proteins from complex mixtures present in biological samples and also differentiate different glycosylation patterns present on the PSA molecules.

6.2.2 Boronic Acid and the Importance of pKa

In this thesis .we have demonstrated the use of a *bis*-boronic acid group for the selective detection of monosaccharides. An interesting avenue for further research would be the use of multiple intramolecular boronic acids to facilitate the selective detection of different complex sugar structures, such as those found in post-translational modifications of proteins. Publications which describe the synthesis and application of this class of bis-boronic acid have, to date, focused on how the intramolecular spacing of the boronic acid groups is able to influence selectivity.

A second element of boronic acids which has received attention is the influence of their pKa on their interactions with sugars - the pKa of boronic acids has been shown to be vital to the functionality of boronic acid based sensors. Previous works by several groups have produced libraries of boronic acid derivatives which demonstrate the ability to tune the pKa via substitution of substituents (Figure 94). [2] However, to date, the use of bis-boronic acids with differing intramolecular pKa values has not been explored for the sensing and profiling of complex carbohydrates. Furthermore, it is known that malignant disease results in the incorporation of sugar groups with different pKas into glycosylation structures, which can allow the differentiation between health and disease. Recently,

selective interactions between sialic acids (a saccharide with low pKa) and modified phenyl boronic acid have been achieved, highlighting the importance of the ligand pKa in binding events[342]. Thus we propose that through the design of *bis*-boronic acids species in which pKas of each boronic acid group can be independently controlled selectivity for complex glycosylation groups could be achieved.

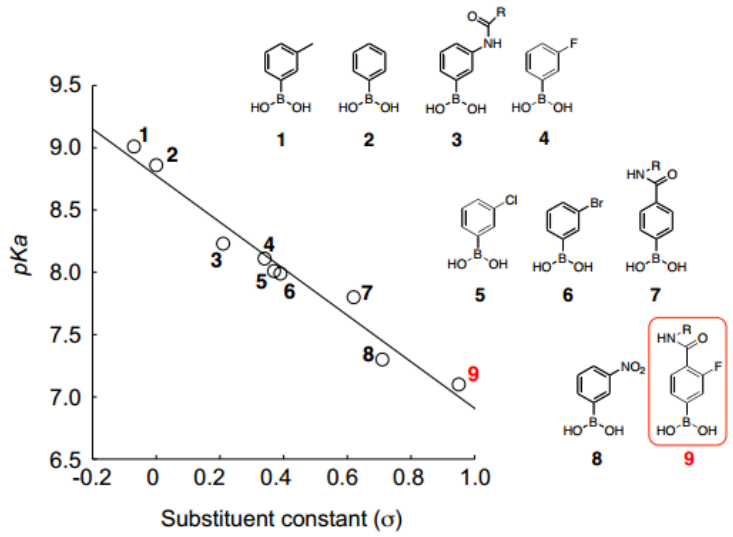

Figure 94: Examples of boronic acid species with their pKa values [1, 2].

6.2.3 Proposed Future Research

We propose that one element of future research would be to produce a library of compounds which contain multiple intramolecular boronic acids, each of which will have a different pKa and will be suitable for use in the molecular imprinting sensor systems described in this thesis. Thus, the aim of this work will be to synthesise a small library of *bis*-boronic acid compounds with each intramolecular boronic acid being varied with reference to its pKa. The compounds produced should then be screened to assess their binding with oligosaccharides. Compounds which show promise should then be incorporated into modified surfaces to produce surface sensors selective for specific oligosaccharides present on glycoproteins.

6.3.4 Target Compound General Design and Requirements

The design of the compounds should meet these strict requirements in order to be useful: The synthetic route should be modular- simple changes of reagents should produce the variety with the compounds without the need for changing the synthetic process. The compounds should be water soluble, as they will need to be compatible with aqueous biological samples.

In addition, molecular design will need to be highly adaptable, allowing tuning of molecular properties. These properties will include: pKa of the constituent boronic acids, linker length and linker properties- such as charge, flexibility polarity etc. The rational of the compounds to be produced will be that by producing compounds with different intramolecular boronic acids, each with different pKa, the compounds will allow the production of a novel class of boronic acid glycan receptors. These molecules should allow the interactions of glycans to be selectively targeted through control of pH, boronic acid spacing, linker properties and boronic acid pKa to produce tuneable glycosylation carbohydrate binding motifs (Figure 95).

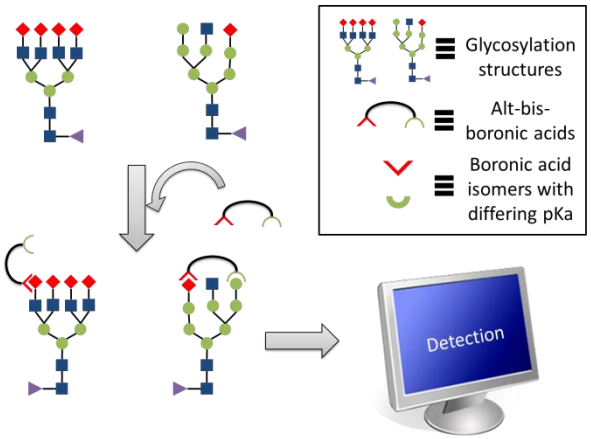

Figure 95: alt-bis-boronic acids will be able to display different affinity to different glycosylation

CHAPTER 7: METHODS

7.1 General methods

7.1.1 Contact Angle

Contact angles were determined using a home-built contact angle apparatus, equipped with a charged coupled device (CCD) KP-M1E/K camera (Hitachi) that was attached to a personal computer for video capture. The dynamic contact angles were recorded as a micro-syringe was used to quasi-statically add or remove water from the drop. The drop was shown as a live video image on the PC screen and the acquisition rate was 4 frames per second. FTA Video Analysis software v1.96 (First Ten Angstroms) was used for the analysis of the contact angle of a droplet of UHP H_2O at the three-phase intersection. The averages and standard errors of contact angles were determined from five different measurements made for each type of SAM.

7.1.2 Ellipsometry

The thickness of the deposited monolayers was determined by spectroscopic ellipsometry. A Jobin-Yvon UVISEL ellipsometer with a xenon light source was used for the measurements. The angle of incidence was fixed at 70 ° . A wavelength range of 280–820 nm was used. The DeltaPsi software was employed to determine the thickness values and the calculations were based on a three-phase ambient/SAM/Au model, in which the SAM was assumed to be isotropic and assigned a refractive index of 1.51. The thickness reported is the average and standard error of six measurements taken on each SAM.

7.1.3 X-ray photoelectron spectroscopy (XPS)

Elemental composition of the SAMs were analysed using an Escalab 250 system (Thermo VG Scientific) operating with Avantage v1.85 software under a pressure of ~ 5 x 10^{-9} mbar. An Al Kα X-ray source was used, which provided a monochromatic X-ray beam with incident energy of 1486.68 eV. A circular spot size of ~ 0.2 mm^2 was employed. The

samples were attached onto a stainless steel holder using double-sided carbon sticky tape (Shintron tape). In order to minimise charge retention on the sample, the samples were clipped onto the holder using stainless steel or Cu clips. The clips provided a link between the sample and the sample holder for electrons to flow, which the glass substrate inhibits. Low resolution survey spectra were obtained using a pass energy of 150 eV over a binding energy range of 0 eV to 1250 eV obtained using 1 eV increments. The spectra recorded were an average of 3 scans. The high resolution spectra were obtained using a pass energy of 20 eV and 0.1 eV increments over a binding energy range of 20–30 eV, centred on the binding energy of the electron environment being studied. A dwell time of 50 ms was employed between each binding energy increment. The spectra recorded were an average of between 5-250 scans (N (1s) = 100 , Au (4f) =5, S (2p) = 150, B (1s) = 250, O (1s) = 50, C (1s) = 50). Sensitivity factors used in this study were: N (1s), 1.8; Au (4f), 17.1; S (2p), 1.68; B (1s), 0.486; O (1s), 2.93; C (1s), 1.0.

7.1.4 Surface Plasmon Resonance (SPR)

SPR experiments were performed with a Reichert SR7000DC Dual Channel Spectrometer (Buffalo, NY, USA) at 25 °C. Prior to the binding studies, a baseline for the SAMs was established by running degassed buffer through the machine at a flow rate of 25 µl/min. Data was analysed using Scrubber 2 (BioLogic Software, Aus.).

7.2.1 Chromatography

Flash chromatography was performed on a Teledyne Isco CombiFlash Rf 200 using RediSep Rf silica flash columns. Ethyl acetate and hexane where used as solvents. Detection of eluted compounds was achieved using UV and evaporative light scattering detectors (ELSD).

7.2.2 NMR Spectroscopy

^{1}H and ^{13}C NMR spectra were recorded on a Bruker AV300 (at 300MHz and 75MHz respectively) or a Bruker AVIII400 (at 400 MHz and 100 MHz respectively) at room

temperature. All ^{13}C NMR spectra were recorded using the PENDANT pulse sequence. Where necessary, COSY, HSQC and NOSEY experiments were carried out to allow unequivocal assignment of signals. Chemical shifts are expressed in parts per million (ppm) down field from tetramethylsilane or relative to residual NMR solvent peak. Data was processed on MestReNova LITE v.5.2 (Mestrelab Research) and Topspin 2.0 (Bruker). The multiplicity of signals is expressed as follows: s= singlet, d=doublet, t=triplet q=quartet, m= multiplet. Coupling constants (*J*) are reported in Hz. 11B NMR spectra were recorded at 96 MHz on a Bruker AVANCE 300 NMR spectrometer and are proton decoupled all spectra were recorded at room temperature unless otherwise stated.

7.2.3 Mass Spectrometry

All samples were analysed by means of the Synapt G2-S HDMS system (Waters, Manchester, UK). All experimental data were acquired with a resolution of 20000. Samples were introduced into the mass spectrometer *via* the nanoAcquity system (Waters, Manchester, UK). Electrospray ionisation was performed with a capillary voltage of 3.2 kilovolts, and the sample cone was set at 40 volts.

7.2.4 Infrared Spectroscopy (IR)

IR spectra were recorded using a PerkinElmer Spectrum 100 FTIR Spectrometer, using a universal ATR sampler (PerkinElmer). Frequencies (in wavenumbers) are listed, with the relative strength and a brief assignment of what type of bond is resonating listed in parentheses. Peaks are listed in descending numerical order. Strengths: s = strong, m = medium, w = weak, br = broad.

7.2.5 Melting points

Melting points (mp) were recorded using a Stuart SMP10, using closed ended melting point tubes. Values stated are uncorrected.

7.2.6 Thin-layer chromatography (TLC)

TLC was carried out on aluminium plates coated with silica gel 60 F254 (Merck 5554). The TLC plates were visualised using either potassium manganate or ninhydrin dip and dried with a heat gun.

7.3 Synthesis of DFC

7.3.1 (2*R*,2'*R*)-Bis(2,5-dioxopyrrolidin-1-yl)3,3'-disulfanediylbis(2-((tert-butoxycarbonyl)amino)propanoate)

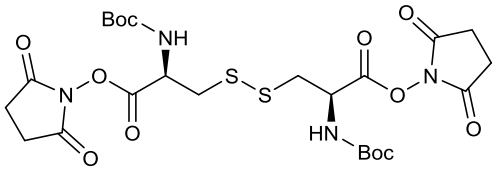

To a solution of Di-Boc-L-cystine (2.161 g, 5.14 mmol) in dry THF (50 mL) was added, *N*-hydroxysuccinimide (1.355 g, 11.3 mmol) and dicyclohexylcarbodiimide (2.327 g, 11.3 mmol) in dry THF and stirred for 18 hours at room temperature. During which time a precipitate developed. The precipitate was separated by filtration and the filtrate concentrated *in vacuo*, re-dissolved in DCM (20 mL) and again filtered. The filtrate was washed with aqueous saturated sodium bicarbonate solution (3 x 25 mL). The combined aqueous phases where then extracted into DCM (25 mL x 3), dried over magnesium sulphate, filtered and evaporated to dryness to give **1**, as a colourless crystalline solid (1.857 g, 57 %). IR (cm^{-1}) [3376.15; m, br; N-H] [1749; S; ester]; ^{1}H NMR (400 MHz, $CDCl_3$) δ 5.41 (d, *J* = 7.3, 2H, N*H*CHCH$_2$), 4.62 (dd, *J* = 12.5, 5.2, 2H, NHC*H*CH$_2$), 3.78 (s, 8H, NCOC*H*$_2$C*H*$_2$), 3.18 (d, *J* = 5.0, 4H, NHCHC*H*$_2$), 1.46 (s, 18H, NHCOOC*H*$_3$); ^{13}C NMR (101 MHz, $CDCl_3$) δ 52.78 (s, SHCH$_2$*C*H), 52.65 (s, NCO*C*H$_2$*C*H$_2$), 41.30 (s, SH*C*H$_2$CH), 28.30 (s, NHCOO*C*H$_3$); Mass spec: calculated: 657.2 $[M+Na]^+$, observed: 657.2 $[M+Na]^+$ $C_{24}H_{34}N_4O_{12}S_2$; mp:97-99 °C.

7.3.2 Di-tert-butyl((2*R*,2'*R*)-disulfanediylbis(1-oxo-1-(prop-2-yn-1-ylamino)propane-3,2-diyl))dicarbamate (2).

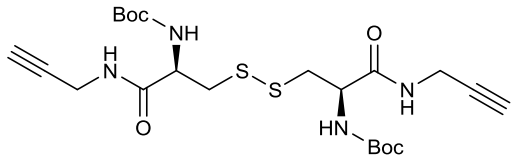

To a solution of **1** (0.420 g, 0.66 mmol) in THF (50 mL), was added propaglyamine (0.091 g, 1.65 mmol) at 0 °C. The solution was stirred and allowed to warm to room temperature over four hours. The resulting precipitate was removed by filtration and the filtrate was washed with saturated aqueous sodium bicarbonate solution (3 x 25 mL). The combined aqueous phases were extracted with dichloromethane (3 x 25 mL). The organic phases were dried over magnesium sulphate, filtered and solvent removed *in vacuo*. The crude material was purified by automated flash chromatography, using a silica column and ethyl acetate/hexane gradient. Compound, **2** isolated as colourless solid (0.235 g, 69 %). IR (cm^{-1}) 3290; s, br; NH 1655; S; amide 1518; S; carboxyl; ^{1}H NMR (400 MHz, $CDCl_3$) δ 8.10 (t, *J* = 5.3, 2H, N*H*CH_2CCH), 5.57 (d, *J* = 9.7, 2H, N*H*COO), 4.94 (td, *J* = 10.5 and 3.7, 2H, SHCH_2C*H*), 4.09 (ddd, *J* 17.6, 5.4 and 2.6, 4H, NHC*H*$_2$CCH), 2.98 (dd, *J* = 14.7 and 3.8, 2H, SHCH*H*CH), 2.88 (dd, *J* = 14.5 and 11.1, 2H, SHC*H*HCH), 2.20 (t, *J* = 2.5, 2H, NHCH2CC*H*), 1.50 (s, 18H, NHCOOC*H*$_3$); ^{13}C NMR (101 MHz, $CDCl_3$) δ 54.46 (s, SCH_2*C*H), 47.48 (s, S*C*H_2), 28.86 (s, NH*C*H2CCH), 28.54 (s, NHCOOC*C*H_3). Mass spec: calculated 537.2 $[M+Na]^+$, observed 537.2 $[M+Na]^+$ $C_{22}H_{34}N_4O_6S_2$; HRMS: calculated 537.1817 observed 537.1827 [M+Na] $C_{22}H_{34}N_4O_6S_2$; Mp 170-171 °C.

7.3.3 (2*R*,2'*R*)-3,3'-Disulfanediylbis(2-amino-*N*-(prop-2-yn-1-yl)propanamide) (3).

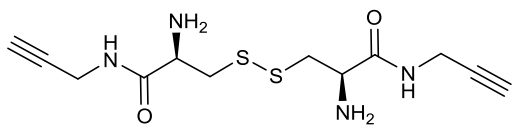

To a solution of **2** (0.410 g, 0.79 mmol) in THF (50 mL), was added trifluoroacetic acid (1.5 mL) and the resultant mixture was stirred at room temperature for 4 hours. The solvent was removed *in vacuo* to yield the product, **3**, as a light brown solid (0.246 g, 97 %). IR (cm^{-1}) 3289; w, br; N-H 1526 M/S Br; NH_2 1660; S; amide; ^{1}H NMR (400 MHz, MeOD) δ 4.24 (dd, *J* = 8.4, 5.0 Hz, 2H, SCH_2C*H*NH_2), 4.08 (d,

J = 2.6 Hz, 4H, NH_2CH_2CH), 3.40 (dd, *J* = 14.8, 5.0 Hz, 2H, SC*H*HCH), 3.10 (dd, *J* = 14.8, 8.4 Hz, 2H, SCH*H*CH), 2.70 (t, *J* = 2.6 Hz, 2H, NH_2CH_2CCH). ^{13}C NMR (101 MHz, MeOD) δ 78.03 (s, SCH_2CHC=O), 71.66 (s, $NHCH_2CCH$), 51.45 (s SCH_2CH), 37.30 (s, SCH_2), 33.34 (s, $NHCH_2CCH$), 28.93 (s, $NHCH_2CCH$).Mass spec: calculated 315.1 $[M+H]^+$, observed 315.1 $[M+H]^+$ $C_{18}H_{19}N_4O_2S_2$; HRMS: observed: 315.0943 calc: 315.0949 $[M+H]^+$ $C_{18}H_{19}NaN_4O_2S_2$; Mp 79-81 °C.

6.3.4 *N*,*N*'-((2*R*,2'*R*)-Disulfanediylbis(1-oxo-1-(prop-2-yn-1-ylamino)propane-3,2-diyl))diacrylamide (4 (DFC)).

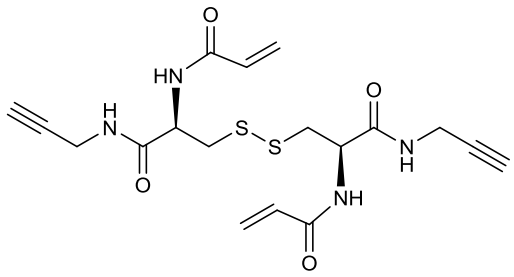

To a stirred solution of **3** (0.060 g, 0.11 mmol) and TEA (0.056 g, 0.55 mmol) in THF (25 mL) was added, acryloyl chloride (0.050 g, 0.55 mmol) dropwise at 0 °C. The stirred mixture was allowed to reach room temperature over four hours. The solution was then washed with saturated aqueous sodium bicarbonate solution (3 x 15 mL) and the aqueous phases were extracted with DCM. All organic phases were combined, dried over magnesium sulphate, filtered and solvent removed *in vacuo*. The crude product was purified by automated column chromatography, silica column and ethyl acetate/ hexane gradient, to produce the final product **DFC** as an off-white solid (0.032 g, 68 %). IR (cm^{-1}) 3277; m, br; NH 1623; S; C=O amide 1647; S; C=O amide 1529; S; alkene; ^{1}H NMR (400 MHz, $CDCl_3$) δ 8.73 (t, *J* = 4.6, 2H, N*H*CH_2CH), 6.67 (d, *J* = 9.3, 2H, SCH_2CHNH), 6.44 (dd, *J* = 16.8, 1.4, 2H C=OCHC*H*H), 6.21 (dd, *J* = 16.8, 10.2, 2H, C=OC*H*CH_2), 5.77 (dd, *J* = 10.2, 1.4, 2H, C=OCHCH*H*), 5.67 – 5.52 (m, 2H, SCH_2CH), 4.16 – 4.00 (m, 4H, $NHCH_2CH$), 3.08 (dd, *J* = 14.8, 3.7, 2H, SC*H*HCH), 2.93 (dd, *J* = 14.8, 11.0, 2H, SCH*H*CH), 2.26 (t, *J* = 2.6, 2H, $NHCH_2CH$); ^{13}C NMR (101 MHz, MeOD) δ 130.09 (s, C=O*C*HCH_2), 126.33 (s, C=OCH*C*H_2), 52.45 (s, SCH_2CH), 40.68 (s, SCH_2), 28.28 (s, $NHCH_2CH$); ^{1}H NMR (400 MHz, MeOD) δ 6.35 (dd, *J* = 17.1, 9.1 Hz, 2H, NHC=OC*H*), 6.29 (dd, *J* = 17.1, 2.8 Hz, 2H,

NHC=OCH*CH*H), 5.73 (dd, *J* = 9.1, 2.8 Hz, 2H, NHC=OCH*C*H*H*), 4.87 (dd, *J* = 8.9, 5.3 Hz, 2H, SCH_2CH), 4.01 (d, *J* = 2.5 Hz, 4H, $NHCH_2CH$), 3.21 (dd, *J* = 13.9, 5.3 Hz, 2H, SC*H*HCH), 2.97 (dd, *J* = 13.9, 8.9 Hz, 2H, SCH*H*CH), 2.62 (t, *J* = 2.5 Hz, 2H, $NHCH_2CH$). Mass spec calculated 445.1$[M+Na]^+$, observed: 445.1 $[M+Na]^+$ $C_{18}H_{22}NaN_4O_4S_2$; HRMS: calculated: 445.0980 observed: 445.0967 [M+Na] $C_{18}H_{22}NaN_4O_4$; mp 232-235 °C.

7.4 Glucose Selective Surface Preparation and Affinity Calculations

7.4.1 SAM Preparation

Polycrystalline gold substrates were purchased from George Albert PVD., Germany, and consisted of a 50 nm gold layer deposited onto a glass covered with a thin layer of chromium. The Au substrates were cleaned by immersion in piranha solution (7:3, H_2SO_4 : H_2O_2) at room temperature for 10 min. (*Caution: Piranha solution reacts violently with all organic compounds and should be handled with care.*) Samples removed from the piranha solution were immediately rinsed with Ultra High Pure (UHP) H_2O, followed by HPLC grade methanol (Fischer Scientific) for 1 min. Immediately after cleaning, the substrates were immersed in freshly prepared 0.1 mM methanol solutions of the either pure or mixed *bis*-BA, TEGT or diamine compound. Post-immersion in the SAM forming solution, the substrates were rinsed with HPLC MeOH and dried with a stream of argon. Brief details of the synthetic pathways used to produce the *bis*-BA and diamine compounds along with characterisation information are reproduced below. Synthesis and characterisation was conducted by collaborators at the University of Bath. For full details please see manuscripts [305] and [240].

7.4.2 Kinetics Study

Investigation of SAM formation kinetics was accomplished by conducting contact angle and ellipsometry at various time points over a 48 hour period. In order to form the SAMs at the indicated time intervals cleaned gold substrates were placed in solutions of each surfactant for the specified time. Gold chips were cleaned by immersion in piranha solution for 10 minutes, before being rinsed with liberal amounts of water for 1 minute, and then rinsed with HPLC grade methanol for a further minute. Following immersion in the SAM solution for the specified time, the chips were removed and rinsed with pure HPLC grade methanol, to 'quench' the SAM formation. Chips were then dried with argon prior to analysis by contact angle or ellipsometry.

7.4.3 Saccharide affinity via Surface Plasmon Resonance (SPR)

SPR experiments were performed with a Reichert SR7000DC Dual Channel Spectrometer (Buffalo, NY, USA) at 25 °C. Modified gold-coated SPR chips were deposited on the base of the prism using index-matching oil. Prior to the binding studies, a baseline was established by running degassed running buffer (PBS) through the machine at a flow rate of 25 µL/min. The modified gold surfaces were subsequently exposed to solutions of each sacchride injected at 25 µL/min for 5 min, after which a ten min dissociation phase was introduced by flowing buffer over the surface. Data sets were processed and analyzed using Scrubber 2 (BioLogic Software, Campbell, Australia). The SPR responses at equilibrium (R_{eq}) were plotted against the concentration of injected protein (C_p) and fitted to a 1:1 steady-state affinity model. The model utilises a nonlinear least-squares regression method to fit data to the Langmuir adsorption isotherm (Equation 12). K_D is the dissociation constant for binding of the proteins to the MI surfaces and R_{max} is the maximum response if all available MI binding sites are occupied.

Eq. 12
$$R_{eq} = \left(\frac{C_P}{C_P + K_D}\right) R_{max}$$

7.5 DFC Surface Preparation, Modification and Affinity Calculations

7.5.1 Self-assembled monolayer (SAM) preparation

Polycrystalline gold substrates were purchased from George Albert PVD. (Germany), and consisted of a 50 nm gold layer deposited onto a glass covered with a thin layer of chromium. The Au substrates were cleaned by immersion in piranha solution (7:3, H_2SO_4:H_2O_2) at room temperature for 10 min. (*Caution: Piranha solution reacts violently with all organic compounds and should be handled with care.*) Samples removed from the piranha solution were immediately rinsed with UHP water, followed by HPLC grade methanol (Fischer Scientific) for 1 min. Immediately after cleaning, the substrates were immersed in freshly prepared 0.1 mM methanolic solutions of DFC. Samples where then left at room temperature to allow SAM formation for at least 18 hours. Chips where then removed from the SAM solution, rinsed with methanol and dried with argon.

7.5.2 Crosslinking between the DFC SAM and AM-BA

Crosslinking between the DFC SAM and AM-BA was initiated using ammonium per sulfate. SAMs of DFC were placed in an aqueous solution of AM-BA (1 mM, 1 mL) which also contained 0.1 % (v/v) tetramethylethylenediamine (TEMED), to which 100 µL of ammonium per sulfate was added (40 mg/mL). The resulting solution was allowed to react for between 0.5 to 24 hours. The modified gold surfaces were subsequently removed from this solution, rinsed for one minute with UHQ water and dried under a stream of argon.

7.5.3 O-(2-Azidoethyl)heptaethylene glycol (Az-OEG) immobilisation on the DFC SAM via a copper catalysed azide alkyne cycloaddition (Cu-AACA)

Click reactions were carried out between DFC SAMs and Az-OEG. An aqueous solution of Az-OEG (5 mM, 1.2 mL) was mixed with copper sulfate (50 μL of a 40 mM solution) and sodium ascorbate (50 μL of a 100 mM solution). SAMs of DFC were placed in the Cu-AACA reaction solutions and allowed to react for between 0.5 to 24 hours. After reaction, the gold modified surfaces were removed from Cu-AACA reaction solution and rinsed well with UHQ water and sonicated in ethylenediaminetetraacetic acid (EDTA) solution (0.1 mM) to remove any residual copper.

7.5.4 Fabrication of molecularly imprinted surfaces

SAMs of DFC were formed as described above. A solution of AM-BA (20 μL of a 7.5 mM solution) was mixed with 20 μl solution of template protein (20 μL of a 250 μM solution) in phosphate buffer solution (2 mL PBS at pH 8.5), and incubated for 30 minutes to permit the formation of AM-BA: protein complexes. To the solution thus obtained the DFC SAMs were placed. To this, a solution of APS (100 μL of a 175 mM solution) and TEMED (1 μL) was added to trigger the crosslinking between the DFC SAMs and the AMBA:protein complex. To this solution, Az-OEG (1 μL) was added. After 30 minutes, the Cu-AACA reaction was initiated by the addition of a solution of pre-prepared catalyst (copper sulfate (25 μL of a 40 mM solution) and sodium ascorbate (25 μL of a 100 mM solution)). The mixture was allowed to react for a further 4 hours, after which time, the modified gold substrates were rinsed liberally with UHQ water for 3 min to remove the bound template protein.

7.5.5 Protein interactions with MI sensor via Surface Plasmon Resonance (SPR)

SPR experiments were performed with a Reichert SR7000DC Dual Channel Spectrometer (Buffalo, NY, USA) at 25 °C. Modified gold-coated SPR chips were deposited on the base of the prism using index-matching oil. Prior to the binding studies, a baseline was established by running degassed running buffer (PBS with 1mM HEPES, 96mM glycine 0.005% SDS at pH 8.5) through the machine at a flow rate of 25 µL/min. The modified gold surfaces were subsequently exposed to protein solutions in buffer injected at 25 µL/min for 5 min, after which a ten min dissociation phase was introduced by flowing buffer over the surface. Data sets were processed and analyzed using Scrubber 2 (BioLogic Software, Campbell, Australia). The SPR responses at equilibrium (R_{eq}) were plotted against the concentration of injected protein (C_p) and fitted to a 1:1 steady-state affinity model. Where indicated, results obtained through equilibrium analysis were validated using a global fitting method, using a single site model in Scrubber 2. The model utilises a nonlinear least-squares regression method to fit data to the Langmuir adsorption isotherm (Equation 12). K_D is the dissociation constant for binding of the proteins to the MI surfaces and R_{max} is the maximum response if all available MI binding sites are occupied.

7.5. NMR Spectra

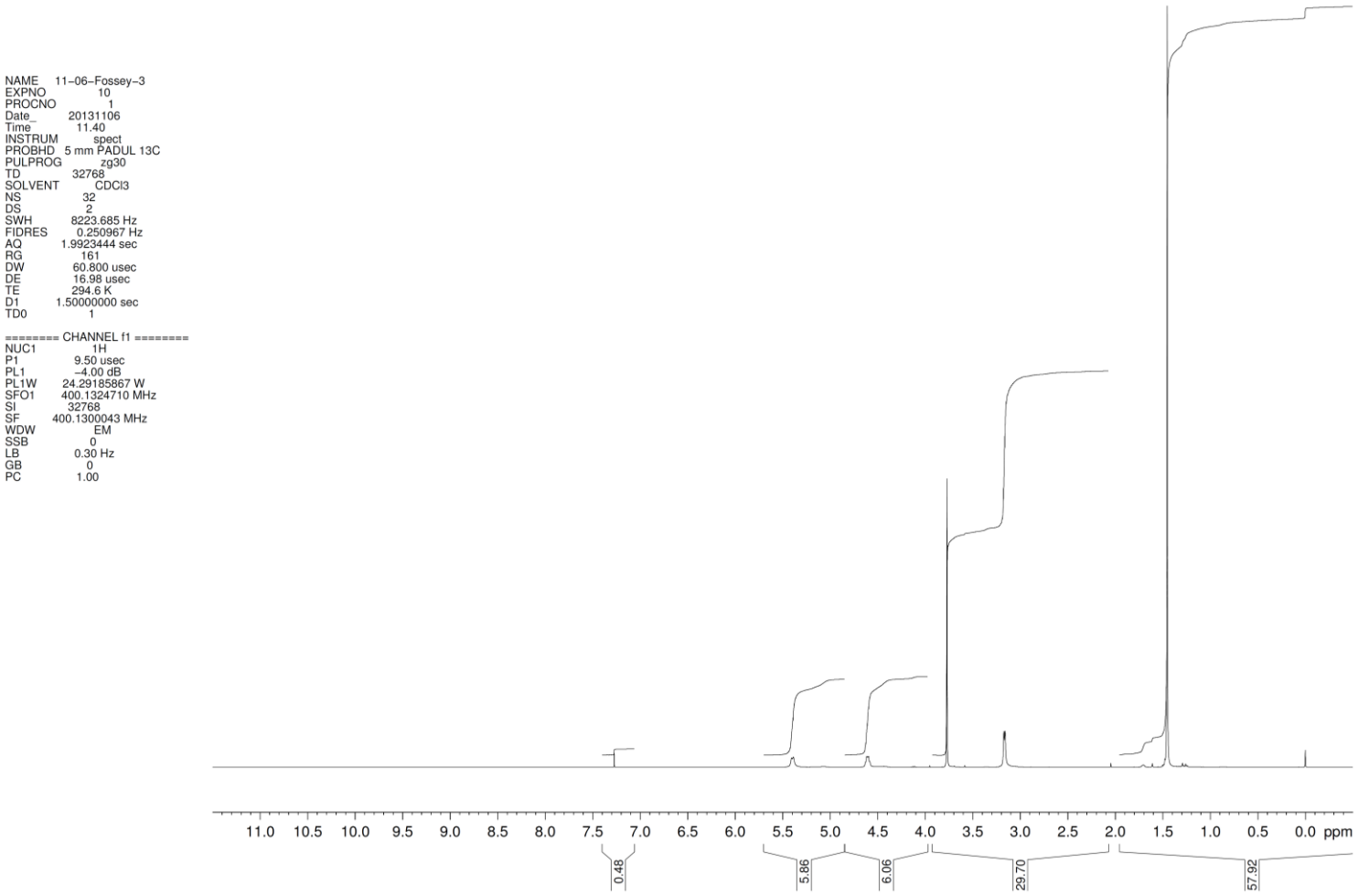

Figure 99 ^{1}H NMR spectrum of (2R,2'R)-bis(2,5-dioxopyrrolidin-1-yl)3,3'-disulfanediylbis(2-((tert-butoxycarbonyl)amino)propanoate) (**1**)

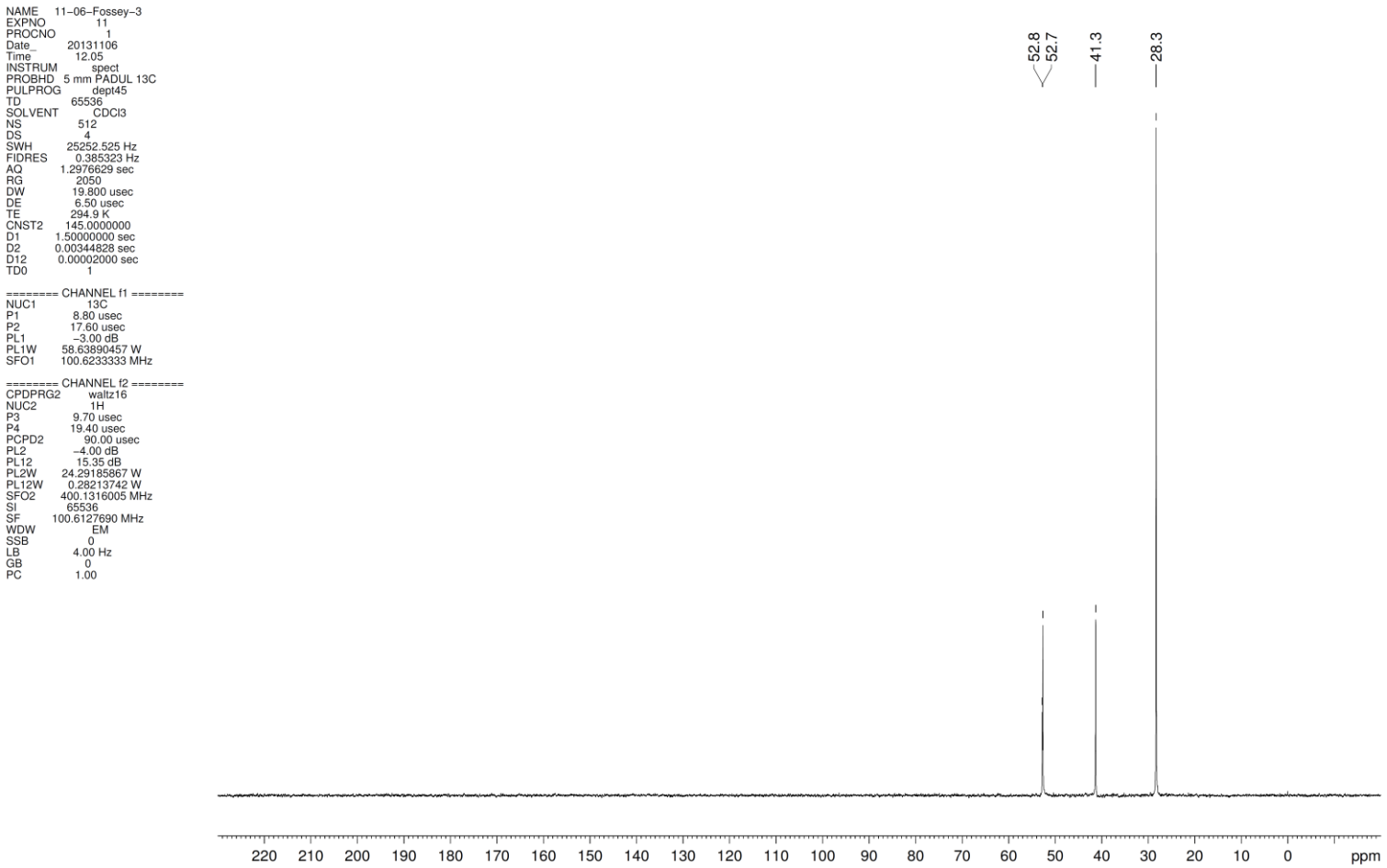

Figure 100 ^{13}C NMR spectrum of (2R,2'R)-bis(2,5-dioxopyrrolidin-1-yl)3,3'-disulfanediylbis(2-((tert-butoxycarbonyl)amino)propanoate) (**1**)

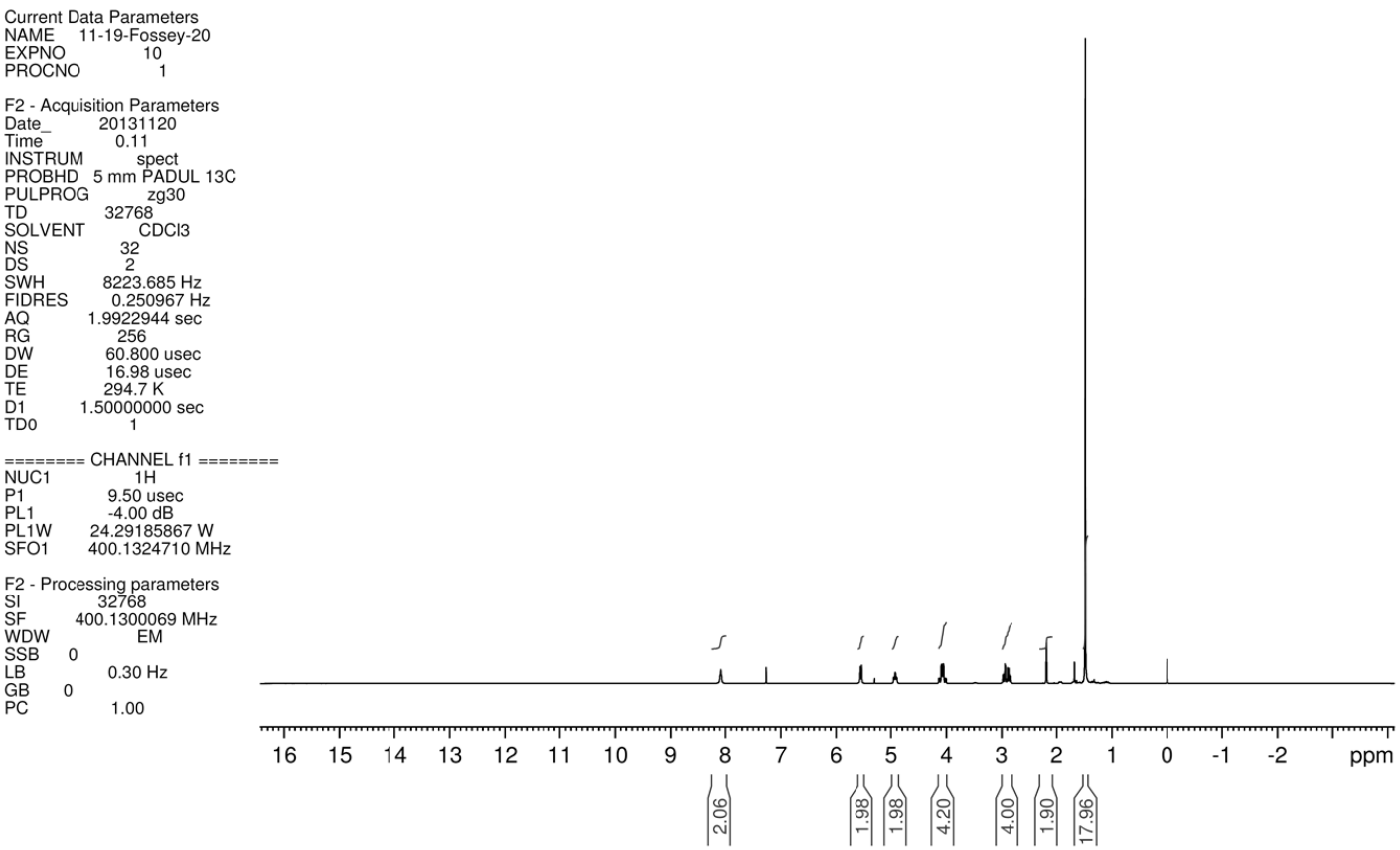

Figure 101 ^{1}H NMR spectrum of Di-tert-butyl((2*R*,2'*R*)-disulfanediylbis(1-oxo-1-(prop-2-yn-1-ylamino)propane-3,2-diyl))dicarbamate (**2**).

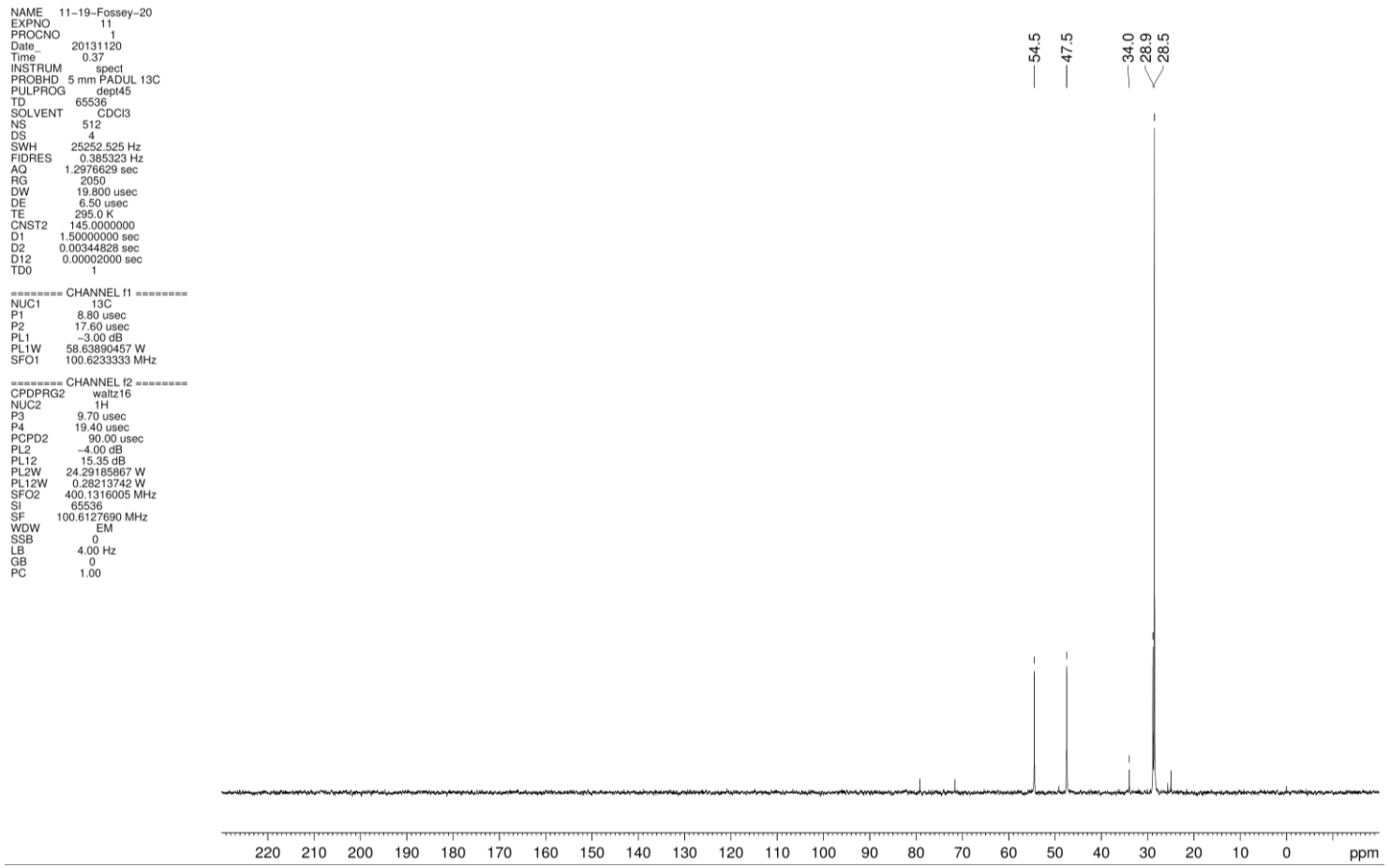

Figure 102 ^{13}C NMR spectrum of Di-tert-butyl((2*R*,2'*R*)-disulfanediylbis(1-oxo-1-(prop-2-yn-1-ylamino)propane-3,2-diyl))dicarbamate (**2**).

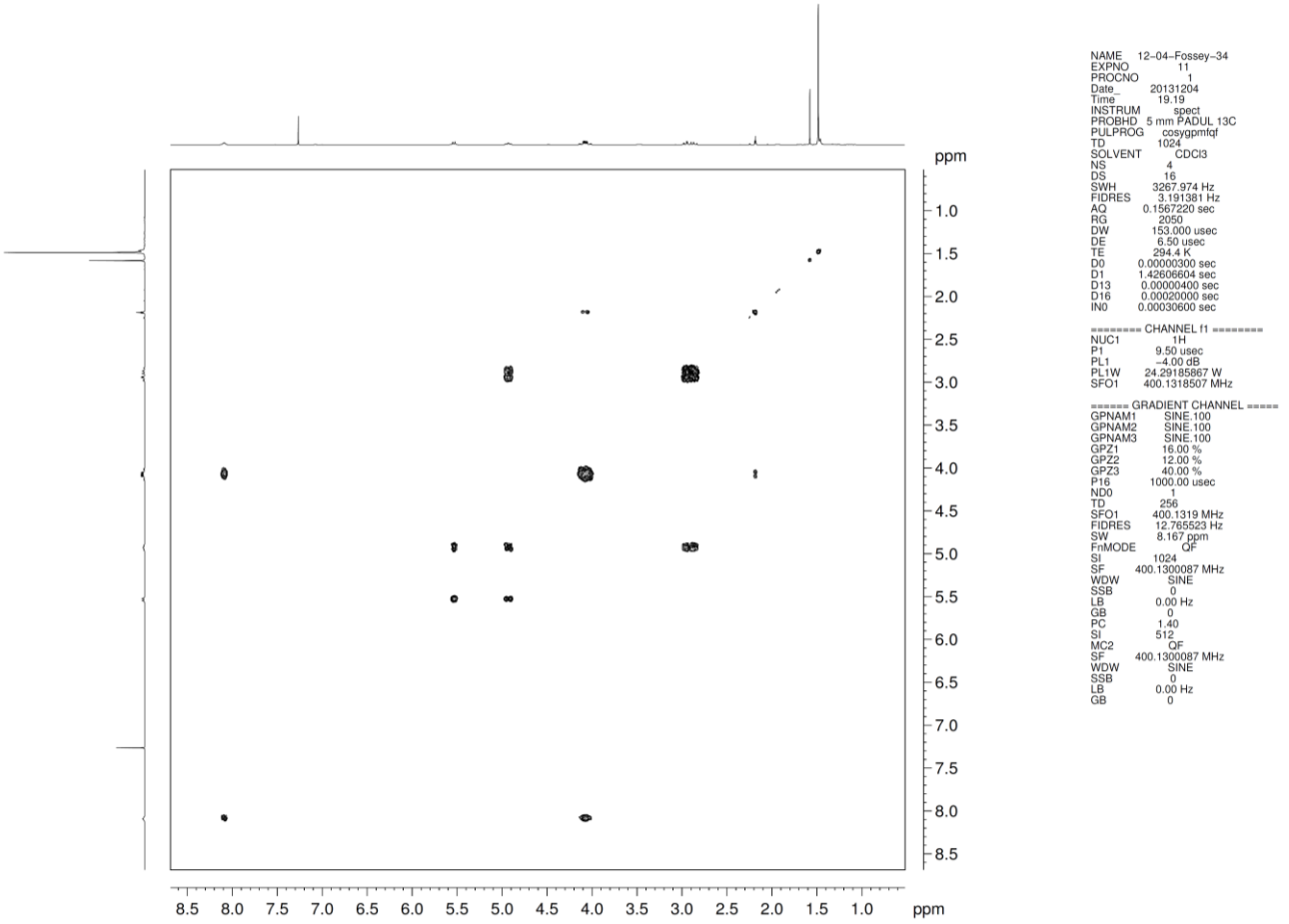


```
NAME      12-04-Fossey-34
EXPNO             11
PROCNO             1
Date_          20131204
Time           19.19
INSTRUM         spect
PROBHD   5 mm PADUL 13C
PULPROG    cosygpmfqf
TD              1024
SOLVENT         CDCl3
NS                 4
DS                16
SWH         3267.974 Hz
FIDRES        3.191381 Hz
AQ          0.1567220 sec
RG               2050
DW            153.000 usec
DE              6.50 usec
TE             294.4 K
D0          0.00000300 sec
D1          1.42606604 sec
D13         0.00000400 sec
D16         0.00020000 sec
IN0         0.00030600 sec

======== CHANNEL f1 ========
NUC1              1H
P1              9.50 usec
PL1            -4.00 dB
PL1W       24.29185867 W
SFO1       400.1318507 MHz

====== GRADIENT CHANNEL =====
GPNAM1        SINE.100
GPNAM2        SINE.100
GPNAM3        SINE.100
GPZ1           16.00 %
GPZ2           12.00 %
GPZ3           40.00 %
P16          1000.00 usec
ND0                1
TD               256
SFO1       400.1319 MHz
FIDRES     12.765523 Hz
SW          8.167 ppm
FnMODE            QF
SI               1024
SF         400.1300087 MHz
WDW              SINE
SSB                0
LB              0.00 Hz
GB                 0
PC              1.40
SI               512
MC2               QF
SF         400.1300087 MHz
WDW              SINE
SSB                0
LB              0.00 Hz
GB                 0
```

Figure 103 COSY NMR spectra of Di-tert-butyl((2*R*,2'*R*)-disulfanediylbis(1-oxo-1-(prop-2-yn-1-ylamino)propane-3,2-diyl))dicarbamate (**2**).

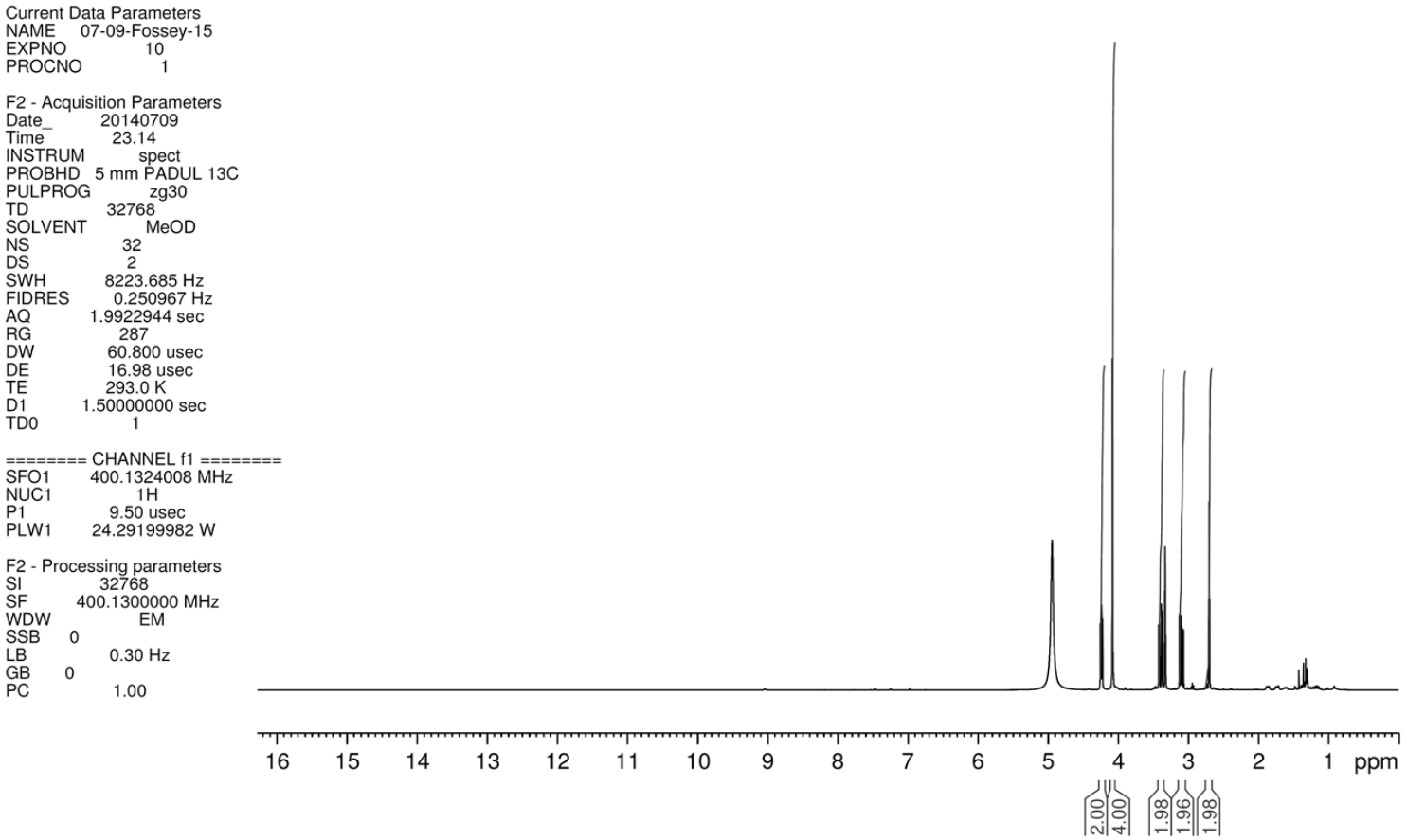

Figure 104 ^{1}H NMR spectrum of (2*R*,2'*R*)-3,3'-disulfanediylbis(2-amino-*N*-(prop-2-yn-1-yl)propanamide) (**3**).

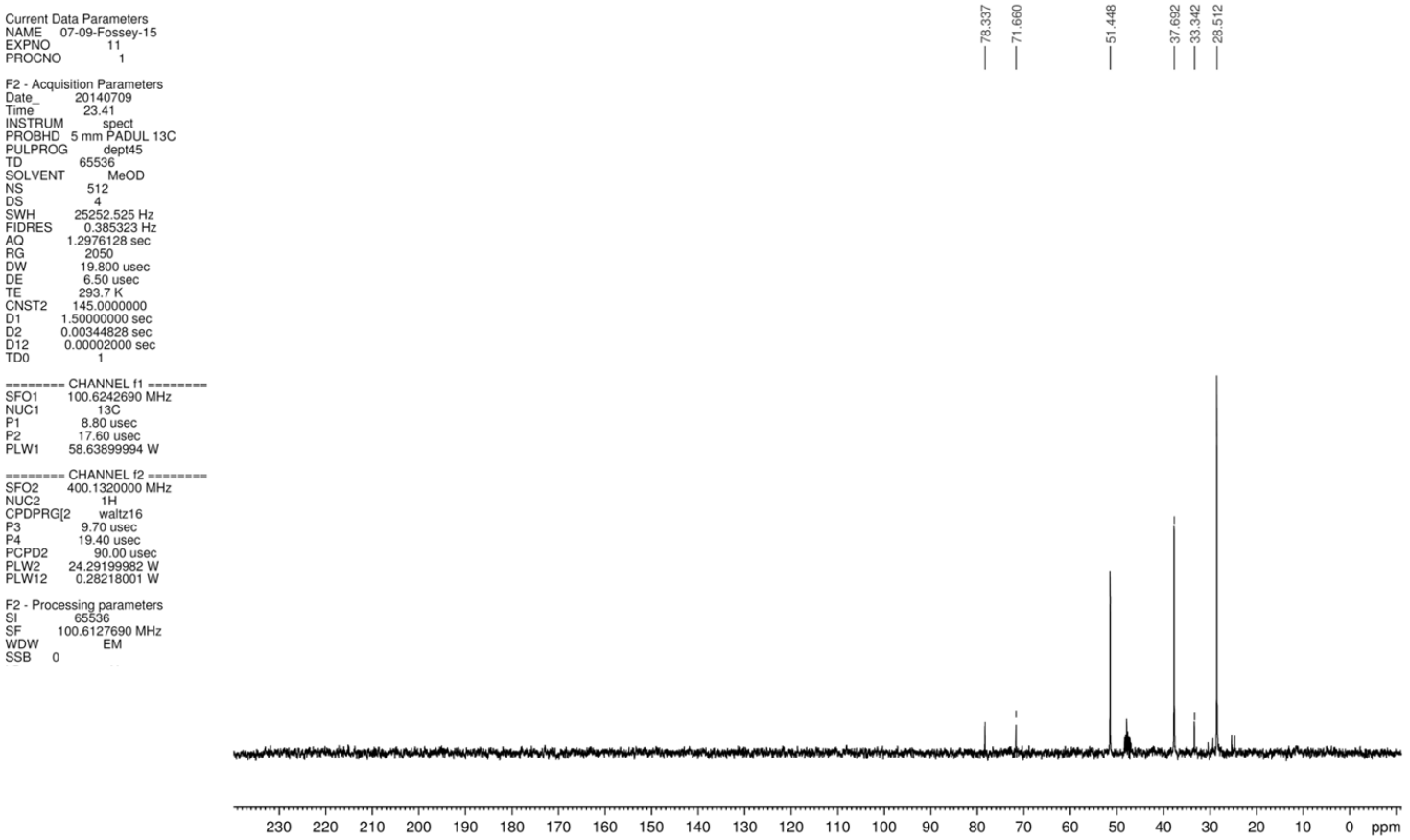

Figure 105 ^{13}C NMR spectrum of (2*R*,2'*R*)-3,3'-disulfanediylbis(2-amino-*N*-(prop-2-yn-1-yl)propanamide) (**3**).

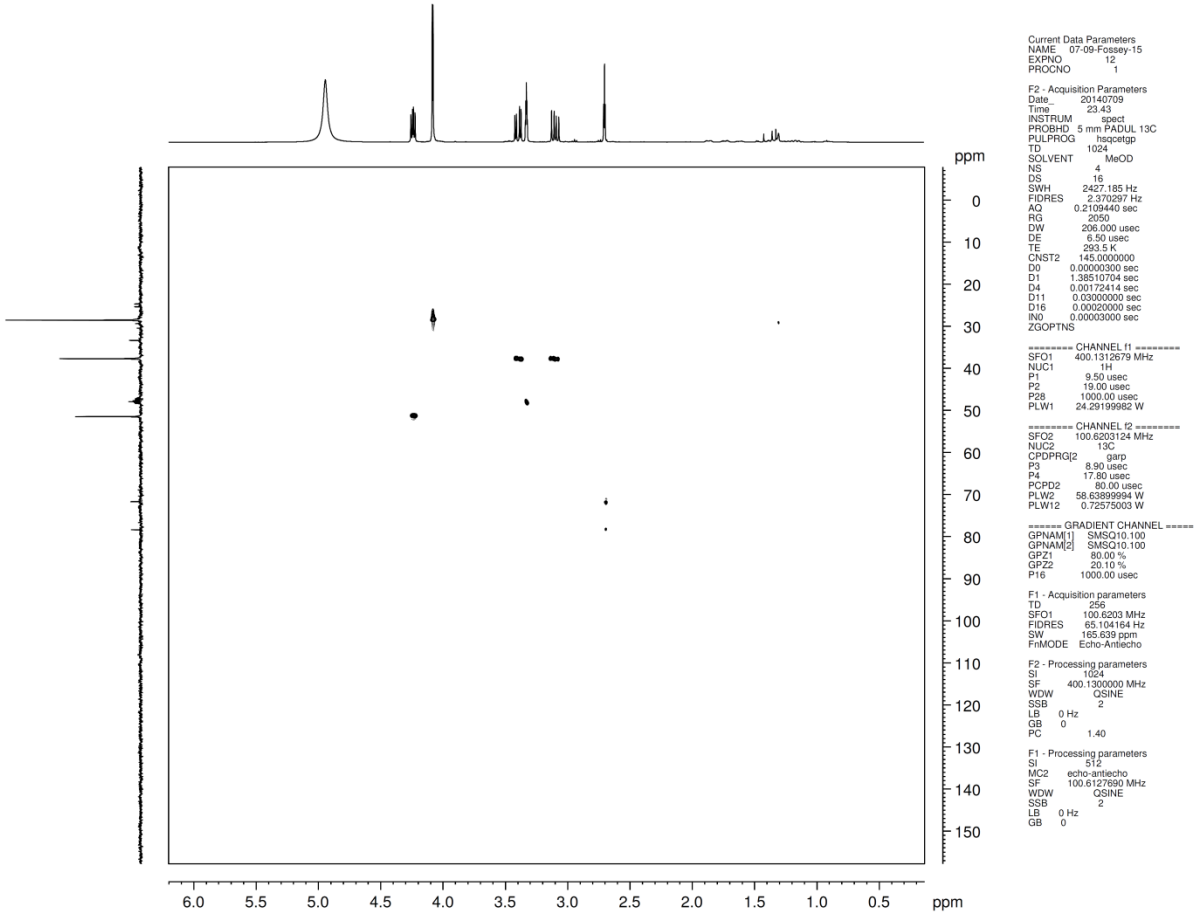

Current Data Parameters
NAME 07-09-Fossey-15
EXPNO 12
PROCNO 1

F2 - Acquisition Parameters
Date_ 20140709
Time 23.43
INSTRUM spect
PROBHD 5 mm PADUL 13C
PULPROG hsqcetgp
TD 1024
SOLVENT MeOD
NS 4
DS 16
SWH 2427.185 Hz
FIDRES 2.370297 Hz
AQ 0.2109440 sec
RG 2050
DW 206.000 usec
DE 6.50 usec
TE 293.5 K
CNST2 145.0000000
D0 0.00000300 sec
D1 1.38510704 sec
D4 0.00172414 sec
D11 0.03000000 sec
D16 0.00020000 sec
IN0 0.00003000 sec
ZGOPTNS

======== CHANNEL f1 ========
SFO1 400.1312679 MHz
NUC1 1H
P1 9.50 usec
P2 19.00 usec
P28 1000.00 usec
PLW1 24.29199982 W

======== CHANNEL f2 ========
SFO2 100.6203124 MHz
NUC2 13C
CPDPRG[2 garp
P3 8.90 usec
P4 17.80 usec
PCPD2 80.00 usec
PLW2 58.63899994 W
PLW12 0.72575003 W

====== GRADIENT CHANNEL =====
GPNAM[1] SMSQ10.100
GPNAM[2] SMSQ10.100
GPZ1 80.00 %
GPZ2 20.10 %
P16 1000.00 usec

F1 - Acquisition parameters
TD 256
SFO1 100.6203 MHz
FIDRES 65.104164 Hz
SW 165.639 ppm
FnMODE Echo-Antiecho

F2 - Processing parameters
SI 1024
SF 400.1300000 MHz
WDW QSINE
SSB 2
LB 0 Hz
GB 0
PC 1.40

F1 - Processing parameters
SI 512
MC2 echo-antiecho
SF 100.6127690 MHz
WDW QSINE
SSB 2
LB 0 Hz
GB 0

Figure 106 HSQC NMR Spectra of (2*R*,2'*R*)-3,3'-disulfanediylbis(2-amino-*N*-(prop-2-yn-1-yl)propanamide) (**3**).

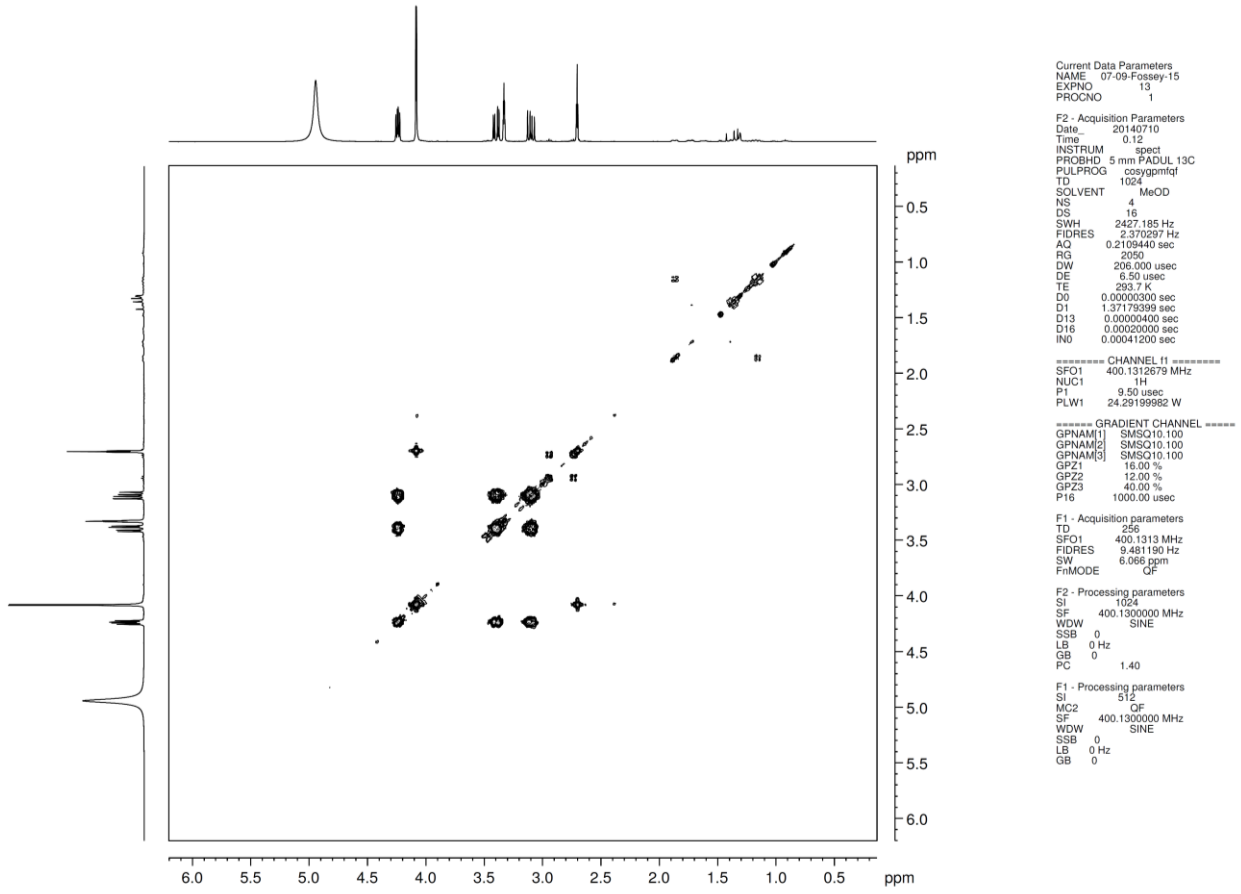

Figure 107 COSY NMR Spectra of (2*R*,2'*R*)-3,3'-disulfanediylbis(2-amino-*N*-(prop-2-yn-1-yl)propanamide) (**3**).

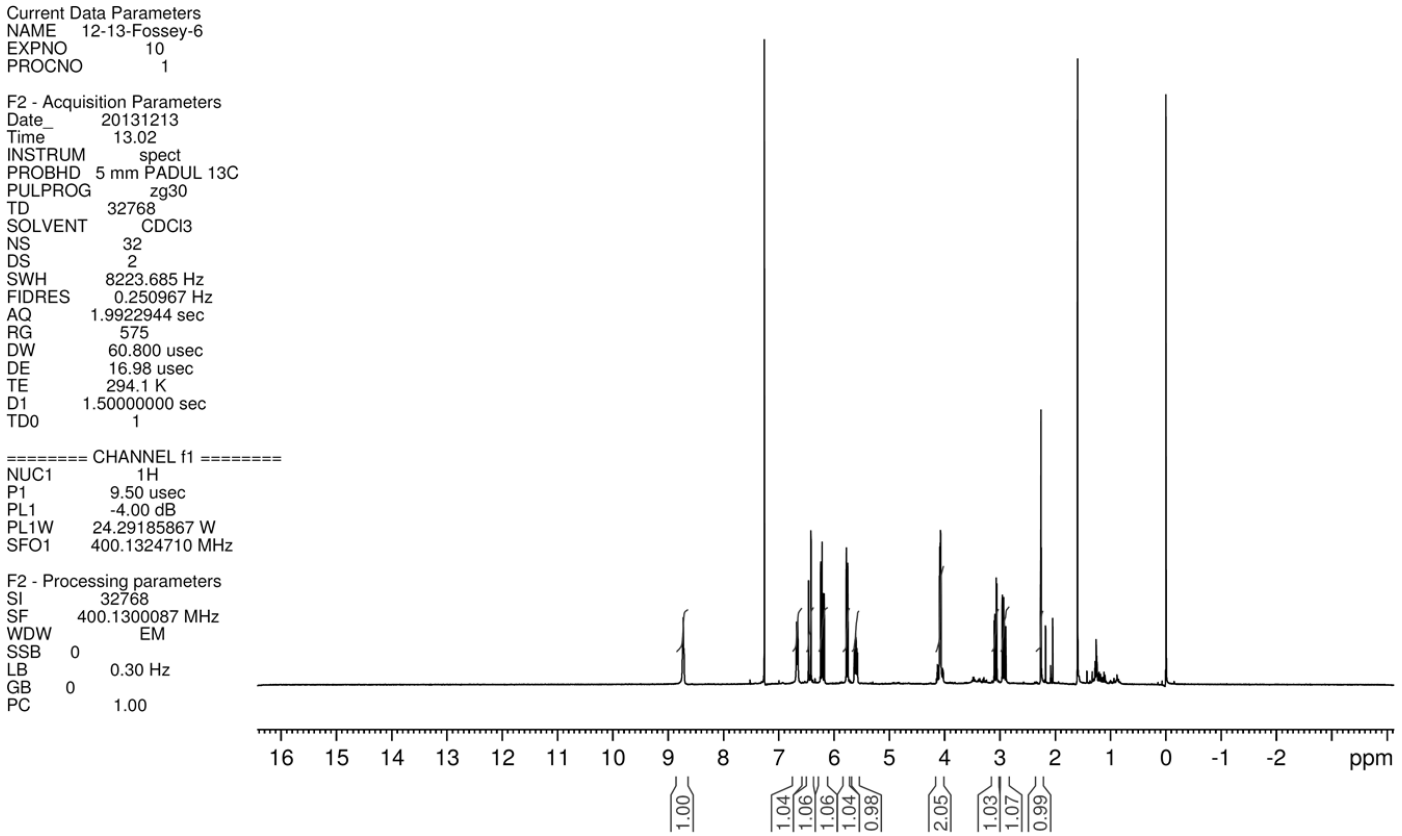

Figure 108 ^{1}H NMR spectrum of *N*,*N*'-((2*R*,2'*R*)-disulfanediylbis(1-oxo-1-(prop-2-yn-1-ylamino)propane-3,2-diyl))diacrylamide (**4** (**DFC**)).

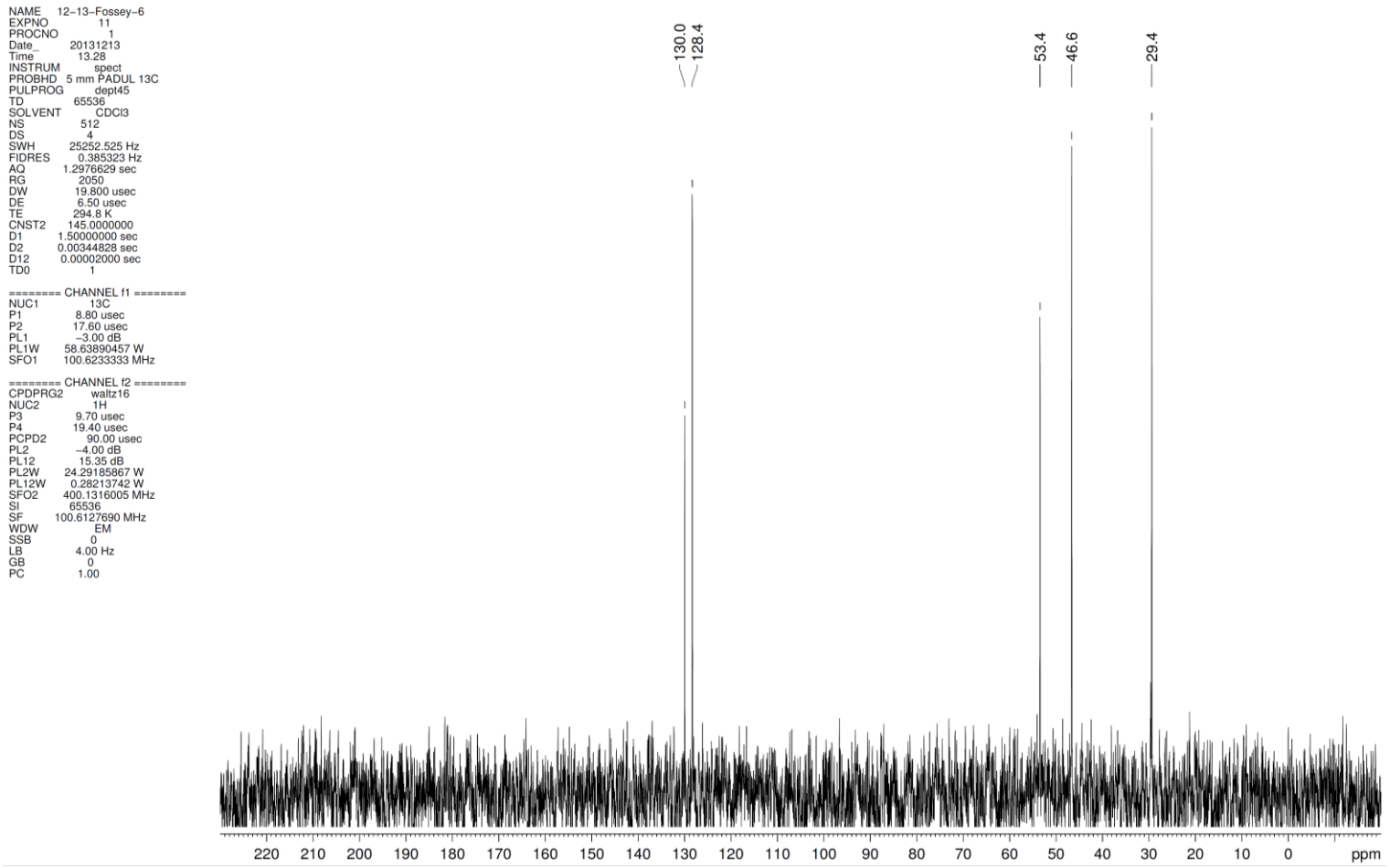

Figure 109 ^{13}C *N*,*N*'-((2*R*,2'*R*)-disulfanediylbis(1-oxo-1-(prop-2-yn-1-ylamino)propane-3,2-diyl))diacrylamide (**4** (**DFC**)).

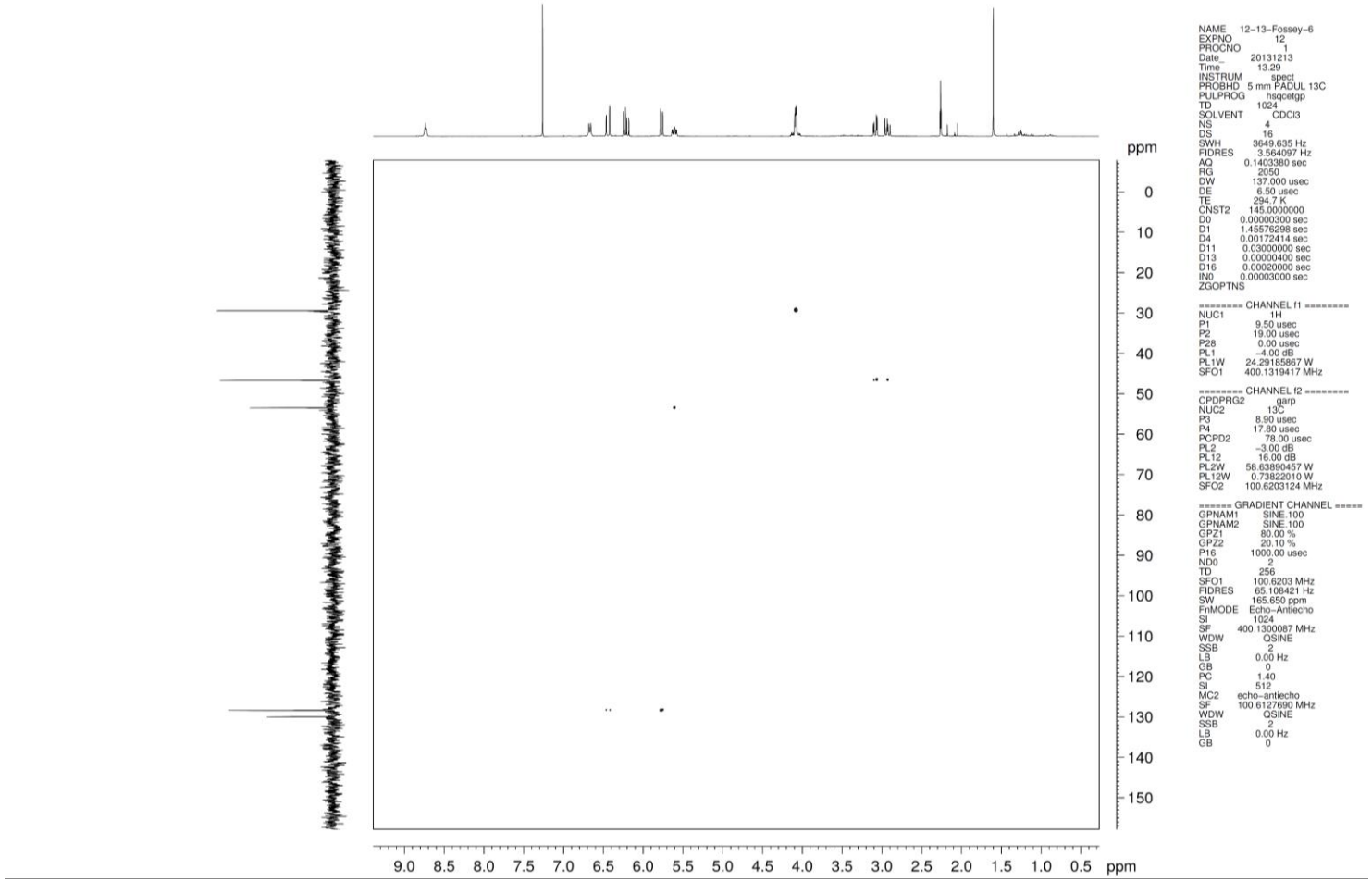

Figure 110 HSQC spectra of *N*,*N*'-((2*R*,2'*R*)-disulfanediylbis(1-oxo-1-(prop-2-yn-1-ylamino)propane-3,2-diyl))diacrylamide (**4** (**DFC**)).

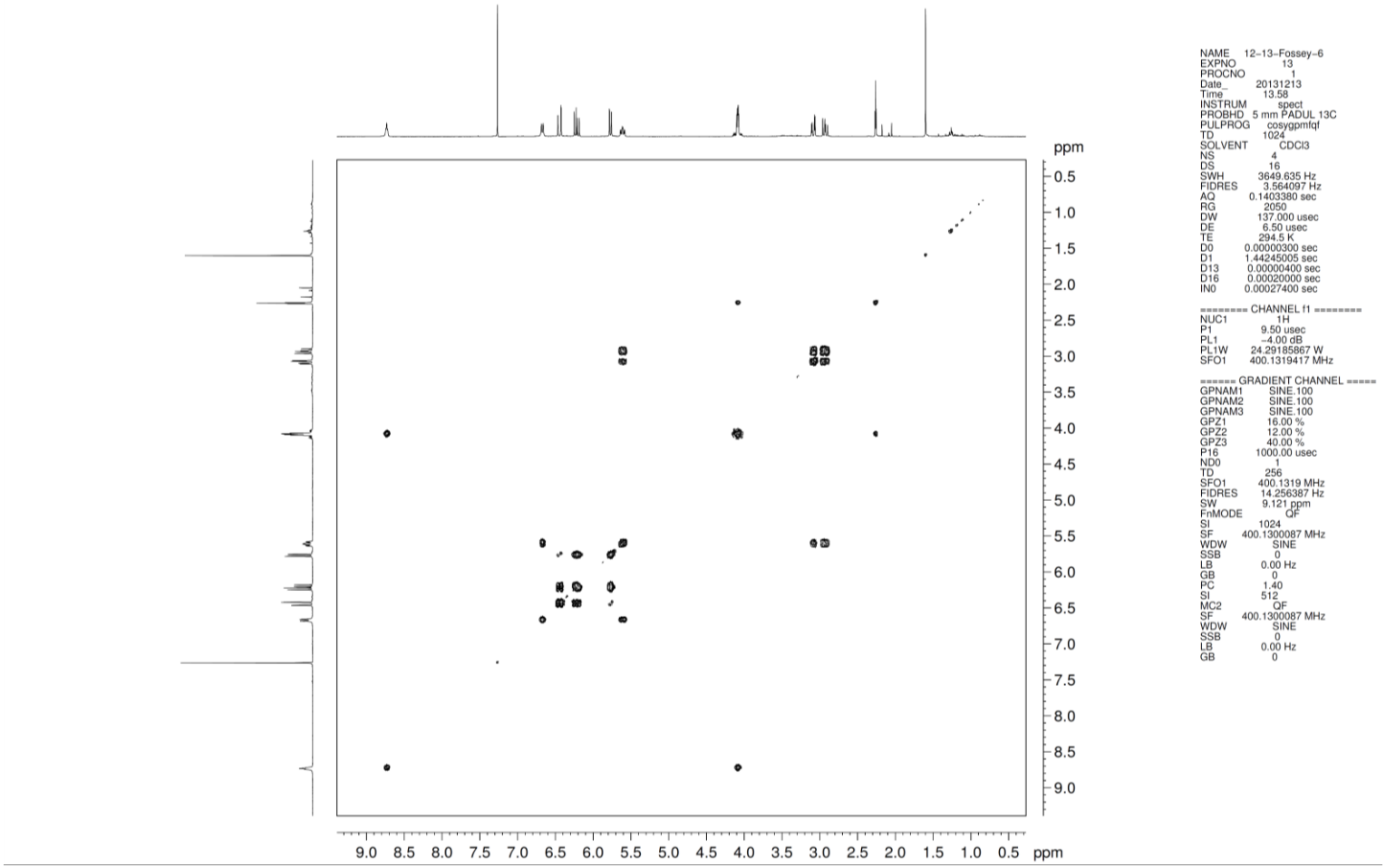

Figure 111 COSY spectra of *N*,*N*'-((2*R*,2'*R*)-disulfanediylbis(1-oxo-1-(prop-2-yn-1-ylamino)propane-3,2-diyl))diacrylamide (**4** (**DFC**)).

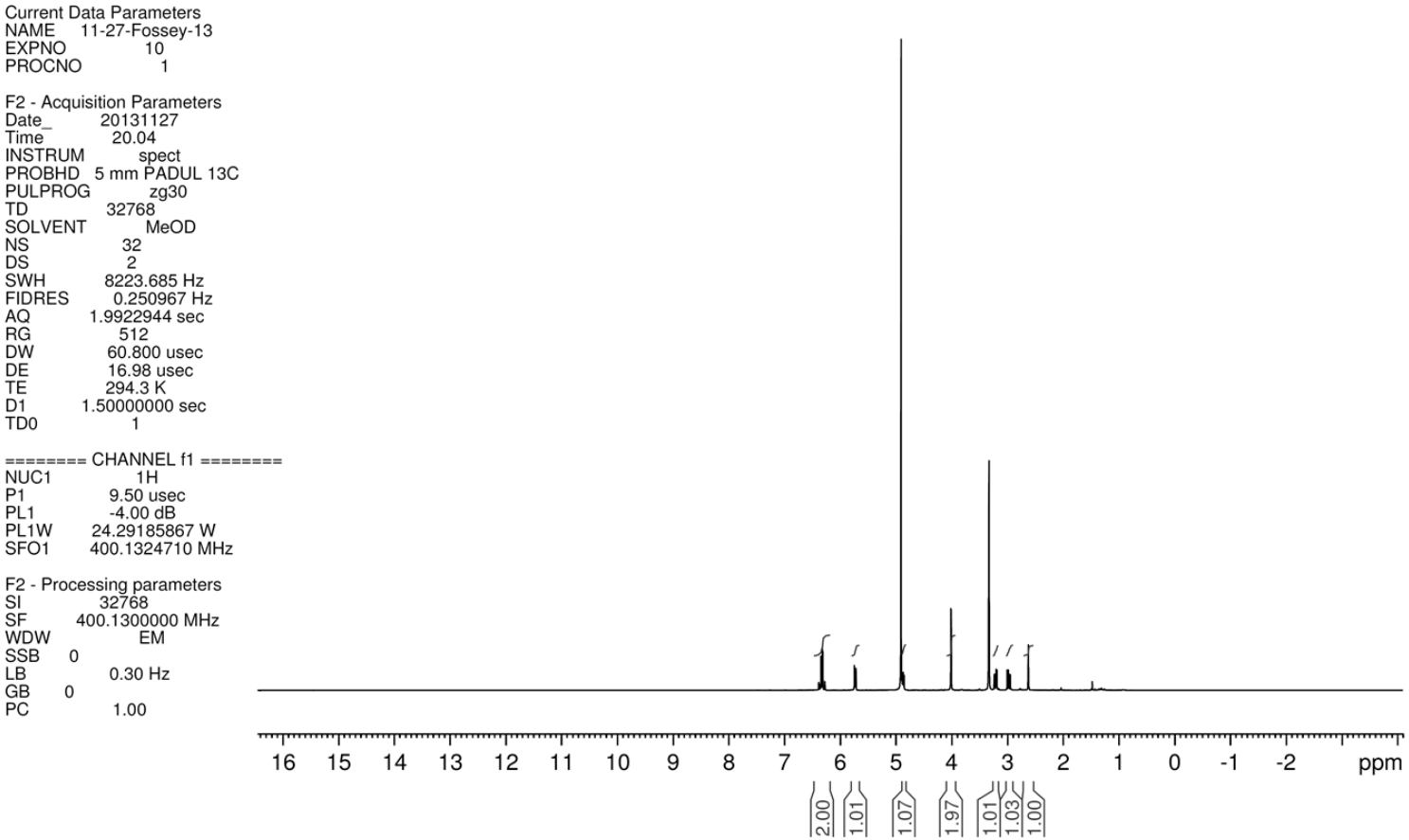

Figure 112 ^{1}H NMR spectrum of *N*,*N*'-((2*R*,2'*R*)-disulfanediylbis(1-oxo-1-(prop-2-yn-1-ylamino)propane-3,2-diyl))diacrylamide (**4** (**DFC**)) in MeOD.

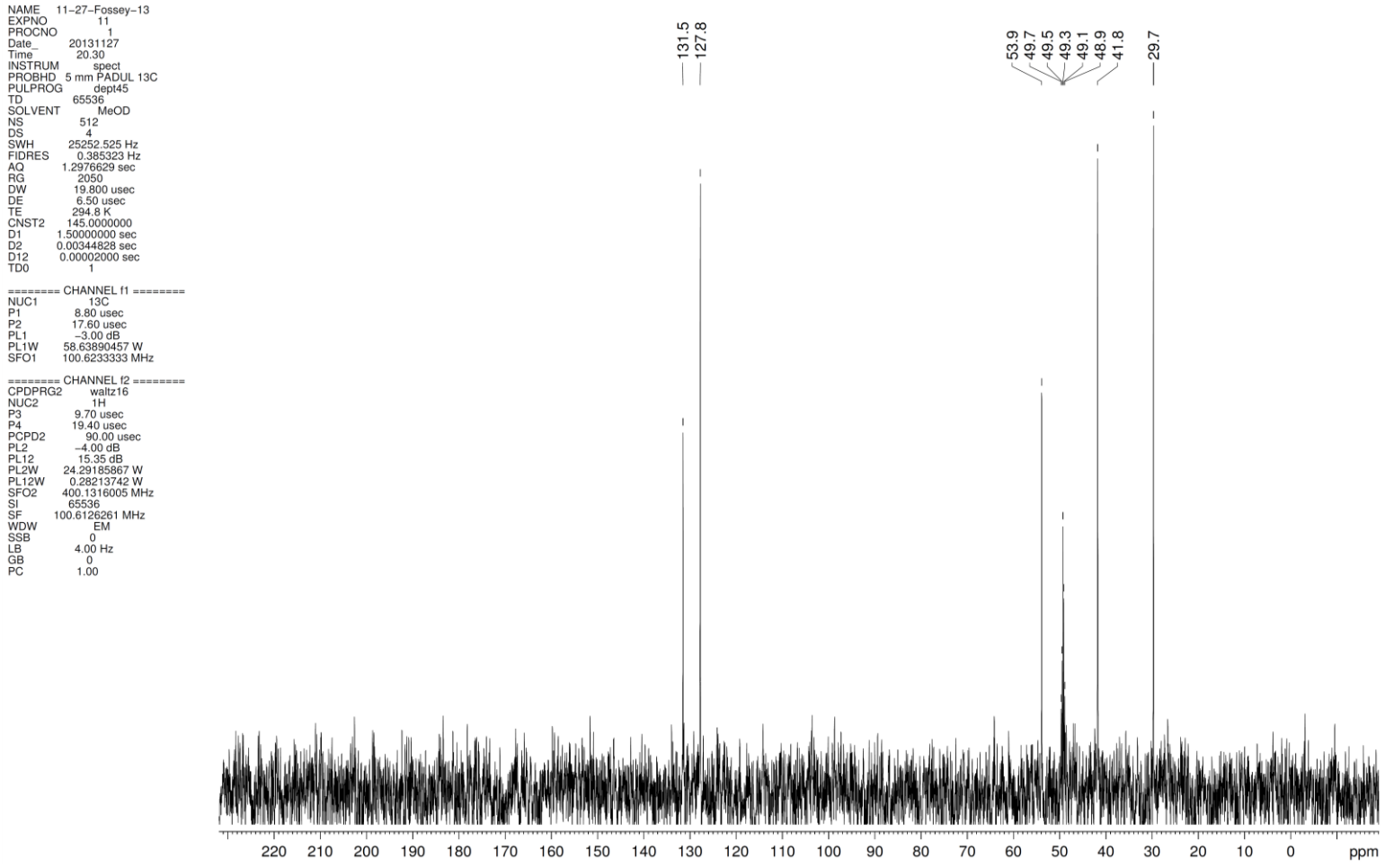

Figure 113 ^{13}C *N*,*N*'-((2*R*,2'*R*)-disulfanediylbis(1-oxo-1-(prop-2-yn-1-ylamino)propane-3,2-diyl))diacrylamide (**4** (**DFC**)), in MeOD.

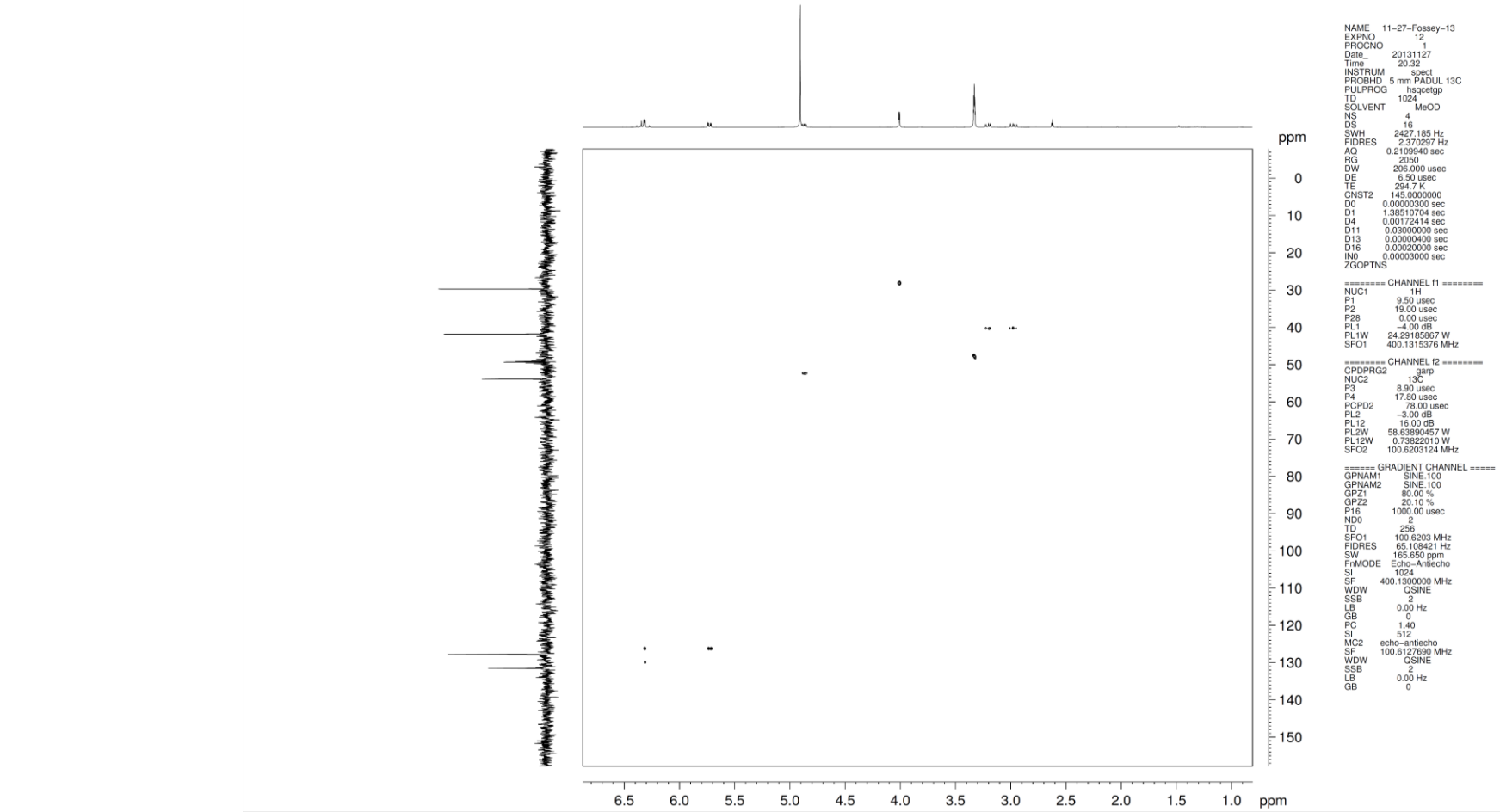

Figure 114 HSQC spectra of *N*,*N*'-((2*R*,2'*R*)-disulfanediylbis(1-oxo-1-(prop-2-yn-1-ylamino)propane-3,2-diyl))diacrylamide (**4** (**DFC**)) in MeOD.

CHAPTER 8: REFERENCES

1. Matsumoto, A., et al., *A synthetic approach toward a self-regulated insulin delivery system.* Angew Chem Int Ed Engl, 2012. **51**(9): p. 2124-8.
2. Phillips, M.D., *Synthetic strategies in the design and construction of saccharide selective fluorescent sensors*, 2005, University of Bath (United Kingdom): Ann Arbor.
3. Varki A and L. JB, *Biological Roles of Glycans.* , in *Essentials of Glycobiology*2009, Cold Spring Harbor Laboratory Press: Cold Spring Harbor (NY):.
4. Saldova, R., et al., *Glycosylation Changes on Serum Glycoproteins in Ovarian Cancer May Contribute to Disease Pathogenesis.* Disease markers, 2008. **25**(4-5): p. 219-232.
5. Shoji, E. and M.S. Freund, *Potentiometric Saccharide Detection Based on the pKaChanges of Poly(aniline boronic acid).* J. Am. Chem. Soc., 2002. **124**(42): p. 12486-12493.
6. Jeremy M Berg, John L Tymoczko, and L. Stryer., *Biochemistry*. 5th edition ed2002, New York: W H Freeman.
7. Carey, F.A., *Organic chemistry*. 6th ed2006, Dubuque, IA: McGraw-Hill.
8. Nishiyabu, R., et al., *Boronic acid building blocks: tools for sensing and separation.* Chem Commun (Camb), 2011. **47**(4): p. 1106-23.
9. Silva, A.M., E.C. da Silva, and C.O. da Silva, *A theoretical study of glucose mutarotation in aqueous solution.* Carbohydr. Res., 2006. **341**(8): p. 1029-40.
10. Lefort, R., et al., *Mutarotational kinetics and glass transition of lactose.* Solid State Commun., 2006. **140**(7-8): p. 329-334.
11. James, T.D., M.D. Phillips, and S. Shinkai, *Boronic Acids in Saccharide Recognition*. Monographs in Supramolecular Chemistry2006, Cambridge: Royal Society of Chemistry.
12. Casu, B., et al., *Hydroxyl proton resonances of sugars in dimethylsulphoxide solution.* Tetrahedron Lett, 1964. **5**(39): p. 2839-2843.
13. Casu, B., et al., *NMR Spectra and conformation of glucose and some related carbohydrates in dimethylsulphoxide solution.* Tetrahedron Lett, 1965. **6**(27): p. 2253-2259.
14. Perlin, A.S., *Hydroxyl Proton Magnetic Resonance in Relation to Ring Size, Substituent Groups, and Mutarotation of Carbohydrates.* Can. J. Chem., 1966. **44**(5): p. 539-550.
15. Kiessling, L.L. and R.A. Splain, *Chemical approaches to glycobiology.* Annu Rev Biochem, 2010. **79**: p. 619-53.
16. Weijers, C.A., M.C. Franssen, and G.M. Visser, *Glycosyltransferase-catalyzed synthesis of bioactive oligosaccharides.* Biotechnology advances, 2008. **26**(5): p. 436-56.
17. Wild, S., et al., *Global Prevalence of Diabetes: Estimates for the year 2000 and projections for 2030.* Diabetes care, 2004. **27**(5): p. 1047-1053.
18. Gough, D.A., J.C. Armour, and D.A. Baker, *Advances and prospects in glucose assay technology.* Diabetologia, 1997. **40**(0): p. S102-S107.
19. Su, L., et al., *Colorimetric detection of urine glucose based ZnFe2O4 magnetic nanoparticles.* Anal. Chem., 2012. **84**(13): p. 5753-8.
20. Liu, Y., et al., *Nonenzymatic glucose sensor based on renewable electrospun Ni nanoparticle-loaded carbon nanofiber paste electrode.* Biosens. Bioelectron., 2009. **24**(11): p. 3329-34.
21. Ye, J.-S., et al., *Nonenzymatic glucose detection using multi-walled carbon nanotube electrodes.* Electrochem. Commun., 2004. **6**(1): p. 66-70.
22. Dai, L., et al., *Differential profiling studies of N-linked glycoproteins in glioblastoma cancer stem cells upon treatment with gamma-secretase inhibitor.* Proteomics, 2011. **11**(20): p. 4021-8.
23. Lange, T., et al., *Human prostate cancer in a clinically relevant xenograft mouse model: identification of beta(1,6)-branched oligosaccharides as a marker of tumor progression.* Clin Cancer Res, 2012. **18**(5): p. 1364-73.
24. Kariya, Y., et al., *N-Glycosylation of Laminin-332 Regulates Its Biological Functions A Novel Function of the Bisecting GlcNAc.* J. Biol. Chem., 2008. **283**(48): p. 33036-33045.
25. Shumyantseva, V.V., et al., *Electrochemical methods for detection of post-translational modifications of proteins.* Biosens. Bioelectron., 2014. **61**: p. 131-9.
26. Pan, S., et al., *Mass spectrometry based glycoproteomics--from a proteomics perspective.* Mol. Cell. Proteomics, 2011. **10**(1): p. R110 003251.

27. Hart, G.W. and R.J. Copeland, *Glycomics Hits the Big Time.*
28. Dudkin, V.Y., et al., *Toward a prostate specific antigen-based prostate cancer diagnostic assay: preparation of keyhole limpet hemocyanin-conjugated normal and transformed prostate specific antigen fragments.* J. Am. Chem. Soc., 2008. **130**(41): p. 13598-607.
29. Schjoldager, K.T.B.G. and H. Clausen, *Site-specific protein O-glycosylation modulates proprotein processing - Deciphering specific functions of the large polypeptide GalNAc-transferase gene family.* Bba-Gen Subjects, 2012. **1820**(12): p. 2079-2094.
30. Laczy, B., et al., *Protein O-GlcNAcylation: a new signaling paradigm for the cardiovascular system.* Am J Physiol-Heart C, 2009. **296**(1): p. H13-28.
31. Mann, M. and O.N. Jensen, *Proteomic analysis of post-translational modifications.* Nat. Biotechnol., 2003. **21**(3): p. 255-61.
32. de Lima, A.L., et al., *Histochemical evaluation of human prostatic tissues with Cratylia mollis seed lectin.* J Biomed Biotechnol, 2010. **2010**: p. 179817.
33. Armeanu, S., et al., *Natural killer cell-mediated lysis of hepatoma cells via specific induction of NKG2D ligands by the histone deacetylase inhibitor sodium valproate.* Cancer Res., 2005. **65**(14): p. 6321-9.
34. Avril, T., et al., *Distinct effects of human glioblastoma immunoregulatory molecules programmed cell death ligand-1 (PDL-1) and indoleamine 2,3-dioxygenase (IDO) on tumour-specific T cell functions.* J. Neuroimmunol., 2010. **225**(1-2): p. 22-33.
35. Batista, B.S., et al., *Identification of a conserved glycan signature for microvesicles.* J Proteome Res, 2011. **10**(10): p. 4624-33.
36. Bhaskar, A.S., N. Gupta, and P.V. Rao, *Transcriptomic profile of host response in mouse brain after exposure to plant toxin abrin.* Toxicology, 2012. **299**(1): p. 33-43.
37. Comelli, E.M., et al., *A focused microarray approach to functional glycomics: transcriptional regulation of the glycome.* Glycobiology, 2006. **16**(2): p. 117-31.
38. Freire-de-Lima, L., et al., *Involvement of O-glycosylation defining oncofetal fibronectin in epithelial-mesenchymal transition process.* Proc. Natl. Acad. Sci. U. S. A., 2011. **108**(43): p. 17690-5.
39. Bi, J., et al., *Overexpression of YKL-40 is an independent prognostic marker in gastric cancer.* Human pathology, 2009. **40**(12): p. 1790-7.
40. Brown, J.R., et al., *Expression patterns of alpha 2,3-sialyltransferases and alpha 1,3-fucosyltransferases determine the mode of sialyl Lewis X inhibition by disaccharide decoys.* J. Biol. Chem., 2003. **278**(26): p. 23352-9.
41. Castelletti, D., et al., *Apical transport and folding of prostate-specific membrane antigen occurs independent of glycan processing.* J. Biol. Chem., 2006. **281**(6): p. 3505-12.
42. Haslam, S.M., et al., *Characterizing the glycome of the mammalian immune system.* Immunol Cell Biol, 2008. **86**(7): p. 564-73.
43. Prokazova, N.V., et al., *Ganglioside GM3 and its biological functions.* Biochemistry (Moscow), 2009. **74**(3): p. 235-249.
44. Yamada, T., et al., *Genetically engineered humanized anti-ganglioside GM2 antibody against multiple organ metastasis produced by GM2-expressing small-cell lung cancer cells.* Cancer Sci., 2011. **102**(12): p. 2157-63.
45. Raval, G., et al., *TNF-alpha induction of GM2 expression on renal cell carcinomas promotes T cell dysfunction.* J. Immunol., 2007. **178**(10): p. 6642-52.
46. Biswas, S., et al., *Elevated levels of select gangliosides in T cells from renal cell carcinoma patients is associated with T cell dysfunction.* J. Immunol., 2009. **183**(8): p. 5050-8.
47. Stephan, C., et al., *PSA and other tissue kallikreins for prostate cancer detection.* Eur J Cancer, 2007. **43**(13): p. 1918-26.
48. Gilgunn, S., et al., *Aberrant PSA glycosylation--a sweet predictor of prostate cancer.* Nat Rev Urol, 2013. **10**(2): p. 99-107.
49. Vermassen, T., et al., *Glycosylation of prostate specific antigen and its potential diagnostic applications.* Clin Chim Acta, 2012. **413**(19-20): p. 1500-5.
50. Saldova, R., et al., *Core fucosylation and alpha2-3 sialylation in serum N-glycome is significantly increased in prostate cancer comparing to benign prostate hyperplasia.* Glycobiology, 2011. **21**(2): p. 195-205.

51. Shimojo, H., et al., *Reduced glycosylation of alpha-dystroglycans on carcinoma cells contributes to formation of highly infiltrative histological patterns in prostate cancer.* The Prostate, 2011. **71**(11): p. 1151-7.
52. Kuzmanov, U., et al., *Separation of kallikrein 6 glycoprotein subpopulations in biological fluids by anion-exchange chromatography coupled to ELISA and identification by mass spectrometry.* Proteomics, 2012. **12**(6): p. 799-809.
53. Rini, J.M., *Lectin structure.* Annu. Rev. Biophys. Biomol. Struct., 1995. **24**: p. 551-77.
54. Zhang, X.A., et al., *Lectin-Based Biosensor Strategy for Electrochemical Assay of Glycan Expression on Living Cancer Cells.* Anal Chem, 2010. **82**(22): p. 9455-9460.
55. Chrispeels, M.J. and N.V. Raikhel, *Lectins, lectin genes, and their role in plant defense.* The Plant cell, 1991. **3**(1): p. 1-9.
56. Subramanyam, S., et al., *Functional characterization of HFR1, a high-mannose N-glycan-specific wheat lectin induced by Hessian fly larvae.* Plant physiology, 2008. **147**(3): p. 1412-26.
57. Fossey, J.S. and T.D. James, *Boronic Acid Based Modular Fluorescent Saccharide Sensors.* 2009. **2007**: p. 103-118.
58. Lorand, J.P. and J.O. Edwards, *Polyol Complexes and Structure of the Benzeneboronate Ion.* J Org Chem, 1959. **24**(6): p. 769-774.
59. Fossey, J.S., et al., *The development of boronic acids as sensors and separation tools.* Chem. Rec., 2012. **12**(5): p. 464-78.
60. Elfeky, S.A., et al., *A surface plasmon enhanced fluorescence sensor platform.* New J. Chem., 2009. **33**: p. 1466.
61. Fossey, J.S. and T.D. James, *Boronic Acid Based Modular Fluorescent Saccharide Sensors*, in *Reviews in Fluorescence 2007*, C.D. Geddes, Editor 2009, Springer New York: New York, NY. p. 103-118.
62. Nishiyabu, R., et al., *Boronic acid building blocks: tools for self assembly.* Chem. Commun., 2011. **47**(4): p. 1124-50.
63. Nishiyabu, R., et al., *Boronic acid building blocks: tools for sensing and separation.* Chem. Commun., 2011. **47**(4): p. 1106-23.
64. Schuller, T.A., et al., *Field-effect saccharide sensing using AlGaN/GaN heterostructures and boronic acid based chemical receptors.* Sensor. Actuat. B-Chem., 2011. **160**(1): p. 1078-1081.
65. Edwards, N.Y., et al., *Boronic acid based peptidic receptors for pattern-based saccharide sensing in neutral aqueous media, an application in real-life samples.* J. Am. Chem. Soc., 2007. **129**(44): p. 13575-83.
66. Yan, J., et al., *The relationship among pKa, pH, and binding constants in the interactions between boronic acids and diols—it is not as simple as it appears.* Tetrahedron, 2004. **60**(49): p. 11205-11209.
67. Lauer, M. and G. Wulff, *Arylboronic acids with intramolecular B–N interaction: convenient synthesis through ortho-lithiation of substituted benzylamines.* J Organomet Chem, 1983. **256**(1): p. 1-9.
68. Wulff, G., M. Lauer, and H. Böhnke, *Rapid Proton Transfer as Cause of an Unusually Large Neighboring Group Effect.* Angew. Chem., Int. Ed. Engl., 1984. **23**(9): p. 741-742.
69. Wiskur, S.L., et al., *pKaValues and Geometries of Secondary and Tertiary Amines Complexed to Boronic AcidsImplications for Sensor Design.* Org Lett, 2001. **3**(9): p. 1311-1314.
70. Bosch, L.I., T.M. Fyles, and T.D. James, *Binary and ternary phenylboronic acid complexes with saccharides and Lewis bases.* Tetrahedron, 2004. **60**(49): p. 11175-11190.
71. Liang, L. and Z. Liu, *A self-assembled molecular team of boronic acids at the gold surface for specific capture of cis-diol biomolecules at neutral pH.* Chem Commun (Camb), 2011. **47**(8): p. 2255-7.
72. Deshayes, S., et al., *Phenylboronic Acid-installed polymeric micelles for targeting sialylated epitopes in solid tumors.* J. Am. Chem. Soc., 2013. **135**(41): p. 15501-7.
73. D'Hooge, F., et al., *Biotinylated boronic acid fluorophore conjugates: Quencher elimination strategy for imaging and saccharide detection.* Rsc Adv, 2012. **2**(8): p. 3274.
74. Scrafton, D.K., et al., *"Click-fluors": modular fluorescent saccharide sensors based on a 1,2,3-triazole ring.* J Org Chem, 2008. **73**(7): p. 2871-4.
75. Hall, D.G., *Boronic acids : preparation and applications in organic synthesis, medicine and materials*. 2nd completely rev. ed2011, Weinheim: Wiley-VCH.
76. Lu, J., G. Xie, and W. Jia, *Metabolomics in human type 2 diabetes research.* Front Med, 2013. **7**(1): p. 4-13.

77. James, T.D., et al., *Novel Saccharide-Photoinduced Electron Transfer Sensors Based on the Interaction of Boronic Acid and Amine.* J. Am. Chem. Soc., 1995. **117**(35): p. 8982-8987.
78. James, T.D., K.R.A.S. Sandanayake, and S. Shinkai, *Novel photoinduced electron-transfer sensor for saccharides based on the interaction of boronic acid and amine.* J. Chem. Soc., Chem. Commun., 1994(4): p. 477.
79. Phillips, M. and T. James, *Boronic Acid Based Modular Fluorescent Sensors for Glucose.* J. Fluoresc., 2004. **14**(5): p. 549-559.
80. Pan, M., et al., *Boronic Acid-functionalized Core-shell-shell Magnetic Composite Microspheres for Selective Enrichment of Glycoprotein.* ACS Appl Mater Interfaces, 2013.
81. Ben-Amram, Y., M. Riskin, and I. Willner, *Selective and enantioselective analysis of mono- and disaccharides using surface plasmon resonance spectroscopy and imprinted boronic acid-functionalized Au nanoparticle composites.* The Analyst, 2010. **135**: p. 2952-9.
82. Lawrence, K., et al., *Pyrene-anchored boronic acid receptors on carbon nanoparticle supports: fluxionality and pore effects.* New J Chem, 2013. **37**(7): p. 1883-1888.
83. Mohapatra, S., N. Panda, and P. Pramanik, *Boronic acid functionalized superparamagnetic iron oxide nanoparticle as a novel tool for adsorption of sugar.* Mat Sci Eng C-Mater, 2009. **29**(7): p. 2254-2260.
84. Zhang, J., C.D. Geddes, and J.R. Lakowicz, *Complexation of polysaccharide and monosaccharide with thiolate boronic acid capped on silver nanoparticle.* Anal Biochem, 2004. **332**(2): p. 253-260.
85. Zhang, J., C.D. Geddes, and J.R. Lakowicz, *Complexation of Dextran and glucose with thiolate boronic acid capped on nanoparticle*, in *Biomedical Vibrational Spectroscopy and Biohazard Detection Technologies*2004. p. 293-301.
86. Lerner, M.B., et al., *Scalable, non-invasive glucose sensor based on boronic acid functionalized carbon nanotube transistors.* Appl Phys Lett, 2013. **102**(18).
87. Tamesue, S., et al., *Hierarchical carbon nanotube assemblies created by sugar-boric or boronic acid interactions.* Chem Commun, 2008(37): p. 4478-4480.
88. Kato, D., et al., *Electrochemically amplified detection for lipopolysaccharide using ferrocenylboronic acid.* Biosens. Bioelectron., 2007. **22**(7): p. 1527-1531.
89. Xia, N., et al., *Sandwich-type electrochemical biosensor for glycoproteins detection based on dual-amplification of boronic acid-gold nanoparticles and dopamine-gold nanoparticles.* Biosens. Bioelectron., 2013. **43**: p. 155-159.
90. Zhang, X., et al., *Boronic acid modified magnetic nanoparticles for enrichment of glycoproteins via azide and alkyne click chemistry.* J Mater Chem, 2012. **22**(32): p. 16520.
91. Qu, Y., et al., *Boronic Acid functionalized core-shell polymer nanoparticles prepared by distillation precipitation polymerization for glycopeptide enrichment.* Chemistry, 2012. **18**(29): p. 9056-62.
92. Whitesides, G.M. and B. Grzybowski, *Self-assembly at all scales.* Science, 2002. **295**(5564): p. 2418-21.
93. Whitesides, G.M. and M. Boncheva, *Beyond molecules: self-assembly of mesoscopic and macroscopic components.* Proc. Natl. Acad. Sci. U. S. A., 2002. **99**(8): p. 4769-74.
94. Wiener, N., *The Human Uses of Human Beings: Cybernetics and Society*, 1950, Houghton Mifflin Co: Boston. p. 36.
95. Ubbelohde, A.R., *Experimental Aspects of the Relation between Thermodynamics and Life*, in *Time and Thermodynamics*1947, Oxford University Press.: Oxford. p. 100-105.
96. Zhang, S., *Fabrication of novel biomaterials through molecular self-assembly.* Nat. Biotechnol., 2003. **21**(10): p. 1171-8.
97. Gardner, M.K., et al., *Microtubule assembly dynamics: new insights at the nanoscale.* Curr. Opin. Cell Biol., 2008. **20**(1): p. 64-70.
98. Jamalyaria, F., R. Rohlfs, and R. Schwartz, *Queue-based method for efficient simulation of biological self-assembly systems.* J. Comput. Phys., 2005. **204**(1): p. 100-120.
99. Castle, B.T. and D.J. Odde, *Brownian dynamics of subunit addition-loss kinetics and thermodynamics in linear polymer self-assembly.* Biophys. J., 2013. **105**(11): p. 2528-40.
100. Vericat, C., et al., *Self-assembled monolayers of thiols and dithiols on gold: new challenges for a well-known system.* Chem. Soc. Rev., 2010. **39**(5): p. 1805-34.
101. Ulman, A., *Formation and Structure of Self-Assembled Monolayers.* Chem. Rev., 1996. **96**(4): p. 1533-1554.

102. Vericat, C., M.E. Vela, and R.C. Salvarezza, *Self-assembled monolayers of alkanethiols on Au(111): surface structures, defects and dynamics.* Physical chemistry chemical physics : PCCP, 2005. **7**(18): p. 3258-68.
103. Nakatsu, S., et al., *A study of the glycoantigens of neonatal porcine islet-like cell clusters using a lectin microarray.* Transplant. Proc., 2012. **44**(4): p. 1134-5.
104. Nishijima, Y., et al., *Glycan profiling of endometrial cancers using lectin microarray.* Genes to cells : devoted to molecular & cellular mechanisms, 2012. **17**(10): p. 826-36.
105. Bertok, T., et al., *Label-free detection of glycoproteins by the lectin biosensor down to attomolar level using gold nanoparticles.* Talanta, 2013. **108**: p. 11-8.
106. Neves, B.R.A., et al., *Self-healing on OPA self-assembled monolayers.* Nanotechnology, 2001. **12**(3): p. 285-289.
107. Schwartz, D.K., *Mechanisms and kinetics of self-assembled monolayer formation.* Annu. Rev. Phys. Chem., 2001. **52**: p. 107-37.
108. Rouhana, L.L., M.D. Moussallem, and J.B. Schlenoff, *Adsorption of short-chain thiols and disulfides onto gold under defined mass transport conditions: coverage, kinetics, and mechanism.* J. Am. Chem. Soc., 2011. **133**(40): p. 16080-91.
109. Thanh, N.T.K. and L.A.W. Green, *Functionalisation of nanoparticles for biomedical applications.* Nano Today, 2010. **5**(3): p. 213-230.
110. Schönherr, H. and G.J. Vancso, *Lattice Imaging of Self-Assembled Monolayers of Partially Fluorinated Disulfides and Thiols on Sputtered Gold by Atomic Force Microscopy*. Langmuir, 1997. **13**(14): p. 3769-3774.
111. Castner, D.G., K. Hinds, and D.W. Grainger, *X-ray Photoelectron Spectroscopy Sulfur 2p Study of Organic Thiol and Disulfide Binding Interactions with Gold Surfaces.* Langmuir, 1996. **12**(21): p. 5083-5086.
112. Bain, C.D., H.A. Biebuyck, and G.M. Whitesides, *Comparison of self-assembled monolayers on gold: coadsorption of thiols and disulfides.* Langmuir, 1989. **5**(3): p. 723-727.
113. Love, J.C., et al., *Self-assembled monolayers of thiolates on metals as a form of nanotechnology.* Chem. Rev., 2005. **105**(4): p. 1103-69.
114. Thompson, M.S., et al., *Synthesis and applications of heterobifunctional poly(ethylene oxide) oligomers.* Polymer, 2008. **49**(2): p. 345-373.
115. Kolega, R.R. and J.B. Schlenoff, *Self-Assembled Monolayers of an Aryl Thiol: Formation, Stability, and Exchange of Adsorbed 2-Naphthalenethiol and Bis(2-naphthyl) Disulfide on Au.* Langmuir, 1998. **14**(19): p. 5469-5478.
116. Limbut, W., et al., *A comparative study of capacitive immunosensors based on self-assembled monolayers formed from thiourea, thioctic acid, and 3-mercaptopropionic acid.* Biosens. Bioelectron., 2006. **22**(2): p. 233-40.
117. Xu, Q.-M., et al., *New Structure ofl-Cysteine Self-Assembled Monolayer on Au(111): Studies by In Situ Scanning Tunneling Microscopy.* Langmuir, 2001. **17**(20): p. 6203-6206.
118. Filimon, A.D., et al., *Study on the reversible changes of the surface properties of an L-cysteine self-assembled monolayer on gold as a function of pH.* Langmuir, 2012. **28**(23): p. 8692-9.
119. Dijksma, M., et al., *Formation and Electrochemical Characterization of Self-Assembled Monolayers of Thioctic Acid on Polycrystalline Gold Electrodes in Phosphate Buffer pH 7.4.* Langmuir, 2000. **16**(8): p. 3852-3857.
120. Zhang, J., et al., *Two-Dimensional Cysteine and Cystine Cluster Networks on Au(111) Disclosed by Voltammetry and in Situ Scanning Tunneling Microscopy.* Langmuir, 2000. **16**(18): p. 7229-7237.
121. Cooper, E. and G.J. Leggett, *Static Secondary Ion Mass Spectrometry Studies of Self-Assembled Monolayers: Influence of Adsorbate Chain Length and Terminal Functional Group on Rates of Photooxidation of Alkanethiols on Gold.* Langmuir, 1998. **14**(17): p. 4795-4801.
122. Oh, S.-Y., et al., *Formation of a Self-Assembled Monolayer of Diaminododecane and a Heteropolyacid Monolayer on the ITO Surface.* Langmuir, 1999. **15**(14): p. 4690-4692.
123. Lewis, P.A., et al., *The Role of Buried Hydrogen Bonds in Self-Assembled Mixed Composition Thiols on Au{111}.* J. Phys. Chem. B, 2001. **105**(43): p. 10630-10636.
124. Badia, A., R.B. Lennox, and L. Reven, *A Dynamic View of Self-Assembled Monolayers.* Acc. Chem. Res., 2000. **33**(7): p. 475-481.

125. Hager, G. and A.G. Brolo, *Adsorption/desorption behaviour of cysteine and cystine in neutral and basic media: electrochemical evidence for differing thiol and disulfide adsorption to a Au(111) single crystal electrode.* J Electroanal Chem, 2003. **550-551**: p. 291-301.
126. Mateo Marti, E., C. Methivier, and C.M. Pradier, *(S)-cysteine chemisorption on Cu110, from the gas or liquid phase: an FT-RAIRS and XPS study.* Langmuir, 2004. **20**(23): p. 10223-30.
127. Zhang, J., et al., *Submolecular electronic mapping of single cysteine molecules by in situ scanning tunneling imaging.* Langmuir, 2009. **25**(4): p. 2232-40.
128. Liang, G.L., et al., *Gauche Defects, Positional Disorder, Dislocations, and Slip Planes in Crystals of Long Methylene Sequences.* J. Phys. Chem., 1994. **98**(45): p. 11739-11744.
129. Frederix, F., et al., *Enhanced Performance of an Affinity Biosensor Interface Based on Mixed Self-Assembled Monolayers of Thiols on Gold.* Langmuir, 2003. **19**(10): p. 4351-4357.
130. Yeung, C.L., et al., *Tuning Specific Biomolecular Interactions Using Electro-Switchable Oligopeptide Surfaces.* Adv Funct Mater, 2010. **20**(16): p. 2657-2663.
131. Valley, D.T., et al., *Steric hindrance of photoswitching in self-assembled monolayers of azobenzene and alkane thiols.* Langmuir, 2013. **29**(37): p. 11623-31.
132. Pranzetti, A., et al., *An electrically reversible switchable surface to control and study early bacterial adhesion dynamics in real-time.* Adv Mater, 2013. **25**(15): p. 2181-5.
133. Collman, J.P., N.K. Devaraj, and C.E.D. Chidsey, *"Clicking" Functionality onto Electrode Surfaces.* Langmuir, 2004. **20**(4): p. 1051-1053.
134. Chaki, N.K. and K. Vijayamohanan, *Self-assembled monolayers as a tunable platform for biosensor applications.* Biosens. Bioelectron., 2002. **17**(1-2): p. 1-12.
135. Geijtenbeek, T.B., et al., *Self- and nonself-recognition by C-type lectins on dendritic cells.* Annu. Rev. Immunol., 2004. **22**: p. 33-54.
136. Kalluri, R., *Basement membranes: structure, assembly and role in tumour angiogenesis.* Nat. Rev. Cancer, 2003. **3**(6): p. 422-33.
137. Geng, J. and N. Henry, *Short time-scale bacterial adhesion dynamics.* Advances in experimental medicine and biology, 2011. **715**: p. 315-31.
138. Flemming, H.-C., *Microbial Biofouling: Unsolved Problems, Insufficient Approaches, and Possible Solutions.* 2011. **5**: p. 81-109.
139. Worz, A., et al., *Protein-resistant polymer surfaces.* J Mater Chem, 2012. **22**(37): p. 19547-19561.
140. Feng, W., et al., *Protein resistant surfaces: Comparison of acrylate graft polymers bearing oligo-ethylene oxide and phosphorylcholine side chains.* Biointerphases, 2006. **1**(1): p. 50-60.
141. Pranzetti, A., et al., *Model Organic Surfaces to Probe Marine Bacterial Adhesion Kinetics by Surface Plasmon Resonance.* Adv Funct Mater, 2012. **22**(17): p. 3672-3681.
142. Mendes, P.M., *Cellular nanotechnology: making biological interfaces smarter.* Chem. Soc. Rev., 2013. **42**(24): p. 9207-18.
143. Herrwerth, S., et al., *Factors that determine the protein resistance of oligoether self-assembled monolayers --internal hydrophilicity, terminal hydrophilicity, and lateral packing density.* J. Am. Chem. Soc., 2003. **125**(31): p. 9359-66.
144. Hansson, K.M., et al., *Whole blood coagulation on protein adsorption-resistant PEG and peptide functionalised PEG-coated titanium surfaces.* Biomaterials, 2005. **26**(8): p. 861-872.
145. Bremmell, K.E., L. Britcher, and H.J. Griesser, *Steric and electrostatic surface forces on sulfonated PEG graft surfaces with selective albumin adsorption.* Colloids Surf B Biointerfaces, 2013. **106**: p. 102-8.
146. Wu, J., et al., *Investigation of the interaction between poly(ethylene glycol) and protein molecules using low field nuclear magnetic resonance.* Acta biomaterialia, 2013. **9**(5): p. 6414-20.
147. PY, J.Y., et al., *Self-assembled monothiol-terminated hyperbranched polyglycerols on a gold surface: a comparative study on the structure, morphology, and protein adsorption characteristics with linear poly(ethylene glycol)s.* Langmuir, 2008. **24**(9): p. 4907-16.
148. Feng, W., et al., *Characterization of protein resistant, grafted methacrylate polymer layers bearing oligo(ethylene glycol) and phosphorylcholine side chains by neutron reflectometry.* Biointerphases, 2007. **2**(1): p. 34-43.
149. Du, H., P. Chandaroy, and S.W. Hui, *Grafted poly-(ethylene glycol) on lipid surfaces inhibits protein adsorption and cell adhesion.* Biochimica et biophysica acta, 1997. **1326**(2): p. 236-48.

150. Fujimoto, K., H. Inoue, and Y. Ikada, *Protein adsorption and platelet adhesion onto polyurethane grafted with methoxy-poly(ethylene glycol) methacrylate by plasma technique.* J Biomed Mater Res, 1993. **27**(12): p. 1559-67.
151. Du, H., P. Chandaroy, and S.W. Hui, *Grafted poly-(ethylene glycol) on lipid surfaces inhibits protein adsorption and cell adhesion.* Biochimica et Biophysica Acta (BBA) - Biomembranes, 1997. **1326**(2): p. 236-248.
152. Schlenoff, J.B., *Zwitteration: coating surfaces with zwitterionic functionality to reduce nonspecific adsorption.* Langmuir, 2014. **30**(32): p. 9625-36.
153. Wu, Z.Q., et al., *Protein-Resistant and Fibrinolytic Polyurethane Surfaces.* Macromol Biosci, 2012. **12**(1): p. 126-131.
154. Siegers, C., M. Biesalski, and R. Haag, *Self-assembled monolayers of dendritic polyglycerol derivatives on gold that resist the adsorption of proteins.* Chemistry, 2004. **10**(11): p. 2831-8.
155. Holmberg, K., et al., *Grafting with hydrophilic polymer chains to prepare protein-resistant surfaces.* Colloid Surf. A., 1997. **123**: p. 297-306.
156. Holmlin, R.E., et al., *Zwitterionic SAMs that Resist Nonspecific Adsorption of Protein from Aqueous Buffer.* Langmuir, 2001. **17**(9): p. 2841-2850.
157. Norde, W., *Driving forces for protein adsorption at solid surfaces.* Macromol. Symp., 1996. **103**(1): p. 5-18.
158. Ostuni, E., et al., *Adsorption of Proteins to Hydrophobic Sites on Mixed Self-Assembled Monolayers.* Langmuir, 2003. **19**(5): p. 1861-1872.
159. Thudi, L., et al., *Adsorption induced enzyme denaturation: the role of protein surface in adsorption induced protein denaturation on allyl glycidyl ether (AGE)-ethylene glycol dimethacrylate (EGDM) copolymers.* Colloids Surf B Biointerfaces, 2012. **90**: p. 184-90.
160. Samanta, D. and A. Sarkar, *Immobilization of bio-macromolecules on self-assembled monolayers: methods and sensor applications.* Chem. Soc. Rev., 2011. **40**(5): p. 2567-92.
161. Van Dorst, B., et al., *Recent advances in recognition elements of food and environmental biosensors: a review.* Biosens. Bioelectron., 2010. **26**(4): p. 1178-94.
162. Arya, S.K., et al., *Recent advances in self-assembled monolayers based biomolecular electronic devices.* Biosens. Bioelectron., 2009. **24**(9): p. 2810-7.
163. Sarma, A.K., et al., *Recent advances in material science for developing enzyme electrodes.* Biosens. Bioelectron., 2009. **24**(8): p. 2313-22.
164. Lazcka, O., F.J. Del Campo, and F.X. Munoz, *Pathogen detection: a perspective of traditional methods and biosensors.* Biosens. Bioelectron., 2007. **22**(7): p. 1205-17.
165. Wang, J., et al., *Glucose detection with surface plasmon resonance spectroscopy and molecularly imprinted hydrogel coatings.* Talanta, 2011. **86**: p. 133-41.
166. Homola, J., *Present and future of surface plasmon resonance biosensors.* Anal. Bioanal. Chem., 2003. **377**(3): p. 528-39.
167. Olivier, G.K., et al., *Antibody-mimetic peptoid nanosheets for molecular recognition.* ACS nano, 2013. **7**(10): p. 9276-86.
168. Tse Sum Bui, B. and K. Haupt, *Molecularly imprinted polymers: synthetic receptors in bioanalysis.* Anal. Bioanal. Chem., 2010. **398**(6): p. 2481-92.
169. Cai, D., et al., *A molecular-imprint nanosensor for ultrasensitive detection of proteins.* Nat. Nanotechnol., 2010. **5**(8): p. 597-601.
170. Wei, S., M. Jakusch, and B. Mizaikoff, *Capturing molecules with templated materials--analysis and rational design of molecularly imprinted polymers.* Analytica chimica acta, 2006. **578**(1): p. 50-8.
171. Turner, N.W., et al., *From 3D to 2D: a review of the molecular imprinting of proteins.* Biotechnol. Prog., 2006. **22**(6): p. 1474-89.
172. Sibrian-Vazquez, M. and D.A. Spivak, *Molecular imprinting made easy.* J. Am. Chem. Soc., 2004. **126**(25): p. 7827-33.
173. Zayats, M., et al., *Molecular Imprinting of Maltose Binding Protein: Tuning Protein Recognition at the Molecular Level.* Macromolecules, 2011. **44**(10): p. 3966-3972.
174. Andersson, L.I., *Molecular imprinting for drug bioanalysis.* J Chromatogr B, 2000. **739**(1): p. 163-173.
175. Wulff, G., *Molecular Imprinting in Cross-Linked Materials with the Aid of Molecular Templates— A Way towards Artificial Antibodies.* Angewandte Chemie International Edition in English, 1995. **34**(17): p. 1812-1832.

176. Chen, L., S. Xu, and J. Li, *Recent advances in molecular imprinting technology: current status, challenges and highlighted applications.* Chemical Society reviews, 2011. **40**(5): p. 2922-42.
177. Vlatakis, G., et al., *Drug assay using antibody mimics made by molecular imprinting.* Nature, 1993. **361**(6413): p. 645-7.
178. He, H., et al., *Imprinting of protein over silica nanoparticles via surface graft copolymerization using low monomer concentration.* Biosens. Bioelectron., 2010. **26**: p. 760-765.
179. Whitcombe, M.J., et al., *A New Method for the Introduction of Recognition Site Functionality into Polymers Prepared by Molecular Imprinting: Synthesis and Characterization of Polymeric Receptors for Cholesterol.* J. Am. Chem. Soc., 1995. **117**(27): p. 7105-7111.
180. Li, F., J. Li, and S. Zhang, *Molecularly imprinted polymer grafted on polysaccharide microsphere surface by the sol-gel process for protein recognition.* Talanta, 2008. **74**(5): p. 1247-55.
181. Hayden, O., et al., *Surface imprinting strategies for the detection of trypsin.* The Analyst, 2006. **131**(9): p. 1044-50.
182. Bossi, A., et al., *Surface-Grafted Molecularly Imprinted Polymers for Protein Recognition.* Anal Chem, 2001. **73**(21): p. 5281-5286.
183. Verheyen, E., et al., *Challenges for the effective molecular imprinting of proteins.* Biomaterials, 2011: p. 1-13.
184. Shi, H., et al., *Template-imprinted nanostructured surfaces for protein recognition.* Nature, 1999. **398**(6728): p. 593-7.
185. Lépinay, S., et al., *In-situ polymerized molecularly imprinted polymeric thin films used as sensing layers in surface plasmon resonance sensors: Mini-review focused on 2010–2011.* Chem. Pap., 2012. **66**(5): p. 340-351.
186. Cecil, R.L., L. Goldman, and A.I. Schafer, *Goldman's Cecil medicine*. 24th ed2012, Philadelphia: Elsevier/Saunders/. xlii, 2569, 86 p.
187. Kennedy, M.A. and R.J. Parks, *Adenovirus virion stability and the viral genome: size matters.* Mol. Ther., 2009. **17**(10): p. 1664-6.
188. Gunawardena, H.P., R.A. O'Hair, and S.A. McLuckey, *Selective disulfide bond cleavage in gold(I) cationized polypeptide ions formed via gas-phase ion/ion cation switching.* J Proteome Res, 2006. **5**(9): p. 2087-92.
189. Choi, S., Y. Yang, and J. Chae, *Surface plasmon resonance protein sensor using Vroman effect.* Biosens. Bioelectron., 2008. **24**(4): p. 899-905.
190. Zhang, D., et al., *Gold nanoparticles can induce the formation of protein-based aggregates at physiological pH.* Nano letters, 2009. **9**(2): p. 666-71.
191. Wang, Y., et al., *Potentiometric sensors based on surface molecular imprinting: Detection of cancer biomarkers and viruses.* Sensor. Actuat. B-Chem., 2010. **146**(1): p. 381-387.
192. Maier, R.M., I.L. Pepper, and C.P. Gerba, *Environmental microbiology*. 2nd ed. Methods in enzymology,2009, Amsterdam ; Boston: Elsevier/Academic Press. xxii, 598 p.
193. Hoffmann, D., *Paul Drude (1863–1906).* Ann. Phys. (Berlin), 2006. **15**(7-8): p. 449-460.
194. Gonçalves, D. and E.A. Irene, *Fundamentals and Applications of Spectroscopic Ellipsometry.* Quim. Nova, 2002. **25**(5): p. 794-800.
195. Ulman, A., *An introduction to ultrathin organic films : from Langmuir-Blodgett to self-assembly*1991, Boston: Academic Press. xxiii, 442 p.
196. Motschmann, H. and R. Teppner, *Ellipsometry in interface science.* 2001. **11**: p. 1-42.
197. Schubert, M., *Another century of ellipsometry.* Ann. Phys. (Berlin), 2006. **15**(7-8): p. 480-497.
198. Kim, S.-H., et al., *Photoinduced refractive index change of self-assembled spiroxazaine monolayer based on surface plasmon resonance.* Dyes Pigments, 2000. **46**(1): p. 55-62.
199. Mittal, K.L., *Advances in contact angle, wettability and adhesion*. Adhesion and adhesives: fundamental and applied aspects2013, Beverly, USA: Wiley. 440.
200. Yuan, Y. and T.R. Lee, *Contact Angle and Wetting Properties.* 2013. **51**: p. 3-34.
201. Kwok, D.Y. and A.W. Neumann, *Contact angle measurement and contact angle interpretation.* Adv. Colloid Interface Sci., 1999. **81**(3): p. 167-249.
202. Krishnan, A., et al., *An evaluation of methods for contact angle measurement.* Colloids Surf B Biointerfaces, 2005. **43**(2): p. 95-8.
203. Andrade, J.D., *X-ray Photoelectron Spectroscopy (XPS).* 1985: p. 105-195.
204. Briggs, D. and M.P. Seah, *Practical surface analysis volume 1- auger and X-ray photoelectron spectroscopy.*1996, Chichester (UK): John Wiley & Sons.

205. Watts, J.F. and J. Wolstenholme, *An introduction to surface analysis by XPS and AES*2003, Chichester, West Sussex, England ; New York: J. Wiley. x, 212 p.
206. Briggs, D. and J.T. Grant, *Surface analysis by Auger and x-ray photoelectron spectroscopy*2003, Chichester, West Sussex, U.K.: IM Publications. xi, 899 p.
207. Seah, M.P., *A review of the analysis of surfaces and thin films by AES and XPS.* Vacuum, 1984. **34**(3-4): p. 463-478.
208. Baer, D.R., et al., *Approaches to analyzing insulators with Auger electron spectroscopy: Update and overview.* J Electron Spectrosc, 2010. **176**(1–3): p. 80-94.
209. Briggs, D., *Surface analysis of polymers by XPS and static SIMS*. Digitally printed 1st pbk. ed. Cambridge solid state science series2005, Cambridge ; New York: Cambridge University Press. xiv, 198 p.
210. Mahmood, N., et al., *Graphene-based nanocomposites for energy storage and conversion in lithium batteries, supercapacitors and fuel cells.* J Mater Chem A, 2014. **2**(1): p. 15.
211. Homola, J., S.S. Yee, and G. Gauglitz, *Surface plasmon resonance sensors: review.* Sensor. Actuat. B-Chem., 1999. **54**(1-2): p. 3-15.
212. Hoa, X.D., A.G. Kirk, and M. Tabrizian, *Towards integrated and sensitive surface plasmon resonance biosensors: a review of recent progress.* Biosens. Bioelectron., 2007. **23**(2): p. 151-60.
213. Tudos, A.J. and R.B.M. Schasfoort, *Handbook of Surface Plasmon Resonance*2008, Cambridge, UK: The Royal Society of Chemistry.
214. Sarid, D. and W.A. Challener, *Modern introduction to surface plasmons : theory, Mathematica modeling, and applications*2010, Cambridge ; New York: Cambridge University Press. xiv, 371 p.
215. Homola, J., *Surface plasmon resonance sensors for detection of chemical and biological species.* Chem. Rev., 2008. **108**(2): p. 462-93.
216. Pluchery, O., R. Vayron, and K.-M. Van, *Laboratory experiments for exploring the surface plasmon resonance.* Eur. J. Phys., 2011. **32**(2): p. 585-599.
217. Boozer, C., et al., *Looking towards label-free biomolecular interaction analysis in a high-throughput format: a review of new surface plasmon resonance technologies.* Curr. Opin. Biotechnol., 2006. **17**(4): p. 400-5.
218. Armstrong-James, M., et al., *Quantitative ionophoresis of catecholamines using multibarrel carbon fibre microelectrodes.* J. Neurosci. Methods, 1981. **4**(4): p. 385-406.
219. Millar, J. and T.G. Barnett, *Basic instrumentation for fast cyclic voltammetry.* J. Neurosci. Methods, 1988. **25**(2): p. 91-95.
220. Stamford, J.A., *In vivo voltammetry: Promise and perspective.* Brain Res. Rev., 1985. **10**(2): p. 119-135.
221. Compton, R.G. and C.E. Banks, *Understanding voltammetry*2007, Singapore ; Hackensack, NJ: World Scientific. xii, 371 p.
222. Manesh, K.M., et al., *Electrospun poly(vinylidene fluoride)/poly(aminophenylboronic acid) composite nanofibrous membrane as a novel glucose sensor.* Anal. Biochem., 2007. **360**(2): p. 189-95.
223. Taylor, S.I., *Deconstructing Type 2 Diabetes.* Cell, 1999. **97**(1): p. 9-12.
224. Mizrachi, E., S.D. Mansfield, and A.A. Myburg, *Cellulose factories: advancing bioenergy production from forest trees.* New Phytol., 2012. **194**(1): p. 54-62.
225. Scrafton, D.K., et al., *" Click-fluors ": Modular Fluorescent Saccharide Sensors Based on a 1 , 2 , 3-Triazole Ring.* J. Org. Chem., 2008. **73**: p. 2871-2874.
226. Kang, X., et al., *Glucose oxidase-graphene-chitosan modified electrode for direct electrochemistry and glucose sensing.* Biosens. Bioelectron., 2009. **25**(4): p. 901-5.
227. Holtz, J.H. and S.A. Asher, *Polymerized colloidal crystal hydrogel films as intelligent chemical sensing materials.* Nature, 1997. **389**(6653): p. 829-32.
228. Alexeev, V.L., et al., *High ionic strength glucose-sensing photonic crystal.* Anal. Chem., 2003. **75**(10): p. 2316-23.
229. Yang, D.-H., et al., *Fabrication of glucose-sensitive TiO 2 ultrathin films by molecular imprinting and selective detection of monosaccharides.* Sensor. Actuat. B-Chem, 2008. **130**(1): p. 379-385.
230. Park, S., H. Boo, and T.D. Chung, *Electrochemical non-enzymatic glucose sensors.* Anal. Chim. Acta., 2006. **556**(1): p. 46-57.
231. Arimori, S., et al., *Modular fluorescence sensors for saccharides.* J. Chem. Soc., Perkin Trans. 1, 2002: p. 803-808.

232. Lee, M., et al., *Formation of a self-assembled phenylboronic acid monolayer and its application toward developing a surface plasmon resonance-based monosaccharide sensor.* Anal Biochem, 2002. **310**(2): p. 163-170.
233. Shoji, E. and M.S. Freund, *Potentiometric saccharide detection based on the pK(a) changes of poly(aniline boronic acid).* J. Am. Chem. Soc., 2002. **124**(42): p. 12486-93.
234. Hall, D.G., *Boronic acids*, ed. D.G. Hall2005, Weinheim: Wiley-VCH.
235. James, T.D., M.D. Phillips, and S. Shinkai, *Boronic Acids in Saccharide Recognition*. Monographs in Supramolecular Chemistry, ed. J.F. Stoddard. Vol. 129. 2007, Cambridge: The Royal Society of Chemistry. 10964-10964.
236. D'Hooge, F., et al., *Biotinylated boronic acid fluorophore conjugates: Quencher elimination strategy for imaging and saccharide detection.* RSC Advances, 2012. **2**: p. 3274.
237. Bain, C.D., et al., *Formation of monolayer films by the spontaneous assembly of organic thiols from solution onto gold.* J. Am. Chem. Soc., 1989. **111**: p. 321-335.
238. Arimori, S., et al., *Modular fluorescence sensors for saccharides.* J. Chem. Soc., Perkin Trans. 1, 2002(6): p. 803-808.
239. Bielecki, M., H. Eggert, and J.C. Norrild, *A fluorescent glucose sensor binding covalently to all five hydroxy groups of α-D-glucofuranose. A reinvestigation.* J. Chem. Soc., Perkin Trans. 2, 1999(3): p. 449-456.
240. Wang, H.C., et al., *A bis-boronic acid modified electrode for the sensitive and selective determination of glucose concentrations.* The Analyst, 2013. **138**(23): p. 7146-51.
241. He, Y.Q., et al., *A study on the sizes and concentrations of gold nanoparticles by spectra of absorption, resonance Rayleigh scattering and resonance non-linear scattering.* Spectrochim Acta A Mol Biomol Spectrosc, 2005. **61**(13-14): p. 2861-6.
242. Briand, E., et al., *Building of an immunosensor: how can the composition and structure of the thiol attachment layer affect the immunosensor efficiency?* Biosens. Bioelectron., 2006. **22**(3): p. 440-8.
243. Wink, T., et al., *Self-assembled Monolayers for Biosensors.* The Analyst, 1997. **122**(4): p. 43R-50R.
244. Yam, C.M., et al., *Protein-resistant monolayers prepared by hydrosilylation of alpha-oligo(ethylene glycol)-omega-alkenes on hydrogen-terminated silicon (111) surfaces.* Chem Commun (Camb), 2004(21): p. 2510-1.
245. Wang, L., et al., *A new approach for the fabrication of an alternating multilayer film of poly(4-vinylpyridine) and poly(acrylic acid) based on hydrogen bonding.* Macromol Rapid Comm, 1997. **18**(6): p. 509-514.
246. Efimenko, K., et al., *Formation of Self-Assembled Monolayers of Semifluorinated and Hydrocarbon Chlorosilane Precursors on Silica Surfaces from Liquid Carbon Dioxide.* Langmuir, 2002. **18**(16): p. 6170-6179.
247. Harder, P., et al., *Molecular Conformation in Oligo(ethylene glycol)-Terminated Self-Assembled Monolayers on Gold and Silver Surfaces Determines Their Ability To Resist Protein Adsorption.* J. Phys. Chem. B, 1998. **102**(2): p. 426-436.
248. Bain, C.D., H.A. Biebuyck, and G.M. Whitesides, *Comparison of Self -Assembled Monolayers on Gold: Coadsorption of Thiols and Disulfides.* Langmuir, 1989. **5**(3): p. 723-727.
249. Shen, C.-H. and J.-C. Lin, *Improving the surface biocompatibility with the use of mixed zwitterionic self-assembled monolayers prepared by a proper solvent.* Langmuir, 2011. **27**(11): p. 7091-7098.
250. Cassie, A.B.D., *Contact Angles.* Discuss. Faraday Soc., 1948. **3**: p. 11-16.
251. Carey, R.I., J.P. Folkers, and G.M. Whitesides, *Self-Assembled Monolayers Containing .omega.-Mercaptoalkyl boronic Acids Adsorbed onto Gold Form a Highly Cross-Linked, Thermally Stable Borate Glass Surface.* Langmuir, 1994. **10**(7): p. 2228-2234.
252. Mendes, P.M., et al., *Electrochemically controllable conjugation of proteins on surfaces.* Bioconj. Chem., 2007. **18**(6): p. 1919-1923.
253. Yeung, C.L., et al., *Tuning Specific Biomolecular Interactions Using Electro-Switchable Oligopeptide Surfaces.* Adv. Funct. Mater., 2010. **20**: p. 2657–2663.
254. Sancenón, F., et al., *Open-chain polyazaalkanes functionalised with pyrene groups as sensing fluorogenic receptors for metal ions.* Polyhedron, 2002. **21**(14-15): p. 1397-1404.
255. Kankate, L., et al., *Protein resistant oligo(ethylene glycol) terminated self-assembled monolayers of thiols on gold by vapor deposition in vacuum.* Biointerphases, 2010. **5**(2): p. 30-36.
256. Cerruti, M., et al., *Poly(ethylene glycol) monolayer formation and stability on gold and silicon nitride substrates.* Langmuir, 2008. **24**(19): p. 10646-53.

257. Frey, S., et al., *Structure of Thioaromatic Self-Assembled Monolayers on Gold and Silver.* Langmuir, 2001. **17**(8): p. 2408-2415.
258. Ishida, T., et al., *Surface-Conditioning Effect of Gold Substrates on Octadecanethiol Self-Assembled Monolayer Growth.* Langmuir, 1997. **13**(17): p. 4638-4643.
259. Godsland, I.F., J.A. Jeffs, and D.G. Johnston, *Loss of beta cell function as fasting glucose increases in the non-diabetic range.* Diabetologia, 2004. **47**(7): p. 1157-66.
260. Schuck, P., *Use of surface plasmon resonance to probe the equilibrium and dynamic aspects of interactions between biological macromolecules.* Annu. Rev. Biophys. Biomol. Struct., 1997. **26**: p. 541-66.
261. Hsieh, H.V., et al., *Direct detection of glucose by surface plasmon resonance with bacterial glucose/galactose-binding protein.* Biosens. Bioelectron, 2004. **19**(7): p. 653-660.
262. Hill, D.G. and B.A. Thumm, *The Mutarotation of Glucose in Water-Methanol Mixtures—Acetate Ion Catalysis.* J. Am. Chem. Soc., 1952. **74**(6): p. 1380-1382.
263. Zhang, X., et al., *Lectin-based biosensor strategy for electrochemical assay of glycan expression on living cancer cells.* Anal Chem, 2010. **82**(22): p. 9455-60.
264. Brooks, C.L., et al., *Antibody recognition of a unique tumor-specific glycopeptide antigen.* Proc. Natl. Acad. Sci. U. S. A., 2010. **107**(22): p. 10056-61.
265. Wang, W., et al., *Antibody structure, instability, and formulation.* J Pharm Sci, 2007. **96**(1): p. 1-26.
266. Manning, M.C., et al., *Stability of protein pharmaceuticals: an update.* Pharm Res, 2010. **27**(4): p. 544-75.
267. Singh, S.K., et al., *Frozen state storage instability of a monoclonal antibody: aggregation as a consequence of trehalose crystallization and protein unfolding.* Pharm Res, 2011. **28**(4): p. 873-85.
268. Zhang, A., et al., *Distinct aggregation mechanisms of monoclonal antibody under thermal and freeze-thaw stresses revealed by hydrogen exchange.* Pharm Res, 2012. **29**(1): p. 236-50.
269. Witkiewicz, P.L. and C.F. Shaw, *Oxidative cleavage of peptide and protein disulphide bonds by gold(III): a mechanism for gold toxicity.* J. Chem. Soc., Chem. Commun., 1981(21): p. 1111.
270. Lee, J.M., et al., *Direct immobilization of protein g variants with various numbers of cysteine residues on a gold surface.* Anal Chem, 2007. **79**(7): p. 2680-7.
271. Haupt, K. and K. Mosbach, *Molecularly Imprinted Polymers and Their Use in Biomimetic Sensors.* Chem. Rev., 2000. **100**(7): p. 2495-2504.
272. Marx, S. and Z. Liron, *Molecular Imprinting in Thin Films of Organic−Inorganic Hybrid Sol−Gel and Acrylic Polymers.* Chem Mater, 2001. **13**(10): p. 3624-3630.
273. Kolb, H.C., M.G. Finn, and K.B. Sharpless, *Click Chemistry: Diverse Chemical Function from a Few Good Reactions.* Angew. Chem., Int. Ed., 2001. **40**(11): p. 2004-2021.
274. Amblard, F., J.H. Cho, and R.F. Schinazi, *Cu(I)-catalyzed Huisgen azide-alkyne 1,3-dipolar cycloaddition reaction in nucleoside, nucleotide, and oligonucleotide chemistry.* Chem. Rev., 2009. **109**(9): p. 4207-20.
275. Rostovtsev, V.V., et al., *A Stepwise Huisgen Cycloaddition Process: Copper(I)-Catalyzed Regioselective "Ligation" of Azides and Terminal Alkynes.* Angew. Chem., Int. Ed., 2002. **41**(14): p. 2596-2599.
276. Tornøe, C.W., C. Christensen, and M. Meldal, *Peptidotriazoles on Solid Phase: [1,2,3]-Triazoles by Regiospecific Copper(I)-Catalyzed 1,3-Dipolar Cycloadditions of Terminal Alkynes to Azides.* J. Org. Chem., 2002. **67**(9): p. 3057-3064.
277. Bertozzi, C.R., *A decade of bioorthogonal chemistry.* Acc. Chem. Res., 2011. **44**(9): p. 651-3.
278. Bock, V.D., H. Hiemstra, and J.H. van Maarseveen, *CuI-Catalyzed Alkyne-Azide "Click" Cycloadditions from a Mechanistic and Synthetic Perspective.* Eur J Org Chem, 2006. **2006**(1): p. 51-68.
279. Shao, C., et al., *Carboxylic acid-promoted copper(I)-catalyzed azide-alkyne cycloaddition.* J Org Chem, 2010. **75**(20): p. 7002-5.
280. Berg, R. and B.F. Straub, *Advancements in the mechanistic understanding of the copper-catalyzed azide-alkyne cycloaddition.* Beilstein J Org Chem, 2013. **9**: p. 2715-2750.
281. Ashworth, I.W., B.G. Cox, and B. Meyrick, *Kinetics and mechanism of N-Boc cleavage: evidence of a second-order dependence upon acid concentration.* J Org Chem, 2010. **75**(23): p. 8117-25.
282. Mehta, A., et al., *Improved efficiency and selectivity in peptide synthesis: Use of triethylsilane as a carbocation scavenger in deprotection of t-butyl esters and t-butoxycarbonyl-protected sites.* Tetrahedron Lett, 1992. **33**(37): p. 5441-5444.

283. Castellano, S. and J. Lorenc, *Nuclear Magnetic Resonance Spectra of Phenyl- and Diphenylacetylene.* J. Phys. Chem., 1965. **69**(10): p. 3552-3564.
284. Ciampi, S., et al., *Functionalization of acetylene-terminated monolayers on Si(100) surfaces: a click chemistry approach.* Langmuir, 2007. **23**(18): p. 9320-9.
285. Schultz, M.J., et al., *Synthesis of linked carbon monolayers: films, balloons, tubes, and pleated sheets.* Proc. Natl. Acad. Sci. U. S. A., 2008. **105**(21): p. 7353-8.
286. James, M., et al., *Nanoscale water condensation on click-functionalized self-assembled monolayers.* Langmuir, 2011. **27**(17): p. 10753-62.
287. Lilge, I. and H. Schönherr, *Covalently cross-linked poly(acrylamide) brushes on gold with tunable mechanical properties via surface-initiated atom transfer radical polymerization.* Eur Polym J, 2013. **49**(8): p. 1943-1951.
288. Chechik, V., et al., *Self-Assembled Monolayers of Branched Thiols and Disulfides on Gold: Surface Coverage, Order and Chain Orientation.* Langmuir, 1998. **14**(11): p. 3003-3010.
289. Weidner, T., et al., *Correlation between the molecular structure and photoresponse in aliphatic self-assembled monolayers with azobenzene tailgroups.* Langmuir, 2008. **24**(20): p. 11691-11700.
290. Dodero, G., et al., *l-Cysteine chemisorption on gold: an XPS and STM study.* Colloids Surf., A, 2000. **175**(1-2): p. 121-128.
291. Booz, M.L., *Electrophoresis*, in *Molecular Biology Problem Solver: A Laboratory Guide*, A.S. Gerstein, Editor 2001, Wiley-Liss: Hoboken, New Jersey.
292. Seabrook, S.A. and R.G. Gilbert, *Photo-initiated polymerization of acrylamide in water.* Polymer, 2007. **48**(16): p. 4733-4741.
293. Zhao, M., et al., *Inhibition of Electrochemical Reactions at Gold Surfaces by Grafted, Highly Fluorinated, Hyperbranched Polymer Films.* Langmuir, 1997. **13**(6): p. 1388-1391.
294. Park, S., et al., *Surface modification of poly(ethylene terephthalate) angioplasty balloons with a hydrophilic poly(acrylamide-co-ethylene glycol) interpenetrating polymer network coating.* J Biomed Mater Res, 2000. **53**(5): p. 568-576.
295. Neuhaus, S., C. Padeste, and N.D. Spencer, *Functionalization of Fluropolymers and Polyolefins via Grafting of Polyelectrolyte Brushes From Atmospheric-Pressure Plasma Activated Surfaces.* Plasma Process Polym, 2011. **8**(6): p. 512-522.
296. Chetty, A.S., *Thermoresponsive 3D scaffolds for non-invasive cell culture*, in *Adv Eng Res*2013, University of Pretoria: Pretoria.
297. Kissinger, P.T. and W.R. Heineman, *Cyclic voltammetry.* J Chem Educ, 1983. **60**(9): p. 702.
298. Shin, M.J. and W.H. Hong, *Sensing capability of molecularly imprinted self-assembled monolayer.* Biochem. Eng. J., 2011. **54**(1): p. 57-61.
299. Van Benschoten, J.J., et al., *Cyclic voltammetry experiment.* J Chem Educ, 1983. **60**(9): p. 772.
300. Kang, H., et al., *Two-dimensional ordering of benzenethiol self-assembled monolayers guided by displacement of cyclohexanethiols on Au(111).* Chem Commun (Camb), 2008(41): p. 5197-9.
301. Jansen, R.J.J. and H. van Bekkum, *XPS of nitrogen-containing functional groups on activated carbon.* Carbon, 1995. **33**(8): p. 1021-1027.
302. Moulder, J.F., et al., *Handbook of X-ray Photoelectron Spectroscopy*1992, Eden Prairie, MN, USA: Perkin-Elmer Corp.
303. Wu, W., et al., *Sensitive dopamine recognition by boronic acid functionalized multi-walled carbon nanotubes.* Chem Commun, 2007(23): p. 2345.
304. Lee, J.K., Y.S. Chi, and I.S. Choi, *Reactivity of Acetylenyl-Terminated Self-Assembled Monolayers on Gold: Triazole Formation.* Langmuir, 2004. **20**(10): p. 3844-3847.
305. Stephenson-Brown, A., et al., *Glucose selective Surface Plasmon Resonance-based bis-boronic acid sensor.* The Analyst, 2013.
306. Han, J.H. and J.Y. Yoon, *Reusable, polyethylene glycol-structured microfluidic channel for particle immunoassays.* J Biol Eng, 2009. **3**: p. 6.
307. James, M., et al., *Nanoscale condensation of water on self-assembled monolayers.* Soft Matter, 2011. **7**(11): p. 5309.
308. Maalouli, N., et al., *Comparison of photo- and Cu(I)-catalyzed "click" chemistries for the formation of carbohydrate SPR interfaces.* The Analyst, 2013. **138**(3): p. 805-12.
309. Ciampi, S., et al., *The rapid formation of functional monolayers on silicon under mild conditions.* Phys. Chem. Chem. Phys., 2014. **16**(17): p. 8003-11.

310. Ciampi, S., et al., *The detailed characterization of electrochemically switchable molecular assemblies on silicon electrodes.* Phys. Chem. Chem. Phys., 2013. **15**(24): p. 9879-90.
311. Chapman, R.G., et al., *Preparation of Mixed Self-Assembled Monolayers (SAMs) That Resist Adsorption of Proteins Using the Reaction of Amines with a SAM That Presents Interchain Carboxylic Anhydride Groups.* Langmuir, 2000. **16**(17): p. 6927-6936.
312. Heuberger, M., T. Drobek, and N.D. Spencer, *Interaction forces and morphology of a protein-resistant poly(ethylene glycol) layer.* Biophys. J., 2005. **88**(1): p. 495-504.
313. O'Brien Ii, M.J., et al., *SPR biosensors: simultaneously removing thermal and bulk-composition effects*, in *Biosens. Bioelectron.*1999. p. 145-154.
314. Jin, Z., et al., *Protein-resistant polyurethane prepared by surface-initiated atom transfer radical graft polymerization (ATRgP) of water-soluble polymers: effects of main chain and side chain lengths of grafts.* Colloids Surf B Biointerfaces, 2009. **70**(1): p. 53-9.
315. Wang, X., et al., *Investigation of the Interaction between Ferroceneboronic Acid and Sugars and Its Application in Probing of Enzyme Activity.* Int J Electrochem Sc, 2013. **8**(12): p. 12557-12565.
316. Springsteen, G. and B. Wang, *A detailed examination of boronic acid–diol complexation.* Tetrahedron, 2002. **58**(26): p. 5291-5300.
317. Sienkiewicz, P.A. and D.C. Roberts, *Chemical affinity systems—I.* J. Inorg. Nuc. Chem., 1980. **42**(11): p. 1559-1575.
318. Tsilikounas, E., C.A. Kettner, and W.W. Bachovchin, *Boron-11 NMR spectroscopy of peptide boronic acid inhibitor complexes of .alpha.-lytic protease. Direct evidence for tetrahedral boron in both boron-histidine and boron-serine adduct complexes.* Biochemistry, 1993. **32**(47): p. 12651-12655.
319. Leung, I.K.H., et al., *An approach to enzyme inhibition employing reversible boronate ester formation.* MedChemComm, 2011. **2**(5): p. 390.
320. Halo, T.L., et al., *Selective recognition of protein tetraserine motifs with a cell-permeable, pro-fluorescent bis-boronic acid.* J. Am. Chem. Soc., 2009. **131**(2): p. 438-9.
321. Uegaki, K., et al., *Simultaneous estimation of the association constants of glycoprotein glycoforms to a common protein by capillary electrophoresis.* Anal Biochem, 2002. **309**(2): p. 269-278.
322. Kallberg, K., K. Becker, and L. Bulow, *Application of a pH responsive multimodal hydrophobic interaction chromatography medium for the analysis of glycosylated proteins.* J Chromatogr A, 2011. **1218**(5): p. 678-83.
323. Keefe, S.E. and E.H. Grant, *Dipole-Moment and Relaxation-Time of Ribonuclease.* Phys. Med. Biol., 1974. **19**(5): p. 701-707.
324. Yaminsky, I.V., et al., *Atomic force microscopy study of lysozyme crystallization.* Crystallogr. Rep., 2002. **47**: p. S149-S158.
325. Kroschwitz, J.I. and H.F. Mark, *Encyclopedia of polymer science and technology*. 3rd ed2003, Hoboken, N.J.: Wiley-Interscience.
326. Perkins, S.J., et al., *Two-domain structure of the native and reactive centre cleaved forms of C inhibitor of human complement by neutron scattering.* J Mol Biol, 1990. **214**(3): p. 751-763.
327. Reh, E., B. Hahn, and S. Lamotte, *Evaluation of stationary phases for 2-dimensional HPLC of proteins Part 1. Validation of commercial RP-columns.* J Chromatogr B Analyt Technol Biomed Life Sci, 2006. **844**(2): p. 204-12.
328. Shamim, N., et al., *Adsorption, desorption, and conformational changes of lysozyme from thermosensitive nanomagnetic particles.* J. Colloid Interface Sci., 2008. **320**(1): p. 15-21.
329. Fournier, T., N. Medjoubi-N, and D. Porquet, *Alpha-1-acid glycoprotein.* BBA Protein Struct. M., 2000. **1482**(1-2): p. 157-171.
330. Ge, S.R., et al., *Bovine serum albumin adsorption onto immobilized organotrichlorosilane surface: Influence of the phase separation on protein adsorption patterns.* J Biomat Sci-Polym E, 1998. **9**(2): p. 131-150.
331. Asingh, P., et al., *Grauballe Man : an Iron Age bog body revisited*. Jutland Archaeological Society publications ,2007, Moesgaard: Moesgaard Museum, Jutland Archaeological Society. 351 p.
332. Noel-Georis, I., et al., *Database of bronchoalveolar lavage fluid proteins.* J Chromatogr B Analyt Technol Biomed Life Sci, 2002. **771**(1-2): p. 221-36.
333. Yaminsky, I.V., et al., *Atomic force microscopy study of lysozyme crystallization.* Crystallogr. Rep., 2002. **47**(S1): p. S149-S158.
334. Zervosen, A., et al., *Unexpected tricovalent binding mode of boronic acids within the active site of a penicillin-binding protein.* J. Am. Chem. Soc., 2011. **133**(28): p. 10839-48.

335. Meany, D.L., et al., *Glycoproteomics for prostate cancer detection: changes in serum PSA glycosylation patterns.* J Proteome Res, 2009. **8**(2): p. 613-9.
336. Drake, R.R., et al., *Clinical collection and protein properties of expressed prostatic secretions as a source for biomarkers of prostatic disease.* J Proteomics, 2009. **72**(6): p. 907-17.
337. Ferlay, J., et al., *Cancer incidence and mortality patterns in Europe: estimates for 40 countries in 2012.* Eur J Cancer, 2013. **49**(6): p. 1374-403.
338. Li, Y., et al., *Simultaneous analysis of glycosylated and sialylated prostate-specific antigen revealing differential distribution of glycosylated prostate-specific antigen isoforms in prostate cancer tissues.* Anal Chem, 2011. **83**(1): p. 240-5.
339. Klueh, U., D.I. Dorsky, and D.L. Kreutzer, *Enhancement of implantable glucose sensor function in vivo using gene transfer-induced neovascularization.* Biomaterials, 2005. **26**(10): p. 1155-63.
340. Wijesuriya, D., et al., *Regeneration of immobilized antibodies on fiber optic probes.* Biosens. Bioelectron., 1994. **9**(8): p. 585-592.
341. Lofgren, J.A., et al., *Comparing ELISA and surface plasmon resonance for assessing clinical immunogenicity of panitumumab.* J. Immunol., 2007. **178**(11): p. 7467-72.
342. Matsumoto, A., et al., *Assessment of tumor metastasis by the direct determination of cell-membrane sialic acid expression.* Angew Chem Int Ed Engl, 2010. **49**(32): p. 5494-7.